National and Kapodistrian University of Athens
School of Science
Department of Physics
Nuclear and Particle Physics Section

Doctoral Thesis

Cosmological Implications of Theories Beyond the Standard Model of Particle Physics

Ioannis D. Gialamas

Athens 2021

This research is co-financed by Greece and the European Union (European Social Fund- ESF) through the Operational Programme "Human Resources Development, Education and Lifelong Learning" in the context of the project "Strengthening Human Resources Research Potential via Doctorate Research - 2nd Cycle" (MIS-5000432), implemented by the State Scholarships Foundation (IKY).

Three-member advisory committee:

- Vassilis C. Spanos (Supervisor) – Associate Professor, NKUA
- Konstantinos Sfetsos – Professor, NKUA
- Nikolaos Tetradis – Professor, NKUA

Seven-member PhD thesis examination committee:

- Vassilis C. Spanos (Supervisor) – Associate Professor, NKUA
- Konstantinos Sfetsos – Professor, NKUA
- Nikolaos Tetradis – Professor, NKUA
- George Diamandis – Associate Professor, NKUA
- Vassileios Georgalas – Associate Professor, NKUA
- Panagiota Kanti – Professor, UOI
- Alexandros Kehagias – Professor, NTUA

“ *Ὅποιος ἐλεύθερα συλλογᾶται, συλλογᾶται καλά.*”

Ῥήγας Βελεστινλῆς

Φυσικῆς Ἀπάνθισμα, Βιέννη 1790

Abstract

In this thesis, we first calculate the gravitino production rate, computing its one-loop thermal selfenergy and we provide a convenient formula for it and its thermal abundance, as a function of the reheating temperature of the Universe. The gravitino yield is compared to the observed dark matter.

In the second part we consider quadratic gravity in the Palatini formulation of gravity assuming the existence of scalar fields coupled to gravity in the most general manner. Once the scalar fields develop vacuum expectation values the Planck scale is dynamically generated. The effect of the quadratic in curvature terms is to reduce the value of the tensor-to-scalar ratio. The inflationary predictions of all the models under consideration are found to comply with the latest bounds set by the Planck collaboration for a wide range of parameters.

Acknowledgements

First and foremost, my sincere gratitude goes to my supervisor prof. Vassilis Spanos who first introduced me to this exciting topic of physics. His knowledge on theoretical and computational physics was invaluable to my education and his insightful feedback pushed me to sharpen my thinking and brought my work to a higher level.

I would also like to thank my collaborators, emeritus prof. Athanasios Lahanas for his help in many topics of physics and Dr. Helmut Eberl for our collaboration and for our illuminating discussions. Thanks also to my collaborator and supervisor during my Master's studies, prof. Nikolaos Tetradis for his help and for introducing me to the amazing topics of cosmology and particle physics. Many thanks to the member of my advisory committee prof. Konstantinos Sfetsos for his kind assistance and support. I thank also many members of the Nuclear and Particle Physics section of NKUA and especially prof. George Diamandis for his support in many issues during the latest years. I also wish to thank D. Canko, Dr. A. Karam, G. Kodaxis, A. Lykkas, Dr. T. Pappas and Dr. A. Racioppi , for our very nice collaboration and communication during the last four years.

I am also very grateful to Xenia for her support all of these years. Last but not least, my deepest gratitude go to my parents and my sister for their support throughout my studies. Without their encouragement and love, nothing would be possible.

Contents

Preface

This thesis gathers some of the main results I have obtained during my PhD studies, for the *Doctorate Degree in Physical Sciences*, from November 2017 to July 2021. These studies have been performed at the National and Kapodistrian University of Athens, under the supervision of Vassilis C. Spanos.

The thesis is organised as follows:

- Chapter 1 is an introduction to the main subjects that follow in the next chapters, i.e. to gravitino dark matter and to cosmic inflation in the Palatini formulation of gravity.
- In Chapter 2 we give a brief introduction to Supersymmetry and Supergravity. These concepts are essential for understanding the calculation of gravitino abundance.
- Chapters 3-5, based on [1, 2], give the main results of the first part of this thesis. More precisely in Chapter 3 we present the finite temperature effects that are taken place in the calculation of the gravitino selfenergy. In Chapters 4 and 5 the gravitino production rate and its abundance are calculated.
- In Chapter 6 we give the basic tools for the calculation of the cosmological observables in the chapters that follow.
- In Chapter 7, based on [3], we discuss the inflationary predictions of basic models of inflation with the presence of a R^2 term in the Palatini formulation of gravity.
- Chapter 8, is based on [4, 5]. In this we study Scale-invariant models of inflation with the presence of quadratic in curvature terms in the usual Einstein-Hilbert action, again in the context of Palatini formulation of gravity. Also, in these models the Planck scale is dynamically generated through nonminimal couplings between gravity and scalar fields.
- Finally, in Chapter 9 we summarize and conclude.

Additional papers and conference proceedings:

During the last four years I have also participated in writing the papers [6–8] which did not fit within the story line of this thesis and are not included. Furthermore, the conference proceedings [9], based on [4, 5], have been presented in HEP–2021 and the [10], based on [1, 2], have been presented in BSM–2021.

Author: Ioannis D. Gialamas
Student ID: 2017503

Περίληψη

Οι επεκτάσεις του Καθιερωμένου Προτύπου στο πλαίσιο της υπερβαρύτητας μας παρέχουν ένα υποψήφιο σωματίδιο σκοτεινής ύλης (ΣΥ), το βαρυτίνο, τον υπερσυμμετρικό εταίρο του βαρυτονίου. Αλληλεπιδρά με τα άλλα σωματίδια καθαρά βαρυτικά κι έτσι αποφεύγει φυσικά την άμεση ή έμμεση ανίχνευση του, όπως προτείνεται από τα τρέχοντα πειραματικά και παρατηρησιακά δεδομένα αναζήτησης ΣΥ. Επομένως, η ακριβής γνώση της κοσμολογικής αφθονίας του είναι απαραίτητη για την εφαρμογή κοσμολογικών περιορισμών σε αυτά τα μοντέλα. Τα βαρυτίνα μπορούν να παραχθούν με διάφορους τρόπους: (i) μη θερμικά, από τη διασπάση του ίνφλατον [11–18], (ii) πολύ αργότερα κατά την περιόδο της νουκλεοσύνθεσης, μέσω της διάσπασης ασταθών σωματιδίων [19–22] και (iii) τέλος, θερμικά μέσω ενός μηχανισμού παραγωγής ψύξης καθώς το Σύμπαν ψύχεται από τη θερμοκρασία επαναθέρμανσης (T_{reh}) μέχρι τώρα [16, 23–37]. Συγκεκριμένα, υπό την προϋπόθεση ότι η υπερσυμμετρία σπάει μέσω ενός διαμεσολαβητή βαθμίδας, ένας διαφορετικός μηχανισμός παραγωγής πρέπει να χρησιμοποιηθεί [38–41][1]. Πρόσφατα, ένα εναλλακτικό σενάριο που περιλαμβάνει τη λεγόμενη "καταστροφική" μη θερμική παραγωγή αργών βαρυτίνων έχει προσελκύσει την προσοχή [60–67].

Αξίζει να σημειωθεί ότι ανάλογα με την ιεραρχία μαζών των μοντέλων υπερβαρύτητας, στην περίπτωση της διατήρησης της R ομοτιμίας, το βαρυτίνο μπορεί είτε να είναι το σταθερό ελαφρύτερο υπερσυμμετρικό σωματίδιο (ΕΥΣ) που παίζει τον ρόλο της ΣΥ (όπως υιοθετείται σε αυτήν τη διατριβή) ή μπορεί να είναι βαρύτερο από το ΕΥΣ και επομένως ασταθές. Στην τελευταία περίπτωση, είναι σημαντικό να υπολογιστεί το πλάτος της διάσπασης του βαρυτίνου στο ελαφρύτερο ουδέτερο φερμιόνιο βαθμίδας, το οποίο στην περίπτωση αυτή είναι το ΕΥΣ [68–79].

Οι προσπάθειες για τον υπολογισμό της θερμικής αφθονίας των βαρυτίνων χρησιμοποιώντας διάφορες τεχνικές, μεθόδους και προσεγγίσεις έχουν επεκταθεί τις τελευταίες τέσσερις δεκαετίες. Δεδομένου ότι τα βαρυτίνα παράγονται κυρίως θερμικά σε πολύ υψηλές θερμοκρασίες, χρησιμοποιήθηκε αρχικά η αποτελεσματική θεωρία των ελαφρών βαρυτίνων, η λεγόμενη προσέγγιση χωρίς παραγώγους που περιλαμβάνει μόνο τις συνιστώσες γκολντστίνο με ιδιοστροφορμή 1/2. Σε αυτό το πλαίσιο, δεδομένου ότι ορισμένα από τα πλάτη παραγωγής παρουσιάζουν υπέρυθρες (ΥΕ) αποκλίσεις, κανονικοποιήθηκαν εισάγοντας είτε μια πεπερασμένη θερμική μάζα γλουονίου είτε μια γωνιακή κλίμακα ανακοπής. Με αυτόν τον τρόπο, στο [24] οι βασικές διαδικασίες παραγωγής βαρυτίνων $2 \to 2$ καταγράφηκαν και υπολογίστηκαν για πρώτη φορά. Αυτός ο υπολογισμός βελτιώθηκε περαιτέρω στα [26, 27].

Η μέθοδος Braaten, Pisarski, Yuan (BPY) [80, 81] που κατέστησε δυνατό τον υπολογισμό της θερμικής αφθονίας του αξιονίου, στο [29] εφαρμόστηκε στο βαρυτίνο, με το κίνητρο του γεγονότος ότι το αξιόνιο που έχει κοινά στοιχεία με το βαρυτίνο, αλληλεπιδρά εξαιρετικά ασθενώς με το υπόλοιπο του φάσματος. Παρόλο που στο [30] χρησιμοποιήθηκε η προηγούμενη τεχνική κανονικοποίησης ΥΕ, στα [31, 34] χρησιμοποιήθηκε η μέθοδος BPY λαμβάνοντας επιπλέον υπόψη τη συμβολή της συνιστώσας του βαρυτίνου με ιδιοστροφορμή 3/2.

Τελικά στο [36] η μέθοδος υπολογισμού βελτιώθηκε σημαντικά. Εκεί υποστηρίχθηκε ότι η βασική απαίτηση για την εφαρμογή της μεθόδου BPY, *δηλ.* $g \ll 1$, όπου g είναι η σταθερά σύζευξης βαθμίδας, δεν ικανοποιείται σε ολόκληρο το εύρος θερμοκρασιών του υπολογισμού, ιδίως όταν το g είναι η ισχυρή σταθερά σύζευξης g_3. Ως εκ τούτου, οι συγγραφείς υπολόγισαν τη θερμική ιδιοενέργεια του βαρυτίνου σε επίπεδο ενός βρόχου πέραν της προσέγγισης του σκληρού

[1] Δείτε επίσης τα [41–59] για διάφορους υπολογισμούς παραγωγής βαρυτίνων.

θερμικού βρόχου, έχοντας το πλεονέκτημα ότι αυτό περιλαμβάνει τις διεργασίες $1 \to 2$ πέραν των διεργασιών $2 \to 2$.

Επιπροσθέτως, βρέθηκε ότι το λεγόμενο αφαιρούμενο τμήμα, δηλαδή τμήματα των τετραγωνικών πλατών $2 \to 2$ τα οποία δεν αντιπροσωπεύονται από την ιδιοενέργεια, είναι πεπερασμένα στο ΥΕ. Το κυρίως αριθμητικό αποτέλεσμα στο [36] σχετικά με τον ρυθμό παραγωγής βαρυτίνων διαφέρει σημαντικά, σχεδόν με έναν συντελεστή 2, σε σύγκριση με τα προηγούμενα αποτελέσματα [34, 37]. Δυστυχώς στο [36] τα κύρια αναλυτικά αποτελέσματα φαίνεται να είναι ανεπαρκή. Συγκεκριμένα οι εξισώσεις σχετικά με τη συνεισφορά της ιδιοενέργειας για το ρυθμό παραγωγής βαρυτίνων στην ενότητα IV A φαίνεται να έχουν ασυνέπεια ως προς τις διαστάσεις. Επιπλέον, λόγω των περιορισμένων υπολογιστικών πόρων εκείνης την εποχής, η αριθμητική εκτίμηση αυτής της ιδιοενέργειας υπολογίστηκε μόνο εντός του κώνου φωτός. Τέλος, δύο από τα τέσσερα μη μηδενικά αφαιρούμενα τμήματα στον πίνακα I του [36] αποδεικνύεται ότι είναι μηδέν.

Έχοντας αυτό ως κίνητρο, υπολογίζουμε εκ νέου [1] τη θερμικά διορθωμένη ιδιοενέργεια του βαρυτίνου χωρίς αριθμητικές προσεγγίσεις σε επίπεδο ενός βρόχου. Τέλος, δεδομένου ότι το τελικό μας αποτέλεσμα για τον ρυθμό παραγωγής βαρυτίνων είναι αριθμητικό όπως στο [36], παρουσιάζουμε μια εύχρηστη παραμετροποίηση ακολουθώντας το [16]. Το τελικό μας αποτέλεσμα διαφέρει από αυτό που εμφανίζεται στο [36] κατά περίπου 10 %. Υπολογίζουμε επίσης τη θερμική αφθονία των βαρυτίνων και συζητούμε πιθανές φαινομενολογικές συνέπειες.

Η συνδυασμένη ανάλυση των πιο πρόσφατων κοσμολογικών δεδομένων που βασίζεται σε διάφορες παρατηρήσεις όπως το κοσμικό υπόβαθρο μικροκυμάτων, οι δομές μεγάλης κλίμακας, τα δεδομένα των σουπερνόβα, κ.α. ευνοεί [82] την ύπαρξη ένος επιπέδου, ομογενούς και ισοτροπικού Σύμπαντος. Ο κοσμικός πληθωρισμός [83–86] όχι μόνο εξηγεί φυσικά τις παραπάνω ιδιότητες του Σύμπαντος, αλλά το πιο σημαντικό είναι ότι όταν αντιμετωπίζεται κβαντικά, παρέχει επίσης έναν μηχανισμό για τη δημιουργία των απαραίτητων αρχέγονων ανισοτροπιών που εξυπηρετούν τη δημιουργία των δομών μεγάλης κλίμακας που παρατηρούμε σήμερα. Τα δεδομένα της αποστολής Planck [87] έχουν περιορίσει σοβαρά τον παραμετρικό χώρο των πληθωριστικών μοντέλων, ουσιαστικά αποκλείοντας πολλά από αυτά, συμπεριλαμβανομένων των απλούστερων όπου ένα βαθμωτό πεδίο συνδέεται ελάχιστα με τη βαρύτητα. Από την άλλη πλευρά, πιο περίπλοκα μοντέλα, όπως το Starobinsky [88], όπου ένας όρος $\mathcal{R}^2$ προστίθεται στη δράση Einstein-Hilbert, φαίνεται να βρίσκονται εντός της επιτρεπόμενης περιοχής. Αυτός ο τύπος μη ελάχιστα συζευγμένων μοντέλων ανήκει στη γενική κατηγορία θεωριών βαθμωτού-τανυστή [8, 89–103]. Σε τέτοια μοντέλα, το βαθμωτό πεδίο ϕ συνήθως συνδέεται με τη βαρύτητα μέσω ενός όρου της μορφής $\xi_\phi \phi^2 \mathcal{R}$, όπου το ξ_ϕ είναι μια σταθερά σύζευξης χωρίς διαστάσεις και $\mathcal{R}$ είναι το βαθμωτό Ricci. Αξίζει να σημειωθεί ότι αυτός ο τύπος σύζευξης επιτρέπει στην κλίμακα Planck να δημιουργείται δυναμικά όταν το ϕ πάρει την αναμενόμενη τιμή του κενού του.

Η δυναμική παραγωγή της κλίμακας Planck επιτυγχάνεται συνήθως σε θεωρίες αναλλοίωτης κλίμακας [4, 5, 9, 104–149] στις οποίες το "τρέξιμο" της τεταρτικής σταθεράς σύζευξης του ίνφλατον προκαλεί ένα σπάσιμο συμμετρίας αλά Coleman–Weinberg. Η αναλλοιώτητα κλίμακας υπαινίσσεται ότι η Λανκρανζιανή μιας θεωρίας δεν πρέπει να περιέχει παραμέτρους μάζας επί τούτου. Εκμεταλλευόμενος την περιοριστική ισχύ της αναλλοιώτητας κλίμακας, μπορεί κανείς να δημιουργήσει τρεις επιπλέον όρους που σέβονται τη συμμετρία: τον όρο Starobinsky $\alpha\mathcal{R}^2$ και τους όρους $\beta\mathcal{R}_{\mu\nu}\mathcal{R}^{\mu\nu}$ και $\gamma\mathcal{R}_{\mu\nu\sigma\lambda}\mathcal{R}^{\mu\nu\sigma\lambda}$, όπου $\mathcal{R}_{\mu\nu\sigma\lambda}$ και $\mathcal{R}_{\mu\nu}$ είναι ο Riemann και ο Ricci τανυστής αντίστοιχα και α, β και γ είναι αδιάστατες σταθερές. Αυτή η θεωρία της βαρύτητας ονομάζεται *τετραγωνική βαρύτητα* και τελευταία λαμβάνει μεγάλη προσοχή ως μία πιθανή θεωρίας κβαντικής βαρύτητας [116, 128, 143, 149–159]. Φυσικά, οι εκτεταμένες θεωρίες της βαρύτητας εγείρουν το ερώτημα της σωστής διατύπωσης, *δηλ.* εάν θα χρησιμοποιήσουμε τον μετρικό ή τον Palatini φορμαλισμό κατά τη μεταβολή της δράσης.

Είναι γνωστό ότι ο Palatini φορμαλσιμός [160, 161] της γενικής θεωρίας της σχετικότητας (ΓΘΣ) (φορμαλισμός πρώτης τάξης) είναι μια εναλλακτική εκδοχή του πιο διαδεδομένου μετρικού φορμαλισμού (φορμαλισμός δεύτερης τάξης). Στον τελευταίο, η σύνδεση του χωροχρόνου είναι η συνήθης Levi-Civita, ενώ στον Palatini φορμαλισμό η σύνδεση $\Gamma^{\lambda}_{\mu\nu}$ και ο μετρικός τανυστής $g_{\mu\nu}$ αντιμετωπίζονται ως ανεξάρτητες μεταβλητές. Στα πλαίσια της ΓΘΣ, οι δύο φορμαλισμοί είναι ισοδύναμοι στο επίπεδο των εξισώσεων πεδίου, με τη σύνδεση Levi-Civita να ανακτάται μετά την ελαχιστοποίηση της δράσης στον Palatini φορμαλσιμό. Όταν λαμβάνονται υπόψη μη ελάχιστες σταθερές σύζευξης μεταξύ της βαρύτητας και της ύλης [8, 102, 103, 145, 162–199] ή/και $f(R)$ θεωρίες[2] [3–5, 9, 149, 158, 200–218], οι προκύπτουσες εξισώσεις πεδίου δεν είναι πλέον οι ίδιες κι έτσι οι δύο φορμαλισμοί οδηγούν σε διαφορετικές κοσμολογικές προβλέψεις.

Ένα αξιοσημείωτο παράδειγμα είναι το μοντέλο πληθωρισμού Starobinsky [88], όπου η προσθήκη ενός όρου $\mathcal{R}^2$ στη συνηθισμένη δράση Einstein-Hilbert μεταφράζεται σε έναν νέο διαδιδόμενο βαθμωτό βαθμό ελευθερίας (ΒΕ) που παίζει το ρόλο του ίνφλατον. Στον Palatini φορμαλισμό δεν υπάρχει επιπλέον διάδοση ΒΕ, επομένως το ίνφλατον πρέπει να προστεθεί εκ των προτέρων στη δράση. Το πλεονέκτημα του Palatini φορμαλισμού είναι ότι η προσθήκη του όρου R^2 μπορεί να χρησιμοποιηθεί για τη μείωση του λόγου τανυστή-βαθμωτού r [202], κάτι που είναι συνέπεια ενός πιο επίπεδου βαθμωτού δυναμικού στο πλαίσιο Einstein. Αυτό επιτρέπει σε διάφορα μοντέλα στα οποία ο πληθωρισμός καθοδηγείται από ένα βαθμωτό πεδίο να καταστούν συμβατά με τις παρατηρήσεις και πάλι [203, 204]. Επιπλέον, η προσθήκη ενός συμμετρικού τανυστή Ricci στο τετράγωνο $R_{(\mu\nu)}R^{(\mu\nu)}$ στη δράση Einstein-Hilbert έχει το ίδιο αποτέλεσμα με τον απλό R^2 όρο (βλέπε [219, 220]), τουλάχιστον όσον αφορά την τροποποίηση του βαθμωτού δυναμικού και κατά συνέπεια οδηγεί στη μείωση του λόγου τανυστή-βαθμωτού [202]. Η κύρια αλλά όχι σημαντική διαφορά μεταξύ αυτών των δύο τετραγωνικών όρων αναλλοίωτης κλίμακας είναι ότι στο πλαίσιο Einstein ο όρος R^2 οδηγεί επίσης σε έναν κινητικό όρο δεύτερης τάξης, ενώ ο $R_{(\mu\nu)}R^{(\mu\nu)}$ όρος αποδίδει μια σειρά κινητικών όρων ανώτερης τάξης. Ωστόσο, αυτοί οι κινητικοί όροι ανώτερης τάξης είναι αμελητέοι, τουλάχιστον κατά τη διάρκεια της αργής κύλισης.

[2]Σε αυτήν τη διατριβή χρησιμοποιούμε διαφορετικά σύμβολα για τη βαθμωτή και την τανυστική καμπυλότητα, τα οποία στον μετρικό φορμαλισμό δηλώνονται με $\mathcal{R}$, ενώ στον Palatini με R.

Dedicated to my family

Chapter 1

Introduction and summary

Extensions of Standard Model (SM) in the context of supergravity (SUGRA) provide us with a candidate particle for dark matter (DM), the gravitino, the superpartner of the graviton. It interacts with other particles purely gravitationally and thus naturally eludes direct or indirect detection, as suggested by current experimental and observational data from the DM search. Therefore, accurate knowledge of its cosmological abundance is essential to apply cosmological constraints to these models. Gravitinos can be produced in several ways: (i) nonthermally, from the inflaton decays [11–18], (ii) much later around the time of big bang nucleosynthesis, through the decays of unstable particles [19–22] and (iii) last but not least, thermally, through a freeze-in production mechanism as the Universe cools down from the reheating temperature ($T_{\rm reh}$) until now [16, 23–37]. In particular, under the assumption of gauge-mediated supersymmetry breaking a different production mechanism (freeze-out) must be used [38–41][1]. Recently, an alternative scenario involving the so-called "catastrophic" nonthermal production of slow gravitinos has attracted attention [60–67].

It is worth noting that depending on the mass hierarchy of the SUGRA models, in the case of R-parity conservation, the gravitino can either be the stable lightest supersymmetric particle (LSP) playing the role of the DM (as it is assumed in this thesis), or it can be heavier than the LSP and thus unstable. In the latter case, it is important to calculate the width of the gravitino decays to the lightest neutralino, which in this case is the LSP [68–79].

Efforts to calculate the thermal gravitino abundance using various techniques, methods, and approximations have spanned nearly the last four decades. Since gravitinos are mainly thermally produced at very high temperatures, the effective theory of light gravitinos, the so-called nonderivative approach, involving only the spin 1/2 goldstino components, was initially used. In this context, since some of the production amplitudes exhibit infrared (IR) divergences, they were regularized by introducing either a finite thermal gluon mass or an angular cutoff. In this way, in [24] the basic $2 \to 2$ gravitino production processes were tabulated and calculated for the first time. This calculation was further improved in [26, 27].

As the Braaten, Pisarski, Yuan (BPY) method [80, 81] succeeded in calculating the axion thermal abundance, in [29] it was further applied to the gravitino, motivated by the fact that the gravitinolike axion, interacts extremely weakly with the rest of the spectrum. Although in [30] the previous IR regularization technique was used, in [31, 34] the BPY method was employed, taking in addition into account the contribution of the spin 3/2 pure gravitino components.

Eventually, in [36] the method of calculation was considerably improved. There it was argued that the basic requirement for the application of the BPY prescription, *i.e.* $g \ll 1$, where g is the gauge coupling constant, is not satisfied in the whole temperature range of the calculation, in particular when g is the strong coupling constant g_3. Therefore, the authors calculated the one-loop thermal gravitino selfenergy numerically beyond the hard thermal loop approximation, with the advantage that this includes the $1 \to 2$ processes in addition to the $2 \to 2$ processes. More importantly, it was found that the so-called subtracted part, *i.e.*

[1]See also [41–59] for various gravitino production calculations.

parts of the $2 \to 2$ squared amplitudes for which the selfenergy may not account for, are IR finite. The main numerical result in [36] on the gravitino production rate differs significantly, almost by a factor of 2, compared to the earlier works [34, 37]. Unfortunately, in [36] the main analytical results seem to be insufficient. In particular, the equations on the selfenergy contribution for the gravitino production rate in section IV A even seem to be dimensionally inconsistent. Moreover, due to the limited computational resources at the time, the numerical estimation of this self-energy was computed only within the light cone. Moreover, two of the four nonzero subtracted parts in the corresponding Table I in [36] turn out to be zero.

Motivated by this, we recalculate [1] the thermally corrected gravitino selfenergy without numerical approximations at the one-loop level. Finally, since our final result for the gravitino production rate is numerical as in [36], we present an updated handy parametrization of it following [16]. Our final result differs from that shown in [36] by about 10%. We also calculate the thermal gravitino abundance and discuss possible phenomenological consequences.

The combined analysis of the latest cosmological data based on various observations such as the cosmic microwave background (CMB), large scale structures, supernova data, *etc.* favor [82] a flat, homogeneous and isotropic Universe. Cosmic inflation [83–86] not only naturally explains the above properties of the Universe, but, most importantly, when treated quantum mechanically, it also provides a mechanism for the generation of the necessary primordial anisotropies that serve as seeds for the generation of the large-scale structures we observe today. The Planck mission data combined with earlier observation [87] have severely constrained the parameter space of inflationary models, essentially ruling out many of them, including the simplest ones where a scalar field is minimally coupled to gravity. On the other hand, more complicated models such as the Starobinsky [88], where a $\mathcal{R}^2$ term is added to the Einstein-Hilbert action, seem to be within the allowed range. This type of nonminimal models belongs to the general class of scalar-tensor (ST) theories [8, 89–103]. In such models, the scalar field ϕ typically couples to gravity via a term of the form $\xi_\phi \phi^2 \mathcal{R}$, where ξ_ϕ is a dimensionless coupling constant and $\mathcal{R}$ is the Ricci scalar. It is worth noting that this type of coupling allows the Planck scale to be dynamically generated when ϕ evolves a vacuum expectation value (VEV).

Dynamical generation of the Planck scale is usually achieved in scale-invariant theories [4, 5, 9, 104–149], in which the running of the inflaton quartic coupling induces symmetry breaking à la Coleman–Weinberg. Scale invariance postulates that the Lagrangian of a theory should not contain any ad hoc mass parameters. Exploiting the restrictive power of scale invariance, one can form three additional terms that respect symmetry: the Starobinsky term $\alpha\mathcal{R}^2$ and the terms $\beta\mathcal{R}_{\mu\nu}\mathcal{R}^{\mu\nu}$ and $\gamma\mathcal{R}_{\mu\nu\sigma\lambda}\mathcal{R}^{\mu\nu\sigma\lambda}$, where $\mathcal{R}_{\mu\nu\sigma\lambda}$ and $\mathcal{R}_{\mu\nu}$ are the Riemann and Ricci tensors, respectively, and α, β and γ are dimensionless constants. This theory of gravity is called *quadratic gravity* and has recently received much attention as a possible realization of quantum gravity [116, 128, 143, 149–159]. Of course, extended theories of gravity raise the question of the correct formulation, *i.e.* whether to use the metric or the Palatini formalism when varying the action.

It is well known that the Palatini formulation [160, 161] of general relativity (GR) (first-order formalism) is an alternative to the well-known metric formulation (second-order formalism). In the latter, the spacetime connection is the usual Levi-Civita, while in the Palatini approach the connection $\Gamma^\lambda_{\mu\nu}$ and the metric $g_{\mu\nu}$ are treated as independent variables. In the context of GR, the two formalisms are equivalent at the level of field equations, with the Levi-Civita connection recovered on-shell in the Palatini approach. When nonminimal couplings between gravity and matter [8, 102, 103, 145, 162–199] or/and $f(R)$ theories[2] [3–5, 9, 149, 158, 200–218] are considered, the resulting field equations are no longer the same

[2]Throughout this thesis we use different symbols for the curvature scalar and tensors, which in the metric formulation we denote by $\mathcal{R}$, while in the Palatini approach by R.

and thus the two formalisms lead to different cosmological predictions. A notable example is the Starobinsky model of inflation [88], where the addition of a $\mathcal{R}^2$ term in the usual Einstein-Hilbert action is translated into a new propagating scalar degree of freedom (DOF) which plays the role of the inflaton. In the Palatini formalism there are no extra propagating DOF, therefore the inflaton has to be added ad hoc in the action. The advantage of considering the Palatini formulation is that the addition of the R^2 term can be used to reduce the tensor-to-scalar ratio r [202], as a consequence of a flatter scalar potential in the Einstein frame (EF) This allows various models in which inflation is driven by a scalar field to be made compatible with the observations again [203, 204]. Moreover, the addition of a symmetric Ricci tensor squared term $R_{(\mu\nu)}R^{(\mu\nu)}$ in the Einstein-Hilbert action has the same effect as the pure R^2 term (see [219, 220]), at least as far as the modification of the scalar potential is concerned, and consequently leads to the reduction of the tensor-to-scalar ratio [202]. The main, but not significant, difference between these two quadratic scale-invariant terms is that in the EF the R^2 term also leads to a second-order kinetic term, while the $R_{(\mu\nu)}R^{(\mu\nu)}$ term yields a series of higher-order kinetic terms. However, these higher order kinetic terms are negligible, at least during slow roll.

In this thesis we use natural units, by setting $\hbar = c = k_B = 1$. We also use $M_{\mathrm{P}} = (8\pi G)^{-1/2} = 1$ in most formulas except when we want the dimensionality to be explicit.

Chapter 2

Supersymmetry and supergravity

Supersymmetry (SUSY) (see [221] for a review) is an extension of the SM that aims to fill some of the gaps. It provides us extra particles that can play the roll of DM, predicts a unification of all fundamental forces of nature (see Fig. 2.2), and manages to solve the hierarchy problem as analyzed in Sec. 2.1. SUGRA (see [222] for a review) is a supersymmetric theory of gravity, or a theory of local SUSY. It involves the graviton described by GR, and extra matter, in particular a fermionic partner of the graviton called gravitino. A natural framework to connect these theories with particle and/or cosmological experiments are the no-scale SUGRA models [223–227], with many applications to cosmic inflation [228–239]. The predictions of such inflationary models [240–275] mimic those of the Starobinsky model [88].

2.1 Supersymmetry

The SM of particle physics, provides a remarkably successful description in a plethora of known phenomena. Although the SM has demonstrated great successes in providing experimental predictions into the TeV range, it leaves some phenomena unexplained and thus needs to be extended at higher energies up to the Planck scale $M_{\rm P} = (8\pi G)^{-1/2} = 2.435 \times 10^{18}$ GeV, where quantum gravity arises. The electroweak sector of the SM contains within it an experimentally calculated parameter, namely the electroweak scale $v_h \simeq 246\,$GeV which is related to the VEV of the Higgs field written in the unitary gauge $H^\dagger = (0, v_h + h)/\sqrt{2}$. The well known hierarchy problem [276–278] of particle physics, *i.e.* the fact that the ratio $v_h/M_{\rm P} \simeq 10^{-16} \ll 1$, lead us to explore physics beyond the SM. In order to analyze the hierarchy problem in more detail we recall the SM higgs field classical potential

$$V = \mu^2(H^\dagger H) + \lambda_h (H^\dagger H)^2 \,. \tag{2.1}$$

The requirement of a non-vanishing VEV for the Higgs field at the minimum of the potential (2.1), occurs if $\lambda_h > 0$ and $\mu^2 < 0$, resulting in a VEV $v_h^2 = -\mu^2/\lambda_h$ and in a Higgs mass $m_h = \sqrt{2\lambda_h v_h^2}$. If $\mu^2 > 0$ the VEV is at the origin in field space, which would imply $v_h = 0$, in which case all particles would remain massless. It has been almost a decade since the discovery of the Higgs boson with a mass $m_h \simeq 125\,$GeV in the Large Hadron Collider (LHC) [279, 280]. This experimental value of the Higgs mass implies that $\lambda_h \simeq 0.13$ and $\mu^2 \simeq -(90\ GeV)^2$. The problem is that μ^2 and thus m_h^2 receives enormous radiative quantum corrections which are generally proportional to a cutoff energy scale Λ, that is used to regulate the fermion loop integral given on the left of Figure 2.1. Assuming the Yukawa interaction between Higgs and fermions $\mathcal{L}_{Yukawa} = -\lambda_f H \bar{f} f$, the left Feynman diagram in Figure 2.1 yields a correction

$$\Delta\mu^2 = -\frac{|\lambda_f|^2}{8\pi^2}\Lambda^2 + \cdots \tag{2.2}$$

where the ellipses represent terms proportional to the fermion mass squared, which grow at most logarithmically with Λ. If $\Lambda \sim M_{\rm P}$ or even much smaller, the 1-loop correction in

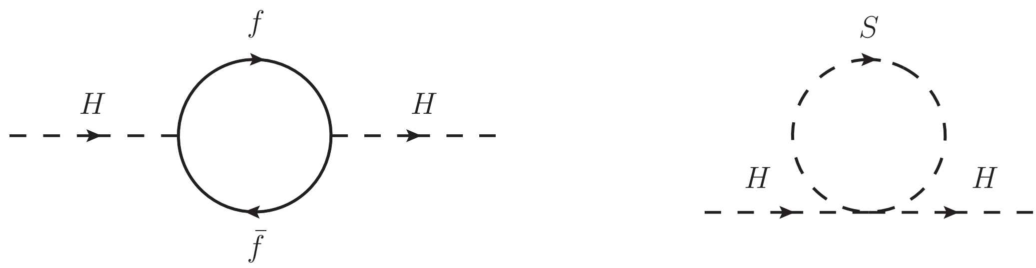

Figure 2.1: The one-loop quantum corrections to the Higgs mass parameter μ^2, due to a fermion f (left) and a scalar S (right).

Eq. (2.2) is vastly greater than the electroweak scale which is the order of magnitude of the mass parameter μ. The observed hierarchy between the electroweak scale and the Planck scale must be achieved with extraordinary fine tuning.

A possible solution to this comes by assuming a complex scalar particle S that couples to the Higgs boson as $-\lambda_{hs}|H|^2|S|^2$. This four-point interaction which is illustrated in the right Feynman diagram in Figure 2.1 would give a new correction to the mass μ^2 which reads

$$\Delta\mu^2 = \frac{\lambda_S}{16\pi^2}\Lambda^2 + \cdots . \tag{2.3}$$

Now, if there is one scalar boson for each of the two spin states of the SM fermions, then the quadratic in Λ quantum corrections of (2.2) and (2.3) will neatly cancel, provided that $\lambda_{hs} = |\lambda_f|^2$ [281–285]. Such bosons could arise in supersymmetric theories as we will see next.

A SUSY transformation relates bosonic and fermionic states in such a way that

$$Q\,|\text{boson}\rangle = |\text{fermion}\rangle\,, \qquad\qquad Q\,|\text{fermion}\rangle = |\text{boson}\rangle\,, \tag{2.4}$$

where Q is an anti-commuting Weyl spinor that generates such transformations. The $\mathcal{N}=1$ Super–Poincare algebra for the 4−momentum generator of spacetime translations P_μ, the generators of the Lorentz group (boosts + rotations) $M_{\mu\nu}$ and the SUSY generators Q are summarized in the following,

$$\begin{aligned}
[P_\mu, P_\nu] &= 0\,,\\
[M_{\mu\nu}, M_{\rho\sigma}] &= i\left(g_{\mu\sigma}M_{\nu\rho} - g_{\mu\rho}M_{\nu\sigma} + g_{\nu\rho}M_{\mu\sigma} - g_{\nu\sigma}M_{\mu\rho}\right)\,,\\
[M_{\mu\nu}, P_\rho] &= i\left(g_{\rho\nu}P_\mu - g_{\mu\rho}P_\nu\right)\,,\\
[Q_\alpha, P_\mu] &= \left[\overline{Q}_{\dot\alpha}, P_\mu\right] = 0\,,\\
[Q_\alpha, M_{\mu\nu}] &= \left(\sigma_{\mu\nu}\right)_\alpha^{\ \beta} Q_\beta\,,\\
\left[\overline{Q}_{\dot\alpha}, M_{\mu\nu}\right] &= \left(\overline{\sigma}_{\mu\nu}\right)_{\dot\alpha}^{\ \dot\beta}\,\overline{Q}_{\dot\beta}\,,\\
\left\{Q_\alpha, \overline{Q}_{\dot\alpha}\right\} &= 2\left(\sigma^\mu\right)_{\alpha\dot\alpha} P_\mu\,,\\
\{Q_\alpha, Q_\beta\} &= \left\{\overline{Q}_{\dot\alpha}, \overline{Q}_{\dot\beta}\right\} = 0\,,
\end{aligned} \tag{2.5}$$

where [,] and { , } stand for the commutator and anti-commutator respectively. The definitions of the Pauli σ matrices along with the used metric signature in this thesis are presented in Appendix A. In the same appendix the notation of Weyl, Dirac and Majorana spinors is displayed. The supersymmetric extension of the SM as described by the algebra (2.5) will extend the known SM particle spectrum with new particles. More precisely each of the "old" particles must have a superpartner with spin differing by 1/2 unit.

2.2 Minimal supersymmetric Standard Model

The minimal supersymmetric Standard Model (MSSM) is the most "economical" extension of the SM that realizes SUSY. It is called "Minimal" as considers only the minimum number of new particles and interactions consistent with phenomenology. As discussed in Sec. 2.1, SUSY pairs bosons with fermions, so every SM particle has its own superpartner. Unfortunately, LHC has not yet discovered any supersymmetric particle, as of the writing of this thesis.

Before continuing with more formal work, we would like to indicate our notation following [37]. The matter fermions are described in terms of the left-handed four-spinors χ^i_L and the corresponding scalar superpartners are denoted as ϕ^i, where i runs over all chiral superfields. Gauge multiplets consist of gauge bosons A^a_μ and their superpartners, the gauginos, which are Majorana fermions are denoted by λ^a, with $a = 1, \ldots,$ "dimension of the gauge group". The gravity sector that contains the graviton and its superpartner gravitino will be analyzed in the next section. In terms of the above particles, the gauge part of the Lagrangian is given by

$$\begin{aligned}
\mathcal{L}^{(\alpha)}_{\text{gauge}} &= \mathcal{D}^{(\alpha)}_\mu \phi^i \mathcal{D}^{(\alpha)\mu} \phi^{*i} - \frac{1}{2} g^2_\alpha \left(\phi^{*i} T^{(\alpha)}_{a,\,ij} \phi^j \right)^2 \\
&+ i\,\overline{\chi}^i_L \gamma^\mu \mathcal{D}^{(\alpha)}_\mu \chi^i_L - \frac{1}{4} F^{(\alpha)\,a}_{\mu\nu} F^{(\alpha)\,b,\,\mu\nu} + \frac{i}{2} \overline{\lambda}^{(\alpha)\,a} \gamma^\mu \mathcal{D}^{(\alpha)}_\mu \lambda^{(\alpha)\,a} \\
&- \sqrt{2} g_\alpha \overline{\lambda}^{(\alpha)\,a} \phi^{*i} T^{(\alpha)}_{a,\,ij} \chi^j_L - \sqrt{2} g_\alpha \overline{\chi}^i_L T^{(\alpha)}_{a,\,ij} \phi^j \lambda^{(\alpha)\,a} \,,
\end{aligned} \tag{2.6}$$

where the index $\alpha = 1, 2\,\text{or}\,3$ indicating the $U(1)_Y$, $SU(2)_L$ or $SU(3)_c$ gauge group. Accordingly the gauge couplings g_α are given by $g_1 = g_Y$, $g_2 = g$ and $g_3 = g_s$ with hypercharge coupling g_Y and the weak and strong couplings g and g_s, respectively. In Table 2.1 are displayed the gauge fields of the MSSM. In the second column are presented the gauge bosons of the SM, while the third one shows the supersymmetric gauginos. In Table 2.2 the full particle content of MSSM is displayed. The generators $T^{(\alpha)}_{a,\,ij}$ in (2.6) for the SM gauge groups are given by

$$\begin{aligned}
T^{(1)}_{a,\,ij} &= \frac{1}{2} Y_i \delta_{ij} \delta_{a1} \,, \\
T^{(2)}_{a,\,ij} &= \frac{1}{2} \sigma_{a,\,ij} \,, \\
T^{(3)}_{a,\,ij} &= \frac{1}{2} \lambda_{a,\,ij} \,,
\end{aligned} \tag{2.7}$$

where Y_i is the hypercharge as given in the fourth column of Tables 2.1 and 2.2. The Pauli σ matrices are given in (A.2) and λ_a are the eight Gell-Mann matrices. The covariant derivatives for bosons, fermions and gauginos are

$$\begin{aligned}
\mathcal{D}^{(\alpha)}_\mu \phi^i &= \partial_\mu \phi^i + i g_\alpha A^{(\alpha)\,a}_\mu T^{(\alpha)}_{a,\,ij} \phi^j \,, \\
\mathcal{D}^{(\alpha)}_\mu \chi^i_L &= \partial_\mu \chi^i_L + i g_\alpha A^{(\alpha)\,a}_\mu T^{(\alpha)}_{a,\,ij} \chi^j_L \,, \\
\mathcal{D}^{(\alpha)}_\mu \lambda^{(\alpha)\,a} &= \partial_\mu \lambda^{(\alpha)\,a} - g_\alpha f^{(\alpha)\,abc} A^{(\alpha)\,b}_\mu \lambda^{(\alpha)\,c} \,,
\end{aligned} \tag{2.8}$$

where the structure constants $f^{(\alpha)\,abc}$ for the three gauge groups are given by

$$\begin{aligned}
f^{(1)\,abc} &= 0 \,, \\
f^{(2)\,abc} &= \epsilon^{abc} \,, \\
f^{(3)\,abc} &= f^{abc} \,.
\end{aligned}$$

Table 2.1: Gauge fields of the MSSM and the corresponding quantum numbers for the three gauge groups.

Name	Gauge bosons $A_\mu^{(\alpha)\,a}$	Gauginos $\lambda^{(\alpha)\,a}$	$(SU(3)_c, SU(2)_L, U(1)_Y)$
B-boson - bino	$A_\mu^{(1)\,a} = B_\mu\,\delta^{a1}$	$\lambda^{(1)\,a} = \widetilde{B}\,\delta^{a1}$	$(\mathbf{1}\,,\mathbf{1}\,,0)$
W-bosons - winos	$A_\mu^{(2)\,a} = W_\mu^a$	$\lambda^{(2)\,a} = \widetilde{W}^a$	$(\mathbf{1}\,,\mathbf{3}\,,0)$
gluon - gluino	$A_\mu^{(3)\,a} = g_\mu^a$	$\lambda^{(3)\,a} = \widetilde{g}^a$	$(\mathbf{8}\,,\mathbf{1}\,,0)$

See Appendix A for more details about the totally antisymmetric structure constants ϵ^{abc} and f^{abc}. In detail, we present the three covariant derivatives for the bosons ϕ^i

$$\begin{aligned}
\mathcal{D}_\mu^{(1)}\phi &= \partial_\mu\phi + i\frac{g_1}{2}B_\mu Y\phi\,,\\
\mathcal{D}_\mu^{(2)}\begin{pmatrix}\phi^1\\ \phi^2\end{pmatrix} &= \left(\begin{pmatrix}\partial_\mu & 0\\ 0 & \partial_\mu\end{pmatrix} + i\frac{g_2}{2}\begin{pmatrix}s_W A_\mu + c_W Z_\mu & \sqrt{2}W_\mu^+\\ \sqrt{2}W_\mu^- & -s_W A_\mu - c_W Z_\mu\end{pmatrix}\right)\begin{pmatrix}\phi^1\\ \phi^2\end{pmatrix}\,,\\
\mathcal{D}_\mu^{(3)}\phi^r &= \partial_\mu\phi^r + i\frac{g_3}{2}g_\mu^a\lambda_{rs}^a\phi^s\,,
\end{aligned} \tag{2.9}$$

where r, s are color indices. We have already substituted $B_\mu = cos\,\theta_W A_\mu - sin\,\theta_W Z_\mu$, $W_\mu^3 = sin\,\theta_W A_\mu + cos\,\theta_W Z_\mu$, $W_\mu^1 = (W_\mu^+ + W_\mu^-)/\sqrt{2}$ and $W_\mu^2 = i(W_\mu^+ - W_\mu^-)/\sqrt{2}$, in order to get the physical gauge bosons A_μ, Z_μ, W_μ^+ and W_μ^-. With θ_W we denote the mixing angle. The corresponding gaugino mixtures are the so-called photino, zino and winos. The field strength tensor $F_{\mu\nu}^{(\alpha)\,a}$ reads

$$F_{\mu\nu}^{(\alpha)\,a} = \partial_\mu A_\nu^{(\alpha)\,a} - \partial_\nu A_\mu^{(\alpha)\,a} - g_\alpha f^{(\alpha)\,abc}A_\mu^{(\alpha)\,b}A_\nu^{(\alpha)\,c}\,, \tag{2.10}$$

so for the three gauge groups we get

$$\begin{aligned}
F_{\mu\nu}^{(1)} &= \partial_\mu B_\nu - \partial_\nu B_\mu\,,\\
F_{\mu\nu}^{(2)\,a} &= \partial_\mu W_\nu^a - \partial_\nu W_\mu^a - g_2\epsilon^{abc}W_\mu^b W_\nu^c\,,\\
F_{\mu\nu}^{(3)\,a} &= \partial_\mu g_\nu^a - \partial_\nu g_\mu^a - g_3 f^{abc}g_\mu^b g_\nu^c\,.
\end{aligned} \tag{2.11}$$

As already mentioned, in Table 2.2 are presented the matter fields of the MSSM, namely

$$\text{leptons}: \begin{bmatrix} \nu_L^I = (\nu_{e^-}\,,\nu_{\mu^-}\,,\nu_{\tau^-}) \\ e_L^{-\,I} = (e_L^-\,,\mu_L^-\,,\tau_L^-) \\ e_R^{-\,c\,I} = (e_R^{-\,c},\mu_R^{-\,c},\tau_R^{-\,c}) \end{bmatrix}, \quad \text{sleptons}: \begin{bmatrix} \widetilde{\nu}_L^I = (\widetilde{\nu}_{e^-}\,,\widetilde{\nu}_{\mu^-}\,,\widetilde{\nu}_{\tau^-}) \\ \widetilde{e}_L^{-\,I} = (\widetilde{e}_L^-\,,\widetilde{\mu}_L^-\,,\widetilde{\tau}_L^-) \\ \widetilde{e}_R^{-\,*\,I} = (\widetilde{e}_R^{-\,*},\widetilde{\mu}_R^{-\,*},\widetilde{\tau}_R^{-\,*}) \end{bmatrix}, \tag{2.12}$$

$$\text{quarks}: \begin{bmatrix} u_L^I = (u_L\,,c_L\,,t_L) \\ u_R^{c\,I} = (u_R^c\,,c_R^c\,,t_R^c) \\ d_L^I = (d_L\,,s_L\,,b_L) \\ d_R^{c\,I} = (d_R^c\,,s_R^c\,,b_R^c) \end{bmatrix} \quad \text{and} \quad \text{squarks}: \begin{bmatrix} \widetilde{u}_L^I = (\widetilde{u}_L\,,\widetilde{c}_L\,,\widetilde{t}_L) \\ \widetilde{u}_R^{*\,I} = (\widetilde{u}_R^*\,,\widetilde{c}_R^*\,,\widetilde{t}_R^*) \\ \widetilde{d}_L^I = (\widetilde{d}_L\,,\widetilde{s}_L\,,\widetilde{b}_L) \\ \widetilde{d}_R^{*\,I} = (\widetilde{d}_R^*\,,\widetilde{s}_R^*\,,\widetilde{b}_R^*) \end{bmatrix}. \tag{2.13}$$

In the forth column the weak hypercharge Y is given by $Y = 2(Q_{\text{EM}} - T_3)$, where Q_{EM} is the

Table 2.2: Matter fields of the MSSM and the corresponding quantum numbers for the three gauge groups. The family index I refers to one out of three generations of leptons, sleptons, quarks and squarks for $I = 1, 2, 3$ respectively.

Name	Bosons ϕ^i	Fermions χ^i_L	$(SU(3)_c, SU(2)_L, U(1)_Y)$
Sleptons - leptons	$\widetilde{L}^I = \begin{pmatrix} \widetilde{\nu}^I_L \\ \widetilde{e}^{-\,I}_L \end{pmatrix}$	$L^I = \begin{pmatrix} \nu^I_L \\ e^{-\,I}_L \end{pmatrix}$	$(\mathbf{1}, \mathbf{2}, -1)$
	$\widetilde{E}^{*I} = \widetilde{e}^{-\,*\,I}_R$	$E^{c\,I} = e^{-\,c\,I}_R$	$(\mathbf{1}, \mathbf{1}, 2)$
Squarks - quarks	$\widetilde{Q}^I = \begin{pmatrix} \widetilde{u}^I_L \\ \widetilde{d}^I_L \end{pmatrix}$	$Q^I = \begin{pmatrix} u^I_L \\ d^I_L \end{pmatrix}$	$(\mathbf{3}, \mathbf{2}, 1/3)$
	$\widetilde{U}^{*I} = \widetilde{u}^{*I}_R$	$U^{c\,I} = u^{cI}_R$	$(\overline{\mathbf{3}}, \mathbf{1}, -4/3)$
	$\widetilde{D}^{*I} = \widetilde{d}^{*I}_R$	$D^{c\,I} = d^{cI}_R$	$(\overline{\mathbf{3}}, \mathbf{1}, 2/3)$
Higgs - higgsinos	$H_d = \begin{pmatrix} H^0_d \\ H^-_d \end{pmatrix}$	$\widetilde{H}_d = \begin{pmatrix} \widetilde{H}^0_d \\ \widetilde{H}^-_d \end{pmatrix}$	$(\mathbf{1}, \mathbf{2}, -1)$
	$H_u = \begin{pmatrix} H^+_u \\ H^0_u \end{pmatrix}$	$\widetilde{H}_u = \begin{pmatrix} \widetilde{H}^+_u \\ \widetilde{H}^0_u \end{pmatrix}$	$(\mathbf{1}, \mathbf{2}, 1)$

electric charge and T_3 is the third component of the weak isospin, being $\pm 1/2$ for doublets and 0 for $SU(2)_L$ singlets. The Higgs part of the MSSM is slightly complicated in comparison with the one of the SM by the fact that there are two complex Higgs doublets H_d and H_u instead of one in the SM. The corresponding fermionic superpartners are also two complex doublets called Higgsinos. The MSSM is specified by the superpotential

$$W = y_u^{IJ}\, \widetilde{U}^{*\,I}\, \widetilde{Q}^J \cdot H_u - y_d^{IJ} \widetilde{D}^{*\,I}\, \widetilde{Q}^J \cdot H_d - y_e^{IJ}\, \widetilde{E}^{*\,I}\, \widetilde{L}^J \cdot H_d + \mu H_u \cdot H_d \,, \tag{2.14}$$

where the antisymmetric symbol $\epsilon^{\alpha\beta}$ (see (A.3)) is used in order to tie up the indices of the $SU(2)_L$ structure. The $\mu-$term in Eq. (2.14) is the SUSY verison of the Higgs boson mass introduced in Eq. (2.1). Since the heaviest fermions in the SM are the top quark, the bottom quark and the tau, the Yukawa couplings y^{IJ} can be approximated as

$$y_u^{IJ} \simeq \begin{pmatrix} 0 & 0 & 0 \\ 0 & 0 & 0 \\ 0 & 0 & y_t \end{pmatrix} , \quad y_d^{IJ} \simeq \begin{pmatrix} 0 & 0 & 0 \\ 0 & 0 & 0 \\ 0 & 0 & y_b \end{pmatrix} , \quad y_e^{IJ} \simeq \begin{pmatrix} 0 & 0 & 0 \\ 0 & 0 & 0 \\ 0 & 0 & y_\tau \end{pmatrix} . \tag{2.15}$$

In the calculation of the thermal gravitino production in Sec. 4 we will consider only the top quark contribution as first done in [36].

The idea [286] that the three gauge couplings should unify at a common high energy scale does not, in fact, prove to be the case in the SM, but it works very convincingly in the MSSM [287–291]. The evolution of the gauge couplings is determined by the gauge and matter content of the MSSM that has been already analyzed. The 1−loop renormalization

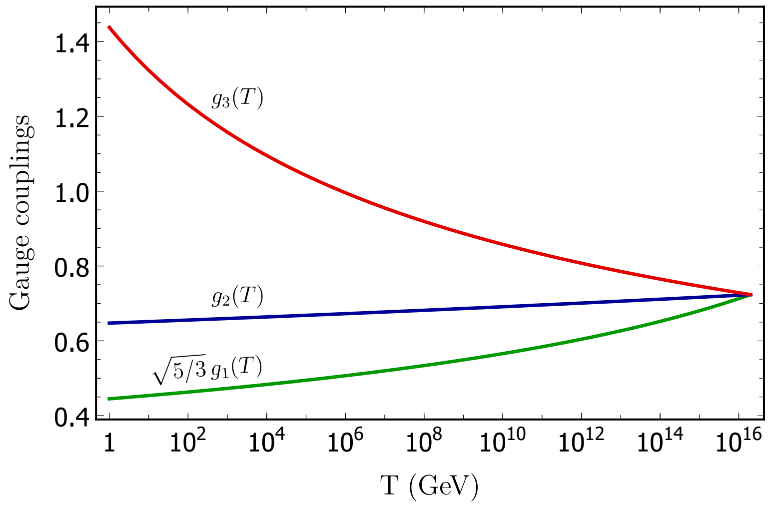

Figure 2.2: Gauge coupling unification in the MSSM at the scale $M_{\rm GUT} \simeq 2 \times 10^{16}$ GeV.

group equations (RGE) for the MSSM gauge couplings $g_{\tilde{1}} = \sqrt{5/3}\, g_1$, g_2 and g_3 are[1]

$$\frac{\mathrm{d}}{\mathrm{d}t} g_\alpha = \frac{1}{16\pi^2} b_\alpha g_\alpha^3, \qquad (b_1, b_2, b_3) = (33/5, 1, -3)\,, \tag{2.16}$$

where t is the logarithm of the energy scale and b_α are coefficients related to the particle spectrum. In the SM the coefficients $(b_1, b_2, b_3) = (41/10, -19/6, -7)$ are smaller, because of the less particles in the loops, so the unification at some energy scale is not achieved. Solving Eq. (2.16) we obtain

$$g_\alpha^2(T) = \frac{g_\alpha^2(M_{\rm GUT})}{1 - \frac{b_\alpha}{8\pi^2} g_\alpha^2(M_{\rm GUT}) \ln(T/M_{\rm GUT})}\,, \tag{2.17}$$

where the grand unification scale, $M_{\rm GUT} \simeq 2 \times 10^{16}$ GeV is defined at the point where the normalized hypercharge coupling $g_{\tilde{1}} = \sqrt{5/3}\, g_1$, the weak coupling g_2 and the strong coupling g_3 meet, having the common value $g_{\tilde{1},2,3}(M_{\rm GUT}) = \sqrt{\pi/6}$. In Fig. 2.2 we present the running of the gauge couplings from low energies ~ 1 GeV till the $M_{\rm GUT}$.

For future use we will also give the running of the gaugino masses. The 1−loop RGE for the three gaugino masses $m_{\lambda^{(\alpha)}} = \{M_1, M_2, M_3\}$ in the MSSM are

$$\frac{\mathrm{d}}{\mathrm{d}t} m_{\lambda^{(\alpha)}} = \frac{1}{8\pi^2} b_\alpha g_\alpha^2 m_{\lambda^{(\alpha)}}, \qquad (b_1, b_2, b_3) = (33/5, 1, -3)\,. \tag{2.18}$$

It follows that the ratios $m^2_{\lambda^{(\alpha)}}/g^2_\alpha$ are RG scale independent (up to small two-loop corrections). A popular but not imperative assumption is that the gaugino masses also unify at the scale $M_{\rm GUT}$, with a value called $m_{1/2}$, thus

$$m_{\lambda^{(\alpha)}}(T) = \left(\frac{g_\alpha(T)}{g_\alpha(M_{\rm GUT})}\right)^2 m_{1/2}\,. \tag{2.19}$$

In Fig. 2.3 we present the gaugino masses for $m_{1/2} = 750$ GeV (left) and $m_{1/2} = 4$ TeV (right). In both sides of this figure, the solid lines correspond to a universal gaugino mass unification at the scale $M_{\rm GUT} \simeq 2 \times 10^{16}$ GeV, while the dashed ones coincide with a non-universal scenario assuming that $M_1/2 = M_2/2 = M_3 = m_{1/2}$ at $M_{\rm GUT}$.

[1] In Eq. (2.16)-(2.19) with $\alpha = 1$ we invoke the normalized hypercharge coupling $g_{\tilde{1}} = \sqrt{5/3}\, g_1$.

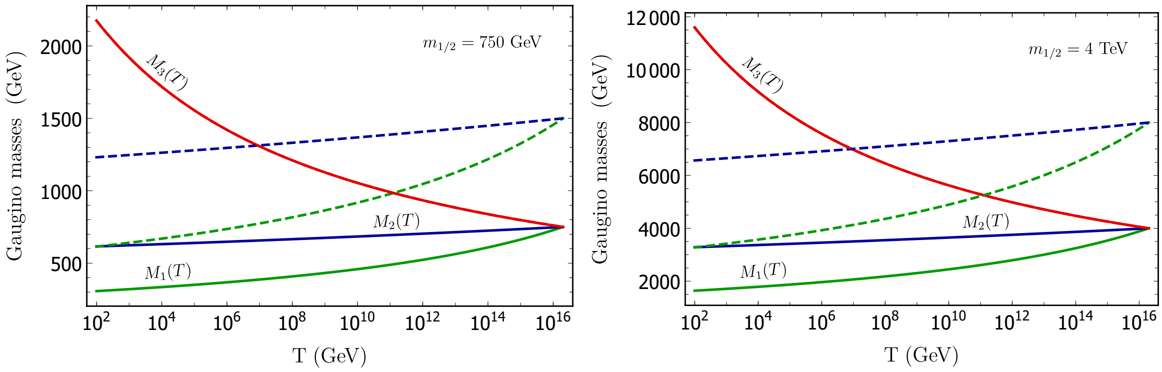

Figure 2.3: The three gaugino masses of the MSSM for $m_{1/2} = 750$ GeV (left) and $m_{1/2} = 4$ TeV (right), assuming a universal gaugino mass unification at the scale $M_{\text{GUT}} \simeq 2 \times 10^{16}$ GeV (solid lines) and a non-universal scenario with $M_1/2 = M_2/2 = M_3 = m_{1/2}$ (dashed lines).

2.3 The gravitino field

In this section we begin to assemble the ingredients of SUGRA by studying the free spin$-3/2$ field, the so-called Rarita-Schwinger field or gravitino.

The SUGRA model contains the graviton field $e_\mu{}^m$ (or vielbein)[2] and its superpartner the gravitino ψ_μ. Since the gravitino is the superpartner of the graviton it is massless in the limit of unbroken SUSY and can be written in terms of a Majorana vector spinor as

$$\psi_\mu = \begin{pmatrix} -i\,\psi_{\mu\,\alpha} \\ i\,\overline{\psi}_\mu{}^{\dot{\alpha}} \end{pmatrix} . \tag{2.20}$$

The Lagrangian of the SUGRA model [292] incorporates the usual Einstein-Hilbert term

$$e^{-1}\mathcal{L}_{EH} = -\frac{M_{\text{P}}^2}{2}\mathcal{R}\,, \tag{2.21}$$

where $\mathcal{R}$ is the Ricci scalar and $e \coloneqq \det e_\mu{}^m$, and the free gravitino Lagrangian which is given by[3]

$$e^{-1}\mathcal{L}_{3/2}^{\text{free}} = \epsilon^{\mu\nu\rho\sigma}\overline{\psi}_{L\mu}\gamma_\nu\partial_\rho\psi_{L\sigma} - \frac{1}{4}m_{3/2}\overline{\psi}_{R\mu}[\gamma^\mu,\gamma^\nu]\psi_{L\nu}\,. \tag{2.22}$$

In the above Lagrangian $\epsilon^{\mu\nu\rho\sigma}$ is the totally anti-symmetric tensor and $m_{3/2}$ is the gravitino mass. The interaction part of the gravitino Lagrangian will be discussed separately in Sec. 2.4.

In the SM, the Higgs mechanism is essential to explain the generation of masses for the particle spectrum. An analogous super-Higgs mechanism [293, 294] is crucial in order to achieve the spontaneous symmetry breaking of SUGRA. The supersymmetric goldstone boson is now a spin-1/2 fermion called goldstino, and it is "eaten" by the gravitino which acquires thus its $\pm 1/2$ helicity components. The gravitino mass arises when the superpotential W and the Kähler potential K get their VEVs $\langle W_h \rangle$ and $\langle K_h \rangle$ respectively. Here the subscript h denotes the hidden sector, *i.e.* the part that is independent of the observable fields. The relevant term which is responsible for the generation of the gravitino mass in the full SUGRA

[2] Here m is the flat spacetime index and μ is the Einstein index.

[3] The covariant derivative acting on the gravitino field can be written as $\mathcal{D}_\mu\psi_\nu = \partial_\mu\psi_\nu$, as we have dropped the spin-connection contributions in the covariant derivatives of all the fermion fields. This assumption matches with the choice of a flat spacetime.

Lagrangian is $-\frac{1}{4M_{\rm P}^2}e^{K/2M_{\rm P}^2}W^*\overline{\psi}_{R\mu}[\gamma^\mu,\gamma^\nu]\psi_{L\nu}$, thus the gravitino mass is given by

$$m_{3/2}=\frac{1}{M_{\rm P}^2}e^{\langle K_h\rangle/2M_{\rm P}^2}\,\langle W_h^*\rangle\,. \tag{2.23}$$

Avoiding total derivatives the free gravitino Lagrangian (2.22) can be rewritten as

$$e^{-1}\mathcal{L}_{3/2}^{\rm free}=-\frac{1}{2}\epsilon^{\mu\nu\rho\sigma}\overline{\psi}_\mu\gamma_5\gamma_\nu\partial_\rho\psi_\sigma-\frac{1}{4}m_{3/2}\overline{\psi}_\mu[\gamma^\mu,\gamma^\nu]\psi_\nu\,, \tag{2.24}$$

which obeys the equations of motion

$$\frac{\partial\mathcal{L}_{3/2}}{\partial\overline{\psi}_\mu}-\partial_\nu\frac{\partial\mathcal{L}_{3/2}}{\partial\left(\partial_\nu\overline{\psi}_\mu\right)}=-\frac{1}{2}\epsilon^{\mu\nu\rho\sigma}\gamma_5\gamma_\nu\partial_\rho\psi_\sigma-\frac{1}{4}m_{3/2}[\gamma^\mu,\gamma^\nu]\psi_\nu=0\,, \tag{2.25}$$

that finally lead to the well-known Rarita-Schwinger equations [295] for the massive gravitino field

$$\gamma^\mu\psi_\mu=0\qquad\text{and}\qquad\left(i\partial\!\!\!/-m_{3/2}\right)\psi_\mu=0\,. \tag{2.26}$$

These equations additionally imply the constraint $\partial^\mu\psi_\mu=0$. The gravitino production calculated in Chapter 4 involves squared matrix elements which are summed over all four gravitino helicity states $s=\pm3/2,\pm1/2$. The polarization tensor for a gravitino with mass $m_{3/2}$ and momentum P can be accordingly written as

$$\begin{aligned}\Pi_{\mu\nu}(P)&=\sum_{s=\pm3/2,\pm1/2}\psi_\mu^{(s)}\,\overline{\psi}_\nu^{(s)}\\&=-(P\!\!\!/+m_{3/2})\left(g_{\mu\nu}-\frac{P_\mu P_\nu}{m_{3/2}^2}\right)-\frac{1}{3}\left(\gamma^\mu+\frac{P_\mu}{m_{3/2}}\right)(P\!\!\!/-m_{3/2})\left(\gamma^\nu+\frac{P_\nu}{m_{3/2}}\right)\,.\end{aligned} \tag{2.27}$$

We are interested in the production of gravitinos at energies much larger than the gravitino mass. In this case the polarization tensor (2.27) splits into two parts [31]

$$\Pi_{\mu\nu}(P)\simeq-P\!\!\!/g_{\mu\nu}+\frac{2}{3}P\!\!\!/\frac{P_\mu P_\nu}{m_{3/2}^2}\,. \tag{2.28}$$

The first term in (2.28) corresponds to the sum over the helicity $\pm3/2$ states whereas the second one to the sum over $\pm1/2$ helicity states, *i.e.* is the goldstino part of the gravitino. In [36] the polarization tensor for the case of a massless gravitino is presented to have the form

$$\Pi_{\mu\nu}^{3/2}(P)=-\frac{1}{2}\gamma_\mu P\!\!\!/\gamma_\nu-P\!\!\!/g_{\mu\nu}\,, \tag{2.29}$$

in which only the sum over the two physical transverse polarizations has been done.

2.4 Gravitino Interactions

So far we have considered the theory of SUSY and how the gravitino emerges in the framework of SUGRA. Let us now discuss about the gravitino interactions with the rest particle spectrum.

Many of the interaction terms concerning the gravitino in the full SUGRA Lagrangian [292] are irrelevant for our analysis, since the considered centre of mass energy $\sqrt{s}$ is much lower than the Planck scale $M_{\rm P}$ and so some operators are suppressed at least by a factor $\sim 1/M_{\rm P}$.

Also, in our analysis in Chapter 4, gravitinos appear only as external lines. Thus, by invoking (2.26), terms which contain $\gamma^\mu\psi_\mu$ or $\overline{\psi}_\mu\gamma^\mu$ can be ignored. Therefore, the relevant interaction Lagrangian is

$$\begin{aligned}\mathcal{L}^{(\alpha)}_{3/2,\,\mathrm{int}} &= -\frac{i}{\sqrt{2}M_{\mathrm{P}}}\overline{\psi}_\mu S^\mu_{\mathrm{MSSM}} + \mathrm{h.c.} \\ &= -\frac{i}{\sqrt{2}M_{\mathrm{P}}}\left[\mathcal{D}^{(\alpha)}_\mu\phi^{*i}\overline{\psi}_\nu\gamma^\mu\gamma^\nu\chi^i_L - \mathcal{D}^{(\alpha)}_\mu\phi^i\overline{\chi}^i_L\gamma^\nu\gamma^\mu\psi_\nu\right] - \frac{i}{8M_{\mathrm{P}}}\overline{\psi}_\mu[\gamma^\rho,\gamma^\sigma]\gamma^\mu\lambda^{(\alpha)\,a}F^{(\alpha)\,a}_{\rho\sigma}\,,\end{aligned} \tag{2.30}$$

where in the first line S^μ_{MSSM} denotes the contribution from MSSM to the supercurrent. Before We will present in more detail the relevant Lagrangians coming from (2.30), for the $SU(3)_c$ gauge group. These Lagrangians along with the corresponding vertices are listed below.

- $$\mathcal{L}_{gg\tilde{g}\psi} = -\frac{i}{8M_{\mathrm{P}}}\left(2\partial_\rho g^a_\sigma - g_3 f^{abc}g^b_\rho g^c_\sigma\right)\left(\overline{\psi}_\mu[\gamma^\rho,\gamma^\sigma]\gamma^\mu\tilde{g}^a + \overline{\tilde{g}^a}\gamma^\mu[\gamma^\rho,\gamma^\sigma]\psi_\mu\right)\,. \tag{2.31}$$

This Lagrangian describes the three-point interactions between $g-\tilde{g}-\psi$ and the four-point interaction $g-g-\tilde{g}-\psi$, with vertex rules[4]

$$\begin{aligned}\triangleright\ \mathrm{Vertex}(g^b_\rho(P)\,\overrightarrow{\tilde{g}^a\,\psi_\mu}) &= -\frac{i}{4M_{\mathrm{P}}}\delta_{ab}[\not{P},\gamma^\rho]\gamma^\mu\,, \\ \triangleright\ \mathrm{Vertex}(g^b_\rho(P)\,\overleftarrow{\tilde{g}^a\,\psi_\mu}) &= -\frac{i}{4M_{\mathrm{P}}}\delta_{ab}\gamma^\mu[\not{P},\gamma^\rho]\,,\end{aligned} \tag{2.32}$$

and

$$\begin{aligned}\triangleright\ \mathrm{Vertex}(g^b_\nu\,g^c_\rho\,\overrightarrow{\tilde{g}^a\,\psi_\mu}) &= -\frac{g_3}{4M_{\mathrm{P}}}f^{abc}[\gamma^\nu,\gamma^\rho]\gamma^\mu\,, \\ \triangleright\ \mathrm{Vertex}(g^b_\nu\,g^c_\rho\,\overleftarrow{\tilde{g}^a\,\psi_\mu}) &= -\frac{g_3}{4M_{\mathrm{P}}}f^{abc}\gamma^\mu[\gamma^\nu,\gamma^\rho]\,.\end{aligned} \tag{2.33}$$

- $$\mathcal{L}_{\tilde{q}q\psi} = \frac{1}{\sqrt{2}M_{\mathrm{P}}}\delta_{rt}\left[\overline{q}^t\gamma^\nu\gamma^\mu\alpha^{i*}_{RL}\psi_\nu(i\partial_\mu\tilde{q}^r_i) - \overline{\psi}_\nu\gamma^\mu\gamma^\nu\alpha^i_{LR}q^t(i\partial_\mu\tilde{q}^{*r}_i)\right]\,. \tag{2.34}$$

This Lagrangian describes the three-point interaction $\tilde{q}-q-\psi$ with vertex rules

$$\begin{aligned}\triangleright\ \mathrm{Vertex}(\tilde{q}^r_i(P)\,\overrightarrow{q^t\,\psi_\mu}) &= -\frac{i}{\sqrt{2}M_{\mathrm{P}}}\delta_{rt}\not{P}\gamma^\nu\alpha^i_{LR}\,, \\ \triangleright\ \mathrm{Vertex}(\tilde{q}^r_i(P)\,\overleftarrow{q^t\,\psi_\mu}) &= \frac{i}{\sqrt{2}M_{\mathrm{P}}}\delta_{rt}\alpha^{i*}_{RL}\gamma^\nu\not{P}\,.\end{aligned} \tag{2.35}$$

- $$\mathcal{L}_{g\tilde{q}q\psi} = -\frac{1}{\sqrt{2}M_{\mathrm{P}}}\delta_{rt}g_3\left[g^a_\mu T_{a,\,rs}\overline{q}^t\gamma^\nu\gamma^\mu\alpha^{i*}_{RL}\psi_\nu\tilde{q}^s_i + g^a_\mu T_{a,\,sr}\overline{\psi}_\nu\gamma^\mu\gamma^\nu\alpha^i_{LR}q^t\tilde{q}^{*s}_i\right]\,. \tag{2.36}$$

This Lagrangian describes the four-point interaction $g-\tilde{q}-q-\psi$ with vertex rules

$$\begin{aligned}\triangleright\ \mathrm{Vertex}(g^a_\mu\,\tilde{q}^s_i\,\overrightarrow{q^t\,\psi_\nu}) &= -\frac{ig_3}{\sqrt{2}M_{\mathrm{P}}}T_{a,\,rs}\delta_{rt}\gamma^\nu\gamma^\mu\alpha^{i*}_{RL}\,, \\ \triangleright\ \mathrm{Vertex}(g^a_\mu\,\tilde{q}^s_i\,\overleftarrow{q^t\,\psi_\nu}) &= -\frac{ig_3}{\sqrt{2}M_{\mathrm{P}}}T_{a,\,sr}\delta_{rt}\gamma^\mu\gamma^\nu\alpha^i_{LR}\,.\end{aligned} \tag{2.37}$$

[4]The arrow over the gluino or squark and gravitino indicates the fermion flow, *i.e.* an arbitrary orientation of each fermion line. See [296].

In the expressions above the momentum P flows into the vertex. We have also used the shortcuts

$$\begin{aligned} \alpha^i_{RL} &= R_{iL}P_R - R_{iR}P_L \,, \\ \alpha^i_{LR} &= R_{iL}P_L - R_{iR}P_R \,, \end{aligned} \tag{2.38}$$

and we defined the conjugated expressions as

$$\begin{aligned} \alpha^{i*}_{RL} &\equiv R^*_{iL}P_R - R^*_{iR}P_L \,, \\ \alpha^{i*}_{LR} &\equiv R^*_{iL}P_L - R^*_{iR}P_R \,, \end{aligned} \tag{2.39}$$

where P_L, P_R are the left and right projectors and the R_{iL}, R_{iR} can be found in [297]. The Lagrangians of the relevant gauge interactions along with the Feynman rules can be found in Appendix B of [37].

2.5 Effective theory for light gravitinos

As we have mentioned in spontaneously broken SUSY models, the massless gravitino acquires its mass by "eating" the goldstino DOF. Thus the gravitino, apart from the mass, receives two additional DOF, the helicity $\pm 1/2$ components. This fact suggests that the dynamics of the goldstino (χ) can very well approximate the helicity $\pm 1/2$ components of the gravitino (ψ_μ) in the limit of vanishing gravitino mass $m_{3/2}$ [298]. According to the $m_{3/2} \to 0$ limit in the polarization tensor (2.28), the term $\frac{2}{3}\not{P}\frac{P_\mu P_\nu}{m^2_{3/2}}$ dominates at energies greater than the gravitino mass. Since,

$$\sum_{s=\pm 1/2} \chi^{(s)}\overline{\chi}^{(s)} = \not{P} + m_{3/2} \simeq \not{P} \,, \tag{2.40}$$

we can effectively replace

$$\psi_\mu \to \sqrt{\frac{2}{3}}\frac{\partial_\mu \chi}{m_{3/2}} \tag{2.41}$$

in this high energy regime. Therefore after an integration by parts

$$\mathcal{L}^{(\alpha)}_{3/2,\,\mathrm{int}} = -\frac{i}{\sqrt{2}M_{\mathrm{P}}}\overline{\psi}_\mu S^\mu_{\mathrm{MSSM}} + \mathrm{h.c.} \to \mathcal{L}^{(\alpha)}_{1/2,\,\mathrm{eff}} = \frac{i}{\sqrt{3}m_{3/2}M_{\mathrm{P}}}\overline{\chi}\partial_\mu S^\mu_{\mathrm{MSSM}} + \mathrm{h.c.}\,. \tag{2.42}$$

This expression can be simplified further in order to obtain an effective interaction Lagrangian in nonderivative form. In all orders in perturbation theory and for a single external goldstino the nonderivative and the derivative forms are equivalent [299]. The nonderivative Lagrangian reads

$$\begin{aligned} \mathcal{L}^{(\alpha)}_{1/2,\,\mathrm{nonder}} &= i\,\frac{m^2_{\phi^i} - m^2_{\chi^i}}{\sqrt{3}M_{\mathrm{P}}m_{3/2}}\left(\overline{\chi}\chi^i_L\phi^{*i} - \overline{\chi}^i_L\chi\phi^i\right) - \frac{m_{\lambda^{(\alpha)}}}{4\sqrt{6}M_{\mathrm{P}}m_{3/2}}\overline{\chi}[\gamma^\mu,\gamma^\nu]\lambda^{(\alpha)\,a}F^{(\alpha)\,a}_{\mu\nu} \\ &- i\,\frac{g_\alpha m_{\lambda^{(\alpha)}}}{\sqrt{6}M_{\mathrm{P}}m_{3/2}}\phi^{*i}T^{(\alpha)}_{a,\,ij}\phi^j\overline{\chi}\gamma_5\lambda^{(\alpha)\,a}\,. \end{aligned} \tag{2.43}$$

In this, $m^2_{\phi^i}$ and $m^2_{\chi^i}$ are the squared masses of the corresponding matter fields and $m_{\lambda^{(\alpha)}}$ are the gaugino masses, as referred previously. The complete set of the Feynman rules is given in Appendix B of [37].

Chapter 3

Finite temperature effects

In this chapter we summarize some well known results from thermal field theory (TFT), *i.e.* the quantum field theory at finite temperature, that are relevant for our computation of the gravitino abundance. TFT can be successfully described using two different formalisms, the imaginary-time formalism (ITF) (or Matsubara formalism) and the real-time formalism (RTF). In ITF the dynamical time t is traded in for the temperature T, as $t = -i\tau$ with periodicity $1/T$. In contrast, the RTF formalism of TFT contains both time and temperature. Which formalism one chooses to perform computations in thermal equilibrium is a matter of personal taste. For nonequilibrium phenomena only the RTF can be used, as the temperature which plays a crucial role in the ITF is not needed explicitly.

In this thesis we have adopted the RTF, but we have also checked the validity of our results applying the ITF. In RTF the temperature dependent propagators read

$$\begin{aligned} \text{scalar}: &\quad \Delta_S(K) = \frac{i}{K^2} + \Gamma_B(K) \\ \text{fermion}: &\quad S_F(K) = \frac{i\,\not{K}}{K^2} - \not{K}\,\Gamma_F(K) \\ \text{vector}-\text{boson}: &\quad \Delta^{ab}_{\mu\nu}(K) = \delta^{ab} g_{\mu\nu}\left(\frac{-i}{K^2} - \Gamma_B(K)\right) \\ \text{ghost}: &\quad G^{ab}(K) = \delta^{ab}\Delta_S(K), \end{aligned} \tag{3.1}$$

where we have defined

$$\Gamma_{F,B}(K) \equiv 2\pi\,\delta(K^2)\,n_{F,B}(K) \tag{3.2}$$

and have assumed massless particles, at the Feynman $\xi = 1$ gauge. In addition, the fermion and boson particle densities are defined as

$$n_{F,B}(K) = (e^{|K\cdot u|/T} \pm 1)^{-1}\,. \tag{3.3}$$

At the plasma rest frame $u^\mu = (1, 0, 0, 0)$, since $K\cdot u = k_0$, we get

$$n_{F,B}(K) = (e^{|k_0|/T} \pm 1)^{-1}\,. \tag{3.4}$$

This will be used in Eqs. (B.1)–(B.5) of Appendix B, integrated over $\int \mathrm{d}k_0\,\delta(k_0 \pm k)$ and after this $n_{F,B}(K)$ will become $n_{F,B}(k)$.

It is interesting to note that although a ghost behaves like a Grassmann variable, its temperature part follows the boson statistics, since its contribution has to be added up to vector-bosons loops, in order to restore unitarity.

In the rest of this chapter we will use these thermalized propagators in order to compute the thermally corrected vector-boson and fermion selfenergies. The presented results are usually addressed to the $SU(3)_c$ gauge group, but it is easy to expand in the rest gauge groups.

3.1 Vector-boson selfenergy

The thermalized vector-boson selfenergy contains three different contributions arising from scalars, fermions and vector-bosons (+ ghosts). In the following we will analyze these one by one.

3.1.1 Scalar contribution

There are two Feynman graphs, plotted in Fig. (3.1), to calculate in order to evaluate the scalar (squark) contribution to vector-boson vacuum polarization. The three vertices appearing in the graphs are $-ig_3 T_{a,\,st}(2K-P)_\mu$ and $-ig_3 T_{a,\,ts}(2K-P)_\nu$ for the first graph and

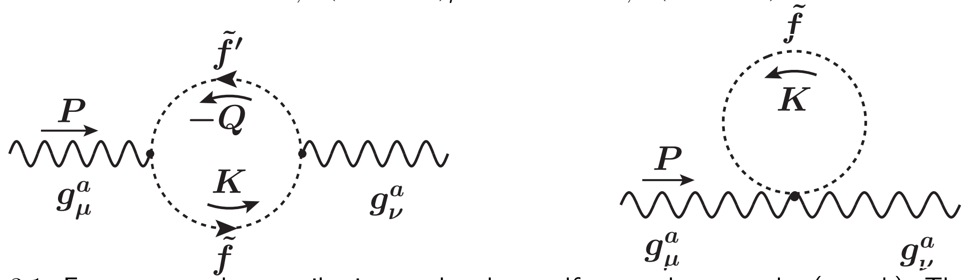

Figure 3.1: Feynman graphs contributing to the gluon selfenergy due to scalar (squark). The color index a is fixed and the momentum Q is defined as $Q = P - K$.

$ig_3^2\left((T_a{\cdot}T_b)_{ss} + (T_a{\cdot}T_b)_{ss}\right) g_{\mu\nu}$ for the second graph, with $a = b$ fixed for a certain gluon. One can calculate the contribution of the first graph(a) as[1]

$$i\Pi^{S(a)}_{\mu\nu}(P) = (-i)^2 g_3^2 N_S |T_{a,\,ss}|^2 \int \frac{\mathrm{d}^4K}{(2\pi)^4}(2K-P)_\mu(2K-P)_\nu \Delta_S(K)\Delta_S(K-P)\,. \tag{3.5}$$

The second graph(b) reads

$$i\,\Pi^{S(b)}_{\mu\nu}(P) = 2ig_3^2 N_S |T_{a,\,ss}|^2 \int \frac{\mathrm{d}^4K}{(2\pi)^4} g_{\mu\nu}\Delta_S(K)\,. \tag{3.6}$$

Using the relations above and the fact that $|T_{a,\,ss}|^2 = 1/2$, we obtain

$$\begin{aligned}\mathrm{Re}[\Pi^S_{\mu\nu}(P)] = -g_3^2 N_S \int \frac{\mathrm{d}^4K}{(2\pi)^4}\Bigg\{ &\frac{1}{2}(2K-P)_\mu(2K-P)_\nu\left[\frac{\Gamma_B(K)}{(K-P)^2} + \frac{\Gamma_B(K-P)}{K^2}\right] \\ &- g_{\mu\nu}(K-P)^2\frac{\Gamma_B(K)}{(K-P)^2}\Bigg\}\,. \end{aligned} \tag{3.7}$$

Now we perform the momentum shift $K \to P - K$ at the second term above. This yields

$$\mathrm{Re}[\Pi^S_{\mu\nu}(P)] = -g_3^2 N_S \int \frac{\mathrm{d}^4K}{(2\pi)^3} I^S_{\mu\nu}\frac{\delta(K^2)}{(K-P)^2} n_B(K)\,, \tag{3.8}$$

with

$$I^S_{\mu\nu} = (2K-P)_\mu(2K-P)_\nu - (K-P)^2 g_{\mu\nu}. \tag{3.9}$$

[1]Here N_s is the number of the scalars in the loop.

Using also that at the plasma rest frame $u^\mu = (1,0,0,0)$ and the fact that scalars in the loop are massless ($K^2 = 0$) we obtain

$$\begin{aligned} g^{\mu\nu} I^S_{\mu\nu} &= 4K{\cdot}P - 3P^2\,, && (3.10)\\ u^\mu u^\nu I^S_{\mu\nu} &= [(2K-P){\cdot}U]^2 - U^2(K-P)^2 \\ &= 4k_0^2 - 4k_0 p_0 + p_0^2 - P^2 + 2K{\cdot}P\,. && (3.11) \end{aligned}$$

Follwing the notation of [36] we define

$$\begin{aligned} g^{\mu\nu}\,\mathrm{Re}(\Pi^S_{\mu\nu}) &= g_3^2 N_S G_S\,,\\ u^\mu u^\nu\,\mathrm{Re}(\Pi^S_{\mu\nu}) &= g_3^2 N_S H_S\,, \end{aligned} \tag{3.12}$$

and using the definitions of basic integrals (B.1)-(B.5) from the Appendix B we have

$$\begin{aligned} G_S &= -4L_5^B(P) + 3P^2\,L_1^B(P)\,,\\ H_S &= -4L_3^B(P) + 4p_0\,L_2^B(P) + (P^2 - p_0^2)\,L_1^B(P) - 2L_5^B(P)\,. \end{aligned} \tag{3.13}$$

Simplifying these equations we finally obtain

$$\begin{aligned} G_S &= \frac{1}{2}\int_0^\infty \frac{\mathrm{d}k}{2\pi^2}\left[4k - \frac{P^2}{4p}L_-(k)\right] n_B(k) \overset{\mathrm{HTL}}{\sim} \frac{T^2}{6}\,,\\ H_S &= \frac{1}{2}\int_0^\infty \frac{\mathrm{d}k}{2\pi^2}\left[2kL + \frac{M(k)}{p} + \frac{p}{4}L_-(k)\right] n_B(k) \overset{\mathrm{HTL}}{\sim} \frac{L+1}{12}T^2\,, \end{aligned} \tag{3.14}$$

where $\overset{\mathrm{HTL}}{\sim}$ denotes the Hard Thermal Loop (HTL) approximation. The functions L, $L_\pm$ and M are defined in Eqs. (B.6), (B.8) and (B.9) of Appendix B, as well as in the Appendix B of [36].

3.1.2 Fermion contribution

The calculation of this part will be used in MSSM for either the quark or gaugino loops. We will calculate the thermal part of a vector selfenergy for the fermion (quark or gluino) loop and then, as before, we can generalize that to $U(1)_Y$, $SU(2)_L$ and $SU(3)_c$ for the SM or the MSSM particle content. The relevant Feynman graph is presented in Fig. 3.2. The vertex

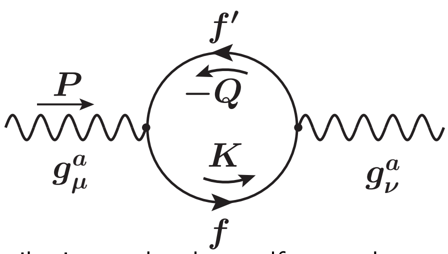

Figure 3.2: Feynman graph contributing to the gluon selfenergy due to the fermion loop. The color index a is fixed and the momentum Q is defined as $Q = P - K$.

rule for vector-boson(g^a_μ)-quark($\bar{q}_s$)-quark(q_t) $= -ig_3 T_{a,\,st}\gamma_\mu$ and for the vectorboson(g^a_μ)-gluino($\bar{\tilde{g}}^b$)-gluino($\tilde{g}^c$) $= -g_3 f_{abc}\gamma_\mu$. Based on these, one can calculate the contribution of the graph in Fig. 3.2 as

$$i\,\Pi^F_{\mu\nu}(P) = -(-i)^2 g_3^2 N_f |T_{a,\,ss}|^2 \int \frac{\mathrm{d}^4K}{(2\pi)^4}\mathrm{Tr}[\gamma_\mu S_F(K-P)\gamma_\nu S_F(K)]\,. \tag{3.15}$$

Using the temperature dependent propagator S_F from (3.1) we obtain

$$\mathrm{Re}[\Pi^F_{\mu\nu}(P)] = -g_3^2 N_f |T_{a,\,ss}|^2 \int \frac{\mathrm{d}^4K}{(2\pi)^4} \mathrm{Tr}\left[\gamma_\mu(\not{K}-\not{P})\gamma_\nu\not{K}\right]\left\{\frac{\Gamma_F(K)}{(K-P)^2}+\frac{\Gamma_F(K-P)}{K^2}\right\}. \tag{3.16}$$

Now we perform the momentum shift $K \to P-K$ at the second term above. This yields

$$\mathrm{Re}[\Pi^f_{\mu\nu}(P)] = -g_3^2\, N_f |T_{a,\,ss}|^2 \int \frac{\mathrm{d}^4K}{(2\pi)^4} \mathrm{Tr}\Big[\gamma_\mu(\not{K}-\not{P})\gamma_\nu\not{K}+\gamma_\mu\not{K}\gamma_\nu(\not{K}-\not{P})\Big]\frac{\Gamma_F(K)}{(K-P)^2}\,.$$

Performing the trace and using the fact that fermions in the loop are massless ($K^2=0$) we get

$$\mathrm{Re}[\Pi^F_{\mu\nu}(P)] = -8g_3^2 N_f\,|T_{a,\,ss}|^2 \int \frac{\mathrm{d}^4K}{(2\pi)^3}\, I^F_{\mu\nu}\,\frac{\delta(K^2)}{(K-P)^2} n_F(K)\,, \tag{3.17}$$

with

$$I^F_{\mu\nu} = K_\mu(K-P)_\nu + K_\nu(K-P)_\mu + K\!\cdot\! P g_{\mu\nu}\,. \tag{3.18}$$

Using also that at the plasma rest frame $u^\mu=(1,0,0,0)$ and (3.18) we get

$$\begin{aligned} g^{\mu\nu} I^F_{\mu\nu} &= 2K\!\cdot\! P\,, \\ u^\mu u^\nu I^F_{\mu\nu} &= 2k_0^2 - k_0 p_0 - \mathbf{p}\!\cdot\!\mathbf{k}\,. \end{aligned} \tag{3.19}$$

Applying the definitions

$$\begin{aligned} g^{\mu\nu}\,\mathrm{Re}\,\Pi^F_{\mu\nu} &\equiv g_3^2 N_f G_F\,, \\ u^\mu u^\nu\,\mathrm{Re}\,\Pi^F_{\mu\nu} &\equiv g_3^2 N_f H_F\,, \end{aligned} \tag{3.20}$$

as well as that $|T_{a,\,ss}|^2 = 1/2$ for fixed color a, one obtains that

$$\begin{aligned} G_F &= -8L_5^F(P)\,, \\ H_F &= -4\Big[2L_3^F(P) - p_0 L_2^F(P) - L_4^F(P)\Big]\,. \end{aligned} \tag{3.21}$$

Eventually using Eqs. (B.1)-(B.5) one gets

$$\begin{aligned} G_F &= \int_0^\infty \frac{\mathrm{d}k}{2\pi^2}\left[4k + \frac{P^2}{2p}L_-(k)\right] n_F(k) \overset{\mathrm{HTL}}{\sim} \frac{T^2}{6}\,, \\ H_F &= \int_0^\infty \frac{\mathrm{d}k}{2\pi^2}\left[2kL + \frac{M(k)}{p}\right] n_F(k) \overset{\mathrm{HTL}}{\sim} \frac{L+1}{12} T^2\,. \end{aligned} \tag{3.22}$$

3.1.3 Vector-boson and ghost contributions

We have three Feynman graphs, plotted in Fig. (3.3), to calculate in order to evaluate the vector-boson contribution to vector-boson vacuum polarization. The graphs involving vector-boson loops must multiplied by a combinatoric factor $1/2$, while the ghost loop is multiplied by -1, due to ghost statistics. On the other hand, as it was noted in (3.1), the ghost thermal propagator follows the boson statistics. These graphs involving trilinear and quartic gauge boson vertices. The trilinear interaction for the vertex $g^a_\mu(P) - g^b_\nu(Q) - g^c_\lambda(R)$, with all the momenta P, Q, R assumed incoming, is

$$\begin{aligned} \mathfrak{TGV}_{\mu\nu\lambda}(P,Q,R) &= -g_3 f_{abc}[g_{\mu\nu}(P-Q)_\lambda + g_{\nu\lambda}(Q-R)_\mu + g_{\lambda\mu}(R-P)_\nu] \\ &\equiv -g_3 f_{abc}\mathfrak{tgv}_{\mu\nu\lambda}(P,Q,R)\,. \end{aligned} \tag{3.23}$$

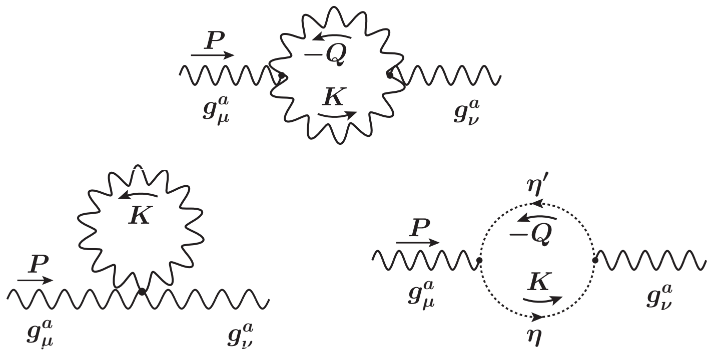

Figure 3.3: Feynman graphs contributing to the gluon selfenergy due to vector-bosons and ghosts. The color index a is fixed and the momentum Q is defined as $Q = P - K$.

The quartic coupling for the vertex $g^a_\mu - g^b_\nu - g^c_\lambda - g^d_\sigma$ does not depend on the momenta

$$\begin{aligned}\mathfrak{FGV}_{\mu\nu\lambda\sigma} \;\; = \;\; & -ig_3^2\,[f_{abe}f_{cde}(g_{\mu\lambda}g_{\nu\sigma} - g_{\mu\sigma}\,g_{\nu\lambda}) \\ & f_{ace}f_{bde}(g_{\mu\nu}\,g_{\lambda\sigma} - g_{\mu\sigma}g_{\nu\lambda}) \\ & f_{ade}f_{cbe}(g_{\mu\lambda}g_{\nu\sigma} - g_{\mu\nu}g_{\lambda\sigma})]\;. \end{aligned} \tag{3.24}$$

The vertex in the ghost graph $g^a_\mu(P) - \eta^b(Q) - \eta^c(R)$, with all the momenta P, Q, R assumed incoming, is

$$ghost_\mu = -g_3 f^{abc} R_\mu\,. \tag{3.25}$$

Using these, one can calculate the contribution of the first graph in Fig. (3.3), as

$$\begin{aligned} i\Pi^{V_1}_{\mu\nu}(P) = -\frac{g_3^2}{2}|f_{abc}|^2 \int \frac{\mathrm{d}^4K}{(2\pi)^4}\mathfrak{tgv}_{\mu\sigma\lambda}(P, K-P, -K)\Delta^{aa}_{\sigma\sigma'}(K-P) \\ \times\, \mathfrak{tgv}^{\lambda'\sigma'}_{\nu}(-P, K, P-K)\Delta^{aa}_{\lambda\lambda'}(K)\,, \end{aligned} \tag{3.26}$$

where the sum $|f_{abc}|^2$, for fixed color a, equals $|f_{abc}|^2 = N_c$. Using the temperature dependent propagator $\Delta^{ab}_{\mu\nu}$ from (3.1) we obtain

$$\begin{aligned} \mathrm{Re}[\Pi^{V_1}_{\mu\nu}(P)] = -\frac{g_3^2}{2}N_c \int \frac{\mathrm{d}^4K}{(2\pi)^4}\mathfrak{tgv}_{\mu\sigma\lambda}(P, K-P, -K)\mathfrak{tgv}^{\lambda\sigma}_{\nu}(-P, K, P-K) \\ \times \left[\frac{\Gamma_B(K)}{(K-P)^2} + \frac{\Gamma_B(K-P)}{K^2}\right]\,. \end{aligned} \tag{3.27}$$

Performing the Lorentz contraction we get

$$\begin{aligned} &\mathfrak{tgv}_{\mu\sigma\lambda}(P, K-P, -K)\mathfrak{tgv}^{\lambda\sigma}_{\nu}(-P, K, P-K) = \\ &= 5(K-P)_\mu K_\nu + 5(K-P)_\nu K_\mu + (5P^2 - 2K{\cdot}P + 2K^2)g_{\mu\nu} - 2P_\mu P_\nu \equiv -I^{V_1}_{\mu\nu}\,, \end{aligned} \tag{3.28}$$

where it is interesting to note that is invariant under the shift $K \to P - K$. Therefore by doing this shift at the second term we get

$$\mathrm{Re}[\Pi^{V_1}_{\mu\nu}(P)] = g_3^2 N_c \int \frac{\mathrm{d}^4K}{(2\pi)^4} I^{V_1}_{\mu\nu}\frac{\Gamma_B(K)}{(K-P)^2}\,. \tag{3.29}$$

Calculating the second and the third diagram of Fig. (3.3) yields, respectively

$$\begin{aligned} I^{V_2}_{\mu\nu} &= 3(P^2 - 2K\cdot P + K^2)g_{\mu\nu}\,, \\ I^{V_3}_{\mu\nu} &= (K-P)_\mu K_\nu + (K-P)_\nu K_\mu\,. \end{aligned} \tag{3.30}$$

In total from the three graphs, and using that $K^2 = 0$ we get

$$\mathrm{Re}[\Pi^V_{\mu\nu}(P)] = g_3^2 N_c \int \frac{\mathrm{d}^4K}{(2\pi)^3} I^V_{\mu\nu} \frac{\delta(K^2)}{(K-P)^2} n_B(K)\,, \tag{3.31}$$

with

$$\begin{aligned} I^V_{\mu\nu} &= I^{V1}_{\mu\nu} + I^{V2}_{\mu\nu} + I^{V3}_{\mu\nu} \\ &= -4(K-P)_\mu K_\nu - 4(K-P)_\nu K_\mu - (2P^2 + 4K\cdot P)g_{\mu\nu} + 2P_\mu P_\nu\,, \end{aligned} \tag{3.32}$$

Starting as usual from the definitions

$$\begin{aligned} g^{\mu\nu}\ \mathrm{Re}(\Pi^V_{\mu\nu}) &\equiv g_3^2 N_c G_V, \\ u^\mu u^\nu\ \mathrm{Re}(\Pi^V_{\mu\nu}) &\equiv g_3^2 N_c H_V\,, \end{aligned} \tag{3.33}$$

and using that

$$\begin{aligned} g^{\mu\nu} I^V_{\mu\nu} &= -8K\cdot P - 6P^2\,, \\ u^\mu u^\nu I^V_{\mu\nu} &= -8k_0^2 + 8k_0 p_0 + 2p_0^2 - 2P^2 - 4K\cdot P\,, \end{aligned} \tag{3.34}$$

we obtain that

$$\begin{aligned} G_V &= -8L_5^B(P) - 6P^2 L_1^B(P)\,, \\ H_V &= -8L_3^B(P) + 8p_0 L_2^B(P) - 2(P^2 - p_0^2)L_1^B(P) - 4L_5^B(P)\,. \end{aligned} \tag{3.35}$$

Using again the Eqs. (B.1)-(B.5) we get

$$\begin{aligned} G_V &= \int_0^\infty \frac{\mathrm{d}k}{2\pi^2}\left[4k + \frac{5}{4}\frac{P^2}{p}L_-(k)\right] n_B(k) \overset{\mathrm{HTL}}{\sim} \frac{T^2}{3}\,, \\ H_V &= \int_0^\infty \frac{\mathrm{d}k}{2\pi^2}\left[2kL + \frac{M(k)}{p} - \frac{p}{4}L_-(k)\right] n_B(k) \overset{\mathrm{HTL}}{\sim} \frac{L+1}{6}T^2\,, \end{aligned} \tag{3.36}$$

where the auxiliary functions $L_\pm$, L and M are defined as before.

3.1.4 Vector spectral densities $\rho_{L,T}$

The free vector-boson propagator is given by

$$\Delta_{\mu\nu} = \frac{i}{P^2}\left(-g_{\mu\nu} + (1-\xi)\frac{P_\mu P_\nu}{P^2}\right), \tag{3.37}$$

so the full vector-boson propagator is

$$D_{\mu\nu} = \Delta_{\mu\nu} + \Delta_{\mu\alpha}(i\Pi^{\alpha\beta})\Delta_{\beta\nu} + \Delta_{\mu\alpha}(i\Pi^{\alpha\beta})\Delta_{\beta\gamma}(i\Pi^{\gamma\delta})\Delta_{\delta\nu} + \cdots\,, \tag{3.38}$$

where $\Pi^{\mu\nu}$ stands for the sum of the three different contributions given by Eqs. (3.8), (3.17) and (3.31). The only tensors that can appear in $\Pi_{\mu\nu}$ are $g_{\mu\nu}$ and $P_\mu P_\nu$. The Ward identity, however tells us that

$$P^\mu \Pi_{\mu\nu} = 0\,. \tag{3.39}$$

It is therefore convenient to extract the tensor structure from $\Pi_{\mu\nu}$ in the following way:

$$\Pi_{\mu\nu} = \left(g_{\mu\nu} - \frac{P_\mu P_\nu}{P^2} \right) \pi(P^2)\,, \tag{3.40}$$

where $\pi(P^2)$ is an arbitrary function of P^2. The presence of a medium will not affect the Ward identity (3.39), but will break the Lorentz covariance and thus terms proportional to the Plasma four-velocity can arise, so

$$\Pi_{\mu\nu} = a_1 g_{\mu\nu} + a_2 u_\mu u_\nu + a_3 P_\mu P_\nu + a_4 P_\mu u_\nu + a_5 P_\nu u_\mu. \tag{3.41}$$

A particular combination is

$$\Pi^T_{\mu\nu} = -g_{\mu\nu} + u_\mu u_\nu - \frac{1}{p^2}(P_\mu - p_0 u_\mu)(P_\nu - p_0 u_\nu) = \begin{pmatrix} 0 & 0 \\ 0 & \delta_{ij} - \frac{p_i p_j}{p^2} \end{pmatrix}. \tag{3.42}$$

We can verify that $P^\mu \Pi^T_{\mu\nu} = 0$ which means that $\Pi^T_{\mu\nu}$ is orthogonal to P^μ (and also to p^i). Therefore it is called transverse. We also define the longitudinal projector (orthogonal to P^μ, but parallel to p^i) by

$$\Pi^L_{\mu\nu} = -g_{\mu\nu} + \frac{P_\mu P_\nu}{P^2} - \Pi^T_{\mu\nu}\,. \tag{3.43}$$

Finally, we define the parallel to P^μ projector

$$\Pi^P_{\mu\nu} = -\frac{P_\mu P_\nu}{P^2}\,. \tag{3.44}$$

Using (3.42)-(3.44) the free propagator (3.37) can be recast to the form

$$\Delta_{\mu\nu}(P) = i \left(\frac{\Pi^T_{\mu\nu}}{P^2} + \frac{\Pi^L_{\mu\nu}}{P^2} + \xi \frac{\Pi^P_{\mu\nu}}{P^2} \right)\,. \tag{3.45}$$

We can also decompose the vector-boson selfenergy as

$$\Pi_{\mu\nu} = -\pi_L \Pi^L_{\mu\nu} - \pi_T \Pi^T_{\mu\nu}\,, \tag{3.46}$$

where the functions π_L and π_T are called transverse and longitudinal selfenergies respectively and encapsulate the thermal corrections analyzed previously. Of course (3.46) satisfies the Ward identity (3.39). We can also check that

$$\begin{aligned} u^\mu u^\nu \Pi^L_{\mu\nu} &= -\frac{p^2}{P^2}\,, && (3.47)\\ u^\mu u^\nu \Pi^T_{\mu\nu} &= 0\,, && (3.48)\\ g^{\mu\nu} \Pi^L_{\mu\nu} &= -1\,, && (3.49)\\ g^{\mu\nu} \Pi^T_{\mu\nu} &= -2\,. && (3.50) \end{aligned}$$

Using the relations above we obtain for the transverse and longitudinal selfenergies that

$$\begin{aligned} \pi_L &= -\frac{P^2}{p^2} u^\mu u^\nu \Pi_{\mu\nu}\,, && (3.51)\\ \pi_T &= -\frac{\pi_L}{2} + \frac{1}{2} g^{\mu\nu} \Pi_{\mu\nu}\,. && (3.52) \end{aligned}$$

Table 3.1: Numerical coefficients in the context of MSSM for the gauge groups, $U(1)_Y$, $SU(2)_L$ and $SU(3)_c$.

Gauge group	N_c	N_F	N_S
$U(1)_Y$	3	9	12
$SU(2)_L$	2	9	14
$SU(3)_c$	0	11	22

Now, our aim is to calculate the full propagator (3.38). It is easy to see that[2]

$$\Delta_{\mu\alpha}(i\Pi^{\alpha\beta})\Delta_{\beta\nu} = \frac{i}{P^2}\left(\pi_L \frac{\Pi^L_{\mu\nu}}{P^2} + \pi_T \frac{\Pi^T_{\mu\nu}}{P^2}\right), \tag{3.53}$$

and

$$\Delta_{\mu\alpha}(i\,\Pi^{\alpha\beta})\Delta_{\beta\gamma}(i\,\Pi^{\gamma\delta})\Delta_{\delta\nu} = \frac{i}{P^2}\left(\pi_L^2 \frac{\Pi^L_{\mu\nu}}{P^4} + \pi_T^2 \frac{\Pi^T_{\mu\nu}}{P^4}\right). \tag{3.54}$$

Using (3.37), (3.38), (3.53) and (3.54) we obtain that the full propagator reads

$$D_{\mu\nu}(P) = \frac{i}{P^2}\Pi^T_{\mu\nu}\left(1 + \frac{\pi_T}{P^2} + \frac{\pi_T^2}{P^4} + \cdots\right) + \frac{i}{P^2}\Pi^L_{\mu\nu}\left(1 + \frac{\pi_L}{P^2} + \frac{\pi_L^2}{P^4} + \cdots\right) - i\xi\frac{P_\mu P_\nu}{P^2}. \tag{3.55}$$

Using the geometric series $1 + x + x^2 + \cdots = \frac{1}{1-x}$ for $x = \frac{\pi_L}{P^2}, \frac{\pi_T}{P^2}$ and dropping the terms proportional to P_μ, P_ν according to the Ward identity, we obtain

$$D^{(T)}_{\mu\nu}(P) = i\frac{\Pi^L_{\mu\nu}}{P^2 - \pi_L} + i\frac{\Pi^T_{\mu\nu}}{P^2 - \pi_T}. \tag{3.56}$$

In (3.56) the superscript (T) indicates that this is only the $T \neq 0$ part, thus the $T = 0$ contribution has to be added additionally. For the $T = 0$ case $u^\mu \to 0$ so the corresponding projectors (3.42) and (3.43) become

$$\Pi^{T\,(0)}_{\mu\nu} = -g_{\mu\nu} - \frac{P_\mu P_\nu}{p^2} \qquad \text{and} \qquad \Pi^{L\,(0)}_{\mu\nu} = -g_{\mu\nu} + \frac{P_\mu P_\nu}{P^2} - \Pi^T_{\mu\nu}. \tag{3.57}$$

The contractions with $g^{\mu\nu}$ are

$$g^{\mu\nu}\Pi^{T\,(0)}_{\mu\nu} = -3 - \frac{p_0^2}{p^2} \qquad \text{and} \qquad g^{\mu\nu}\Pi^{L\,(0)}_{\mu\nu} = \frac{p_0^2}{p^2} \tag{3.58}$$

Then from (3.51) and (3.52) we obtain that

$$\pi_T^{(0)} = \pi_L^{(0)} = \pi_0. \tag{3.59}$$

Finally, the full vector-boson propagator, which includes both the $T = 0$ and $T \neq 0$ parts, reads

$$D_{\mu\nu}(P) = i\frac{\Pi^L_{\mu\nu}}{P^2 - \pi_L - \pi_0} + i\frac{\Pi^T_{\mu\nu}}{P^2 - \pi_T - \pi_0}. \tag{3.60}$$

The final step is the calculation of the functions π_T, π_L and π_0. Firstly, we will calculate the $T = 0$ one-loop correction to the vector selfenergy, assuming the $\overline{\text{DR}}$ renormalization

[2] All the contractions with the gauge dependent term vanish.

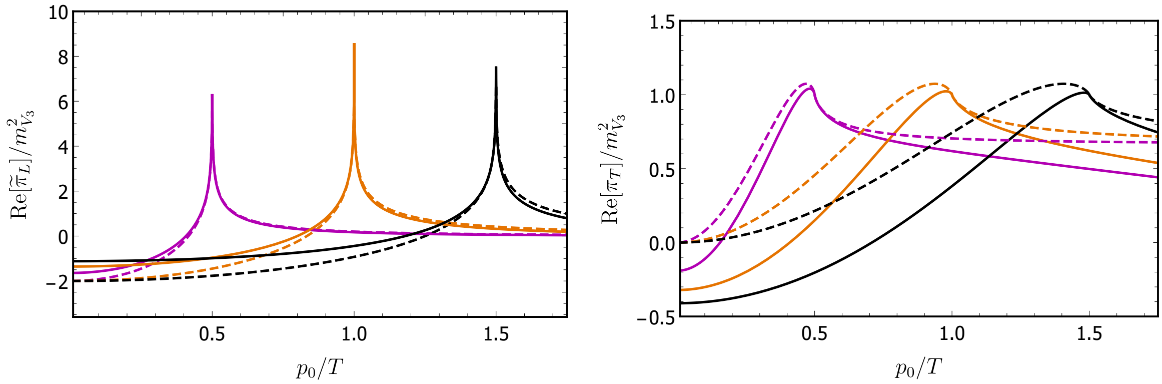

Figure 3.4: Real parts of the longitudinal (left) and transverse (right) selfenergies within the complete 1-loop approximation (solid lines) and their HTL limits (dashed lines) for various momenta, $p/T = 0.5$ (magenta), $p/T = 1.0$ (orange), and $p/T = 1.5$ (black). For illustrative purposes we plot the longitudinal selfenergy with a tilde, $\tilde{\pi}_L = \pi_L/(P^2/p^2)$. All the lines correspond to the $SU(3)_c$ gauge group.

scheme. From (3.43),(3.46) and (3.59) we obtain that

$$\Pi^{(0)}_{\mu\nu} = \left(g_{\mu\nu} - \frac{P_\mu P_\nu}{P^2}\right)\pi_0(p^2)$$

and so in $d = 4$ dimensions

$$\pi_0(p^2) = \frac{g^{\mu\nu}\Pi^{(0)}_{\mu\nu}}{3}\,. \tag{3.61}$$

As in the $T \neq 0$ case there are 3 different contributions (scalar, fermion and vector) which are listed below[3].

$$\begin{aligned}
\bullet\ g^{\mu\nu}\Pi^{S\,(0)}_{\mu\nu} &= -ig^2_\alpha \frac{N_S}{2}\int \frac{d^dK}{(2\pi)^d}\frac{(4-2d)K^2 + (1-2d)P^2 + (4d-4)K\cdot P}{K^2(K-P)^2} \\
&= g^2_\alpha P^2 \frac{N_S/2}{16\pi^2}\ln\left(\frac{-P^2}{\mu^2}\right), \\
\bullet\ g^{\mu\nu}\Pi^{F\,(0)}_{\mu\nu} &= ig^2_\alpha \frac{N_F}{2}\int \frac{d^dK}{(2\pi)^d}\frac{\mathrm{Tr}\left[\gamma^\nu(\not{K}-\not{P})\gamma_\nu\not{K}\right]}{K^2(K-P)^2} = g^2_\alpha P^2\frac{2N_F}{16\pi^2}\ln\left(\frac{-P^2}{\mu^2}\right), \\
\bullet\ g^{\mu\nu}\Pi^{V\,(0)}_{\mu\nu} &= ig^2_\alpha N_c \int \frac{d^dK}{(2\pi)^d}\frac{(2d-4)K^2 + (d/2+1)P^2 + (4-5d)K\cdot P}{K^2(K-P)^2} \\
&= g^2_\alpha P^2 \frac{-5N_c}{16\pi^2}\ln\left(\frac{-P^2}{\mu^2}\right).
\end{aligned} \tag{3.62}$$

Finally, adding these contributions we obtain

$$\pi_0(P^2) = g^2_\alpha\, P^2 \frac{2N_F + N_S/2 - 5N_c}{48\pi^2}\ln\left(\frac{-P^2}{\mu^2}\right). \tag{3.63}$$

The $T \neq 0$ contribution is given by (3.51) and (3.52),

$$\pi_L = -\frac{P^2}{p^2} g^2_\alpha (N_S H_S + N_F H_F + N_c H_V) \overset{\mathrm{HTL}}{\sim} -\frac{P^2}{p^2}(L+1)m^2_V \tag{3.64}$$

and

$$\pi_T = -\frac{\pi_L}{2} + \frac{g^2_\alpha}{2}(N_S G_S + N_F G_F + N_c G_V) \overset{\mathrm{HTL}}{\sim} (1 + \frac{P^2}{p^2}\frac{L+1}{2})m^2_V\,, \tag{3.65}$$

[3]Here we have restored the gauge group index α in order to generalize our results into the rest gauge groups.

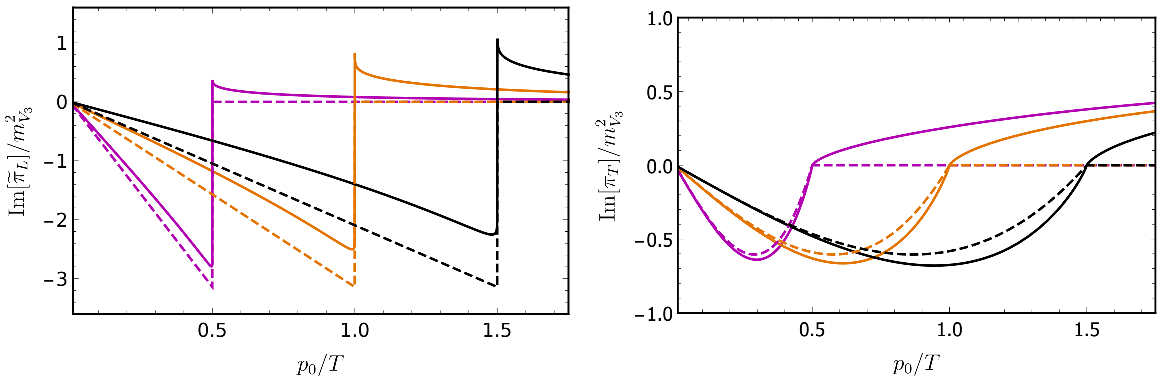

Figure 3.5: Imaginary parts of the longitudinal (left) and transverse (right) selfenergies within the complete 1-loop approximation (solid lines) and their HTL limits (dashed lines) for various momenta, $p/T = 0.5$ (magenta), $p/T = 1.0$ (orange), and $p/T = 1.5$ (black). For illustrative purposes we plot the longitudinal selfenergy with a tilde, $\tilde{\pi}_L = \pi_L/(P^2/p^2)$. All the lines correspond to the $SU(3)_c$ gauge group.

in which the vector thermal mass is given by

$$m_V^2 = \frac{1}{6} g_\alpha^2 T^2 (N_c + N_S/2 + N_F/2)\,. \tag{3.66}$$

The numerical coefficients involved in the thermal mass are given explicitly in Table 3.1 assuming the MSSM content. Figures 3.4 and 3.5 shows the real and imaginary parts of the longitudinal (3.64) and transverse (3.65) selfenergies within the complete 1-loop approximation (solid lines) and their HTL limits (dashed lines) for various momenta, $p/T = 0.5, 1.0, 1.5$, for the $SU(3)_c$ gauge group. As manifested in Fig. (3.5) for $p_0 > p$ the imaginary part for both π_L and π_T vanishes in the HTL limit. This is entirely to be expected as in the HTL approximation both selfenergies depends on the function L which develops imaginary part only below the light cone.

For later use we define the spectral functions ρ_L and ρ_T which are given by (6.74) and (6.75) of [300],

$$\rho_T = -2\,\mathrm{Im}\frac{1}{P^2 - \pi_0 - \pi_T}, \qquad \rho_L = -2\,\mathrm{Im}\frac{P^2}{p^2}\frac{1}{P^2 - \pi_0 - \pi_L}\,. \tag{3.67}$$

These functions can be rewritten as

$$\rho_{L,T}(P) = 2\pi\left[Z_{L,T}(p)\delta(p_0 - \omega_{L,T}(p)) - Z_{L,T}(p)\delta(p_0 + \omega_{L,T}(p))\right] + \rho^{\mathrm{cont}}_{L,T}(P)\,, \tag{3.68}$$

where the δ-functions come from the poles in the definitions (3.67) and $\rho^{\mathrm{cont}}_{L,T}$ are the continuum parts. The residues can be very well approximated by their HTL analytical expressions which read,

$$Z_L(p) = \frac{\omega_L(p)(\omega_L^2(p) - p^2)}{p^2(p^2 + 2m_V^2 - \omega_L^2(p))}\,, \quad Z_T(p) = \frac{\omega_T(p)(\omega_T^2(p) - p^2)}{2m_V^2\omega_T^2(p) - (\omega_T^2(p) - p^2)^2}\,. \tag{3.69}$$

The positions of the poles are denoted by ω_L for the longitudinal and by ω_T for the transverse vectors. They will be calculated in detail in Sec. 3.3.

3.2 Fermion selfenergy

We have two Feynman graphs contributing to the fermion selfenergy. One that is due to vector-boson loop and another due to Yukawa type fermion loop. The relevant $SU(3)_c$

interaction Lagrangian is

$$\mathcal{L} = -g_3 g^a_\mu \bar{f}_s \gamma^\mu T_{a,\,st} f_t + \lambda\phi \bar{f}_s \Gamma_{st} f_t \,. \tag{3.70}$$

This yields the Feynman rules for the vertex vectorboson(g^a_μ)-quark($\bar{f}_s$)-quark(f_t) $= -ig_3 T_{a,\,st}\gamma_\mu$ and for the boson(ϕ)-quark($\bar{f}_s$)-quark(f_t) $= i\lambda\Gamma_{st}$. Because the T dependence of the propa-

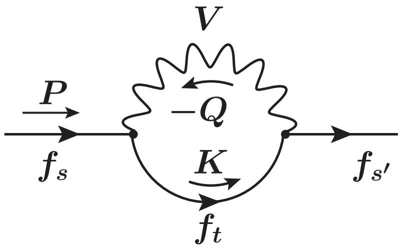

Figure 3.6: Feynman graphs contributing to the fermion selfenergy. The color index a is fixed and the momentum Q is defined as $Q = P - K$.

gators (3.1) is additive, it is easy to separate off the $T = 0$ selfenergy by

$$\Sigma = \Sigma^{(0)} + \Sigma^{(T)} \,. \tag{3.71}$$

The finite temperature correction $\Sigma^{(T)}$ is complex, but as it is discussed in [301] we can ignore the imaginary part and compute only the real part. We will proceed computing the $T \neq 0$ and $T = 0$ parts separately, starting from $\Sigma^{(T)}$.

The contribution to the fermion selfenergy due to vector-boson loop graph is[4]

$$-i\Sigma^{(T)}_V = (-i)^2 g_3^2 C_R \int \frac{\mathrm{d}^4K}{(2\pi)^4}\left[\gamma^\nu S_F(K)\gamma^\mu \Delta^{ab}_{\mu\nu}(K-P)\right], \tag{3.72}$$

where $\Sigma_a T_{a,\,s't} T_{a,\,ts} = C_R \delta_{s's}$ is the quadratic Casimir of the representation. In [301] Table 1 we can see the values of C_R for all the relevant gauge groups. Taking the temperature dependent propagators from (3.1) we get

$$-i\Sigma^{(T)}_V = (-i)^2 g_3^2 C_R \int \frac{\mathrm{d}^4K}{(2\pi)^4}\gamma_\mu \left(\frac{i\not{K}}{K^2} - \Gamma_F(K)\not{K}\right)\gamma^\mu \left(-\frac{i}{(K-P)^2} - \Gamma_B(K-P)\right). \tag{3.73}$$

The real part (correction to the mass term) is

$$\mathrm{Re}\,\Sigma^{(T)}_V = g_3^2 C_R \int \frac{\mathrm{d}^4K}{(2\pi)^4}\left(-\gamma_\mu\not{K}\gamma^\mu \frac{\Gamma_B(K-P)}{K^2} + \gamma_\mu\not{K}\gamma^\mu\frac{\Gamma_F(K)}{(K-P)^2}\right). \tag{3.74}$$

At the first term we make the shift $K \to P - K$ and using the identity $\gamma_\mu\not{K}\gamma^\mu = -2\not{K}$, we get

$$\mathrm{Re}\,\Sigma^{(T)}_V = -2g_3^2\, C_R \int \frac{\mathrm{d}^4K}{(2\pi)^3}\left\{\not{K}\left[n_B(K) + n_F(K)\right] - \not{P} n_B(K)\right\}\frac{\delta(K^2)}{(K-P)^2}\,. \tag{3.75}$$

For the second graph, repeating the same steps, we get

$$\mathrm{Re}\,\Sigma^{(T)}_\phi = -|\lambda^2|\, C' \int \frac{\mathrm{d}^4K}{(2\pi)^3}\left\{\not{K}\left[n_B(K) + n_F(K)\right] - \not{P} n_B(K)\right\}\frac{\delta(K^2)}{(K-P)^2}\,, \tag{3.76}$$

[4]Actually we defined the fermion selfenergy as $-i\Sigma$, as well as this of the vector-boson as $i\Pi_{\mu\nu}$, in order to resume these corrections following $S_F = i(\not{P} - \Sigma)^{-1}$ for fermions and $\Delta = -i(P^2 - \Pi)^{-1}$ for the gauge bosons.

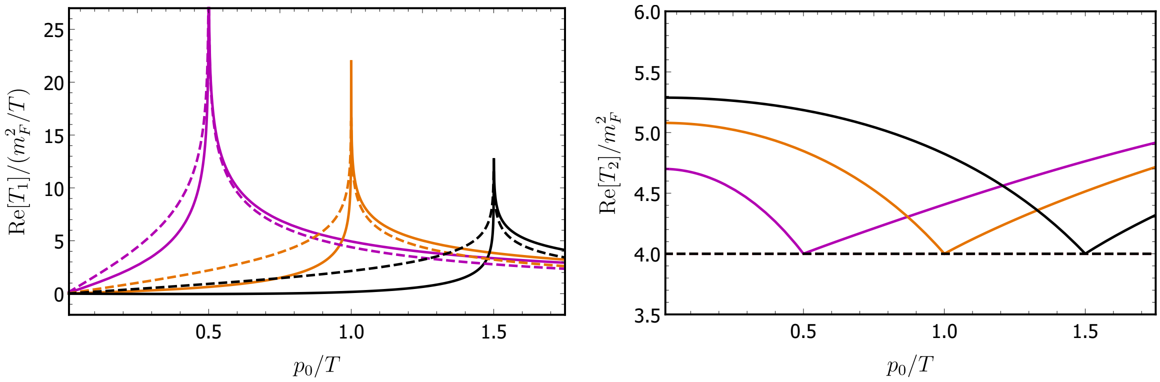

Figure 3.7: Real parts of the functions T_1 (left) and T_2 (right) within the complete 1-loop approximation (solid lines) and their HTL limits (dashed lines) for various momenta, $p/T = 0.5$ (magenta), $p/T = 1.0$ (orange), and $p/T = 1.5$ (black).

where $(\Gamma\Gamma^\dagger)_{s's} = C'\delta_{s's}$. Comparing (3.75) and (3.76) we can see that computing one of them is enough, since they are related with $2g_3^2 C_R \to |\lambda^2| C' = \lambda_q$. Thus we will proceed computing (3.75).

A theory containing fermions with no bare masses is chirally invariant to all orders. At $T = 0$, chiral invariance has two consequences. Firstly there are no $\overline{\chi}\chi$ couplings induced in any finite order of perturbation theory. Secondly the fermion selfenergy is of the form $\Sigma^{(0)} = \tilde{\Sigma}_0 \not{P}$ for a particle with four-momentum P, where $\widetilde{\Sigma}_0$ is a function of P^2. For the same chirally invariant theory at $T \neq 0$, the first consequence still holds but the second does not. At finite temperature the plasma of particles and antiparticles constitutes the heat bath introduces a special Lorentz frame, the rest frame of the plasma. In a general frame the heat bath has four-velocity v^μ with $v^\mu v_\mu = 1$. The presence of this four-velocity means that general Dirac structure of a fermion selfenergy in a thermal heat bath takes the form

$$\Sigma_V^{(T)}(P) = -a_V \not{P} - b_V \not{u}\,, \tag{3.77}$$

with a_V and b_V functions of P^2, see [301, 302]. We just give the formulas for the rest-frame $u^\mu = (1, 0, 0, 0)$ [303],

$$a_V(P) = \frac{1}{4p^2}\Big[T_2^V(P) - p_0 T_1^V(P)\Big]\,, \tag{3.78}$$

$$b_V(P) = \frac{1}{4p^2}\Big[P^2 T_1^V(P) - p_0 T_2^V(P)\Big]\,, \tag{3.79}$$

with

$$T_1^V(P) \equiv \mathrm{Tr}[\not{u}\,\mathrm{Re}\,\Sigma_V^{(T)}(P)] \qquad \text{and} \qquad T_2^V(P) \equiv \mathrm{Tr}[\not{P}\,\mathrm{Re}\,\Sigma_V^{(T)}(P)]\,. \tag{3.80}$$

We will start calculating $T_1^V(P)$, that is,

$$T_1^V(P) = -2g_3^2 C_R \int \frac{\mathrm{d}^4K}{(2\pi)^3}\Big\{(n_B(K) + n_F(K))\mathrm{Tr}[\not{u}\not{K}] - n_B(K)\mathrm{Tr}[\not{u}\not{P}]\Big\}\frac{\delta(K^2)}{(K-P)^2}\,.$$

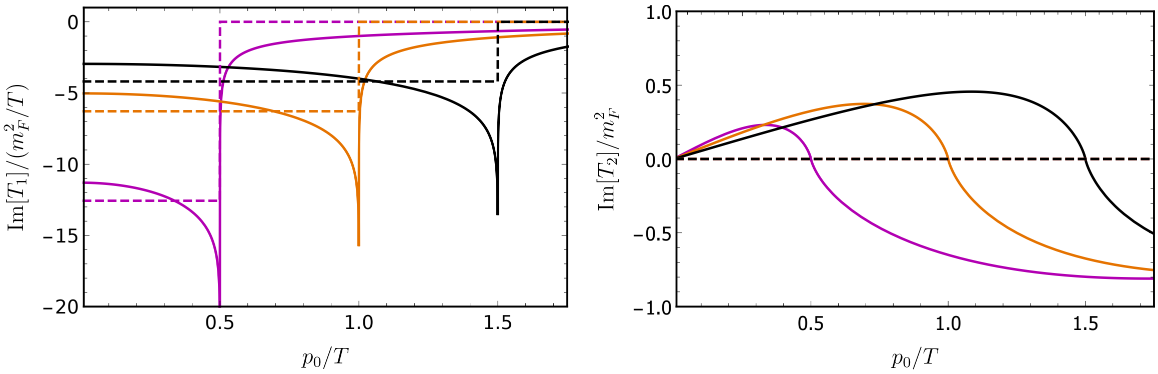

Figure 3.8: Imaginary parts of the functions T_1 (left) and T_2 (right) within the complete 1-loop approximation (solid lines) and their HTL limits (dashed lines) for various momenta, $p/T = 0.5$ (magenta), $p/T = 1.0$ (orange), and $p/T = 1.5$ (black).

At this point using (B.1) and (B.2) we obtain

$$\begin{aligned} T_1^V(P) &= -8g_3^2 C_R \left[L_2^B(P) + L_2^F(P) - p_0 L_1^B(P)\right] \\ &= -g_3^2 C_R \frac{1}{p} \int_0^\infty \frac{\mathrm{d}k}{2\pi^2} \left\{ \left[\frac{2kp}{p_0}\Big(L-1\Big) + kL_+(k)\right] n_F(k) \right. \\ &\quad \left. + \left[\frac{2kp}{p_0}\Big(L-1\Big) + kL_+(k) + p_0 L_-(k)\right] n_B(k) \right\} . \end{aligned} \tag{3.81}$$

We are turning now to $T_2^V(P)$. We have

$$T_2^V(P) = -2g_3^2\, C_R \int \frac{\mathrm{d}^4K}{(2\pi)^3} \{(n_B(K) + n_F(K))\mathrm{Tr}[\not{P}\not{K}] - n_B(K)\mathrm{Tr}[\not{P}\not{P}]\} \frac{\delta(K^2)}{(K-P)^2} .$$

As before, using the Eqs. (B.1) and (B.5) of Appendix B and we get

$$\begin{aligned} T_2^V(P) &= -8g_3^2 C_R \Big[L_5^B(P) + L_5^F(P) - P^2 L_1^B(P)\Big] \\ &= g_3^2 C_R \int_0^\infty \frac{\mathrm{d}k}{2\pi^2} \left\{ \left[4k + \frac{P^2}{2p} L_-(k)\right] n_F(k) + \left[4k - \frac{P^2}{2p} L_-(k)\right] n_B(k) \right\} . \end{aligned} \tag{3.82}$$

Figures 3.7 and 3.8 shows the real and imaginary parts of the "full" (both graphs) T_1 and T_2 within the complete 1-loop approximation (solid lines) and their HTL limits (dashed lines) for various momenta, $p/T = 0.5, 1.0, 1.5$. The HTL limits for these functions are given by

$$T_1(P) \overset{\mathrm{HTL}}{\sim} -\frac{2m_F^2}{p_0}(L-1) \qquad \text{and} \qquad T_2(P) \overset{\mathrm{HTL}}{\sim} 4m_F^2 , \tag{3.83}$$

in which the fermion thermal mass is defined in (3.87). These simple HTL expressions can easily interpret the vanishing $\mathrm{Im}[T_1]$ above the light cone and the the vanishing $\mathrm{Im}[T_2]$ in the whole region.

For the $T = 0$ part in each gauge group we have that[5]

$$\begin{aligned} \Sigma_V^{(0)} &= -i g_\alpha^2 C_R \int \frac{\mathrm{d}^d K}{(2\pi)^d} \left(\gamma^\nu \frac{\not{K}}{K^2} \gamma^\mu \right) \frac{g_{\mu\nu}}{(P-K)^2} \\ &= -g_\alpha^2 C_R \not{P} \frac{1}{16\pi^2} \left(2 - r - \ln \frac{-P^2}{\mu^2} - \gamma + \ln 4\pi \right) \end{aligned} \tag{3.84}$$

Similarly,

$$\Sigma_\phi^{(0)} = i\lambda_q^2 \int \frac{\mathrm{d}^d K}{(2\pi)^d} \frac{\not{K}}{K^2 (P-K)^2} = -\frac{\lambda_q^2}{16\pi^2} \frac{\not{P}}{2} \left(2 - \ln \frac{-P^2}{\mu^2} - \gamma + \ln 4\pi \right) . \tag{3.85}$$

Then using that $\widetilde{\Sigma}_0 \not{P} = \Sigma_V^{(0)} + \Sigma_\phi^{(0)}$ we obtain that

$$\widetilde{\Sigma}_0 = -\frac{1}{2\pi^2} \left[\frac{m_F^2}{T^2} \left(2 - \ln \frac{-P^2}{\mu^2} - \gamma + \ln 4\pi \right) - \frac{g_\alpha^2 C_R}{8} r \right] , \tag{3.86}$$

where we have defined the fermion thermal mass

$$m_F^2 = \left(\frac{g_\alpha^2 C_R}{8} + \frac{\lambda_q^2}{16} \right) T^2 . \tag{3.87}$$

Our aim is to write the result in the helicity basis $\lambda^\pm = \frac{1}{2}(\gamma^0 \pm \hat{p}_i \gamma^i)$ with $\hat{p}_i = p_i/p$, thus $\gamma^0 = \lambda^+ + \lambda^-$ and $\hat{p}_i \gamma^i = (\lambda^+ - \lambda^-)$. So from (3.71) and (3.77) for both graphs of Fig. 3.6 we obtain that

$$\Sigma(P) = -a(p_0 \gamma^0 - p_i \gamma^i) - b\gamma^0 = \Sigma_+(P)\lambda^+ + \Sigma_-(P)\lambda^- \tag{3.88}$$

with

$$\begin{aligned} \Sigma_\pm(P) &= \frac{1}{4p} \Big(\pm T_2(P) - (\pm p_0 - p) T_1(P) \Big) \\ &= \pm 2 \frac{m_F^2}{T^2} \int_0^\infty \frac{\mathrm{d}k}{\pi^2} \left[\frac{\omega_\mp}{p^2} \Big(k L_+ (n_B + n_F) + L_- \left(n_B \omega_\mp + n_F \omega_\pm \right) \Big) \right. \\ &\quad \left. + 2 \frac{L\omega_\mp + \omega_\pm}{p p_0} k (n_B + n_F) \right] . \end{aligned} \tag{3.89}$$

We want to make a decomposition to the propagator into the two helicity eigenstates,

$$-\, i\, S^*(P) = \frac{1}{\not{P} - \Sigma(P)} = \frac{\not{P} - \Sigma(P)}{(\not{P} - \Sigma(P)(\not{P} - \Sigma(P))} , \tag{3.90}$$

which after some algebra takes the form

$$-\, i\, S^*(P) = \frac{\gamma^0 - \hat{p}_i \gamma^i}{2D_+(P)} + \frac{\gamma^0 + \hat{p}_i \gamma^i}{2D_-(P)} , \tag{3.91}$$

[5] Here we have used that in $d = 4 - \epsilon$ dimensions $\frac{(2\pi^4)}{i\pi^2} \mu^{4-d} \int \frac{\mathrm{d}^d K}{(2\pi)^d} \frac{\not{K}}{K^2 (P-K)^2} = \frac{i}{16\pi^2} \frac{\not{P}}{2} \left(\Delta - \ln \frac{-P^2}{\mu^2} + 2 \right)$ where $\Delta = \frac{2}{\epsilon} - \gamma + \ln 4\pi$ and γ is the Euler–Mascheroni constant.

with

$$\begin{aligned} D_\pm(P) &= p_0 \mp p - \Sigma_\pm(P) - (p_0 \mp p)\widetilde{\Sigma}_0 \\ &= 2\omega_\mp \left\{ 1 + \frac{1}{2\pi^2} \left[\frac{m_F^2}{T^2} \left(2 - \gamma + \ln 4\pi - \ln \frac{-P^2}{\mu^2} \right) - \frac{g_\alpha^2 C_R}{8} r \right] \right\} + 2\frac{m_F^2}{T^2} F_\pm \,. \end{aligned} \tag{3.92}$$

The functions $F_\pm$ in (3.92) are defined as

$$F_\pm = \mp \int_0^\infty \frac{\mathrm{d}k}{\pi^2} \frac{\omega_\mp}{p^2} \Big(kL_+ (n_B + n_F) + L_- \left(n_B \omega_\mp + n_F \omega_\pm \right) \Big) \mp \frac{T^2}{2} \frac{L\omega_\mp + \omega_\pm}{pp_0} \,. \tag{3.93}$$

Following [300] (see also [304, 305]), one defines the spectral functions as

$$\rho_\pm(P) = -2\,\mathrm{Im} \left(\frac{1}{D_\pm} \right) \,. \tag{3.94}$$

Assuming $\overline{\mathrm{DR}}$ renormalization scheme ($r = 0$), and consequently ignoring the terms $-\gamma + \ln 4\pi$, we finally get

$$\rho_\pm(P) = \mathrm{Im} \left\{ \omega_\mp \left(1 + \frac{1}{2\pi^2} \left[\frac{m_F^2}{T^2} \left(2 - \ln \frac{-P^2}{\mu^2} \right) \right] \right) + \frac{m_F^2}{T^2} F_\pm \right\}^{-1} \,. \tag{3.95}$$

As in the vector case, the fermionic spectral functions can be written as the sum of a pole and a continuum part,

$$\rho_\pm(P) = 2\pi \left[Z_\pm(p) \delta(p_0 - \omega_\pm(p)) + Z_\mp(p) \delta(p_0 + \omega_\mp(p)) \right] + \rho_\pm^{\mathrm{cont}}(P) \,, \tag{3.96}$$

while the corresponding residues can be very well approximated by their HTL analytical expressions which read,

$$Z_\pm(p) = \frac{\omega_\pm^2(p) - p^2}{2m_F^2} \,. \tag{3.97}$$

The positions of the poles $\omega_\pm(p)$ should not be confused with the shortcuts (B.7).

3.3 Dispersion relations

In this section we will show the full one-loop dispersion relations for vector bosons and fermions. The corresponding HTL results are also given for completeness.

3.3.1 Poles of ρ_L and ρ_T

The $T \neq 0$ dispersion relation for longitudinal (transverse) modes are given by the poles of the longitudinal (transverse) parts of the vector propagator. For the longitudinal one we have to find the zeros of the equation $p^2(1 - \pi_L/P^2) = 0$ as it is dictated from the longitudinal spectral function (3.67). The longitudinal selfenergy defined in (3.46) and calculated in (3.64) can be written as

$$\begin{aligned} \pi_L = -\frac{P^2}{p^2} m_V^2 \Bigg[L + \frac{6}{N_1 T^2} \frac{1}{2\pi^2} \Bigg(&\frac{p_0^2}{4p} N_2 I_1^B + \frac{1}{p} N_2 I_2^B + \frac{p_0}{p} N_2 I_3^B - \frac{p}{2} N_c I_1^B \\ &+ \frac{P^2}{4p} N_F\, I_1^F + \frac{1}{p} N_F I_2^F + \frac{p_0}{p} N_F I_3^F \Bigg) \Bigg] \,, \end{aligned} \tag{3.98}$$

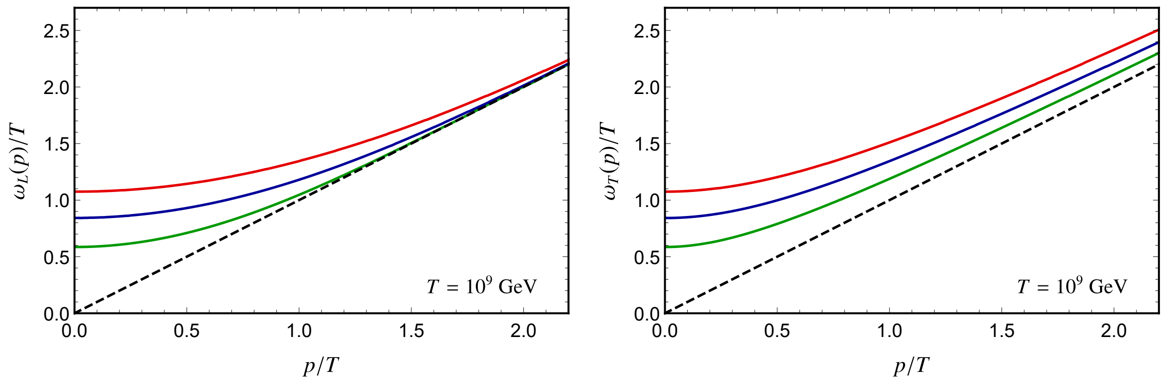

Figure 3.9: Dispersion relation for the longitudinal (left) and transverse (right) vector modes within the complete 1-loop approximation. The solid curves represent in order, the $SU(3)_c$ (red), $SU(2)_L$ (blue), and $U(1)_Y$ (green) case, while the dashed one is the boundary of the light cone. All the lines correspond to the temperature $T = 10^9$ GeV.

where the integrals $I^{F,B}_{1,2,3}$ have been defined in (B.17)-(B.19) and the coefficients N_1 and N_2 are the following combinations

$$N_1 = N_c + N_S/2 + N_F/2 \qquad \text{and} \qquad N_2 = N_c + N_S/2\,. \tag{3.99}$$

Now, the dispersion relation for the longitudinal modes can be written as

$$\begin{aligned} p^3 \;&+\; m_V^2 p\Big(1 - \frac{p_0}{p}\ln\frac{p_0+p}{p_0-p}\Big) + \left(\frac{m_V}{T}\right)^2 \frac{3}{N_1\pi^2}\left[I_1^B\left(\frac{p_0^2}{4}N_2 - \frac{p^2}{2}N_c\right)\right. \\ &+\; \left. I_2^B N_2 + I_3^B p_0 N_2 + I_1^F\frac{p_0^2-p^2}{4}N_F + I_2^F N_F + I_3^F p_0 N_F\right] = 0\,, \end{aligned} \tag{3.100}$$

while its HTL limit is

$$p^3 + 2m_V^2 p - m_V^2 p_0 \ln\frac{p_0+p}{p_0-p} = 0\,, \tag{3.101}$$

and can be found in [300]. In order to go from the full 1−loop (3.100) to the HTL expression (3.101) only the integrals $I_2^{F,B}$ give a sufficient contribution.

For the transverse modes the equation $P^2 - \pi_T = 0$ must be solved. In analogy with (3.98) the transverse selfenergy is written as

$$\pi_T = -\frac{\pi_L}{2} + T^2\left(\frac{m_V}{T}\right)^2\left[1 + \frac{3}{N_1}\frac{1}{2\pi^2}\left(\frac{P^2}{4p}(6N_C - N_2)\,I_1^B + \frac{P^2}{2p}N_F\,I_1^F\right)\right]\,. \tag{3.102}$$

The dispersion relation for the longitudinal modes can be written as

$$\begin{aligned} p^3 \;&-\; m_V^2\frac{p}{2}\Big(1 - \frac{p_0}{p}\ln\frac{p_0+p}{p_0-p}\Big) + m_V^2\frac{p^3}{p^2-p_0^2} - \left(\frac{m_V}{T}\right)^2\frac{3}{2N_1\pi^2}\left[I_1^B\left(\frac{p_0^2-p^2}{4}N_2\right.\right. \\ &+\; \left.\left. p^2 N_c\right) + I_2^B N_2 + I_3^B p_0 N_2 + I_1^F\frac{p_0^2+p^2}{4}N_F + I_2^F N_F + I_3^F p_0 N_F\right] = 0\,, \end{aligned} \tag{3.103}$$

while its HTL limit is

$$p_0^2 p^3 - p^5 - m_V^2 p p_0^2 - m_V^2\frac{p_0}{2}(p^2-p_0^2)\ln\frac{p_0+p}{p_0-p} = 0\,, \tag{3.104}$$

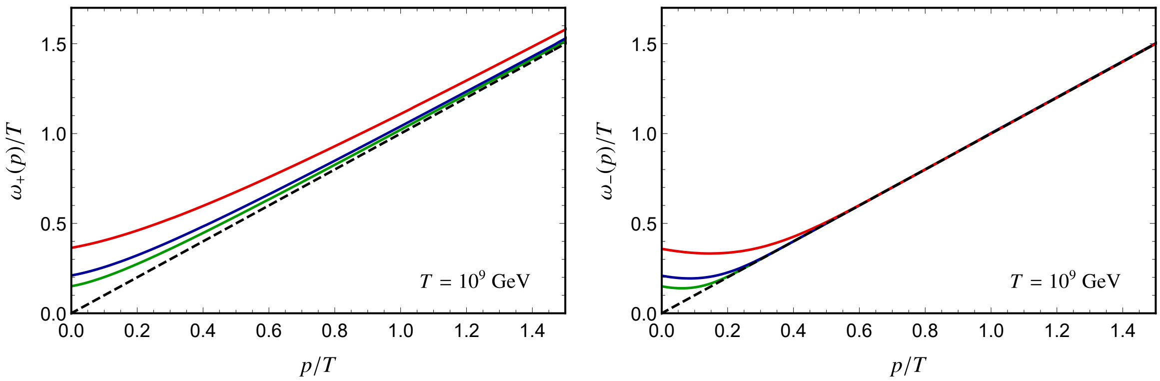

Figure 3.10: Dispersion relation of the longitudinal (left) and transverse (right) vector modes within the complete 1-loop approximation. The solid curves represent in order, the $SU(3)_c$ (red), $SU(2)_L$ (blue), and $U(1)_Y$ (green) case, while the dashed one is the boundary of the light cone. All the lines correspond to the temperature $T = 10^9$ GeV.

in agreement with [300]. Figure 3.9 illustrates the 1−loop dispersion relations for longitudinal (3.100) and transverse (3.103) vectors for the three gauge groups. The gauge group dependence arises from the thermal masses and from the numerical coefficients N (see Table 3.1). The reference temperature in this figure is $T = 10^9$ GeV.

3.3.2 Poles of ρ_+ and ρ_-

For the fermionic modes the $T \neq 0$ dispersion relations arise from the poles of the spectral functions (3.95), *i.e.* when $(p_0 \mp p)/2 + \frac{m_F^2}{T^2} F_\pm = 0$. The functions $F_\pm$ defined in (3.93) can be written with respect to the integrals (B.17)-(B.19) as

$$F_\pm = \mp \frac{\omega_\mp}{\pi^2 p^2} \left(I_3^B + I_3^F + \omega_\mp I_1^B + \omega_\pm I_1^F \right) \mp \frac{T^2}{2} \frac{L\omega_\mp + \omega_\pm}{p p_0} \, , \tag{3.105}$$

in which the shortcuts $\omega_\pm$ (see (B.7)) have nothing to do with the pole positions $\omega_\pm(p)$ coming from the dispersion relation. The 1−loop dispersion relation for both $\rho_\pm$ takes the form

$$\begin{aligned} &p_0 \mp p - \frac{m_F^2}{2p} \left[\left(1 \mp \frac{p_0}{p} \right) \ln \frac{p_0 + p}{p_0 - p} \pm 2 \right] \\ &\mp \left(\frac{m_F}{T} \right)^2 \frac{1}{\pi^2} \frac{p_0 \mp p}{p^2} \left[I_3^B + \frac{p_0 \mp p}{2} I_1^B + I_3^F + \frac{p_0 \pm p}{2} I_1^F \right] = 0 \, . \end{aligned} \tag{3.106}$$

In the HTL approximation the terms contain integrals can be dropped, so (3.106) reduces to

$$p_0 \mp p - \frac{m_F^2}{2p} \left[\left(1 \mp \frac{p_0}{p} \right) \ln \frac{p_0 + p}{p_0 - p} \pm 2 \right] = 0 \, . \tag{3.107}$$

Figure 3.10 illustrates the 1−loop dispersion relations for fermions (3.106) for the three gauge groups. The gauge group dependence arises from the thermal mass m_F. The reference temperature in this figure is again $T = 10^9$ GeV.

Chapter 4

Thermal gravitino production

In this chapter we will calculate the thermal gravitino production following the procedure which was firstly described in [36] and reconsidered in [1, 2].

Since the gravitino is the superpartner of the graviton, its interactions are suppressed by the inverse of the reduced Planck mass $M_{\rm P}$. Therefore, the dominant contributions to its production, in leading order of the gauge group couplings, are processes of the form $a\, b \to c\, \widetilde{G}$, where $\widetilde{G}$ stands for gravitino and a, b, c can be three superpartners or one superpartner and two SM particles. The possible processes and the corresponding squared amplitudes in $SU(3)_c$ are given in Table 4.1, where we follow the "historical" notation of [24] for their designation by the letters A-J. In $SU(3)_c$, the particles a, b, and c could be gluons g, gluinos $\tilde{g}$, quarks q, or/and squarks $\tilde{q}$. Analogous processes occur in $SU(2)_L$ or $U(1)_Y$, where the gluino mass $m_{\tilde{g}} \equiv M_3$ becomes M_2 or M_1, respectively. In the factor $Y_\alpha \equiv 1 + m^2_{\lambda(\alpha)}/(3m^2_{3/2})$, where $m_{\lambda(\alpha)} = \{M_1, M_2, M_3\}$ and $m_{3/2}$ is the gravitino mass, the unity refers to the 3/2 gravitino components and the rest to the 1/2 goldstino part. For the calculation of the spin-3/2 component in the amplitudes, following [36], the gravitino polarization sum (2.29) is used. As in [36], the nonderivative approach is used for the goldstino spin 1/2 part [28, 37]. The result for the full squared amplitude is shown to be the same in either the derivative or the nonderivative approach [299].

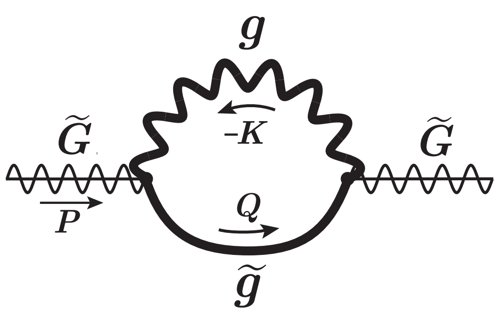

Figure 4.1: The one-loop thermally corrected gravitino self-energy ($D-$graph) for the case of $SU(3)_c$. The thick gluon and gluino lines denote resummed thermal propagators. In our calculation we have also included the equivalent in $SU(2)_L$ and $U(1)_Y$.

The Casimir operators in Table 4.1 are $C_\alpha = \sum_{a,b,c} |f^{(\alpha)\,abc}|^2 = \{0, 6, 24\}$ and $C'_\alpha = \sum^{\phi}_{a,i,j} |T^{(\alpha)}_{a,\,ij}|^2 = \{11, 21, 48\}$, where $\sum^{\phi}_{a,i,j}$ denotes the sum over all involved chiral multiplets and group indices. f^{abc} and T_a are the group structure constants and generators, respectively. The processes A, B and F are not present in $U(1)_Y$ since $C_1 = 0$. The masses for the particles a, b and c are assumed to be zero. In the third column of Table 4.1 we give the square of the total amplitude for each process, which is the sum of the individual amplitudes,

$$|\mathcal{M}_{X,\text{full}}|^2 = |\mathcal{M}_{X,s} + \mathcal{M}_{X,t} + \mathcal{M}_{X,u} + \mathcal{M}_{X,x}|^2\,, \tag{4.1}$$

Table 4.1: Squared matrix elements for gravitino production in $SU(3)_c$ in terms of $g_3^2 Y_3/M_P^2$ assuming massless particles, $Y_3 = 1 + m_{\tilde{g}}^2/(3m_{3/2}^2)$, $C_3 = 24$ and $C_3' = 48$.

X	Process	$\lvert\mathcal{M}_{X,\text{full}}\rvert^2$	$\lvert\mathcal{M}_{X,\text{sub}}\rvert^2$
A	$gg \to \tilde{g}\widetilde{G}$	$4C_3(s + 2t + 2t^2/s)$	$-2sC_3$
B	$g\tilde{g} \to g\widetilde{G}$	$-4C_3(t + 2s + 2s^2/t)$	$2tC_3$
C	$\tilde{q}g \to q\widetilde{G}$	$2sC_3'$	0
D	$gq \to \tilde{q}\widetilde{G}$	$-2tC_3'$	0
E	$\tilde{q}q \to g\widetilde{G}$	$-2tC_3'$	0
F	$\tilde{g}\tilde{g} \to \tilde{g}\widetilde{G}$	$8C_3(s^2 + t^2 + u^2)^2/(stu)$	0
G	$q\tilde{g} \to q\widetilde{G}$	$-4C_3'(s + s^2/t)$	0
H	$\tilde{q}\tilde{g} \to \tilde{q}\widetilde{G}$	$-2C_3'(t + 2s + 2s^2/t)$	0
I	$q\bar{\tilde{q}} \to \tilde{g}\widetilde{G}$	$-4C_3'(t + t^2/s)$	0
J	$\tilde{q}\bar{\tilde{q}} \to \tilde{g}\widetilde{G}$	$2C_3'(s + 2t + 2t^2/s)$	0

where the indices s, t, u denote the diagrams produced by the exchange of a particle in the corresponding channel, and the index x stands for the diagram containing a quartic vertex. The so-called $D-$graph, following the terminology of [36], is shown in Fig. 4.1 for the case of the gluino-gluon loop. Its contribution is the sum of the squared amplitudes for the s, t and u channel graphs,

$$|\mathcal{M}_{X,D}|^2 = |\mathcal{M}_{X,s}|^2 + |\mathcal{M}_{X,t}|^2 + |\mathcal{M}_{X,u}|^2 \,, \tag{4.2}$$

plus $1 \to 2$ processes. This can be understood by applying the optical theorem. Accordingly, from the imaginary part of the loop graphs one computes the sum of the decays ($1 \to 2$) and the scattering amplitudes ($2 \to 2$). In our case, we use resummed thermal propagators for the gauge boson and the gaugino and by applying cutting rules one sees that the $D-$graph describes both the scattering amplitudes occurring in (4.2) and the decay amplitudes.

The subtracted part of the squared amplitudes is the difference between the full amplitudes (4.1) and the amplitudes already contained in the $D-$graph (4.2), *i.e.*

$$|\mathcal{M}_{X,\text{sub}}|^2 = |\mathcal{M}_{X,\text{full}}|^2 - |\mathcal{M}_{X,D}|^2 \,. \tag{4.3}$$

For processes B, F, G, and H, the corresponding amplitudes are IR divergent. For this reason, we follow the more elegant method, which consists in splitting the total scattering rate into two parts, the subtracted and the $D-$graph parts. It is worth noting that for the processes with incoming or/and outgoing gauge bosons, we explicitly checked the gauge invariance for $|\mathcal{M}_{X,\text{full}}|^2$. On the other hand, we note that $|\mathcal{M}_{X,\text{sub}}|^2$ is gauge dependent [1]. In summary, the gravitino production rate $\gamma_{3/2}$ consists of three parts: (i) the subtracted rate γ_{sub} (ii) the $D-$graph contribution γ_{D} and (iii) the top Yukawa rate γ_{top},

$$\gamma_{3/2} = \gamma_{\text{sub}} + \gamma_{\text{D}} + \gamma_{\text{top}} \,. \tag{4.4}$$

Below, these three contributions are discussed in detail.

4.1 $2 \to 2$ scatterings

Now, let's extract in detail the full amplitudes (4.1) for the 10 processes of Table 4.1. We will present the $SU(3)_c$ results, but of course these can be generalized to the rest gauge groups. In all processes we fix the incoming and outgoing momenta by $k_1 + k_2 = p_1 + p_2$ with

[1]As shown in [36] the splitting of the amplitudes in resummed and non-resummed contributions violates the gauge invariance. Therefore a gauge dependence of the result is expected.

$s = (k_1 + k_2)^2$, $t = (k_1 - p_1)^2$, and $u = (k_1 - p_2)^2$. The particle 4 can be the gravitino or the goldstino. The processes A, B, and F are not present for the $U(1)_Y$ gauge group since there is no self-coupling of gauge bosons for an abelian gauge theory, thereby also the SUSY version of the relevant three-gauge boson vertex is absent.The amplitudes are summarized below:

- **Amplitudes for the process A:** $gg \to \tilde{g}\widetilde{G}$

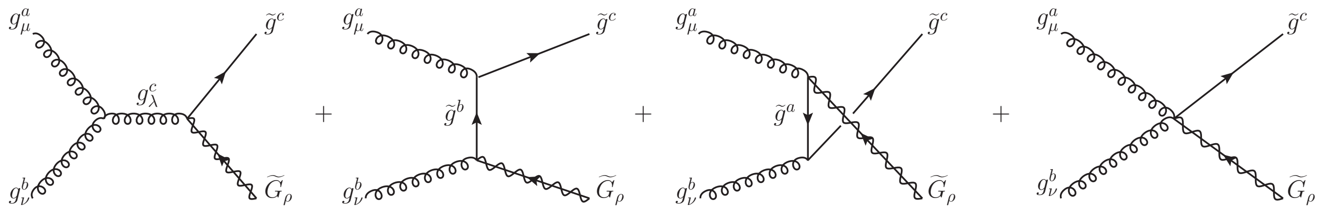

Figure 4.2: Feynman diagrams of process A.

There are four Feynman diagrams, (1): with a g propagator in the s-channel, (2): a $\tilde{g}$ propagator in the t-channel, (3): a $\tilde{g}$ propagator in the u-channel, and (4): with the four-point interaction.

$$\mathcal{M}_{A,s} = \frac{g_3}{4M_{\rm P}s} f^{abc} V^{\mu\nu\delta}(k_1, k_2, -k_1 - k_2)\bar{u}(p_1)\gamma^\rho[\not{k}_1 + \not{k}_2, \gamma_\delta]v_\rho(p_2)\epsilon_\mu(k_1)\epsilon_\nu(k_2)\,, \quad (4.5)$$

$$\mathcal{M}_{A,t} = \frac{g_3}{4M_{\rm P}} \frac{f^{abc}}{t - m_{\tilde{g}}^2} \bar{u}(p_1)\gamma^\mu(\not{k}_2 - \not{p}_2 + m_{\tilde{g}})\gamma^\rho[\not{k}_2, \gamma^\nu]v_\rho(p_2)\epsilon_\mu(k_1)\epsilon_\nu(k_2)\,, \quad (4.6)$$

$$\mathcal{M}_{A,u} = -\frac{g_3}{4M_{\rm P}} \frac{f^{abc}}{u - m_{\tilde{g}}^2} \bar{u}(p_1)\gamma^\nu(\not{k}_1 - \not{p}_2 + m_{\tilde{g}})\gamma^\rho[\not{k}_1, \gamma^\mu]v_\rho(p_2)\epsilon_\mu(k_1)\epsilon_\nu(k_2)\,, \quad (4.7)$$

$$\mathcal{M}_{A,x} = -\frac{g_3}{4M_{\rm P}} f^{abc}\bar{u}(p_1)\gamma^\rho[\gamma^\mu, \gamma^\nu]v_\rho(p_2)\epsilon_\mu(k_1)\epsilon_\nu(k_2)\,. \quad (4.8)$$

For the $\xi = 1$ gauge we also need the matrix elements with the incoming FP-ghosts for the

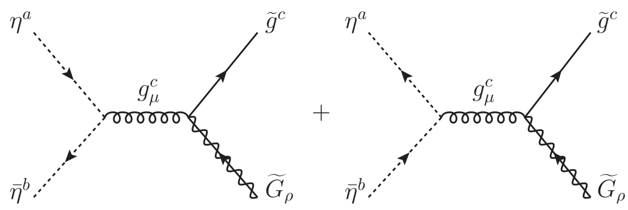

Figure 4.3: Feynman diagrams with FP-ghosts in the $\xi = 1$ gauge for the process A.

gluon. There are two graphs possible,

$$\mathcal{M}_{A,\eta} = \frac{g_3}{4M_{\rm P}} f^{abc}\bar{u}(p_1)\gamma^\rho[\not{k}_1 + \not{k}_2, \not{k}_2]v_\rho(p_2)\,, \quad (4.9)$$

$$\mathcal{M}_{A,\bar{\eta}} = -\frac{g_3}{4M_{\rm P}} f^{abc}\bar{u}(p_1)\gamma^\rho[\not{k}_1 + \not{k}_2, \not{k}_1]v_\rho(p_2)\,. \quad (4.10)$$

Using the amplitudes above along with Eq. (2.27) and Eq. (4.1) we obtain the result for the full squared amplitude

$$|\mathcal{M}_{A,\mathrm{full}}|^2 = \frac{4g_3^2 C_3}{M_\mathrm{P}^2}\left(1+\frac{m_{\tilde g}^2}{3m_{3/2}^2}\right)\left(s+2t+2\frac{t^2}{s}\right). \tag{4.11}$$

- **Amplitudes for the process B:** $g\tilde g \to g\widetilde G$

Due to a crossing symmetry between processes A and B, the squared amplitude of B can be obtained from (4.11) under the exchange $s \leftrightarrow t$ and the addition of an overall minus sign, that is

$$|\mathcal{M}_{B,\mathrm{full}}|^2 = -\frac{4g_3^2 C_3}{M_\mathrm{P}^2}\left(1+\frac{m_{\tilde g}^2}{3m_{3/2}^2}\right)\left(t+2s+2\frac{s^2}{t}\right). \tag{4.12}$$

- **Amplitudes for the process C:** $\tilde q g \to q\widetilde G$

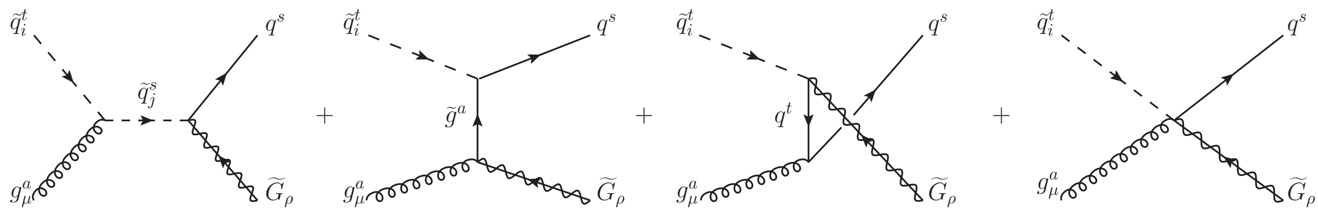

Figure 4.4: Feynman diagrams of process C .

There are four Feynman diagrams, (1): with a $\tilde q$ propagator in the s-channel, (2): a $\tilde g$ propagator in the t-channel, (3): a q propagator in the u-channel, and (4): with the four-point interaction,

$$\mathcal{M}_{C,s} = \frac{ig_3}{\sqrt{2}M_\mathrm{P}}\frac{T_{a,\,st}}{s-m_{\tilde q_i}^2}\bar u(p_1)\gamma^\rho(\not k_1+\not k_2)\alpha_{RL}^{i*}v_\rho(p_2)(2k_1+k_2)^\mu\epsilon_\mu(k_2)\,, \tag{4.13}$$

$$\mathcal{M}_{C,t} = \frac{i\sqrt{2}g_3}{4M_\mathrm{P}}\frac{T_{a,\,st}}{t-m_{\tilde g}^2}\bar u(p_1)\alpha_{RL}^{i*}(\not k_1-\not p_1-m_{\tilde g})\gamma^\rho[\not k_2,\gamma^\mu]v_\rho(p_2)\epsilon_\mu(k_2)\,, \tag{4.14}$$

$$\mathcal{M}_{C,u} = \frac{ig_3}{\sqrt{2}M_\mathrm{P}}\frac{T_{a,\,st}}{u-m_q^2}\bar u(p_1)\gamma^\mu(\not k_1-\not p_2+m_q)\gamma^\rho\not k_1\alpha_{RL}^{i*}v_\rho(p_2)\epsilon_\mu(k_2)\,, \tag{4.15}$$

$$\mathcal{M}_{C,x} = -\frac{ig_3}{\sqrt{2}M_\mathrm{P}}T_{a,\,st}\bar u(p_1)\gamma^\rho\gamma^\mu\alpha_{RL}^{i*}v_\rho(p_2)\epsilon_\mu(k_2)\,. \tag{4.16}$$

The full squared amplitude reads

$$|\mathcal{M}_{C,\mathrm{full}}|^2 = \frac{2g_3^2 C_3'}{M_\mathrm{P}^2}\left(1+\frac{m_{\tilde g}^2}{3m_{3/2}^2}\right)s\,. \tag{4.17}$$

- **Amplitudes for the process D:** $gq \to \tilde q\widetilde G$

Due to a crossing symmetry between processes C and D, the squared amplitude of D can be obtained from (4.17) under the exchange $s \leftrightarrow t$ and the addition of an overall minus sign, that is

$$|\mathcal{M}_{D,\mathrm{full}}|^2 = -\frac{2g_3^2 C_3'}{M_\mathrm{P}^2}\left(1+\frac{m_{\tilde g}^2}{3m_{3/2}^2}\right)t\,. \tag{4.18}$$

- **Amplitudes for the process E:** $\tilde q q \to g\widetilde G$

Due to a crossing symmetry between processes C and E, the squared amplitude of E can be obtained from (4.17) under the exchange $s \leftrightarrow t$ and the addition of an overall minus sign, that is

$$|\mathcal{M}_{E,\text{full}}|^2 = -\frac{2g_3^2 C_3'}{M_\text{P}^2}\left(1 + \frac{m_{\tilde{g}}^2}{3m_{3/2}^2}\right) t\,. \tag{4.19}$$

- **Amplitudes for the process F:** $\tilde{g}\tilde{g} \to \tilde{g}\widetilde{G}$

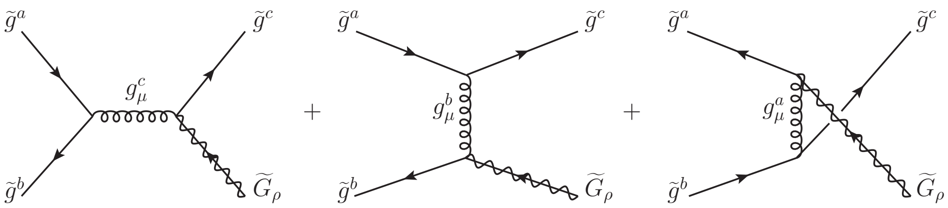

Figure 4.5: Feynman diagrams of process F.

There are three Feynman diagrams, (1): with a g propagator in the s-channel, (2): a g propagator in the t-channel, and (3): a g propagator in the u-channel. Here one has to be careful because $\mathcal{M}_t$ gets an additional minus sign from the fermionic statistics.

$$\begin{aligned}
\mathcal{M}_{F,s} &= -\frac{g_3}{4M_\text{P}s} f^{abc}\bar{v}(k_2)\gamma_\mu u(k_1)\bar{u}(p_1)\gamma^\rho[\not{k}_1 + \not{k}_2, \gamma^\mu]v_\rho(p_2)\,, & (4.20)\\
\mathcal{M}_{F,t} &= \frac{g_3}{4M_\text{P}t} f^{abc}\bar{u}(p_1)\gamma_\mu u(k_1)\bar{v}(k_2)\gamma^\rho[\not{p}_1 - \not{k}_1, \gamma^\mu]v_\rho(p_2)\,, & (4.21)\\
\mathcal{M}_{F,u} &= -\frac{g_3}{4M_\text{P}u} f^{abc}\bar{u}(p_1)\gamma_\mu u(k_2)\bar{v}(k_1)\gamma^\rho[\not{k}_2 - \not{p}_1, \gamma^\mu]v_\rho(p_2)\,. & (4.22)
\end{aligned}$$

The full squared amplitude reads

$$|\mathcal{M}_{F,\text{full}}|^2 = \frac{8g_3^2 C_3}{M_\text{P}^2}\left(1 + \frac{m_{\tilde{g}}^2}{3m_{3/2}^2}\right)\frac{(s^2+t^2+u^2)^2}{stu}\,. \tag{4.23}$$

- **Amplitudes for the process G:** $q\tilde{g} \to q\widetilde{G}$

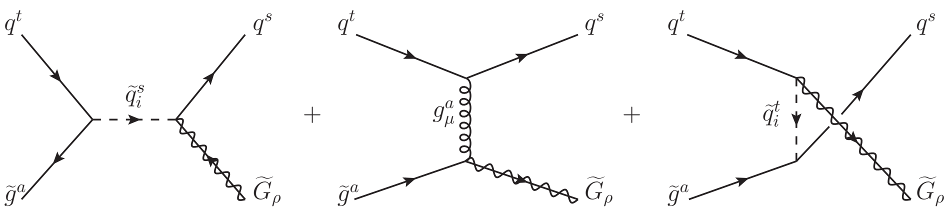

Figure 4.6: Feynman diagrams of process G.

There are three Feynman diagrams, (1): with a $\tilde{q}$ propagator in the s-channel, (2): a g propagator in the t-channel, and (3): a $\tilde{q}$ propagator in the u-channel. Here one has to be careful because $\mathcal{M}_{G,u}$ gets an additional minus sign from the fermionic statistics.

$$\mathcal{M}_{G,s} = -\frac{ig_3}{M_{\rm P}}\frac{T_{a,\,st}}{s-m^2_{\tilde{q}_i}}\bar{v}(k_2)\alpha^i_{LR}u(k_1)\bar{u}(p_1)\gamma^\mu(\not{k}_1+\not{k}_2)\alpha^{i*}_{RL}v_\mu(p_2)\,, \tag{4.24}$$

$$\mathcal{M}_{G,t} = \frac{ig_3}{4M_{\rm P}}\frac{T_{a,\,st}}{t}\bar{u}(p_1)\gamma_\mu u(k_1)\bar{u}_\mu(p_2)[\not{k}_1-\not{p}_1,\gamma^\nu]\gamma^\mu u(k_2)\,, \tag{4.25}$$

$$\mathcal{M}_{G,u} = \frac{ig_3}{M_{\rm P}}\frac{T_{a,\,st}}{u-m^2_{\tilde{q}_i}}\bar{u}(p_1)\alpha^{i*}_{RL}u(k_2)\bar{u}_\mu(p_2)(\not{p}_2-\not{k}_1)\gamma^\mu\alpha^{i*}_{LR}u(k_1)\,. \tag{4.26}$$

The full squared amplitude reads

$$|\mathcal{M}_{G,\rm full}|^2 = \frac{-4g_3^2C_3'}{M_{\rm P}^2}\left(1+\frac{m^2_{\tilde{g}}}{3m^2_{3/2}}\right)\left(s+\frac{s^2}{t}\right)\,. \tag{4.27}$$

- **Amplitudes for the process H:** $\tilde{q}\tilde{g} \to \tilde{q}\widetilde{G}$

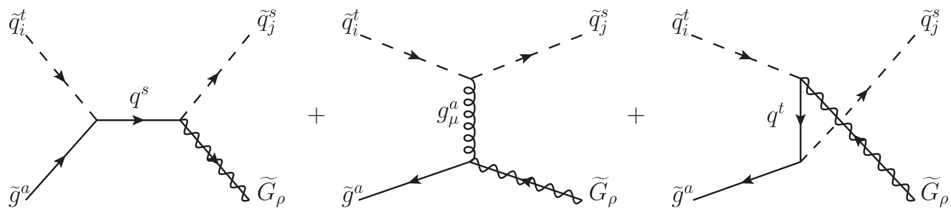

Figure 4.7: Feynman diagrams of process H.

There are three Feynman diagrams, (1): with a q propagator in the s-channel, (2): a g propagator in the t-channel, and (3): a q propagator in the u-channel. Here one has to be careful because $\mathcal{M}_{H,s}$ gets an additional minus sign from the fermionic statistics.

$$\mathcal{M}_{H,s} = -\frac{ig_3}{M_{\rm P}}\frac{T_{a,\,st}}{s-m^2_q}\bar{u}_\rho(p_2)\not{p}_1\gamma^\rho\alpha^j_{LR}(\not{k}_1+\not{k}_2+m_q)\alpha^{i*}_{RL}u(k_2)\,, \tag{4.28}$$

$$\mathcal{M}_{H,t} = \frac{ig_3}{4M_{\rm P}t}T_{a,\,st}\bar{v}(k_2)\gamma^\rho[\not{k}_1-\not{p}_1,\not{k}_1+\not{p}_1]v_\rho(p_2)\delta_{ij}\,, \tag{4.29}$$

$$\mathcal{M}_{H,u} = \frac{ig_3}{M_{\rm P}}\frac{T_{a,\,st}}{u-m^2_q}\bar{v}(k_2)\alpha^j_{LR}(\not{k}_1-\not{p}_2+m_q)\gamma^\rho\not{k}_1\alpha^{i*}_{RL}v_\rho(p_2)\,. \tag{4.30}$$

The full squared amplitude reads

$$|\mathcal{M}_{H,\rm full}|^2 = \frac{-2g_3^2C_3'}{M_{\rm P}^2}\left(1+\frac{m^2_{\tilde{g}}}{3m^2_{3/2}}\right)\left(t+2s+\frac{2s^2}{t}\right)\,. \tag{4.31}$$

- **Amplitudes for the process I:** $q\tilde{q} \to \tilde{g}\widetilde{G}$

Due to a crossing symmetry between processes G and I, the squared amplitude of I can be obtained from (4.27) under the exchange $s \leftrightarrow t$, that is

$$|\mathcal{M}_{I,\rm full}|^2 == \frac{-4g_3^2C_3'}{M_{\rm P}^2}\left(1+\frac{m^2_{\tilde{g}}}{3m^2_{3/2}}\right)\left(t+\frac{t^2}{s}\right)\,. \tag{4.32}$$

- **Amplitudes for the process J:** $\tilde{q}\bar{\tilde{q}} \to \tilde{g}\widetilde{G}$

Due to a crossing symmetry between processes H and J, the squared amplitude of J can be obtained from (4.31) under the exchange $s \leftrightarrow t$ and the addition of an overall minus sign, that is

$$|\mathcal{M}_{J,\mathrm{full}}|^2 = \frac{2g_3^2 C_3'}{M_\mathrm{P}^2}\left(1+\frac{m_{\tilde{g}}^2}{3m_{3/2}^2}\right)\left(s+2t+\frac{2t^2}{s}\right). \tag{4.33}$$

4.1.1 The nonderivative approach

In the nonderivative approach given by Eq. (2.43), one has new Feynman rules, which can be found *e.g.* in [37] or in [32]. The goldstino-fermion-sfermion-gluon vertex vanishes and there occurs a new coupling, goldstino-gaugino-sfermion-sfermion. The goldstino-fermion-sfermion coupling is proportional to $m_f^2 - m_{\tilde{f}}^2$. All the other couplings are proportional to the gaugino mass term $m_{\lambda^{(\alpha)}}$. We are only interested in the massless limit, thus we set the goldstino-fermion-sfermion coupling to zero. We again give only the results for $SU(3)_c$.

We will give in explicit the new amplitudes for the five independent processes (A, C, F, G and H). From these we will calculate the subtracted part (see Table 4.1), which differs from the one calculated in [36]. For convenience we define a prefactor,

$$pre = \frac{m_{\tilde{g}}}{2\sqrt{6}M_\mathrm{P}m_{3/2}}g_3(f^{abc}\,|\,T_{a,rs}), \tag{4.34}$$

where f^{abc} ($T_{a,rs}$) is taken in processes without (with) quarks and squarks.

• **Amplitudes for the process A:** $gg \to \tilde{g}\chi$

For this process we have again four Feynman diagrams, (1): with a g propagator in the s-channel, (2): a $\tilde{g}$ propagator in the t-channel, (3): a $\tilde{g}$ propagator in the u-channel, and (4): with the four-point interaction.

$$\begin{aligned}
\mathcal{M}_{A,s} &= -i\frac{pre}{s}V^{\mu\nu\rho}(k_1,k_2,-k_1-k_2)\bar{u}(p_2)[\not{k}_1+\not{k}_2,\gamma_\rho]v(p_1)\epsilon_\mu(k_1)\epsilon_\nu(k_2), && (4.35)\\
\mathcal{M}_{A,t} &= i\frac{pre}{t}\bar{u}(p_2)[\not{k}_2,\gamma^\nu](\not{k}_1-\not{p}_1)\gamma^\mu v(p_1)\epsilon_\mu(k_1)\epsilon_\nu(k_2), && (4.36)\\
\mathcal{M}_{A,u} &= -i\frac{pre}{u}\bar{u}(p_2)[\not{k}_1,\gamma^\mu](\not{k}_2-\not{p}_1)\gamma^\nu v(p_1)\epsilon_\mu(k_1)\epsilon_\nu(k_2), && (4.37)\\
\mathcal{M}_{A,x} &= i\,pre\,\bar{u}(p_2)[\gamma^\mu,\gamma^\nu]v(p_1)\epsilon_\mu(k_1)\epsilon_\nu(k_2). && (4.38)
\end{aligned}$$

For the $\xi = 1$ gauge we also need the matrix elements with the incoming FP-ghosts for the gluon. There are two graphs possible,

$$\begin{aligned}
\mathcal{M}_{A,\eta} &= -i\,\frac{pre}{s}\,\bar{u}(p_2)\gamma^\rho[\not{k}_1+\not{k}_2,\not{k}_2]v(p_1), && (4.39)\\
\mathcal{M}_{A,\bar{\eta}} &= -i\,\frac{pre}{s}\,\bar{u}(p_2)\gamma^\rho[\not{k}_1+\not{k}_2,\not{k}_1]v(p_1). && (4.40)
\end{aligned}$$

• **Amplitudes for the process C:** $\tilde{q}g \to q\chi$

For this process we have only one graph with a $\tilde{g}$ propagator in the t-channel.

$$\mathcal{M}_{C,t} = ipre\frac{\sqrt{2}}{t}\bar{u}(p_1)\alpha_{RL}^{i*}(\not{k}_1-\not{p}_1)[\not{k}_2,\gamma^\mu]v(p_2)\epsilon_\mu(k_2). \tag{4.41}$$

• **Amplitudes for the process F:** $\tilde{g}\tilde{g} \to \tilde{g}\chi$

For this process we have again three Feynman diagrams, (1): with a g propagator in the

s-channel, (2): a g propagator in the t-channel, and (3): a g propagator in the u-channel.

$$\begin{aligned} \mathcal{M}_{F,s} &= i\frac{pre}{s}\bar{v}(k_2)\gamma_\mu u(k_1)\bar{u}(p_2)[\not{k}_1+\not{k}_2,\gamma^\mu]v(p_1)\,, && (4.42)\\ \mathcal{M}_{F,t} &= -i\frac{pre}{t}\bar{u}(p_1)\gamma_\mu u(k_1)\bar{u}(p_2)[\not{p}_1-\not{k}_1,\gamma^\mu]u(k_2)\,, && (4.43)\\ \mathcal{M}_{F,u} &= i\frac{pre}{t}\bar{u}(p_1)\gamma_\mu u(k_2)\bar{u}(p_2)[\not{p}_2-\not{k}_1,\gamma^\mu]u(k_1)\,,. && (4.44) \end{aligned}$$

- **Amplitudes for the process G:** $qg \to q\chi$

For this process we have only one graph with a g propagator in the t-channel.

$$\mathcal{M}_{G,t} = i\frac{pre}{t}\bar{u}(p_1)\gamma_\mu u(k_1)\bar{u}(p_2)[\not{k}_1-\not{p}_1,\gamma^\mu]u(k_2)\,. \tag{4.45}$$

- **Amplitudes for the process H:** $\tilde{q}\tilde{g} \to \tilde{q}\chi$

For this process we have two graphs, instead of three, (1): with a g propagator in the t-channel, and a new one (2): with a four-point interaction.

$$\begin{aligned} \mathcal{M}_{H,t} &= \frac{pre}{t}\bar{u}(p_2)[\not{k}_1-\not{p}_1,\not{p}_1+\not{k}_1]u(k_2)\,, && (4.46)\\ \mathcal{M}_{H,x} &= 2\,pre\,\bar{u}(p_2)\gamma_5 u(k_2)\,. && (4.47) \end{aligned}$$

4.2 The subtracted contribution

In the fourth column of Table 4.1 we present the so-called subtracted part (4.3), which is the sum of the interference terms between the four types of diagrams (s, t, u, x), plus the x-diagram squared, for each process. If we use the amplitudes computed in the nonderivative approach, we see that the only nonzero contributions are those of processes A and B, which are

$$\begin{aligned} |\mathcal{M}_{A,\mathrm{sub}}|^2 &= \frac{1}{2}\frac{g_3^2}{M_\mathrm{P}^2}\left(1+\frac{m_{\tilde{g}}^2}{3m_{3/2}^2}\right)(-2sC_N)\,, && (4.48)\\ |\mathcal{M}_{B,\mathrm{sub}}|^2 &= \frac{g_3^2}{M_\mathrm{P}^2}\left(1+\frac{m_{\tilde{g}}^2}{3m_{3/2}^2}\right)(2tC_N)\,. && (4.49) \end{aligned}$$

The extra factor 1/2 in (4.48) comes from the 2 identical incoming particles. Note that in [36] the subtracted part for processes H and J is also nonzero; we assume that the authors used the squark-squark-gluino-goldstino Feynman rule as given in [32], where in fact a factor γ_5 is missing. In contrast, we use the correct Feynman rule as given in [37].

To calculate the subtracted rate for the processes $a\,b \to c\,\widetilde{G}$, we use the general form

$$\mathcal{C} = \frac{1}{(2\pi)^8}\int\frac{d^3\mathbf{p}_a}{2E_a}\frac{d^3\mathbf{p}_b}{2E_b}\frac{d^3\mathbf{p}_c}{2E_c}\frac{d^3\mathbf{p}_{\widetilde{G}}}{2E_{\widetilde{G}}}\,|\mathcal{M}|^2\,f_a\,f_b\,(1\pm f_c)\times\delta^4(P_a+P_b-P_c-P_{\widetilde{G}})\,, \tag{4.50}$$

where f_i stands for the usual Bose and Fermi statistical densities

$$f_{B,F} = \frac{1}{e^{\frac{E}{T}}\mp 1}\,. \tag{4.51}$$

In the temperature range of interest, all particles exept the gravitino are in thermal equilibrium. For the gravitino the statistical factor $f_{\widetilde{G}}$ is negligible. Thus, $1-f_{\widetilde{G}} \simeq 1$, as it is already used in (4.50). Moreover, backward reactions are neglected. In addition, the simplification $1\pm f_c \simeq 1$ is usually used, which allows the analytical computation of (4.50). In our case,

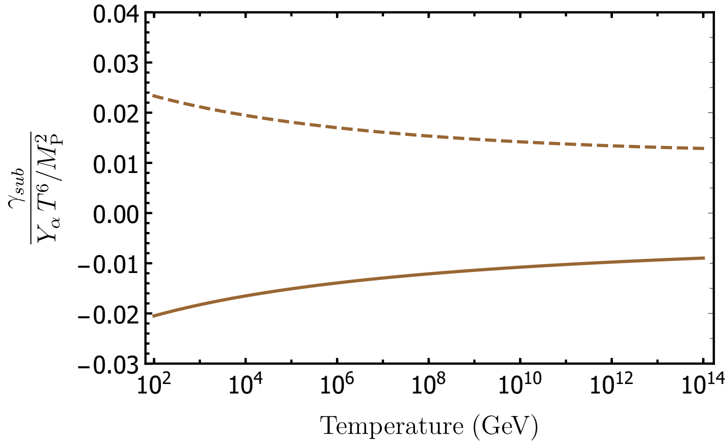

Figure 4.8: The subtracted rate divided by $Y_\alpha T^6/M_{\rm P}^2$. The solid line corresponds to the subtracted rate given by Eq. (4.52), while the dashed one has been calculated in [36].

there is no such reason. We keep the factor $1 \pm f_c$ and consequently proceed numerically in the calculation of the subtracted rate[2]. In Appendix C, following the technique presented in [37], we present the calculation of the subtracted rate in detail, together with other cases of matrix elements not needed for this calculation but shown for completeness. Substituting the Eqs. (4.48) and (4.49) into (4.50), the subtracted rate is obtained as[3]

$$\gamma_{\rm sub} = \frac{T^6}{M_{\rm P}^2} \sum_{\alpha=1}^{3} g_\alpha^2 \left(1 + \frac{m_{\lambda(\alpha)}^2}{3m_{3/2}^2}\right) C_\alpha \left(-\mathcal{C}^s_{\rm BBF} + 2\,\mathcal{C}^t_{\rm BFB}\right) . \tag{4.52}$$

Note that, although in (4.52) we sum over the three gauge groups, the subtracted rate for the $U(1)_Y$ gauge group is identically zero since $C_1 = 0$. The numerical factors, calculated by using the Cuba library [306], are $\mathcal{C}^s_{\rm BBF} = 0.25957 \times 10^{-3}$ and $\mathcal{C}^t_{\rm BFB} = -0.13286 \times 10^{-3}$. The subscripts B and F indicate whether the particles are bosons and fermions, respectively, and the superscripts determine whether the squared amplitude is proportional to s or t. It is easy to see that, unlike in [36], our result for the subtracted part is negative. This is not unphysical, since the total rate, not the subtracted rate, must be positive. Figure 4.8 shows the subtracted rate (4.52) and the one calculated in [36].

4.3 The $D-$graph contribution

As discussed above, Eq. (4.2) describes the relation between the $D-$graph and the sum of squared amplitudes for the channels s, t, and u. In the $D-$graph contribution, we implement the resummed thermal corrections to the gauge boson and gaugino propagators[4]. Although Fig. 4.1 shows the gluino-gluon thermal loop, the contributions of all gauge groups are included in our analysis. The momentum flow used to calculate the $D-$graph can be seen in Fig. 4.1. That is $\widetilde{G}(P) \to g(K) + \tilde{g}(Q)$, with

$$P = (p, p, 0, 0)\,,\; K = (k_0, k\cos\theta_k, k\sin\theta_k, 0)\,,\text{ and } Q = (q_0, q\cos\theta_q, q\sin\theta_q, 0)\,, \tag{4.53}$$

[2]As it was argued in [32] and we have checked numerically, the effect of taking into account the statistical factor f_c can be about -10% ($+20\%$) if c is a fermion (boson). See Table C.3 in Appendix C.

[3]In (4.50) the collision term is denoted by $\mathcal{C}$, while in (4.52) by $\gamma_{\rm sub}$ in order to maintain the previous notation.

[4]Like in [36] using the gravitino polarization sum (2.29), we nullify the corresponding quark-squark $D-$graph.

where $\theta_{k,q}$ are the polar angles of the corresponding 3-momenta $\mathbf{k}, \mathbf{q}$ in spherical coordinates. Here, we have already assumed that the gravitino is massless compared to the high temperature of the thermal bath, that is $P^2 = 0$.

We have 7 variables, p, k, q, k_0, q_0, c_k and c_q, and three non-trivial equations due to the overall momentum conservation, $P^i = K^i + Q^i$, $i = 0, 1, 2$. Thus, we are left with 4 independent variables. Using the momentum conservation we obtain that

$$\begin{aligned} p &= k_0 + q_0\,, &(4.54)\\ c_k &= \frac{p^2 - q^2 + k^2}{2kp}\,, &(4.55)\\ c_q &= \frac{p^2 + q^2 - k^2}{2pq}\,, &(4.56)\\ cos(\theta_k - \theta_q) &= \frac{p^2 - q^2 - k^2}{2kq}\,. &(4.57)\end{aligned}$$

In order to calculate the gravitino selfenergy with vector-gaugino loop in the massless case we need the Feynman rules for the two vertices. The gluon-gluino-gravitino interaction is given by Eq. (2.31) (see also [78]) and after obeying the equivalence theorem, the goldstino interaction can be read from (2.43). Thus, the goldstino selfenergy with gluon-gluino loop including the outer goldstino legs can be written as

$$\Pi = \frac{1}{8M_P^2} n_3 \frac{m_{\tilde{g}}^2}{3m_{3/2}^2} \int \frac{\mathrm{d}^4K}{(2\pi)^4} \mathrm{Tr}\left(\not{P}[\not{K}, \gamma^\mu] S(Q) [\not{K}, \gamma^\nu] D_{\mu\nu}(K)\right)\,, \tag{4.58}$$

in which $S(Q)$ is the gluino propagator, $D_{\mu\nu}(K)$ the gluon propagator, and $n_3 = 8$ from the color running in the loop. Now, we can easily generalize that to the expression $\Pi^<$, including all three groups, $U(1)_Y$, $SU(2)_L$ and $SU(3)_c$, with $n_1 = 1$ and $n_2 = 3$. As we use the non-time ordered selfenergy $\Pi^<$, we get an additonal factor $1/2$, that is

$$\Pi^<(P) = \frac{1}{16M_\mathrm{P}^2} \sum_{\alpha=1}^{3} n_\alpha \left(1 + \frac{m_{\lambda(\alpha)}^2}{3m_{3/2}^2}\right) \int \frac{\mathrm{d}^4K}{(2\pi)^4} \mathrm{Tr}\left(\not{P}[\not{K}, \gamma^\mu]\, {}^*S^<(Q) [\not{K}, \gamma^\nu]\, {}^*D_{\mu\nu}^<(K)\right)\,, \tag{4.59}$$

with the thermally resummed propagators denoted by a *,

$$\begin{aligned} {}^*S^<(Q) &= \frac{f_F(q_0)}{2}\left[(\gamma_0 - \gamma^i \hat{q}^i)\rho_+(Q) + (\gamma_0 + \gamma^i \hat{q}^i)\rho_-(Q)\right]\,, &(4.60)\\ {}^*D_{\mu\nu}^<(K) &= f_B(k_0)\left[\Pi_{\mu\nu}^T \rho_T(K) + \Pi_{\mu\nu}^L \frac{k^2}{K^2}\rho_L(K) + \xi \frac{K_\mu K_\nu}{K^4}\right]\,, &(4.61)\end{aligned}$$

with $\hat{q}^i = q^i/q$. In (4.59) we have also incorporated the helicity $\pm 3/2$ components of the gravitino, as in [31] it has been shown, up to two loop order in the gauge couplings, that one obtains the characteristic factor $1 + m_{\lambda(\alpha)}^2/3m_{3/2}^2$, as well as in the calculation of the $2 \to 2$ scatterings.

Using the paremetrization (4.53) and the abbreviations for cosine and sine, we get for the different spectral function combinations the following results:

$$\begin{aligned} &\propto \rho_-\rho_L : & &16\, p\, k^2 (c_{2k} c_q + s_{2k} s_q + 1)\,, &(4.62)\\ &\propto \rho_+\rho_L : & &16\, p\, k^2 (-c_{2k} c_q - s_{2k} s_q + 1)\,, &(4.63)\\ &\propto \rho_-\rho_T : & &16\, p \left((k_0^2 + k^2)(2 - cos(2\theta_k - \theta_q) - c_q) - 4k_0 k (c_k - cos(\theta_k - \theta_q))\right)\,, &(4.64)\\ &\propto \rho_+\rho_T : & &16\, p \left((k_0^2 + k^2)(2 + cos(2\theta_k - \theta_q) + c_q) - 4k_0 k (c_k + cos(\theta_k - \theta_q))\right)\,. &(4.65)\end{aligned}$$

Note, that $c_{2k}c_q+s_{2k}s_q+1 = 2\cos^2\frac{2\theta_k-\theta_q}{2}$ and $-c_{2k}c_q-s_{2k}s_q+1 = 2\sin^2\frac{2\theta_k-\theta_q}{2}$. Substituting these in Eq. (4.59) we get

$$\begin{aligned}
\Pi^<(P) \;=\; & \frac{1}{32M_{\mathrm{P}}^2}\sum_{\alpha=1}^{3} n_\alpha\left(1+\frac{m_{\lambda(\alpha)}^2}{3m_{3/2}^2}\right)\int\frac{\mathrm{d}^4K}{(2\pi)^4}f_F(q_0)f_B(k_0)\times \\
& \Bigg[\rho_L(K)\rho_-(Q)32\,p\,k^2\cos^2\frac{2\theta_k-\theta_q}{2}+\rho_L(K)\rho_+(Q)32\,p\,k^2\sin^2\frac{2\theta_k-\theta_q}{2} \\
& +\rho_T(K)\rho_-(Q)16\,p\left((k_0^2+k^2)(2-cos(2\theta_k-\theta_q)-c_q)-4k_0k(c_k-cos(\theta_k-\theta_q))\right) \\
& +\rho_T(K)\rho_+(Q)16\,p\left((k_0^2+k^2)(2+cos(2\theta_k-\theta_q)+c_q)-4k_0k(c_k+cos(\theta_k-\theta_q))\right)\Bigg].
\end{aligned} \tag{4.66}$$

In order to compute the integral (4.66) it is convenient to multiply by the 4-momentum δ-function $\int\mathrm{d}^4Q\,\delta^4(K+Q-P)=1$. Also, using the relations

$$\begin{aligned}
\mathrm{d}^4K &= \mathrm{d}k_0\,k^2\mathrm{d}k\,\mathrm{d}cos\theta_k\,\mathrm{d}\phi_k\,, \\
\mathrm{d}^4Q &= \mathrm{d}q_0\,q^2\mathrm{d}q\,\mathrm{d}cos\theta_q\,\mathrm{d}\phi_q\,,
\end{aligned} \tag{4.67}$$

we can perform the integrations $\mathrm{d}q_0$, $\mathrm{d}cos\theta_q$, $\mathrm{d}cos\theta_k$ and $\mathrm{d}\phi_k$ thanks to the δ-function. Nothing depends on $\mathrm{d}\phi_k$, so we get an extra 2π from this integration. After these integrations the Eqs. (4.62)-(4.65) become,

$$\propto \rho_-\rho_L: \quad \frac{8}{q}(p-q)^2((p+q)^2-k^2)\,, \tag{4.68}$$

$$\propto \rho_+\rho_L: \quad \frac{8}{q}(p+q)^2(k^2-(p-q)^2)\,, \tag{4.69}$$

$$\propto \rho_-\rho_T: \quad \frac{8}{q}\left(k^2-(p-q)^2\right)\left(\left(1+\frac{k_0^2}{k^2}\right)\left(k^2+(p+q)^2\right)-4k_0(p+q)\right), \tag{4.70}$$

$$\propto \rho_+\rho_T: \quad \frac{8}{q}\left((p+q)^2-k^2\right)\left(\left(1+\frac{k_0^2}{k^2}\right)\left(k^2+(p-q)^2\right)-4k_0(p-q)\right), \tag{4.71}$$

and the resummed propagator (4.66) takes the form

$$\begin{aligned}
\Pi^<(P) \;=\; & \frac{1}{4(2\pi)^3}\frac{1}{M_{\mathrm{P}}^2}\sum_{\alpha=1}^{3} n_\alpha\left(1+\frac{m_{\lambda(\alpha)}^2}{3m_{3/2}^2}\right)\int_{-\infty}^{\infty}\mathrm{d}k_0\int_0^{\infty}\mathrm{d}k\int_{|k-p|}^{k+p}\mathrm{d}q\,\frac{k}{p}f_B(k_0)f_F(p_0-k_0)\times \\
& \Big[\rho_L(K)\rho_-(Q)(p-q)^2((p+q)^2-k^2)+\rho_L(K)\rho_+(Q)(p+q)^2(k^2-(p-q)^2) \\
& +\rho_T(K)\rho_-(Q)\left(k^2-(p-q)^2\right)\left(\left(1+\frac{k_0^2}{k^2}\right)\left(k^2+(p+q)^2\right)-4k_0(p+q)\right) \\
& +\rho_T(K)\rho_+(Q)\left((p+q)^2-k^2\right)\left(\left(1+\frac{k_0^2}{k^2}\right)\left(k^2+(p-q)^2\right)-4k_0(p-q)\right)\Big],
\end{aligned} \tag{4.72}$$

with $q_0 = p-k_0$. In order to compute the production rate γ_D we will use its definition

$$\gamma_D = \int\frac{\mathrm{d}^3\mathbf{p}}{2p_0(2\pi)^3}\Pi^<(p)\,, \tag{4.73}$$

with $\mathrm{d}^3\mathbf{p} = 4\pi p^2 \mathrm{d}p$ in this frame. Then

$$
\begin{aligned}
\gamma_D \;\; = \;\; & \frac{1}{4(2\pi)^5} \frac{1}{M_\mathrm{P}^2} \sum_{\alpha=1}^{3} n_\alpha \left(1 + \frac{m_{\lambda(\alpha)}^2}{3m_{3/2}^2}\right) \int_0^\infty \mathrm{d}p \int_{-\infty}^{\infty} \mathrm{d}k_0 \int_0^\infty \mathrm{d}k \int_{|k-p|}^{k+p} \mathrm{d}q \, k f_B(k_0) f_F(p_0 - k_0) \times \\
& \Big[\rho_L(K)\rho_-(Q)(p-q)^2((p+q)^2 - k^2) + \rho_L(K)\rho_+(Q)(p+q)^2(k^2 - (p-q)^2) \\
& + \rho_T(K)\rho_-(Q)\left(k^2 - (p-q)^2\right)\left(\left(1 + \frac{k_0^2}{k^2}\right)\left(k^2 + (p+q)^2\right) - 4k_0(p+q)\right) \\
& + \rho_T(K)\rho_+(Q)\left((p+q)^2 - k^2\right)\left(\left(1 + \frac{k_0^2}{k^2}\right)\left(k^2 + (p-q)^2\right) - 4k_0(p-q)\right)\Big] . \qquad (4.74)
\end{aligned}
$$

The spectral functions $\rho_{L,T}$ and $\rho_\pm$ can be found in Eqs. (3.68) and (3.96). The thermally corrected one-loop selfenergies for gauge bosons, scalars and fermions that we have used in calculating these spectral functions can be found in Secs. 3.1 and 3.2 or equivalently in various previous works [301, 303, 307–310]. Comparing (4.74) with the corresponding analytical result given in Eqs. (4.6) and (4.7) in [36], one can notice that they differ on the overall factor and on the number of independent phase-space integrations. Our analytical result has been checked using various frames for the momenta flow into the loop. The four dimensional integral (4.74) has been calculated numerically using the Cuba library [306]. As this result is numerical, inspired by [16], we will give an easy to apply formula for this using a suitable interpolating function (see Sec. 4.5).

4.4 The top quark contribution

Previous works [26–35, 37] considered gravitino production only due to gauge couplings, while the authors of [36] dealt also with the contribution of the top quark Yukawa coupling λ_t. As shown in [36], in scatterings involving fermions only, such as quark-quark $\to$ Higgsino-gravitino, the dominant contribution of order T^6/M_P^2 vanishes. On the other hand, scatterings involving two fermions and two scalars, such as squark-squark $\to$ Higgsino-gravitino, give a sizeable scattering rate. As in the scatterings of Table 4.1 the various top quark Yukawa diagrams populate both the spin 1/2 and the spin 3/2 components. The characteristic factor $m_{\lambda_\alpha}^2/3m_{3/2}^2$ linked with the 1/2 component, becomes $A_t^2/3m_{3/2}^2$, where A_t is the trilinear stop supersymmetry breaking soft parameter. It is worth mentioning that the inclusion of thermal masses is not necessary for obtaining a finite result in this case, as the accompanying diagrams are infrared convergent.

The sum of all top scatterings is given by [36]

$$
\sum |\mathcal{M}_{top}|^2 = 72 \frac{\lambda_t^2}{M_\mathrm{P}^2} \left(1 + \frac{A_t^2}{3m_{3/2}^2}\right) s \, , \qquad (4.75)
$$

where s is the usual Mandelstam variable. The resulting production rate reads

$$
\gamma_\mathrm{top} = \frac{T^6}{M_\mathrm{P}^2} 72 \mathcal{C}^s_\mathrm{BBF} \lambda_t^2 \left(1 + \frac{A_t^2}{3m_{3/2}^2}\right) , \qquad (4.76)
$$

where $\mathcal{C}^s_\mathrm{BBF} = 0.25957 \times 10^{-3}$. Since this contribution stems from the squark-squark $\to$ Higgsino-gravitino process, only the numerical factor $\mathcal{C}^s_\mathrm{BBF}$ is involved.

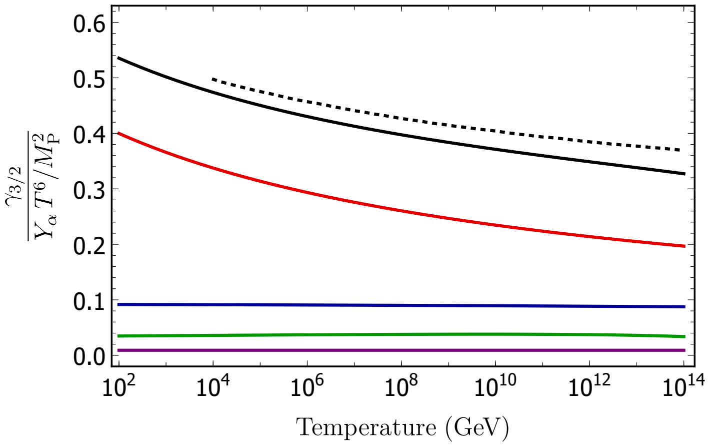

Figure 4.9: Gravitino production rates divided by $Y_\alpha T^6/M_P^2$. The solid curves represent in order the total rate (black) given by (4.4), the $SU(3)_c$ (red), $SU(2)_L$ (blue), and $U(1)_Y$ (green) rates given by (4.77), and the top Yukawa rate (purple) given by (4.76). The upper dashed curve is the total production rate obtained in [36]. The top Yukawa coupling λ_t was set equal to 0.7, so our result can be directly compared with that in [36].

4.5 Total rate and parametrization

Following [16] we parametrize the results (4.52) and (4.74) using the gauge couplings g_1, g_2 and g_3 . Thus

$$\gamma_{\rm sub} + \gamma_{\rm D} = \frac{3\zeta(3)}{16\pi^3}\,\frac{T^6}{M_P^2}\sum_{\alpha=1}^{3} c_\alpha\, g_\alpha^2 \left(1 + \frac{m_{\lambda(\alpha)}^2}{3m_{3/2}^2}\right)\ln\left(\frac{k_\alpha}{g_\alpha}\right), \tag{4.77}$$

where the constants c_α and k_α depend on the gauge group and their values are given in

Table 4.2: The values of the constants c_α and k_α that parametrize our result (4.77) for the subtracted and the $D-$graph part. Each line corresponds to the particular gauge group, $U(1)_Y$, $SU(2)_L$ or $SU(3)_c$.

Gauge group	c_α	k_α
$U(1)_Y$	41.937	0.824
$SU(2)_L$	68.228	1.008
$SU(3)_c$	21.067	6.878

Table 4.2. In Fig. 4.9 we summarize our numerical results for the gravitino production rates divided by $Y_\alpha T^6/M_P^2$. In particular, for the case of the top Yukawa contribution, in Y_α the $m_{\lambda(\alpha)}^2$ must be replaced by A_t^2. The colored solid curves represent the $SU(3)_c$ (red), $SU(2)_L$ (blue), and $U(1)_Y$ (green) rates given by (4.77) and the top Yukawa rate (purple) given by (4.76), while the solid black curve is the total result given by (4.4). The dashed black curve corresponds to the total result from [36]. For comparison, we also chose $\lambda_t = 0.7$. The gauge framework of our calculation is the MSSM gauge group $SU(3)_c \times SU(2)_L \times U(1)_Y$. Using a different gauge structure like SU(5) or flipped SU(5) [236], apparently constitutes a completely new calculation.

Despite the analytical and numerical discrepancies with [36], it is interesting that our result for the total gravitino production rate is only $5\% - 11\%$ smaller than that in [36]. Since we cannot explain this in detail quantitatively, we assume that the above differences have opposite effects on the total result. For convenience, in Fig. 4.9, universal gauge coupling unification is assumed at the grand unification scale $\simeq 2 \times 10^{16}$ GeV, but certainly the result in (4.77) can be used independently of this assumption. Equation (4.77) together with the numbers in Table 4.2 is the main result of the first part of this thesis.

Chapter 5

Gravitino cosmology

Our result (4.77) for the gravitino production rate has important implications for gravitino cosmology. In this chapter, we compute the gravitino abundance from thermal production. The nonthermal production of gravitinos [11–18], which depends on the model of inflation, has been ignored. Comparing the relic gravitino density with the observed DM, an upper bound on the reheating temperature of the Universe is realized.

5.1 The Boltzmann equation

An homogeneous, isotropic and expanding Universe is described in terms of the Friedmann–Lemaitre–Robertson–Walker (FLRW). The FLRW metric also assumes that the spatial component of the metric can be time-dependent. The generic metric which meets these conditions is

$$ds^2 = dt^2 - \alpha(t)^2 \left[\frac{dr^2}{1 - kr^2} + r^2(d\theta^2 + \sin^2\theta \, d\phi^2) \right] , \tag{5.1}$$

where (t, r, θ, ϕ) are comoving coordinates, $\alpha(t)$ is the scale factor, and $k = -1, 0, 1$ is the curvature parameter which equals to zero for a flat geometry. The evolution of $\alpha(t)$ in a flat spacetime is described by the Friedmann equation

$$H^2 = \left(\frac{\dot{\alpha}(t)}{\alpha(t)} \right)^2 = \frac{\rho}{3M_{\mathrm{P}}^2} , \tag{5.2}$$

where H is the Hubble constant and ρ the total energy density of the Universe.

The Boltzmann equation essentially expresses the action of the so-called Liouville operator $L[f]$ on the phase-space density $f(\vec{x}, |\vec{p}|, t)$, in terms of the so-called collision operator $\mathcal{C}[f]$. For more details we refer the interested reader in the literature [311]. In the general case, the former is written as

$$L[f] = \mathcal{C}[f] . \tag{5.3}$$

The general relativistic form of the Liouville operator is given by

$$L[f] = \left[P^\lambda \frac{\partial}{\partial x^\lambda} - \Gamma^\lambda{}_{\mu\nu} P^\mu P^\nu \frac{\partial}{\partial P^\lambda} \right] f , \tag{5.4}$$

where $\Gamma^\lambda{}_{\mu\nu}$ is the Levi-Civita connection. In a FLRW Universe, we have that $f = f(E_{\widetilde{G}}, t)$, where $E_{\widetilde{G}}$ denotes the energy of the dark matter particle, *i.e.* the gravitino. In such a case, upon using the connection for the FLRW (5.1), we obtain from (5.4) that

$$L[f] = E_{\widetilde{G}} \frac{\partial f}{\partial t} - H |\mathbf{p}_{\widetilde{G}}|^2 \frac{\partial f}{\partial E_{\widetilde{G}}} . \tag{5.5}$$

The number density of gravitinos is defined as

$$n_{3/2} = \frac{g_{\widetilde{G}}}{(2\pi)^3} \int \mathrm{d}^3\mathbf{p}_{\widetilde{G}}\, f(E_{\widetilde{G}}, t)\,, \tag{5.6}$$

where $g_{\widetilde{G}} = 4$ is the number of DOF for the massive gravitino. The $(2\pi)^3$ factor comes from the state density $1/h^3$ in the phase space, once we use natural units with $\hbar = h/(2\pi) = 1$. Now, using (5.3), (5.5) and (5.6) we obtain that

$$E_{\widetilde{G}} \frac{\mathrm{d}n_{3/2}}{\mathrm{d}t} - E_{\widetilde{G}} H \int \mathrm{d}|\mathbf{p}_{\widetilde{G}}| \mathrm{d}\Omega |\mathbf{p}_{\widetilde{G}}|^3 \frac{\partial n_{3/2}}{\partial |\mathbf{p}_{\widetilde{G}}|} = \frac{g_{\widetilde{G}}}{(2\pi)^3} \int \mathrm{d}^3\mathbf{p}_{\widetilde{G}}\, \mathcal{C}[f]\,. \tag{5.7}$$

We have used that $\frac{\partial n_{3/2}}{\partial E_{\widetilde{G}}} = \frac{E_{\widetilde{G}}}{|\mathbf{p}_{\widetilde{G}}|} \frac{\partial n_{3/2}}{\partial |\mathbf{p}_{\widetilde{G}}|}$, as a result of the (on-shell) dispersion relation $|\mathbf{p}_{\widetilde{G}}|^2 + m_{3/2}^2 = E_{\widetilde{G}}^2$. By partially integrating the second term on the left-hand-side (LHS) of (5.7), and defining the right-hand-side (RHS) as the collision term (this has been already defined in Eq. (4.50), we obtain the Boltzmann equation for the number density in the form:

$$\dot{n}_{3/2} + 3Hn_{3/2} = \gamma_{3/2}\,, \tag{5.8}$$

where the dot denotes time differentiation. Recall that the production rate $\gamma_{3/2}$ consists of three parts: the subtracted and top quark rates calculated using the collision terms (4.50) and the $D-$graph contribution calculated by means of the gravitino selfenergy. The first term in the LHS of (5.8) depicts the evolution of the number density, while the second term accounts for the dilution of gravitinos due to the expansion of the Universe.

5.2 Gravitino abundance

In this section we compute [1, 2] the gravitino abundance by integrating the relevant Boltzmann equation. The energy density ρ during the radiation dominated epoch of the Universe is given by

$$\rho = g_\star \frac{\pi^2}{30} T^4\,, \tag{5.9}$$

where $g_\star$ are the effective energy DOF. That is, the Hubble parameter given by the Friedmann equation (5.2) takes the form

$$H(T) = \sqrt{\frac{g_\star \pi^2}{90} \frac{T^2}{M_{\mathrm{P}}^2}}\,. \tag{5.10}$$

Equation (5.8) has been written in terms of the gravitino number density, but is also useful to express it in terms of the gravitino abundance

$$Y_{3/2} = \frac{n_{3/2}}{n_{\mathrm{rad}}}\,, \tag{5.11}$$

where $n_{\mathrm{rad}} = \zeta(3)T^3/\pi^2$ is the number density of any single bosonic relativistic DOF. Substituting (5.11) into (5.8) the last takes the form

$$\dot{Y}_{3/2} + 3\left(H + \frac{\dot{T}}{T}\right) Y_{3/2} = \frac{\gamma_{3/2}}{n_{\mathrm{rad}}}\,. \tag{5.12}$$

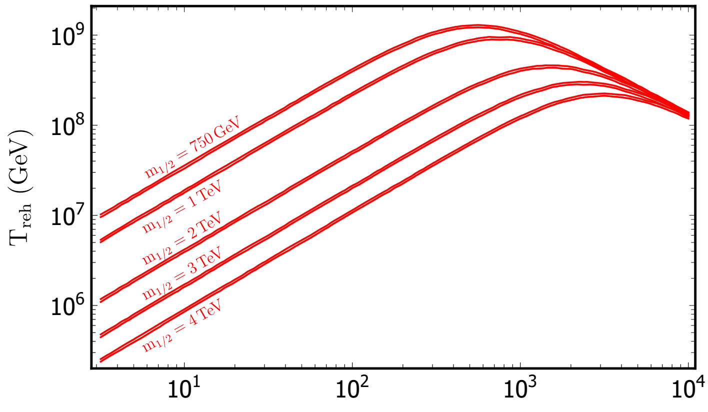

Figure 5.1: The cosmologically accepted 3σ regions for the gravitino thermal abundance for various values of $m_{1/2}$ between $750\,\mathrm{GeV}$ and $4\,\mathrm{TeV}$. The trilinear coupling A_t has been ignored and the top Yukawa coupling is $\lambda_t = 0.7$.

With the conservation of entropy per comoving volume, $g_{\star s} T^3 \alpha^3 = \text{const.}$, the above equation can be rewritten as

$$\frac{\mathrm{d}Y_{3/2}}{\mathrm{d}T} - \frac{\mathrm{d}\ln g_{\star s}}{\mathrm{d}T} Y_{3/2} = -\frac{\gamma_{3/2}}{n_{\rm rad} H T}\left(1 + \frac{T}{3}\frac{\mathrm{d}\ln g_{\star s}}{\mathrm{d}T}\right), \tag{5.13}$$

in which $g_{\star s}$ are the effective entropy DOF. Straightforward integration then yields [16]

$$Y_{3/2}(T) = Y_{3/2}(T_{\rm reh})\frac{g_{\star s}(T)}{g_{\star s}(T_{\rm reh})} - g_{\star s}(T)\int_{T_{\rm reh}}^{T} \frac{\gamma_{3/2}(T')}{n_{\rm rad}(T') g_{\star s}(T') H(T')}\left(1 + \frac{T'}{3}\frac{\mathrm{d}\ln g_{\star s}(T')}{\mathrm{d}T'}\right)\frac{\mathrm{d}T'}{T'}. \tag{5.14}$$

This integration begins at $T_{\rm reh}$ and runs to lower T, coherent with the assumption that inflaton decays and thermalization are instantaneous and simultaneous at the reheating temperature. Speculating that any initial gravitino population has been diluted away during inflation, *i.e.* assuming a vanishing abundance at $T_{\rm reh}$, and disregarding the weak T-dependence of the integrand for $T \ll T_{\rm reh}$, we obtain that

$$Y_{3/2}(T) \simeq \frac{\gamma_{3/2}(T_{\rm reh})}{H(T_{\rm reh})\; n_{\rm rad}(T_{\rm reh})}\;\frac{g_{\star s}(T)}{g_{\star s}(T_{\rm reh})}. \tag{5.15}$$

In [16, 312], the case of not instantaneous inflaton decay was considered. In particular, according to [312], in the case of gravitino DM a correction factor $\sim 10\%$ is expected for not instantaneous inflaton decays.

5.3 Gravitino dark matter

According to the latest data from the Planck satellite, the cosmological accepted value for the DM density in the Universe is $\Omega_{\rm DM} h^2 = 0.1198 \pm 0.0012$ [82]. Assuming that the thermal gravitino density, $\Omega_{3/2} = \rho_{3/2}/\rho_{\rm cr}$ is equal to the observed DM, we obtain that

$$\begin{aligned} \Omega_{\rm DM} h^2 &= \frac{\rho_{3/2}(t_0)\, h^2}{\rho_{\rm cr}} = \frac{m_{3/2}\, Y_{3/2}(T_0)\, n_{\rm rad}(T_0)\, h^2}{\rho_{\rm cr}} \\ &\simeq 1.33 \times 10^{24}\, \frac{m_{3/2}\, \gamma_{3/2}(T_{\rm reh})}{T_{\rm reh}^5}, \end{aligned} \tag{5.16}$$

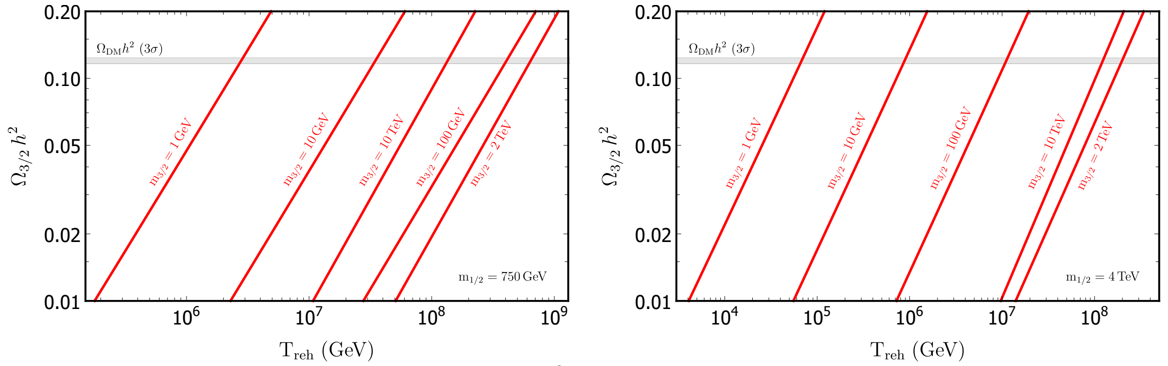

Figure 5.2: The thermal gravitino density $\Omega_{3/2}h^2$ as a function of the reheating temperature $T_{\rm reh}$ for various values of the gravitino mass. In both figures has been adopted universal gaugino masses which are $m_{1/2} = 750\, GeV$ on the left and $m_{1/2} = 4\, TeV$ on the right panel. The shaded regions in gray mark the allowed value (3σ) for the DM density given by [82].

where $\rho_{\rm cr} = 3\, H_0^2 M_{\rm P}^2$ is the critical energy density, $H_0 = 100\, h\, {\rm km}/({\rm s\, Mpc})$ is the Hubble constant today, $T_0 = 2.725\, K$ the current cosmic microwave background temperature and $h = 0.676$ is the reduced Hubble constant. The MSSM entropy DOF at the corresponding temperatures are $g_{\star s}(T_0) = 43/11$ and $g_{\star s}(T_{\rm reh}) = 915/4$. The last number corresponds to the effective energy DOF for $H(T_{\rm reh})$ in the MSSM too. Figure 5.1 shows the 3σ regions resulting from (5.16) for various values of $m_{1/2}$. In this figure the trilinear coupling A_t has been ignored and the top Yukawa coupling is $\lambda_t = 0.7$, as before. As previously, gauge coupling unification is assumed, as well as a universal gaugino mass $m_{1/2}$ at the GUT scale.

For large gravitino masses, the reheating temperature is $m_{1/2}$ independent, since the characteristic factor $m^2_{\lambda(\alpha)}/(3m^2_{3/2})$ becomes negligible for $m_{1/2} \ll m_{3/2}$. Assuming that $m_{1/2} \gtrsim 750\,$GeV, as suggested by the recent LHC data [313, 314] on gluino searches, from Fig. 5.1 we infer that for maximum $T_{\rm reh} \simeq 10^9\,$GeV the corresponding gravitino mass is $m_{3/2} \simeq 550\,$GeV. Considering a reheating temperature one order of magnitude smaller, $T_{\rm reh} \simeq 10^8\,$GeV, for the same gravitino mass, $m_{1/2}$ can go up to $3 - 4\,$TeV.

Finally, Fig. 5.2 illustrates the upper limits on $T_{\rm reh}$ for $m_{1/2} = 750\, GeV$ and $m_{1/2} = 4\, TeV$, respectively. Note that for larger values of $m_{1/2}$ the bounds on $T_{\rm reh}$ are more stringent. If one adds nonthermal production processes the bound on $T_{\rm reh}$ will become more severe.

Chapter 6

Cosmic inflation

In physical cosmology, cosmic inflation [83–86] is a theory which describes a period of exponential expansion of space in the early Universe. The theory of inflation manages to simultaneously solve basic issues of the Big Bang cosmology like the horizon and flatness problems. The simplest theory of inflation assumes the existence of one scalar field ϕ which is minimally coupled to gravity and has a canonical kinetic term.

6.1 Cosmological observables

Concerning the cosmological observables, and assuming the slow roll approximation, we begin by discussing the scalar and tensor power spectra, which play a crucial role in inflationary cosmology. The CMB observations significantly constrain the inflationary predictions, as shown in Fig 6.1. Choosing an arbitrary pivot scale $k_\star$ that exited the horizon, the scalar

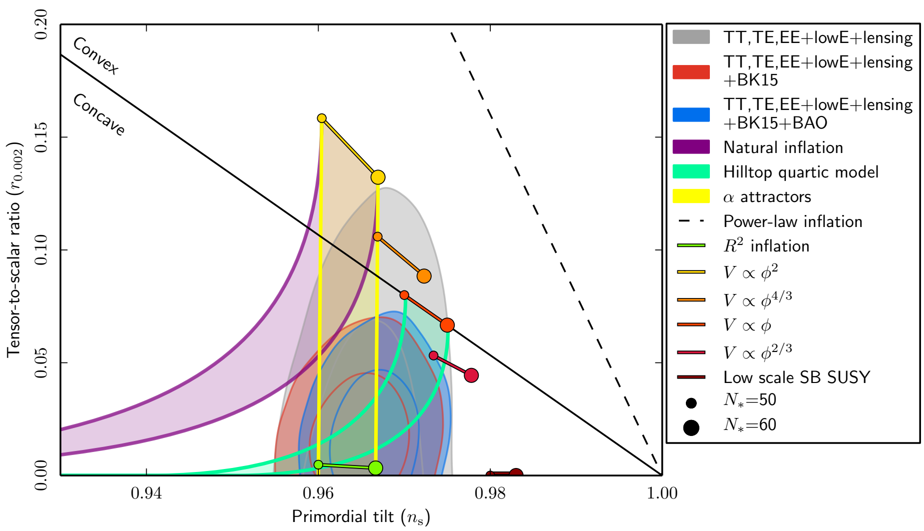

Figure 6.1: Marginalized joint 68% and 95% CL regions for n_s and r at $k = 0.002\,Mpc^{-1}$ from Planck alone and in combination with BK15 or BK15+BAO data, compared to the theoretical predictions of selected inflationary models. This figure has been adapted from [87].

($\mathcal{P}_\zeta$) and tensor ($\mathcal{P}_T$) power spectra can be written as

$$\mathcal{P}_\zeta(k) = A_s\left(\frac{k}{k_\star}\right)^{n_s-1}, \qquad A_s \simeq \frac{1}{24\pi^2}\frac{V(\phi_\star)}{\epsilon_V(\phi_\star)} \qquad \text{and} \qquad \mathcal{P}_T(k) \simeq \frac{2V(\phi_\star)}{3\pi^2}\left(\frac{k}{k_\star}\right)^{n_t}, \tag{6.1}$$

where the scale-dependence of the power spectra is defined by the scalar (n_s) and tensor (n_t) spectral indices given by

$$n_s - 1 = \frac{\mathrm{d}\ln\mathcal{P}_\zeta(k)}{\mathrm{d}\ln k} = -6\epsilon_V + 2\eta_V \qquad \text{and} \qquad n_t = \frac{\mathrm{d}\ln\mathcal{P}_T(k)}{\mathrm{d}\ln k}\,. \tag{6.2}$$

In these we have used the potential slow roll parameters (note that in most formulas we use $M_{\rm P}^2 = 1$ except when we want the dimensionality to be explicit)

$$\epsilon_V = \frac{1}{2}\left(\frac{V'(\phi)}{V(\phi)}\right)^2 \qquad \text{and} \qquad \eta_V = \frac{V''(\phi)}{V(\phi)}\,. \tag{6.3}$$

The tensor-to-scalar ratio is defined as

$$r = \frac{\mathcal{P}_T(k)}{\mathcal{P}_\zeta(k)} = 16\epsilon_V\,. \tag{6.4}$$

The Planck collaboration [87] has set the following bounds on the values of the observables:

$$A_s = (2.10 \pm 0.03) \times 10^{-9}, \qquad n_s = 0.9649 \pm 0.0042 \quad (1\sigma \text{ region}), \qquad r < 0.056\,. \tag{6.5}$$

During inflation the variation of the scalar field is related to the so-called number of e-folds $N_\star$ which has to be between 50 and 60 for the horizon and flatness problems to be solved. Following [87, 315] the number of e-folds is given by

$$\begin{aligned} N_\star \simeq \int_{\phi_{\rm end}}^{\phi_\star} \frac{{\rm d}\phi}{\sqrt{2\epsilon_V}} \;&=\; \ln\left[\left(\frac{\pi^2}{30}\right)^{\frac{1}{4}} \frac{(g_{\star s}(T_0))^{\frac{1}{3}}}{\sqrt{3}} \frac{T_0}{H_0}\right] - \ln\left[\frac{k_\star}{a_0 H_0}\right] + \frac{1}{4}\ln\left[\frac{V^2(\phi_\star)}{\rho_{\rm end}}\right] \\ &+\; \frac{1-3w}{12(1+w)} \ln\frac{\rho_{\rm reh}}{\rho_{\rm end}} + \frac{1}{4}\ln\left[\frac{g_\star(T_{\rm reh})}{g_{\star s}(T_{\rm reh})}\right] - \frac{1}{12}\ln\left[g_{\star s}(T_{\rm reh})\right]\,, \end{aligned} \tag{6.6}$$

where the subscripts “0”, “reh” and “end” denote quantities at the present epoch, at the reheating phase and at the end of inflation, respectively. The entropy density DOF have the values $g_{\star s}(T_0) = 43/11$ and $g_{\star s}(T_{\rm reh}) \simeq g_\star(T_{\rm reh}) = \mathcal{O}(100)$ for $T_{\rm reh} \sim 1\,{\rm TeV}$ or higher. The pivot scale is fixed at $k_\star = 0.05\,{\rm Mpc}^{-1}$ or $k_\star = 0.002\,{\rm Mpc}^{-1}$. The constant w characterizes an effective equation-of-state parameter.

Given an inflationary model, the largest uncertainties in $N_\star$ are mainly in the period of reheating of the Universe. For a review see *e.g.* [316]. For the scales of interest, these uncertainties yield values for $N_\star$ in the range $50-60$, which are commonly used in the literature. The reheating temperature reached by the Universe after its thermalization has been extensively studied and various mechanisms and models have been subjected to theoretical testing [316–327]. The number of e-folds accrued during the reheating period, $\Delta N_{\rm reh}$, is given by

$$\Delta N_{\rm reh} \equiv ln\,\frac{a_{reh}}{a_{\rm end}} = -\frac{1}{3(1+w)}\ln\frac{\rho_{\rm reh}}{\rho_{\rm end}}\,. \tag{6.7}$$

We consider the effective equation-of-state parameter w in the reheating phase as a free parameter. At the end of inflation $w = -1/3$ while the value $w = 1/3$ corresponds to the onset of radiation dominance. In the canonical reheating scenario $w = 0$, but values in the range $\simeq 0.0 - 0.25$, or larger, immediately after inflation, are also possible in some models [327, 328].

For any model given a value of $N_\star$, we have a prediction of ΔN_{reh} and in this sense (6.6) serves as a probe of the reheating process. Conversely, given a reheating mechanism, under a particular inflation model, the value of ΔN_{reh} is fixed, and thus $N_\star$ is predicted. In terms of ΔN_{reh}, for given w, one has for the reheating temperature, (see for instance [323]),

$$T_{\rm reh} = \left(\frac{30}{\pi^2}\frac{\rho_{\rm end}}{g_\star(T_{\rm reh})}\right)^{1/4} exp\left(-\frac{3(1+w)\Delta N_{\rm reh}}{4}\right)\,. \tag{6.8}$$

Note that since $a_{\rm reh} > a_{\rm end}$ we have that $\Delta N_{\rm reh} \geq 0$, and therefore due to $w > -1$ the reheating temperature $T_{\rm reh}$ is bounded from above

$$T_{\rm reh} \leq \left(\frac{30}{\pi^2}\frac{\rho_{\rm end}}{g_\star(T_{\rm reh})}\right)^{1/4} . \tag{6.9}$$

The bound on the RHS of this defines the instantaneous reheating temperature, $T_{\rm ins}$. The temperature $T_{\rm reh}$ reaches this upper bound when the reheating process is instantaneous, in which case $\Delta N_{\rm reh} = 0$. Note that for rapid thermalization we have $\rho_{\rm end} = \rho_{\rm reh}$, from Eq. (6.7). The reheating temperature should be larger than $\sim 1\,\mathrm{MeV}$ so that Big Bang Nucleosynthesis (BBN) is not upset. Lower values on $T_{\rm reh}$ have been established in [329] and recently in [330].

6.2 Cosmological observables with varying speed of sound

In this section we will see how the cosmological observables are differentiated in the case of a varying speed of sound [331–348]. The need for study the sound speed parameter c_s is due to the fact that in the Palatini formulation of R^2 gravity (see next chapters) higher in the velocity terms unavoidably appear, and thus its value deviates from unity. In fact c_s is defined by

$$c_s^2 = \frac{\partial p/\partial X}{\partial \rho/\partial X} , \tag{6.10}$$

where ρ and p are the energy density and pressure. With X we denote the kinetic term, *i.e.* $X = \frac{1}{2}g^{\mu\nu}\partial_\mu\phi\partial_\nu\phi$.

Choosing an arbitrary pivot scale $k_\star$ that exited the sound horizon at $t^\star$, *i.e.* $k_\star c_s(t^\star) = a(t^\star)H(t^\star)$, the scalar and tensor power spectra can be expanded about this pivot. keeping the first order terms in the slow roll parameters, one has

$$\mathcal{P}_\zeta(k) = \frac{H_\star^2}{8\pi^2 M_{\rm P}^2 \epsilon_1^\star c_s^\star} A\left(1 - 2(D+1)\epsilon_1^\star - D\epsilon_2^\star - (2+D)s_1^\star + (-2\epsilon_1^\star - \epsilon_2^\star - s_1^\star)\ln\frac{k}{k_\star}\right) \tag{6.11}$$

and

$$\mathcal{P}_T(k) = \frac{2H_\star^2}{\pi^2 M_{\rm P}^2} A\left(1 - 2(D+1-\ln c_s^\star)\,\epsilon_1^\star + (-2\epsilon_1^\star)\ln\frac{k}{k_\star}\right) . \tag{6.12}$$

A subtle point concerns the dependence of the tensor power spectrum on the speed of sound c_s. Usually this is computed by evaluating all quantities at the time of Hubble horizon, which is generally different, from the time of sound horizon. However, if we want to compare the scalar and tensor spectra using the results of cosmological measurements, the same pivot should be used, for consistency, as has been emphasized in [343, 345–347]. Using a pivot scale $k_\star c_s(t^\star) = a(t^\star)H(t^\star)$ in the scalar spectrum also yields a dependence on c_s in the tensor spectrum.

In these equations the Hubble flow functions (HFF), usually referred to as slow roll parameters, are defined in the usual manner, in terms of the Hubble rate,

$$\epsilon_1 \equiv -\frac{\mathrm{d}lnH}{\mathrm{d}N} = -\frac{\dot{H}}{H^2} \quad , \quad \epsilon_2 \equiv \frac{\mathrm{d}\ln\epsilon_1}{\mathrm{d}N} = \frac{\dot{\epsilon_1}}{\epsilon_1 H} \quad , \quad s_1 \equiv \frac{\mathrm{d}\ln c_s}{\mathrm{d}N} = \frac{\dot{c}_s}{c_s H} ,$$

where $\mathrm{d}N = H\mathrm{d}t$. A star in the HFF in the expressions above means that these are evaluated at $t^\star$. The equations (6.11) and (6.12) can be found in the references [343, 344, 346, 347]. In these references, a slightly different pivot scale is usually quoted, $k_\diamond c_{s\diamond}(\eta_\diamond) = -1/\eta_\diamond$, where $\eta_\diamond$

is the conformal time, and the corresponding expressions are given in terms of $k_\diamond$. However to first order, in HFF, they have the same form when the quantities denoted by a diamond symbol are replaced by the corresponding starred ones. Only the second order terms are affected and the corresponding coefficients differ. Note that higher order corrections have been computed but here we retain the next to leading corrections, *i.e.* first order in the slow roll parameters. In [346] the constants A, D are given analytically. In fact their values are $A = 18e^{-3}$ and $D = 1/3 - \ln 3$, as obtained using the *uniform approximation*, a method that is suitable for theories with varying speed of sound, which is similar to the WKB method. Taking next order corrections in the adiabatic approximation these constants are dressed (renormalized) and A turns out to be very close to unity while D becomes $D = 7/19 - ln3$. For our numerical treatment we will therefore use the renormalized values. For details we refer the reader to reference [346] where a detailed study is presented, including higher order corrections, and a comparison with other calculations is made.

Concerning the spectral index of the scalar power spectrum, following standard definitions, this is given by

$$n_s = 1 - 2\epsilon_1^\star - \epsilon_2^\star - s_1^\star \,, \tag{6.13}$$

while the tensor-to- scalar ratio is given by,

$$r \equiv \frac{\mathcal{P}_T(k_\star)}{\mathcal{P}_\zeta(k_\star)} = 16\epsilon_1^\star \, c_s^\star(1 + 2\ln c_s^\star \epsilon_1^\star + D\epsilon_2^\star + (2 + D)s_1^\star) \,, \tag{6.14}$$

to the same order of approximation. As for the number of e-folds, a $-\ln c_s$ term is included in the expression (6.6), since the speed of sound may not unity. This term is positive and in general can also give a significant contribution.

Chapter 7

R^2 Palatini inflationary models and reheating

The incorporation of popular inflationary models into Palatini gravity in an effort to describe the cosmological evolution of the Universe leads to different cosmological predictions than the metric formulation, because the dynamics of the two approaches differ. A notable example, is the Starobinsky model, in which there is an additional propagating scalar DOF, the scalaron, in addition to the graviton, whose mass is related to the coefficient of the $\mathcal{R}^2$ term. In the EF this shows up as a dynamical scalar field, the inflaton, which moves in a potential, the famous Starobinsky potential [349–351]. In the framework of Palatini gravity, there are no extra propagating DOF in any $f(R)$ theory [352] that can play the role of the inflaton, and therefore the inflaton must be inserted by hand as an extra field coupled to $f(R)$ gravity.

The differences between metric and Palatini formulations in cosmological predictions, as far as inflation is concerned, arise from the nonminimal couplings of the scalars that occupy the role of the inflaton. These couplings are different in the two approaches. This was first pointed out in [162] and has since attracted the interest of many authors [3–5, 8, 9, 164–185, 188, 201–208, 217, 353–360].

7.1 The model

We consider an action in the Jordan frame (JF) where scalar fields ϕ^J are coupled to gravity in the following way

$$S_{\rm JF} = \int \mathrm{d}^4x\sqrt{-g}\left(f(R,\phi) + \frac{1}{2}G_{IJ}(\phi)\partial\phi^I\partial\phi^J - V(\phi)\right) . \tag{7.1}$$

In it R is the scalar curvature in the Palatini formalism and $f(R,\phi)$ is an arbitrary function of the scalars ϕ^J and R. This action is reminiscent of an $f(R)$ theory involving scalar fields with kinetic terms written in the most general way reminiscent of σ - models. Following the standard procedure, we write this action in the following way and introduce the auxiliary field Φ.

$$S = \int \mathrm{d}^4x\sqrt{-g}\left(f(\Phi,\phi) + f'(\Phi,\phi)(R-\Phi) + \frac{1}{2}G_{IJ}(\phi)\partial\phi^I\partial\phi^J - V(\phi)\right) . \tag{7.2}$$

Here $f'(\Phi,\phi)$ denotes the derivative with respect Φ. One can define ψ in the following way

$$\psi = \frac{\partial f(\Phi,\phi)}{\partial\Phi}, \quad \text{with} \quad \text{inverse} \quad \Phi = \Phi(\psi,\phi)\,, \tag{7.3}$$

so the action is written as follows,

$$S = \int \mathrm{d}^4x\sqrt{-g}\left(\psi R + \frac{1}{2}G_{IJ}(\phi)\partial\phi^I\partial\phi^J - \psi\Phi + f(\Phi,\phi) - V(\phi)\right). \tag{7.4}$$

One can go to the EF by doing a Weyl transformation of the metric

$$g_{\mu\nu} = \lambda\bar{g}_{\mu\nu}, \quad \text{with} \quad \lambda\psi = \frac{1}{2}. \tag{7.5}$$

That done the theory in the EF gets the following form,

$$S_{\mathrm{EF}} = \int \mathrm{d}^4x\sqrt{-\bar{g}}\left(\frac{\overline{R}}{2} + \frac{1}{4\psi}G_{IJ}(\phi)\partial\phi^I\partial\phi^J - \frac{1}{4\psi^2}(\psi\Phi - f(\Phi,\phi) + V(\phi))\right). \tag{7.6}$$

The final step is to eliminate the field ψ whose equation of motion is trivially written as

$$\psi(\partial\phi)^2 = \psi\Phi - 2f(\Phi,\phi) + 2V(\phi), \tag{7.7}$$

where, in order to expedite the notation, we have designated $G_{IJ}(\phi)\,\partial\phi^I\partial\phi^J = (\partial\phi)^2$.

Note that (7.7) is not solvable, in general, but we will illustrate it on R^2-theories where it can be solved analytically. In what follows we will focus on such theories, which can be viewed as generalizations of the Starobinsky action. However, there are two main differences, first, the coefficients of the linear and quadratic, in the curvature R, terms are in general not constants, and second, the framework is the Palatini formalism where the connection is not the well-known Christoffel connection, but is treated as an independent field.

We will apply the previous formalism when there is only a single scalar, ϕ, and $f(\phi,R)$ is quadratic in curvature and has the form

$$f(R,\phi) = \frac{g(\phi)}{2}R + \frac{R^2}{12M^2(\phi)}. \tag{7.8}$$

Since a single scalar field is assumed, its kinetic term can always be put into the form $(\partial\phi)^2/2$, *i.e.* in the action (7.1) the field can be taken to be canonically normalized. So in this theory there are three arbitrary functions, namely $g(\phi), M^2(\phi), V(\phi)$, and each choice of these specifies a particular model. We have specified the reduced Planck mass M_{P} dimensionless and equal to one, and thus all quantities in (7.8) are dimensionless. When we reintroduce dimensions, the functions g, V have dimensions $mass^2$, and $mass^4$, respectively, while M^2 is dimensionless. Note that a nontrivial field dependence of the functions $g(\phi)$ and / or $M^2(\phi)$ is a manifestation of nonminimal coupling of the scalar ϕ to Palatini gravity. Note that since we use the Palatini formalism, there is no scalaron field, associated with an additional propagating DOF, which plays the role of the inflaton in the EF of the metric formulation .

With the function $f(R,\phi)$ as given by (7.8) we get from Eq. (7.3),

$$\psi = \frac{g(\phi)}{2} + \frac{\Phi}{6M^2(\phi)}, \tag{7.9}$$

whose inverse is,

$$\Phi = 6M^2(\phi)\left(\psi - \frac{g(\phi)}{2}\right). \tag{7.10}$$

Using these we can solve (7.7) in terms of ψ in a trivial manner,

$$\psi = \frac{4V + 3M^2 g^2}{2(\partial\phi)^2 + 6M^2 g}\,, \tag{7.11}$$

that is ψ, and hence Φ from (7.10), are expressed in terms of $\phi, (\partial\phi)^2$. Plugging ψ, Φ into (7.6) we get, in a straightforward manner,

$$S_{\mathrm{EF}} = \int \mathrm{d}^4x\sqrt{-g}\left(\frac{R}{2} + \frac{K(\phi)}{2}(\partial\phi)^2 + \frac{L(\phi)}{4}(\partial\phi)^4 - \bar{U}(\phi)\right)\,. \tag{7.12}$$

In this action we have suppressed the bar in the scalar curvature and also $\sqrt{-g}$, and to simplify the notation we have denoted $\partial_\mu\phi\partial^\mu\phi$ by $(\partial\phi)^2$ and $(\partial_\mu\phi\partial^\mu\phi)^2$ by $(\partial\phi)^4$. Note the appearance of quartic terms $(\partial\phi)^4$ in the action. As for the functions $K, L, \bar{U}$, appearing in (7.12), they given are analytically by

$$L(\phi) = (3M^2g^2 + 4V)^{-1}\,,\; K(\phi) = 3M^2 g L\,,\; \bar{U}(\phi) = 3M^2 V L\,. \tag{7.13}$$

Note that since terms up to R^2 were considered, in $f(R)$ - gravity, terms higher than $(\partial\phi)^4$ do not occur in the action.

The above Lagrangian may feature, under certain conditions, K - inflation models [361], involving a single field described by an action whose general form is

$$S = \int \mathrm{d}^4x\sqrt{-g}\left(\frac{R}{2} + p(\phi, X)\right)\,. \tag{7.14}$$

where $X \equiv (1/2)\partial_\mu\phi\partial^\mu\phi$. The cosmological perturbations of such models were considered in [362]. However, the importance of a time-dependent sound speed c_s in K - inflation models was emphasized in [343] and cosmological constraints were derived, using improved expressions for the power spectra of density perturbations. Specific models with $p(\phi, X) = F(X) - V(\phi)$ were considered in [363]. In (7.12) the Lagrangian density is identified with $p(\phi, X)$, but the function $F(X)$ is now given by $K(\phi)\,X + L(\phi)\,X^2$, which in addition to X also depends, on the field ϕ, as well, through $K(\phi), L(\phi)$.

In a flat FLRW metric, where the background field ϕ is only time dependent, the energy density and pressure are given by

$$\rho(\phi, X) = K(\phi)X + 3L(\phi)X^2 + \bar{U}(\phi) \quad , \quad p(\phi, X) = K(\phi)X + L(\phi)X^2 - \bar{U}(\phi)\,, \tag{7.15}$$

with X being, in this case, half of the velocity squared, $X = \dot{\phi}^2/2$.

We will assume that the function $L(\phi)$ is always positive to avoid phantoms, leading to an equation-of-state with $w < -1$. This can occur when $L < 0$ and X becomes sufficiently large. However, there is no restriction on the sign of $K(\phi)$ which can be negative in some regions of the field space, signaling that the kinetic term has the wrong sign in these regions. Obviously, the sign of $K(\phi)$ should be positive at the minimum of the potential. Possibilities where K is negative in some regions are interesting but will not be pursued in this thesis. Besides, we will assume that the potential is positive $\bar{U}(\phi) \geq 0$ and it has a Minkowski vacuum. This ensures that the energy density is positive definite. When considering inflationary models, the inflaton rolls towards this minimum, signaling the end of inflation and the beginning of the thermalization of the Universe. These are rather mild conditions.

As for the potential $\bar{U}$ appearing in the Lagrangian (7.12) in the Einstein frame, we see from the last of (7.13) that due to the fact that we have assumed $L, M^2 > 0$, the positivity of $\bar{U} \geq 0$ entails that $V \geq 0$. Moreover, one can trivially show, from (7.13), that $\bar{U}$ can be cast into the following form,

$$\bar{U} = \frac{3M^2}{4}\left(1 - \frac{K^2}{3M^2 L}\right). \tag{7.16}$$

From this it is evident that the potential is not only positive, but is also bounded from above by,

$$\bar{U} \leq \frac{3M^2}{4}. \tag{7.17}$$

This upper bound can be easily saturated, for large ϕ, by suitably choosing the functions involved, namely g, M^2 and V. Indeed, for large ϕ, the asymptotic values of these functions, control the behavior of the potential in this regime[1]. If we opt that the function M^2 approaches a plateau or is constant, this is also true for the potential, which can thus drive successful inflation. The requirement for a Minkowski vacuum is also easily satisfied, so there are many ways to realise potentials with the required properties for the inflationary slow roll mechanism. This is exemplified in specific models discussed later.

To conclude this section, we have presented a general and model independent, framework of R^2 - theories in the Palatini formulation of gravity, which can be useful for studying inflation models and can support slow roll inflation. In the EF these theories have many features in common with the K-inflation models. This formalism will be used to study various inflation models in the following sections.

7.2 The equations of motion and the slow roll

When noncanonical kinetic terms are present, the equations of motion for the inflaton scalar field ϕ deviate from their standard form. As a consequence, the cosmological parameters describing the slow roll evolution should be modified accordingly. Certainly, one can normalize the kinetic term of the scalar field accordingly, but this is not always very convenient. In fact, in most cases, the integrations needed, to go from the noncanonical to the canonical field are not easy, in most of the cases, to be carried and the results cannot be presented in a closed form. Therefore, it turns out to be easier to work directly with the noncanonical fields and express the cosmological observables in a way that is suitable for this treatment.

It is not difficult to see that the field ϕ satisfies the equation of motion given by

$$(K + 3L\dot{\phi}^2)\ddot{\phi} + 3H(K + L\dot{\phi}^2)\dot{\phi} + \bar{U}'(\phi) + \frac{1}{4}(2K' + 3L'\dot{\phi}^2)\dot{\phi}^2 = 0\,. \tag{7.18}$$

Therein all primes denote derivatives with respect to ϕ. If the field were canonical, $K = 1$, and if there were no quartic in the velocity terms, *i.e.* $L = 0$, then the above equation takes its familiar form. In it is encoded the effect of using a nonminimal, in general field ϕ in the function K. The effect of the presence of terms $(\partial\phi)^4$ in the action is encoded in the function L. The terms that depend on L are multiplied by an additional power of the velocity squared, as compared to the K-terms. These cannot be neglected, although as we discuss below, they are small in certain models, during inflation. In terms of the field ϕ and its velocity $\dot{\phi}$, the speed of sound (6.10) has the form

$$c_s^2 = \frac{1 + L\dot{\phi}^2/K}{1 + 3L\dot{\phi}^2/K}\,. \tag{7.19}$$

[1] It is quite easy to see that the saturation of the bound (7.17), for large field values, is easily obtained when $\frac{g^2}{V} \longrightarrow 0\,,$ and $\frac{g^2 M^2}{V} \ll 1\,,$ as $\phi \longrightarrow$ *large*.

c_s is controlled by $L\dot{\phi}^2/K$, the same combination that appears in the equation of motion for the field ϕ, and approaches unity when $L\,\dot{\phi}^2/K \ll 1$.

We can gain more insight by briefly using a canonically normalized field ϕ_c, defined by

$$\phi_c = \int \sqrt{K(\phi)}\mathrm{d}\phi\,. \tag{7.20}$$

To avoid ghosts suppose that $K > 0$, so that the above integration makes sense. Indeed, if K is negative, the kinetic term of the field ϕ has the wrong sign, namely $-(\partial\phi_c)^2/2$. However, it can also happen that this function is negative in one region, but strictly positive at the Minkowski vacuum. In this way, ghosts are also avoided. This case, interesting as it may be, will not be discussed and we prefer to take a more conservative point of view and have $K > 0$ in the whole region. Then equation of motion (7.18) with respect to the field ϕ_c takes the form

$$\left(1+\frac{3L}{K^2}\dot{\phi}_c^2\right)\ddot{\phi}_c + 3H\left(1+\frac{L}{K^2}\dot{\phi}_c^2\right)\dot{\phi}_c + \frac{\mathrm{d}\bar{U}}{\mathrm{d}\phi}_c + \frac{3L}{4K^2}\frac{\mathrm{d}\,\ln\left(L/K^2\right)}{\mathrm{d}\phi_c}\dot{\phi}_c^4 = 0\,. \tag{7.21}$$

From this form it is clear that the smallness of the ∂h^4 terms in the action is quantified by the smallness of the ratio $\frac{L}{K^2}\dot{\phi}_c^2 \ll 1$, which is equivalent to $\frac{L}{K}\dot{\phi}^2 \ll 1$. If we neglect this in the above equation, we get familiar form of the equation of motion for the canonical field ϕ_c.

It should be emphasised, however, that our numerical study properly accounts for the contribution of these terms and no approximation is made, although we have numerically found them to be small, at least in the models considered in this thesis. In Fig. 7.1 we plot on the left panel the evolution of the field ϕ versus the number of e-folds $N_\star = \ln(a_{\mathrm{end}}/a(t))$, from the time when the number of e-folds reaches $N_\star = 70$ to the end of inflation corresponding to $N_\star = 0$. On the right panel, we show the parameter $\epsilon_1 = -\frac{\dot{H}}{H^2}$, the speed of sound squared c_s^2 and the evolution of $\frac{L}{K}\dot{\phi}^2$. For reference, we have also included a vertical band to mark the region $N_\star = 50 - 60$, which is usually given in the literature. These plots consider the minimally coupled model, for which $g = 1, M^2 = \frac{1}{6\alpha}$ and $V = \frac{m^2}{2}\phi^2$. The values of the parameters α, m^2, used in the construction of Fig. 7.1, correspond to Model I (C - case), discussed later in Sec. 7.3.1. for which $\alpha = 10^9$ and $m = 6.32\times10^{-6}$. However, similar results hold for the other models studied in this thesis.

On the left side of this figure one can see the rapid damped oscillations of ϕ, after the end of inflation, when it begins to fall to the minimum of the potential. These are clearly visible in the enlarged inset small figure. On the right pane, one can see that $\epsilon_1 << 1.0$, $c_s^2 \simeq 1.0$, and $\frac{L}{K}\dot{\phi}^2 \sim \mathcal{O}(10^{-2})$, for any number of e-folds that is larger than about 5, or even smaller. For $N \lesssim 5$ the function ϵ_1 starts to grow and $\frac{L}{K}\dot{\phi}^2$ increases significantly, however remains small in magnitude until the end of inflation.

On the other hand, the scales of interest, from CMB observations, are in the range of $10^{-4}Mpc^{-1} \lesssim k \lesssim 10^{-1}\,Mpc^{-1}$ and the number of e-folds remaining until the end of inflation, from the time t_k a scale k crossed the sound horizon, is $N_k = \ln(a_{\mathrm{end}}/a(t_k))$. Even for the largest scale, in the above range, the number of e-folds cannot be smaller than about $\simeq 20$, as we have numerically established. Therefore, any scale k in the range of interest, crossed the sound horizon long before the end of inflation, when $\epsilon_1 << 1.0$, $c_s^2 \simeq 1.0$, and $\frac{L}{K}\dot{\phi}^2$ was small $\mathcal{O}(10^{-2})$. Therefore, for the cosmological scales of interest the contribution of the L - terms is small.

Although small, for a wide range of parameters and for the class of models studied here, the role of $\frac{L}{K}\dot{\phi}^2$ is important in determining the energy density ρ_{end} at the end of inflation, which in turn affects the instantaneous reheating temperature T_{ins}. Even in this case, however, we have found that the values of ρ_{end} differ from the obtained values approximately by factors of order $\mathcal{O}(1)$.

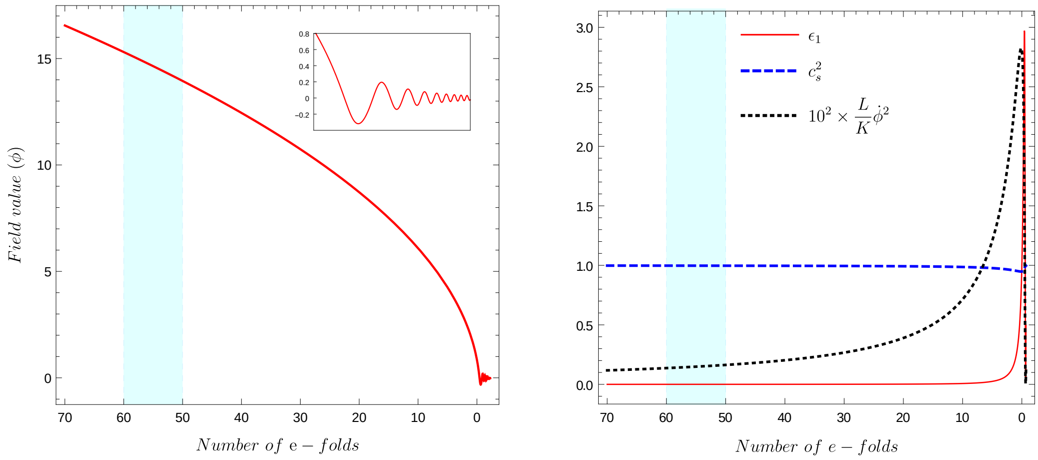

Figure 7.1: The left panel shows the evolution of the field ϕ with the number of e-folds. In the small inset figure, the rapid oscillations of ϕ as it approaches the minimum of the potential are magnified. On the right is the parameter ϵ_1, the speed of sound squared c_s^2 and the quantity $10^2 L\dot{\phi}^2/K$.

The preceding arguments imply that one can use the slow roll approximation for the cases we are interested in and at the same time neglect the L - terms, provided that their omission is sufficiently justified. We reiterate that our results are based on a numerical study and no such an approximation is made. However, this does not deprive us of the right, to present qualitative arguments based on this approximation scheme for an analytical treatment of the models considered, aiming at a better understanding of the results obtained based on a numerical study in which all terms are included and no approximation is made.

Provided that the contribution of the L - term is small, and with $K > 0$, the first slow roll parameters as defined with respect to the potential are given by,

$$\epsilon_V = \frac{1}{2K(\phi)}\left(\frac{\bar{U}'}{\bar{U}}\right)^2 \quad , \quad \eta_V = \frac{\left(K^{-1/2}\bar{U}'\right)'}{K^{1/2}\bar{U}} \, . \tag{7.22}$$

In these equations the primes denote the derivatives with respect to ϕ. It is trivial to show that these definitions are indeed consistent with the known definitions given the canonically normalized field ϕ_c of Eq. (7.20). As for the number of e-folds, left to the end of inflation, this is given by

$$N_\star = \int_{\phi_{\rm end}}^{\phi_\star} K(\phi)\frac{\bar{U}(\phi)}{\bar{U}'(\phi)} \mathrm{d}\phi \, . \tag{7.23}$$

In this $\phi_\star$ is the pivot value and $\phi_{\rm end}$ the value of the field at the end of inflation.

7.3 Quadratic and quartic models

Before we move into the consideration of specific models and present our results, we fell it is appropriate to briefly outline the approach taken in this section. Our predictions are based on a study in which the Friedmann equations and the evolution equation (7.18) are solved numerically without making any approximations. Before doing so, however, we consider it useful to first apply the slow roll approximation, neglecting the contribution of the L - terms. This is done for comparison with the numerical results which are the only reliable source to reach physical conclusions. For the models considered in this thesis, the numerical investigation shows that this approximation scheme is reasonable, since it is justified by the results of the numerical treatment. For this reason, it explains at a very satisfactory level the results derived by our numerical treatment. It should be noted, however, that this is not a generic property and may not hold for other models included in the Palatini R^2 gravity.

As for our numerical analysis, the approximation scheme used is also useful to obtain a first estimate of the magnitudes of the parameters involved, consistent with the bounds imposed by the measurements of the cosmological parameters. In our numerical approach, we scan the parameter space starting from initial values of the parameters that fall within the range proposed by this analysis.

7.3.1 Minimally coupled models with potentials $\sim \phi^n$

In this section, we consider specific models using the formalism presented in previous sections, and discuss their predictions. An interesting class of models is the one in which the potential V is a monomial in the field ϕ, $V \sim \phi^n$, where n is even integer, and g, M^2 are constants, *i.e.* the scalar ϕ couples minimally to gravity. We set $g = 1$ [2] and thus these models are described by

$$g(\phi) = 1 \quad , \; M^2(\phi) = \frac{1}{6\alpha} \quad , \quad V(\phi) = \frac{\lambda}{n}\phi^n \quad \text{with} \;\; n = \text{positive even integer} \, . \tag{7.24}$$

So we are dealing with two parameters, α and λ, which are in principle unknown. Cosmological data will constrain their allowable values, as we will see shortly. To facilitate the analysis, we define the parameter c defined by the combination,

$$c = \frac{8\lambda\alpha}{n} \, . \tag{7.25}$$

Then the functions K, L are given by

$$K(\phi) = (1 + c\phi^n)^{-1} \; , \; L(\phi) \; = \; 2\alpha \, (1 + c\phi^n)^{-1} \, , \tag{7.26}$$

while the potential $\bar{U}$ receives the form

$$\bar{U}(\phi) = \frac{1}{8\alpha} \frac{c\phi^n}{1 + c\phi^n} \, . \tag{7.27}$$

For large values of ϕ this is $\simeq 1/8\alpha$ therefore $1/8\alpha$, which is proportional to M^2, sets actually the inflation scale.

To find the range of parameters α, λ, or equivalently α, c, that is consistent with the cosmological data, we first consider the amplitude of the power spectrum A_s. To do this, it is sufficient to consider the simplified form given by (6.1), take $c_s^\star \simeq 1$ and replace ϵ_V as given by (7.22). Then, from the previously given analytic form of the potential and from (7.22) we obtain the amplitude A_s of Eq. (6.1) in the form,

$$A_s \simeq \frac{1}{24\pi^2} \frac{1}{4n^2} \left(\frac{c}{a} \right) \phi_\star^{n+2} = \frac{1}{12\pi^2} \frac{\lambda}{n^3} \phi_\star^{n+2} \, , \tag{7.28}$$

where $\phi_\star$ is the value of the field at $t^\star$. As it seems, the ratio c/α, or equivalently the parameter λ, that controls the magnitude of the amplitude A_s. For the central value of A_s, which is $A_s \simeq 2.1 \times 10^{-9}$, on account of (7.28) , we have

$$\lambda\phi_\star^{n+2} \simeq (2.5 \times 10^{-7})n^3 \quad \text{or} \quad \left(\frac{c}{\alpha} \right) \phi_\star^{n+2} \simeq (2.0 \times 10^{-6})n^2 \, . \tag{7.29}$$

[2] When the Planck mass is put back into the action, this corresponds to $g = M_{\mathrm{P}}^2$.

To further quantify the admissible range of parameters, we also need an estimate for $\phi_\star$. For this purpose, we use (7.23) from which it follows that

$$N_\star = \frac{1}{2n}\left(\phi_\star^2 - \phi_{\rm end}^2\right), \tag{7.30}$$

which yields

$$\phi_\star^2 = 2nN_\star + \phi_{\rm end}^2 \,. \tag{7.31}$$

$\phi_{\rm end}$ is defined as the value for which $\epsilon_V = 1$. For the specific models

$$\epsilon_V = \frac{n^2}{2}\frac{1}{\phi^2(1+c\phi^n)}, \tag{7.32}$$

therefore $\phi_{\rm end}^2$ is solution of the equation

$$c\phi_{\rm end}^{n+2} + \phi_{\rm end}^2 - \frac{n^2}{2} = 0\,. \tag{7.33}$$

For $c = 0$ the solution is exactly $\phi_{\rm end}^2 = n^2/2$ while for any $c > 0$ the only real and positive solution for $\phi_{\rm end}^2$ is easily found to be bounded by $n^2/2$. From this bound on $\phi_{\rm end}^2$ and using the fact that $N_\star$ is about ~ 50, or so, it follows from (7.31) that $\phi_\star$ is well approximated by

$$\phi_\star = \sqrt{2nN_\star}\,, \tag{7.34}$$

provided that $n << 4N_\star$. This covers a large class of models ranging from $n = 2$ up to $n = 10$ or even larger. Using $\phi_\star$ as given above, A_s from Eq. (7.28) is written, in terms of $N_\star$, as

$$A_s \simeq \frac{1}{12\pi^2}\frac{\lambda}{n^3}(2nN_\star)^{(n/2+1)}\,. \tag{7.35}$$

For $A_s \simeq 2.1\times 10^{-9}$ we have that the coupling λ is constrained to be

$$\lambda \simeq (4.97\times 10^{-7})\,\frac{k^2}{(4k)^k}\,\frac{1}{N_\star^{k+1}} \quad \text{where} \;\; n = 2k\,. \tag{7.36}$$

Note that this is inversely proportional to $N_\star^{k+1}$. For $N_\star = 55$ and $n = 2$, *i.e.* $V \sim \phi^2$, this gives $\lambda \simeq 4.11\times 10^{-11}$ while for $k = 2$, *i.e.* $V \sim \phi^4$ we get $\lambda \simeq 1.87\times 10^{-13}$. Note that for the $n = 4$ case Eq. (7.35) coincides with that given in [205].

For the parameter α a lower bound can be obtained from the observational bound on the tensor-to-scalar ratio r (6.5). Using the analytic form of the potential one finds

$$\frac{1}{8\alpha}\frac{c\phi_\star^n}{1+c\phi_\star^n} < 2.0\times 10^{-9}\,. \tag{7.37}$$

Replacing c in terms of α from (7.25), and using the value of $\phi_\star$ given before in (7.34), we have from (7.37), after some trivial manipulations,

$$\alpha \gtrsim 5\times 10^7\left(1.25 - \frac{N_\star}{50\,n}\right)\,. \tag{7.38}$$

For instance, for the quartic potential $V \sim \phi^4$ and for $N_\star = 55$ this yields $\alpha \geq 0.485\times 10^8$, resulting to an inflationary scale, lower than $\sim 10^{-5}$, or so.

The previously given constraints on the parameters are obtained from the amplitude of the power spectrum in combination with the bound on r, and define the range in which acceptable values for A_s can be obtained, However, the spectral index n_s puts additional constraints and in order to have an estimate of it we use the approximate formula given by (6.2) The parameter ϵ_V is given by (7.32) and for η_V we employ (7.22) from which it follows that

$$\eta_V = \frac{n\,(n-1-(n/2+1)c\phi^n)}{\phi^2(1+c\phi^n)}\,. \tag{7.39}$$

From this, and ϵ_V of Eq. (7.32), we get, on account of (6.2),

$$n_s = 1 - \frac{n^2+2n}{\phi^2}\,. \tag{7.40}$$

Replacing ϕ by $\phi_\star = \sqrt{2nN_\star}$ a rather simple expression for n_s is obtained given by

$$n_s = 1 - \frac{n+2}{2N_\star}\,. \tag{7.41}$$

Note that for $n = 2$ and $N_\star = 55$ the above formula gives $n_s = 0.9636$ which is well within the observational limits but for $n = 4$ a rather large value of $N_\star$ is needed to get an acceptable value for n_s. In fact $N_\star > 76$ is required to have $n_s = 0.9607$, the lowest allowed value when using the data $n_s = 0.9649 \pm 0.0042$. This is a rather large value for the number of e-folds $N_\star$. The situation gets even worse for models with $n > 4$.

In the context of this qualitative discussion, it is important to have estimates of the variations in the quantities of interest as the parameters of the present models vary. Starting from the amplitude of the power spectrum given by (7.35), it is a trivial task to see that such variation yields

$$\delta A_s = \left(\frac{\delta\lambda}{\lambda} + \frac{n+2}{2}\frac{\delta N_\star}{N_\star}\right) A_s\,. \tag{7.42}$$

The first term stems from the explicit dependence of A_s on λ. With λ fixed, and only α varying, the second term contributes. In this case, one can see that, varying the e-folds about the order of unity can lead to a significant change in A_s, of the same order of magnitude as the errors accompanying the measurements of A_s. Because of the prefactor $(n+2)/2$, on the RHS of (7.42), this is larger for models with larger n.

On the other hand, the corresponding variation of the spectral index n_s is found, from (7.41),

$$\delta n_s = \frac{n+2}{2N_\star^2}\delta N_\star\,. \tag{7.43}$$

This is proportional to the relative change $\delta N_\star/N_\star$ but is accompanied by an extra $N_\star$ in the denominator. As a result, one expects n_s to change little as the number of e-folds changes.

To estimate the variations $\delta N_\star$, and thus $\delta A_s, \delta n_s$, when varying the involved couplings, namely α and λ for the models under study, one should start from Eq. (6.6) and vary $N_\star$ with respect to α, λ for a fixed value of the reheating temperature. The only dependence on these is through the logarithm of $3H_\star^2$, which equals $\bar{U}(\phi_\star)$ in the slow roll regime, and the logarithm with ρ_{end}. We skip the details of such an analysis. We simply note that the final result is of the form.

$$\delta N_\star = \frac{\delta\alpha}{\alpha} f_\alpha + \frac{\delta\lambda}{\lambda} f_\lambda\,, \tag{7.44}$$

where the factors $f_{\alpha,\lambda}$ depend on the model under consideration.

A final remark concerns the instantaneous reheating temperature $T_{\rm ins}$, which is determined once we know $\rho_{\rm end}$, see Eq. (6.9) and the discussion that follows. With $g_\star(T_{\rm reh}) = 106.75$, we have

$$T_{\rm ins} = 0.411\rho_{\rm end}^{1/4}\,, \tag{7.45}$$

which is generally true. However, $\rho_{\rm end}$ depends on the details of the model under consideration.

The end of inflation is determined by $\epsilon_1 = 1$, equivalent to $\rho + 3p = 0$. In the absence of L - terms, this leads to $\rho_{\rm end} = \sigma\,\bar{U}$, where $\sigma = 1.5$. However, in their presence a more refined analysis is required. In this case, the equation $\epsilon_1 = 1$ can be trivially solved, using (7.15), to obtain $L\dot{\phi}^2/K$ in terms of the potential $\bar{U}$, both evaluated at the end of the inflation. This makes it a fairly straightforward task to compute $\rho_{\rm end}$,

$$\rho_{\rm end} = \sigma f(c_s)\bar{U}(\bar{\phi}_{\rm end}) \quad . \tag{7.46}$$

In this equation, to avoid confusion, we have denoted by $\bar{\phi}_{\rm end}$ the value of the field at the end of inflation. This implicitly depends on L and can only be extracted numerically. The function $f(c_s)$ depends on the speed of sound squared, c_s^2, evaluated at the end of inflation, and is given by $f(c_s) = 8c_s^2/(9c_s^2-1)$. Due to the fact that $1/3 \leq c_s^2 \leq 1$, as one can see from (7.19), it is bounded by $1 \leq f(c_s) \leq 4/3$. If we had used the value $\phi_{\rm end}$, as given by $\epsilon_V = 1$, Eq. (7.46) would have been expressed as follows,

$$\rho_{\rm end} = \sigma\, f_\rho\, \bar{U}(\phi_{\rm end}) \quad , \quad f_\rho \equiv f(c_s)\,\frac{\bar{U}(\bar{\phi}_{\rm end})}{\bar{U}(\phi_{\rm end})} \quad . \tag{7.47}$$

This says that the approximate result for $\rho_{\rm end}$ as given by $\sigma\,\bar{U}(\phi_{\rm end})$, is actually dressed by the factor f_ρ. In this factor the function $f(c_s)$ plays no important role because of the bounds quoted earlier, but the ratio $\bar{U}(\bar{\phi}_{\rm end})/\bar{U}(\phi_{\rm end})$ may deviate substantially from unity. This ratio can only be calculated numerically. However, in all models considered, and in a wide range of the parameters, we have found that it lies between $\simeq 0.5$ and 0.65. Moreover, if we take into account the bounds on $f(c_s)$, the factor f_ρ is in the range $0.5 - 0.85$. Thus, the numerically derived result for $\rho_{\rm end}$ is reduced by the factor f_ρ, from the approximate result, $\rho_{\rm end} = \sigma\,\bar{U}(\phi_{\rm end})$. Things look much better for the instantaneous temperature, which depends on the square root of $\rho_{\rm end}$. Therefore, the numerically derived $T_{\rm ins}$ is smaller by a factor in the range $0.84 - 0.95$. Thus the approximate result $\rho_{\rm end} = \sigma\,\bar{U}(\phi_{\rm end})$, that we can derive analytically, yields $T_{\rm ins}$ that are not far from the actual values.

For the models studied in this thesis, referred to as Model I, II as well as Higgs Model, using the equation relating $L\dot{\phi}^2/K$ to $\bar{U}$ at the end of inflation, Eq. (7.46) can be further simplified given by,

$$\rho_{\rm end} = \frac{\sigma}{4\alpha}(1-c_s^2) \quad , \tag{7.48}$$

where the speed of sound is meant at the end of inflation. Simple as may be, the value of c_s^2 depends implicitly on the parameters of the model and it can only be calculated numerically. This is a rather elegant relation, showing that only c_s at the end of inflation is needed, to derive $\rho_{\rm end}$. It also shows the prominent role of the $L\dot{\phi}^2/K$, at the end of inflation, through which c_s^2 is determined, see Eq. (7.19). Using (7.48), the instantaneous reheating temperature can written into the form

$$T_{\rm ins} = 0.321\alpha^{-1/4}(1-c_s^2)^{1/4} \quad . \tag{7.49}$$

From this, using the fact that $c_s^2 \geq 1/3$, an absolute upper bound can be derived, $T_{\rm ins} \leq 0.290\alpha^{-1/4}$, which holds for any model considered in this thesis. From (7.48), one can conclude that for large α the instantaneous temperature falls as $\alpha^{-1/4}$. In reality it can fall much faster, due to the implicit dependence of c_s^2 on the parameters involved.

Following the previous discussion, we can derive analytic expressions for $T_{\rm ins}$, that are good estimates, using the approximate expression $\rho_{\rm end} = \sigma\,\bar{U}(\phi_{\rm end})$. For the class of models studied in this subsection, the latter follows from the solution of (7.33) which depends only on the combination c. Using the analytic form of the potential one finds in a straightforward way that,

$$\rho_{\rm end} = \frac{\sigma}{8\alpha}\left(1 - \frac{2}{n^2}\phi_{\rm end}^2\right) . \tag{7.50}$$

$\rho_{\rm end}$, and hence $T_{\rm ins}$, cannot be quantified further, at this stage, since for this purpose the value of $h_{\rm end}$ is needed. In what follows, we will analyze in detail the predictions for this class of models. As noted at the beginning of this section, in presenting our final results for each model considered, we will solve the associated equations numerically with exact formulas, without approximations, and take into account the temperature dependence of the number of e-folds.

Model I :

We first consider the model (Model I) in which the functions g, M^2 and V are as given by (7.24) with $n = 2$, that is the potential V is quadratic in the field ϕ,

$$V(\phi) = \frac{m^2}{2}\phi^2 . \tag{7.51}$$

For this case we prefer m^2, instead of λ, since it carries the dimension of $mass^2$ when $M_{\rm P}$ is reinstated. Following what we have learned so far, we define, see Eq. (7.25), the constant c as the combination

$$c = 4m^2\alpha . \tag{7.52}$$

The value of $\phi_\star$ in this case is given by, using (7.31),

$$\phi_\star \simeq 2\sqrt{N_\star} . \tag{7.53}$$

Then from (7.36), which appear from the power spectrum amplitude, we get, for values $N_\star = 50 - 60$,

$$m \simeq (6.5 \pm 0.5) \times 10^{-6} \quad \text{or} \quad \frac{c}{\alpha} \simeq (1.7 \pm 0.3) \times 10^{-10} . \tag{7.54}$$

The lowest (largest) limits correspond to $N_\star = 60 (N_\star = 50)$. Therefore, using reasonable approximations we have derived fairly tight bounds on the parameter m. Recall that $m^2 \equiv \lambda$ and thus λ is of the order of 10^{-11}. From the bound (7.38), we get for $N_\star = 50 - 60$, a lower bound which is estimated to be in the range,

$$\alpha \geq (0.32 - 0.37) \times 10^8 . \tag{7.55}$$

Here, the smallest value corresponds to $N_\star = 60$ and the largest to $N_\star = 50$. Thus, the parameter α cannot be chosen arbitrarily. It should be $\sim 10^8$ or larger. In the following, due to (7.55), we take the largest value as the bound set on α, *i.e.* $\alpha \gtrsim 0.37 \times 10^8$, which is valid for any $N_\star$ in the range of interest.

Concerning the instantaneous reheating temperature, in this case, by solving analytically (7.33), and replacing ϕ_{end} into (7.50), we get

$$\rho_{\text{end}} = \frac{\sigma}{8\alpha}\left(1 - \frac{\sqrt{1+8c}-1}{4c}\right). \tag{7.56}$$

We can consider two different regimes, the small c and the large c, for which ρ_{end}, and consequently T_{ins}, have different dependencies on the parameters involved, as we shall see. Since from (7.54) the ratio c/a is of the order of $\sim 10^{-10}$, small c values are obtained when $\alpha < 10^{10}$. On the other hand large c values are obtained when $\alpha > 10^{10}$.

For small c - values one can expand (7.56), and using the fact that $\sigma = 1.5$, the instantaneous temperature, as given by (7.45), receives the form,

$$\rho_{\text{end}} \simeq \sigma\frac{c}{4\alpha} = \sigma m^2 \quad \rightarrow \quad T_{\text{ins}} = 0.455 \times \sqrt{m}\,. \tag{7.57}$$

This, because of (7.54), leads to a temperature that is $T_{\text{ins}} \simeq 2.82 \times 10^{15}\,\text{GeV}$, for $m = 6.5 \times 10^{-6}$. As we will see, this estimate is not far from the one obtained in our numerical treatment. Perhaps more important is the fact that in the regime of small c the power spectrum amplitude, which forces m to be within the limits suggested by (7.54), also determines the maximum reheating temperature.

In the case of large c, ρ_{end}, and hence T_{ins}, have a completely different behavior. In fact in this case, from (7.56) and (7.45), we get

$$\rho_{\text{end}} \simeq \frac{\sigma}{8\alpha} \quad \rightarrow \quad T_{\text{ins}} = 0.270 \times a^{-1/4}\,, \tag{7.58}$$

that is, T_{ins} is controlled by the value of α, since it is proportional to $\alpha^{-1/4}$, and therefore decreases as α increases.. Due to the fact that $\alpha > 10^{10}$, for being within the large c regime, T_{ins} results in smaller values lower than in the case of small c. For example, for $\alpha = 5 \times 10^{11}$ we obtain from (7.58) a temperature $T_{\text{ins}} \simeq 0.783 \times 10^{15}\,\text{GeV}$ and certainly even lower temperatures for larger values of α. Therefore, for the largest possible value for the instantaneous temperature, of the order of $\simeq 10^{15}\,\text{GeV}$, we had better used values $\alpha < 10^{10}$ so that we are in the small c regime.

As advertised earlier, the cosmological predictions of all the models considered are based on a numerical analysis in which no approximation is made. For the present model, predictions for three different inputs, called A, B and C, are presented below. These correspond to the values of the parameters α and c given by $(\alpha, c) = (0.37 \times 10^8,\, 0.006\,),\, (10^8,\, 0.016\,)$ and $(10^9,\, 0.16\,)$ respectively. These were not chosen at random. In fact, the parameter α for the case A touches its lower bound discussed earlier, and c was chosen so that m falls well within the range suggested by (7.54). Indeed, we choose $m \simeq 6.32 \times 10^{-6}$. The rationale for this particular choice for m will be discussed later.

For the other cases, larger values of α's have been chosen, but the values of c are tuned so that in all cases we have the same value for m, *i.e.* $m \simeq 6.32 \times 10^{-6}$. In this way, we can check how the predictions change when the parameter α is changed, since we have kept a fixed m value. Note that from all the cases presented, the case A has the lowest allowed value of α and therefore the Planck upper bound on the tensor-to-scalar ratio parameter r is almost saturated. For the other cases B, C smaller values for r are expected.

Figure 7.2, at the top, shows for the cases A (left) and C (right), the primordial tilt n_s versus the reheating temperature T_{reh}, for different values of the equation-of-state parameter from $w = -1/3$ to $w = 1.0$. The shaded region marks the range $n_s = 0.9649 \pm 0.0042$ that is allowed by observations.

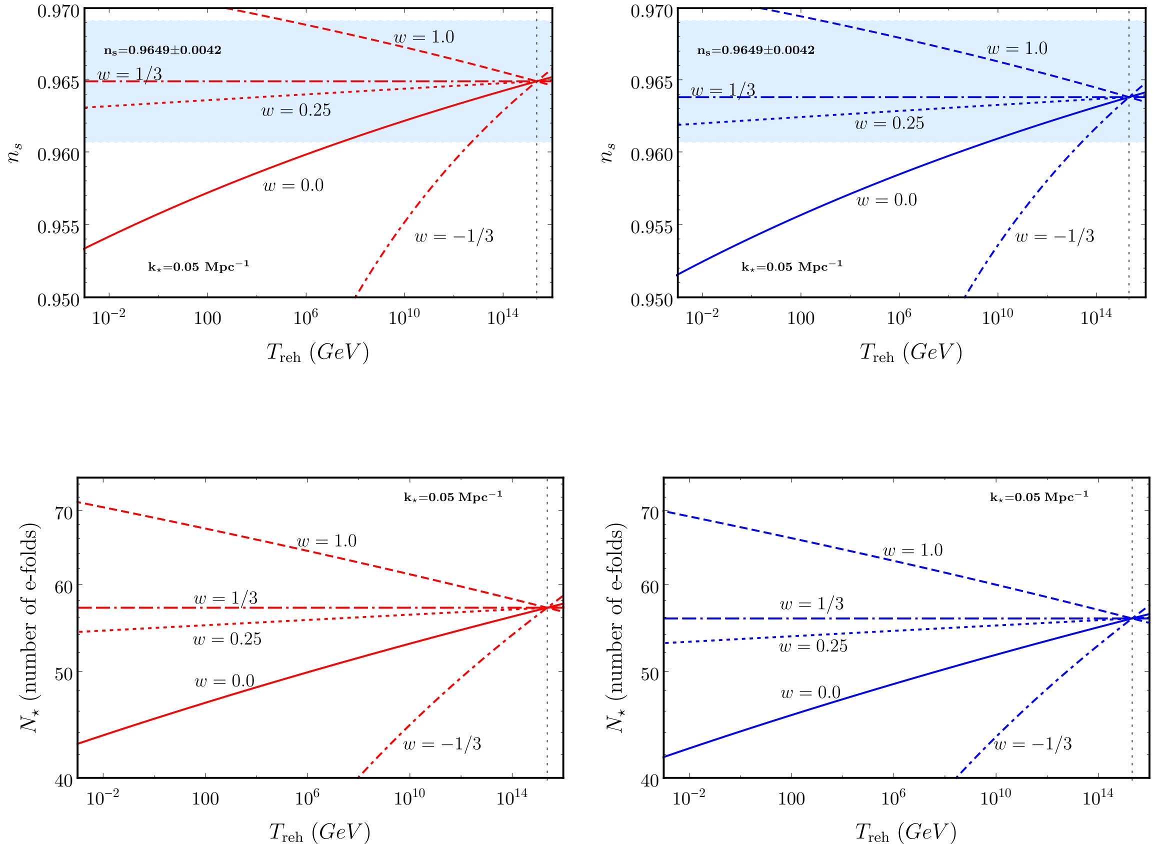

Figure 7.2: The primordial tilt n_s (top) and the number of e-folds $N_\star$ (bottom), vs. the reheating temperature $T_{\rm reh}$, in GeV, for a scale $k_\star = 0.05\,Mpc^{-1}$, and for different values of the equation-of-state parameter, for the cases A (left) and C (right) of Model I, discussed in the text. The shaded region marks the allowed values for the primordial tilt $n_s = 0.9649 \pm 0.0042$ while the vertical dashed line indicates the instantaneous reheating temperature.

All lines intersect at a common temperature, the instantaneous reheating temperature $T_{\rm ins}$, marked by thin vertical dashed lines, which for case A equals to $T_{\rm ins} = 2.337 \times 10^{15}$ GeV, and for case C to $T_{\rm ins} = 2.099 \times 10^{15}$ GeV. Values for $T_{\rm reh}$ beyond this point, are shown, but are not allowed. The data shown correspond to a pivot scale $k_\star = 0.05\,Mpc^{-1}$. Note that the n_s data by themselves are not a constraint on the reheating temperature as long as the equation-of-state parameter is in the range 0.25 to values slightly below $\simeq 1.0$. For these values of w, any temperature is allowed. For $w < 0.25$ a lower reheating temperature is specified which is larger for smaller values of w. For example for the canonical reheating scenario, $w = 0$, this is $\simeq 10^7 - 10^9$ GeV while for $w = -1/3$ this is $\approx 10^{13}$ GeV. At the bottom of the same figure, and for the same set of inputs, the corresponding numbers of e-folds, $N_\star$, are shown, for cases A (left) and C (right).

Notice that both n_s and $N_\star$, shown in the figures, are very similar for both cases A and C. In particular, both observables move slightly downward as one goes from A (left) to C (right), *i.e.* , by increasing the value of α from 0.37×10^8 to 10^9, leaving the other parameter fixed. In fact, varying only the parameter α, keeping $\lambda = m^2$ fixed, which is the case for the inputs we are using, we obtain from (7.44),

$$\delta N_\star = \frac{\delta\alpha}{\alpha} f_\alpha \,. \tag{7.59}$$

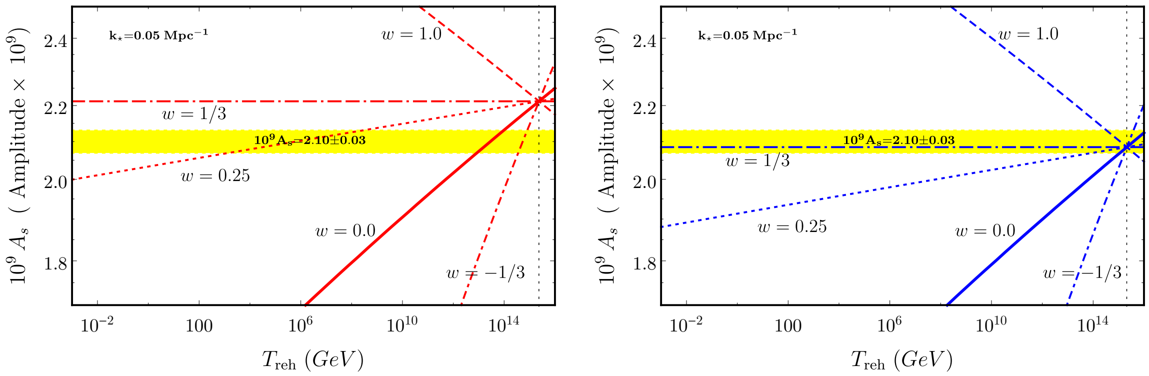

Figure 7.3: The amplitude $10^9\,A_s$ vs. the reheating temperature $T_{\rm reh}$, in GeV, for $k_\star = 0.05\,Mpc^{-1}$, for different values of the equation-of-state parameter. The shaded region marks the allowed values $10^9\,A_s = 2.10 \pm 0.03$. Case A is shown on the left and case C on the right. The instantaneous temperatures are marked by thin dashed vertical lines in each case.

For our input values, we find that the factor f_a is of order unity and negative. It follows that as the value of the parameter α increases, the relative change $\delta N_\star/N_\star$, is negativ and thus decreases due to (7.43), n_s. This decrease is small, as we have already discussed, what is indeed imprinted on this figure.

The amplitude of the scalar power spectrum impose tighter bounds on $T_{\rm reh}$ than n_s, as shown in Fig. 7.3. In this figure we plot the amplitude $10^9 \times A_s$ vs. the reheating temperature $T_{\rm reh}$, in GeV, for $k_\star = 0.05\,Mpc^{-1}$, and for different values of the equation-of-state parameter, as in the previous figure. The shaded area marks the allowed range $10^9 \times A_s = 2.10 \pm 0.03$. Case A is shown on the left and case C on the right. The lines are as in Fig. 7.2. It can be seen that for case A the values $w \gtrsim 1/3$ are completely excluded by the data of A_s, while for $w \lesssim 0.25$ bounds are set for the minimum and maximum allowed temperature. In this case, the maximum temperature, for any allowed value of w, can never reach the instantaneous temperature. For the C-case, right panel, one sees, by comparing this figure with the n_s plot, top and right panel of Fig. 7.2, that the bounds on the reheating temperature are tighter. In particular, for values of w, different from $w \simeq 1/3$, a lower reheating temperature is set, much higher than that imposed by the n_s data.

Comparing the two cases, A and C, we find that A_s is in accordance with (7.42), and the fact that λ, or equivalently m, is fixed and $\delta N_\star/N_\star$ is negative. However the change in A_s is relatively large, unlike n_s, in the sense that its variation reaches the order of magnitude of the observational error of A_s, as discussed earlier.

It is worth noting that for given a value for the parameter α there is a fine-tuned value of m, in the range suggested by (7.54), for which the case $w = 1/3$ falls within the allowed range by A_s observations[3]. In this case, the instantaneous reheating temperature is reached for each value of w in the range $-1/3 \leq w \leq 1$. However, in this case, for each w that differs from the value $1/3$, a lowest temperature is determined that is close to the instantaneous temperature. This includes the values $0.0 \lesssim w \lesssim 0.25$, which are preferred in some reheating scenarios. This is clearly seen, for example, in Case C, where for $\alpha = 10^9$ the value $m = 6.32 \times 10^{-6}$ forces the line $w = 1/3$ within the A_s boundaries, as shown on the right panel of Fig. 7.3. Keeping α fixed, any slight change in the value of the parameter m, which essentially controls A_s, causes the line $w = 1/3$, to be shifted down or up out of the allowed range, and in this case

[3]This assumes that the case $w = 1/3$ is compatible with $N_\star$ in the range $\approx 50 - 60$, which is always the case unless the parameter α takes extremely high values.

Table 7.1: Example outputs for Model I, for inputs corresponding to cases A, C (see main text), for the cosmological observables n_s, r, A_s and $N_\star$, for different values of the equation-of-state parameter. The values shown for the reheating temperature $T_{\rm reh}$, in GeV, correspond to the minimum (top rows) and maximum (bottom rows) allowed when the observational limits for $A_s \simeq (2.10 \pm 0.03) \times 10^{-9}$ and $n_s = 0.9649 \pm 0.0042$ are respected. Blank entries indicate that there are no values for the specific value of w that are compatible with the observational bounds set on n_s and A_s.

Model I (pivot scale $k_\star = 0.05\,Mpc^{-1}$)						
		A - case			C - case	
w - value	$w = 0.0$	$w = 0.25$	$w = 1.0$	$w = 0.0$	$w = 0.25$	$w = 1.0$
$10^9\,A_s$	2.07	2.07		2.07	2.07	2.13
n_s	0.9637	0.9637		0.9637	0.9637	0.9642
r	0.0616	0.0616		0.0040	0.0040	0.0038
$N_\star$	55.25	55.25		55.65	55.65	56.43
$T_{\rm reh}$	8.542×10^{12}	1.547×10^3		1.138×10^{15}	9.741×10^{13}	3.667×10^{14}
$10^9\,A_s$	2.13	2.13		2.08	2.08	2.08
n_s	0.9642	0.9642		0.9638	0.9638	0.9638
r	0.0602	0.0602		0.0039	0.0039	0.0039
$N_\star$	56.03	56.03		55.85	55.85	55.85
$T_{\rm reh}$	8.861×10^{13}	1.855×10^8		2.099×10^{15}	2.099×10^{15}	2.099×10^{15}

the instantaneous reheating scenario is no longer supported. At the same time, depending on the value of m, lower and upper limits of reheating temperatures are imposed, which are different for each w. However, some values of w are completely excluded. By increasing m, the line $w = 1/3$ is raised and moves above the upper observational limit on A_s. In this case, all values in the range $1/3 \leq w \leq 1$ are excluded. On the other hand if one decreases m, the line $w = 1/3$ moves below the lower bound of A_s and values $-1/3 \leq w \leq 1/3$ are excluded. Further Increasing or decreasing the value of m excludes all possible cases $-1/3 \leq w \leq 1$. Thus, there is a range of m outside of which no agreement with the data of A_s can be obtained, for any value of w, in the interval $-1/3 \leq w \leq 1$. This range is indeed narrow and falls within the range given by (7.54). Within this range there are fine-tuned values for which the reheating can be instantaneous. Note that the sensitivity of the primordial tilt n_s to the value of m is not so dramatic, and the n_s data leave more room to satisfy observational requirements. Therefore, the conclusion is that for a given α, the value of m should be in a very narrow range, to match the power spectrum data. Moreover, if the reheating is instantaneous, it should be appropriately fine-tuned. This is also true, as we shall see, for other popular models, in particular the Higgs model, which we will discuss later.

Following the numerical procedure already outlined, we show in Table 7.1 example results of the considered model for the choice of parameters corresponding to the inputs A, and C for a pivot scale $k_\star = 0.05\,Mpc^{-1}$. The predicted cosmological observables n_s, r, A_s are shown for different values of the equation-of-state parameter w corresponding to the minimum (top rows) and maximum (bottom rows) allowed reheating temperatures $T_{\rm reh}$ when the limits $A_s \simeq (2.10 \pm 0.03) \times 10^{-9}$, and $n_s = 0.9649 \pm 0.0042$ are satisfied. The corresponding predictions for the number of e-folds $N_\star$, are also shown. Blank entries indicate that there are no values for the specific value of w that are compatible with the observation bounds for n_s, A_s. Note that for the C - case the maximum reheating temperature is the instantaneous reheating temperature, $T_{\rm ins} = 2.099 \times 10^{15}$ GeV. At this temperature, the predictions are independent of w, since $T_{\rm ins}$ marks the intersection of all w-lines. For the same case, the lower bounds for $T_{\rm reh}$ are also shown. For the cases $w = 0.0$, 0.25 and $w = 1.0$, these are not very far from $T_{\rm ins}$, in agreement with Fig. 7.3, right panel, as discussed earlier. For the A - case , on the other hand, both the minimum and maximum reheating temperatures are smaller than the corresponding values for the C - case. Note in particular the predictions for $w = 0.25$, for which the temperature range allowed by all observations is $T_{\rm reh} \simeq (1.5 \times 10^3 - 1.9 \times 10^8)$ GeV.

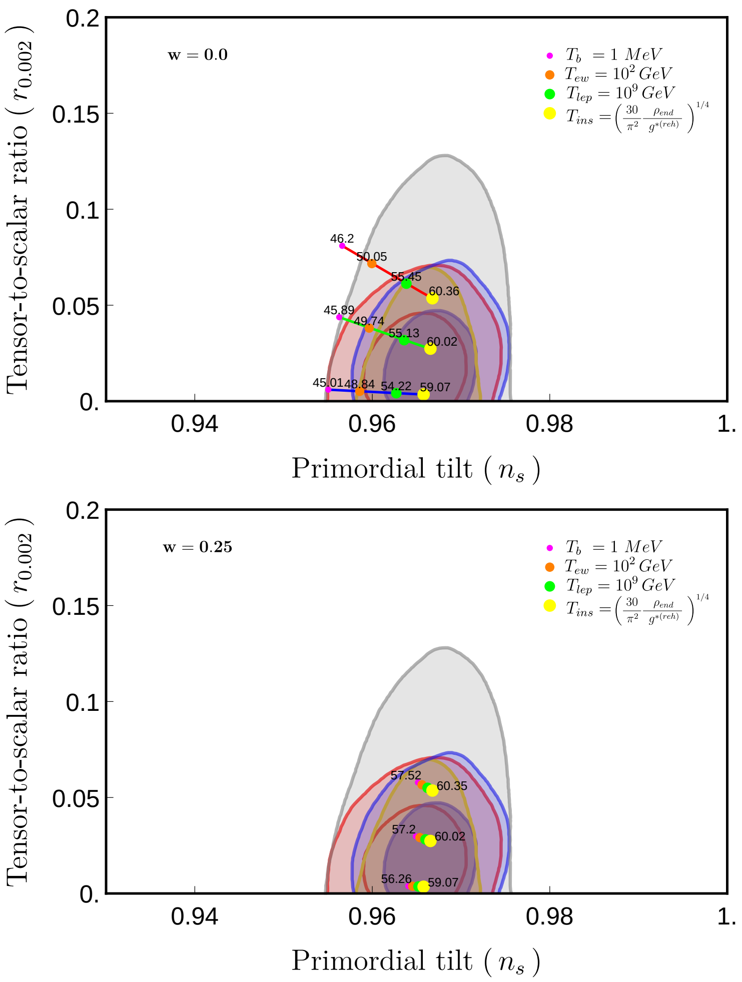

Figure 7.4: The tensor-to-scalar ratio $r_{0.002}$ vs. the primordial tilt n_s for Model I, for the data sets A (red line), B (green line) and C (blue line) corresponding to different inputs of the parameters (see main text). A pivot scale $k_\star = 0.002\,Mpc^{-1}$ is used, allowing a direct comparison with the corresponding Planck 2018 data. The value of the equation-of-state parameter for the upper figure is $w = 0.0$, while for the lower figure $w = 0.25$. The tiny circle (in magenta), the small one (in orange) and the large one (in green) correspond to the reheating temperatures close to BBN, Electroweak and Leptogenesis scenarios, respectively, while the largest one (in yellow) marks the instantaneous reheating temperature. In each case, the numbers indicate the e folds when $k_\star = 0.002\,Mpc^{-1}$.

In Fig. 7.4, for Model I, the tensor-to-scalar ratio $r_{0.002}$ is plotted against the primordial tilt n_s for data sets A (red line), B (green line), and C (blue line). A pivot scale $k_\star = 0.002\,Mpc^{-1}$, was used in drawing this figure so that it can be directly compared to the corresponding Planck 2018 limits [82, 87], which are also plotted. The tiny circle (in magenta), the small one (in orange) and the large one (in green) correspond to the reheating temperatures close to BBN, Electroweak and Leptogenesis scenarios, given by $T_b = 1\,MeV$, $Tew = 10^2$ GeV and $T_{lep} = 10^9$ GeV, respectively. The largest circle (in yellow) marks the instantaneous reheating temperature, see Eq. (6.9), for each case shown. The number next to each circle indicates the corresponding number of e-folds remaining at the pivot scale $k_\star = 0.002\,Mpc^{-1}$. The value of the equation-of-state parameter for the upper figure is $w = 0.0$, while for the lower one $w = 0.25$. In the latter, only the e-folds corresponding to T_b and instantaneous reheating are shown to be clearly visible. In both cases shown, $w = 0$ and $w = 0.25$,one obtains the smallest values for the tensor-to-scalar ratio r in the C - case, *i.e.* for the largest values of the parameters α, c. Recall that the ratio c/a was kept fixed. For smaller values of the parameters, r becomes larger and saturates the Planck upper bound in the A - case, corresponding to the smallest allowed values of α, c, as we have already noted.

We note that in the drawing of Fig. 7.4 the A_s-constraints have not been included. When they are included, the allowed line segments shown in the figure are reduced considerably, since $T_{\rm reh}$ is further constrained by the A_s data. For example, for the C - case, which is well within the range allowed by all observations and also gives the smallest value for r, much of the segment with ends corresponding to temperatures T_b and the minimum allowed temperature as read from Table 7.1 for each w-case, is cut out. Only a tiny part of it, close to the maximum reheating temperature $T_{\rm ins}$, will remain.

Model II :

As a second model (Model II) worth studying, is the one in which the functions g, M^2 are as in (7.24), as in Model I, but the potential is quartic in the involved scalar field, *i.e.*

$$V(\phi) = \frac{\lambda}{4}\phi^4 \,, \tag{7.60}$$

that is $n = 4$. We have already noted from the qualitative arguments presented earlier that this model, as well as all those with $n > 4$, do not satisfy the spectral index observations unless one has a large number of e-folds, probably larger than $N_\star > 76$, or so. However, a more detailed investigation is needed to reach a firm conclusion that also takes the reheating temperature into account.

Applying the general results given at the beginning of this section to this model, we get,

$$\phi_\star \simeq \sqrt{8N_\star} \,. \tag{7.61}$$

Also on account of (7.36) the coupling λ is

$$\lambda \simeq 10^{-8}\,\frac{3.11}{N_\star^3} \,, \tag{7.62}$$

which for e-folds in the range $N_\star = 50 - 60$, yields

$$\lambda \simeq (1.45 - 2.50) \times 10^{-13} \,, \tag{7.63}$$

the lowest value corresponding to $N_\star = 60$. Therefore, the coupling λ must be quite small to satisfy the requirements imposed by the observations. For the parameter α, which sets the inflation scale, employing (7.38), we have a lower bound given by

$$\alpha \gtrsim (0.47 - 0.50) \times 10^8 \,, \tag{7.64}$$

not much different from the bounds given in (7.55).

For $T_{\rm ins}$, as in the case $n = 2$, we must compute $\phi_{\rm end}$ and use (7.50) adapted to the case $n = 4$. Although an analytical solution for $\phi_{\rm end}$ is possible by Eq. (7.33), we will not present it. Instead, we will discuss its behaviour for small and large c-values. For small c-values, omitting the $\mathcal{O}(c^2)$ terms, we find $\phi_{\rm end}^2 \simeq 8(1 - 64\,c)$. Then from (7.50) the leading contribution is,

$$\rho_{\rm end} \simeq \sigma\frac{8c}{\alpha} = 16\sigma\lambda \quad \rightarrow \quad T_{\rm ins} = 0.909 \times \lambda^{1/4} \,. \tag{7.65}$$

With $\lambda = 2 \times 10^{-13}$, the central value in the range (7.63), there is an instantaneous reheating temperature around $T_{\rm ins} \simeq 1.48 \times 10^{15}$ GeV. As in the previously studied model, in the case of $n = 2$ case, the power spectrum determines the maximum reheating temperature, in the regime of small c. In the case of large c, $\phi_{\rm end}^2$ behaves like $c^{-1/3}$ and therefore contributes

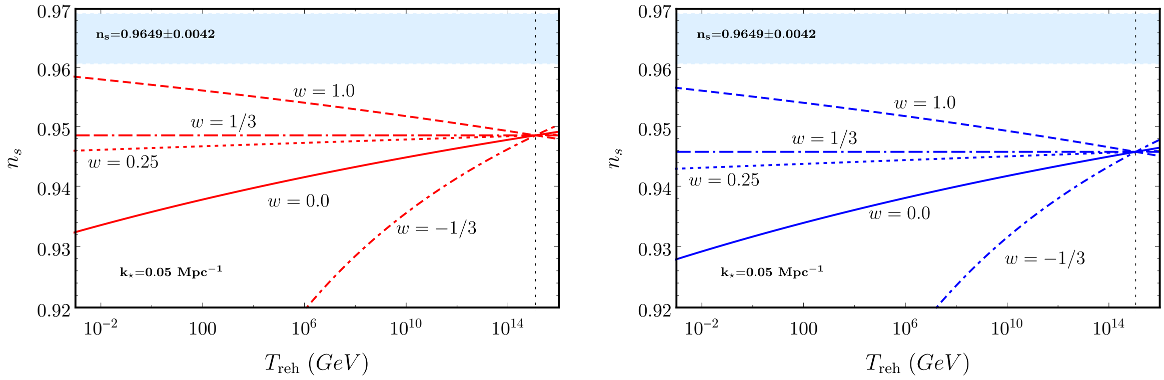

Figure 7.5: The primordial tilt n_s, vs. the reheating temperature $T_{\rm reh}$, in GeV, for a scale $k_\star = 0.05\,Mpc^{-1}$, and for various values of the equation-of-state parameter, for cases A (left) and B (right) of Model II discussed in the text. The shaded regions mark the allowed values for the primordial tilt $n_s = 0.9649 \pm 0.0042$ and the vertical dashed lines the instantaneous reheating temperatures.

little to Eq. (7.50). If we then keep only the leading term in $\rho_{\rm end}$, we get the same result (7.58) as in the previous model, and $T_{\rm ins}$ is again proportional to $\alpha^{-1/4}$.

For this model, we will also present example results of our numerical treatment, considering a fixed value $\lambda = 2.0 \times 10^{-13}$, in the middle of the range proposed by (7.63), and values of α in the range $a = 5 \times 10^7 - 5 \times 10^9$, thus respecting the bound (7.64). The value $a = 5 \times 10^7$ corresponds to the lowest allowed value, and we call it for the future A - case, while 5×10^9 is arbitrarily taken two orders of magnitude larger, which we call B - case. Although in principle one can also consider larger α - values, it is not necessary to do so for reasons that will be briefly explained.

The left panel of Fig. 7.5 shows the predictions for the primordial tilt n_s, for the cases A (left) and B (right), as a function of the reheating temperature for different values of the equation-of-state parameter w. Note that there is not much difference between the two cases, although the parameter α differs by two orders of magnitude. The explanation is the same as for Model I. Note that the lines on the right have been shifted imperceptibly downwards. That is, the trend is toward lower n_s values as the α parameter increases. As for the instantaneous reheating temperature, for the taken values of α, λ, for the A - case it is $T_{\rm ins} = 1.223 \times 10^{15}$ GeV, while for the B - case this is $T_{\rm ins} = 1.129 \times 10^{15}$ GeV. These are marked by vertical thin dashed lines, as in the previous figures. As noted for this model, agreement with n_s observational data is difficult to achieve. In both cases, it is clear from this figure that values for n_s that are just acceptable can only be obtained for very small reheating temperatures and only for $w = 1$. In this case, the number of e-folds is large $N_\star > 70$, as is shown in Fig. 7.6 where the number of e-folds is plotted. We did not consider larger values of α because, as explained, they would predict lower n_s, leading to larger deviations from the data.

Although no agreement with n_s data can be obtained in this model, we give a brief account of the predictions for the amplitude of the power spectrum for the sake of completeness. Agreement with A_s data requires values of w smaller than 0.25 for the A - case, while for the B - case the value $w = 0.25$ is narrowly accepted. Values smaller than $w \simeq 0.25$ are allowed. In any case, such values for the equation-of-state parameter as shown in Fig. 7.5lead to even smaller values of n_s, smaller than $\simeq 0.945$ or so, and thus unacceptable. Models with $n > 4$ give predictions that are also difficult to reconcile with the data according to our general arguments.

From this it is concluded that from the class of models whose initial potential is of the

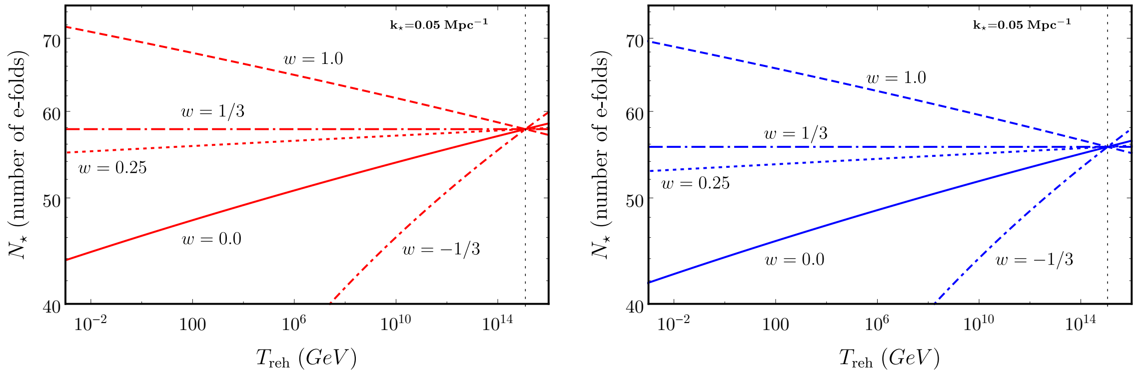

Figure 7.6: As in Figure 7.5 for the number of e-folds $N_\star$.

monomial form $V \sim \phi^n$, and with constant values for the coefficients of the terms R and R^2 in Palatini gravity, only the case $n = 2$, which belongs to the class of cosmological attractors [364], can lead to successful inflation whenall observational constraints are taken into account.

7.3.2 Nonminimally coupled models

Nonminimal coupling arises when the constants g and/or M^2 are field-dependent in the models studied so far. A particularly interesting case is the model in which

$$g(h) = 1 + \xi_h h^2 \ , \ M^2(h) = \frac{1}{6\alpha} \ , \ V(h) = \frac{\lambda_h}{4} h^4 \, . \tag{7.66}$$

This belongs to the class of models (7.24), with quartic potential, but the scalar h is non-minimally coupled to the scalar curvature R, in the Palatini framework, since g is field dependent, in the particular way shown above. This model actually follows from the Higgs coupling (hence we use h instead of ϕ for the scalar field) to Palatini gravity

$$\frac{M_{\rm P}^2 + 2\xi_h H^\dagger H}{2} R + \frac{\alpha}{2} R^2 + |DH|^2 - \lambda_h \left(|H|^2 - \frac{u_h^2}{2} \right)^2 , \tag{7.67}$$

where $u_h \simeq 246\,\text{GeV}$ is the Electroweak scale. In Planck units, this is very small $u_h \sim 10^{-16}$ and plays no significant role in inflation. Thus, setting $u_h = 0$ and working in the unitary gauge, $H^\dagger = (0, h/\sqrt{2})$, (7.67) is actually the model described by g, M^2 and the quartic potential as given in (7.66).

The Higgs coupling to gravity and its role as an inflaton, in the metric formulation, was proposed in [365, 366] and it has been widely studied since then [7, 179, 181, 203–205, 357, 367–388] both in the context of the metric formulation and in Palatini formulation. The importance of the term R^2 in (7.67) was discussed in [179, 203–205]. In this thesis we will show that the quartic coupling λ_h, as in the minimally coupled quartic model studied previously, corresponding to $\xi_h = 0$, is strongly constrained by cosmological data, in particular the power spectrum amplitude A_s. This limits the available options, especially when the reheating of the Universe after inflation is considered.

The functions K, L and $\bar{U}$ in this model are given below, in the limit $u = 0$,

$$K(h) = \frac{1 + \xi_h h^2}{(1 + \xi_h \, h^2)^2 + c h^4} \ , \ L(h) = \frac{2\alpha}{(1 + \xi_h h^2)^2 + c h^4} \, , \tag{7.68}$$

while the potential $\bar{U}$ receives the form

$$\bar{U}(h) = \frac{1}{8\alpha}\,\frac{ch^4}{(1+\xi_h h^2)^2 + ch^4}\,. \tag{7.69}$$

As in the simple quartic potential, the parameter c is the combination $c = 2\alpha\lambda_h$. Note, however, that there is a non-trivial ξ_h-dependence and therefore the Higgs model is different from the simple quartic model studied earlier. Obviously, if $\xi_h = 0$ the functions (7.68), (7.69) smoothly go into (7.26), (7.27).

For large values of h the potential (7.69) approaches a plateau $\simeq 1/8(\alpha + \xi_h^2/2\lambda_h)$, and hence an inflation scale μ can be established. Specifically, reintroducing units, this is defined by $\mu \equiv M_{\mathrm{P}}/\sqrt{6(\alpha+\xi_h^2/2\lambda_h)}$. Then the potential for large field values approaches $\bar{U} \simeq 3\mu^2 M_{\mathrm{P}}^2/4$. For comparison, in the Starobinsky model the inflaton potential reaches $3\,\mu_S^2 M_{\mathrm{P}}^2/4$, where μ_S is the scalaron mass, and in this case cosmological data determine its size, given by $\mu_S \simeq 10^{-5}\,M_{\mathrm{P}}$. In the considered model, the size of μ will be discussed later when bounds are set for the parameters ξ_h, λ_h and α.

In the same way as in the models studied before, the slow roll parameters ϵ_V, η_V are given by, as functions of h,

$$\epsilon_V = \frac{8(1+\xi_h\, h^2)}{h^2(1+2\xi_h h^2 + (\xi_h^2+c)h^4)}\,,\; \eta_V = \frac{4}{h^2}\left(-\frac{3+2\xi_h h^2}{1+\xi_h h^2} + \frac{6(1+\xi_h\, h^2)}{(1+\xi_h\, h^2)^2 + ch^4}\right)\,. \tag{7.70}$$

Although the parameter η_V has a rather complicated form, both the primordial tilt and amplitude of the power spectrum have rather simple expressions. In fact, they are given by

$$n_s = 1 - \frac{16}{h_\star^2} - \frac{8}{h_\star^2(1+\xi_h h_\star^2)} \tag{7.71}$$

and

$$A_s = \frac{\lambda_h}{24\,\pi^2}\,\frac{h_\star^6}{32(1+\xi_h h_\star^2)}\,, \tag{7.72}$$

where we have replaced the field h with its pivot value $h_\star$. These agree with (7.40) and (7.28), respectively, for $n = 4$, when $\xi_h = 0$, as they should. However, the presence of the ξ_h changes the predictions for the cosmological observables, as we will see.

To get further, we need the pivot value $h_\star$. In this case, the number of e-folds $N_\star$ is given by

$$N_\star = \frac{1}{8}\,(h_\star^2 - h_{\mathrm{end}}^2)\,. \tag{7.73}$$

This does not explicitly depend on the parameter ξ_h and is identical to (7.30) if $n = 4$. Hence

$$h_\star^2 = 8N_\star + h_{\mathrm{end}}^2\,, \tag{7.74}$$

which is functionally the same as (7.31), but the value of h_{end} is different. The latter depends on both ξ_h and the combination $c = 2\alpha\lambda_h$ and is given as the solution of equation

$$ch_{\mathrm{end}}^6 + (1+\xi_h h_{\mathrm{end}}^2)(h_{\mathrm{end}}^2(1+\xi_h h_{\mathrm{end}}^2) - 8) = 0\,. \tag{7.75}$$

This is a cubic equation in h_{end}^2, which we prefer to cast in the form (7.75) for reasons that will become clear below. Note that in the limit $\xi_h = 0$ this equation becomes (7.33), if we put $n = 4$ in the latter. In the form represented by (7.75), we see that at $c = 0$ the solution for h_{end}^2 is easily obtained, since it becomes a quadratic equation for h_{end}^2. This observation is useful when we want to study the predictions of the model for small c, expanding in powers of c around the zero-order solution.

Since this is a cubic equation for h_{end}^2, one can obtain an analytic solution, and in our case there is only one real and positive solution. The value of this solution can never be greater than 8 for h_{end}^2. In fact, this value is obtained when h_{end}^2 is less than $\sim 10^{-3}$. For larger values, the root of this equation is smaller. It follows that h_{end}^2 in (7.74) can be neglected and $h_\star$ can be approximated by

$$h_\star \simeq \sqrt{8N_\star}\,, \tag{7.76}$$

as in the simple quartic model. Replacing this value in (7.71) and (7.72) we get

$$n_s = 1 - \frac{2}{N_\star} - \frac{1}{N_\star(1+8\xi_h N_\star)}\,, \tag{7.77}$$

and

$$A_s = \frac{2\lambda_h}{3\,\pi^2}\,\frac{N_\star^3}{(1+8\xi_h N_\star)}\,. \tag{7.78}$$

As expected in the limit $\xi_h = 0$ these smoothly go to (7.41) and (7.35) when in the latter we put $n = 4$.

However, the role of the parameter ξ_h is very important and can improve the case, as far as the primordial tilt n_s is concerned. In the simple quartic model, the predictions for n_s are difficult to reconcile with the cosmological observations, unless one considers large values of the e folds, $N_\star \simeq 70$ or so, as discussed earlier. Such large values of e-folds may not be acceptable, as they require very low values for the reheating temperature, at least in the standard reheating scenarios. If one accepts a large number of e-folds, $N_\star > 70$, this may be consistent with alternative reheating scenarios, which can be interesting in their own right, but we would like to take a more conservative stance in this thesis.

As for ξ_h, we assume that it is positive. Then one sees from (7.77) that n_s is larger than the one obtained in the quartic potential studied before, which corresponds to $\xi_h = 0$. Moreover, for any $N_\star$ the observable n_s increases as ξ_h grows and therefore values within limits may be obtained for sufficiently large values of ξ_h. From (7.77) it can be seen that for values $\xi_h \simeq 0.06$ the primordial tilt can be within observational limits, for e-folds in the range $N_\star \simeq 52 - 60$. That is for this value of ξ_h a large portion of e-folds, in the range $50 - 60$, is covered, which is broadened for larger ξ_h allowing, also, for values of $N_\star$ lower than 52. Values of $\xi_h < 0.06$ are also acceptable, but at the cost of significantly shrinking the range of allowed e-folds, that are compatible with the observational limits imposed by n_s. For example, for $\xi_h \simeq 0.004$ one obtains $n_s = 0.9607$, at the edge of the lower observational limit, which pushes $N_\star$ to $N_\star \simeq 60$. From these arguments, it is apparent that a reasonable range to deal with in our numerical procedure is to focus on values of ξ_h of the order of $\mathcal{O}(10^{-2})$, or larger. In what follows, we will take $\xi_h \gtrsim 0.06$ on the grounds that this is likely to cover a wider range of e-folds, as we explained above.

From (7.78), and accepting that A_s is $\simeq 2.1 \times 10^{-9}$, the quartic coupling is bounded as follows

$$\lambda_h \simeq 3.11 \times 10^{-8}\,\frac{1+8\xi_h N_\star}{N_\star^3}\,. \tag{7.79}$$

In the limit $\xi_h = 0$ this coincides with (7.62), as it should. From this it can be seen that the allowed values for λ_h depend on the parameter ξ_h, and also that in this case there are larger values of the coupling λ_h, than in the simple quartic model. However, even in this case the quartic coupling is small. For $\xi_h = 0.06$, it is of the order $\sim 10^{-12}$. For λ_h to reach values of order $\gtrsim 10^{-6}$, one needs large values $\xi_h \gtrsim 10^4$ when $N_\star \simeq 50-60$.

As for the parameter α, as discussed in the previous models, a lower bound for it can be given by (6.5),

$$\alpha \gtrsim 5\times 10^7 \left(1.25 - \frac{N_\star(1+8\xi_h\, N_\star)}{200}\right) . \tag{7.80}$$

This bound on α depends on ξ_h, it is quadratic in $N_\star$, and there is a critical value of ξ_h beyond which it becomes negative, which means that in this case any positive value of α is actually allowed. Since we prefer to work with values $\xi_h > 0.06$ the RHS of (7.80) is negative, for $N_\star \simeq 50-60$, and for our purposes there is virtually no lower bound on the parameter α. The lack of a lower bound can be important because α in this case can be chosen either larger or smaller than the ratio $\xi_h^2/2\lambda_h$. In the regime

$$\xi_h^2 > 2\alpha\lambda_h\,, \tag{7.81}$$

an upper bound on α is imposed, for given $\xi_h\,,\lambda_h$. Of particular interest, within this regime, is the case where $\xi_h^2 \gg 2\alpha\lambda_h$. In this limit, one sees from (7.68) and (7.69) that the functions $K(h)$ and the potential $\bar{U}(h)$ do not depend on the parameter α. Rather, $K(h)$ depends only on ξ_h and $\bar{U}(h)$ depends on ξ_h, λ_h. Although the function $L(h)$ depends on α, its influence in the equations of motion is small for the cases of interest here, as we have already noted. Therefore, in this case the results are independent of the parameter α, as long as $\xi_h^2 \gg 2\alpha\,\lambda_h$ holds. In this case the inflation scale μ, as previously defined, becomes $\mu \simeq \sqrt{\lambda_h/3\xi_h^2}\, M_{\mathrm{P}}$ and lies in the range $\sim (2\times 10^{-5} - 5\times 10^{-7})\, M_{\mathrm{P}}$, for values of ξ_h in the range $0.06 - 100.0$ and for $N_\star$ between $50-60$, with the smaller (larger) scales being obtained for higher (lower) ξ_h and $N_\star$ values. Obviously, the previously mentioned arguments are no longer valid when the parameters in regime

$$\xi_h^2 < 2\alpha\,\lambda_h\,. \tag{7.82}$$

Then we have a lower bound for α, for given ξ_h, λ_h. Also in this case, the predictions depend on α and ξ_h, λ_h. In particular, if $\xi_h^2 \ll 2\alpha\,\lambda_h$ the inflation scale is $\mu \simeq M_{\mathrm{P}}/\sqrt{3a}$, *i.e.* it is determined solely by α.

The lower and upper bounds of the parameter α, for having $a > \xi_h^2/2\lambda_h$ and $a < \xi_h^2/2\lambda_h$, are given in the fourth and fifth columns, respectively. In preparing this table, the values of $N_\star$ were taken as usual in the range $N_\star \simeq 50-60$.

To obtain an estimation of the instantaneous reheating temperature, which is given by (7.45), we need to know the energy density at the end of inflation. Following similar arguments as for the previously studied models, we find that in this case it is given by

$$\rho_{\mathrm{end}} \;=\; \frac{\sigma}{8\alpha}\left(1 - \frac{h_{\mathrm{end}}^2(1+\xi_h\, h_{\mathrm{end}}^2)}{8}\right) \equiv \frac{\sigma}{8\alpha}\, F(\xi_h, c)\,. \tag{7.83}$$

Recall that $\sigma = 1.5$. The function $F(\xi_h, c)$ is too complicated to be presented, although there is an analytic expression for the unique positive solution h_{end}^2 of Eq. (7.75). We will actually use this for the computation of ρ_{end} by (7.83). Replacing α by $c/2\lambda_h$, where λ_h is given by (7.79), we obtain from (7.45),

$$T_{\mathrm{ins}} \;=\; (0.968\times 10^{-3})\left(\frac{55}{N_\star}\right)^{1/2}\left(\xi_h + 2.27\times 10^{-3}\,\frac{55}{N_\star}\right)^{1/4} R^{1/4}(\xi_h, c)\,, \tag{7.84}$$

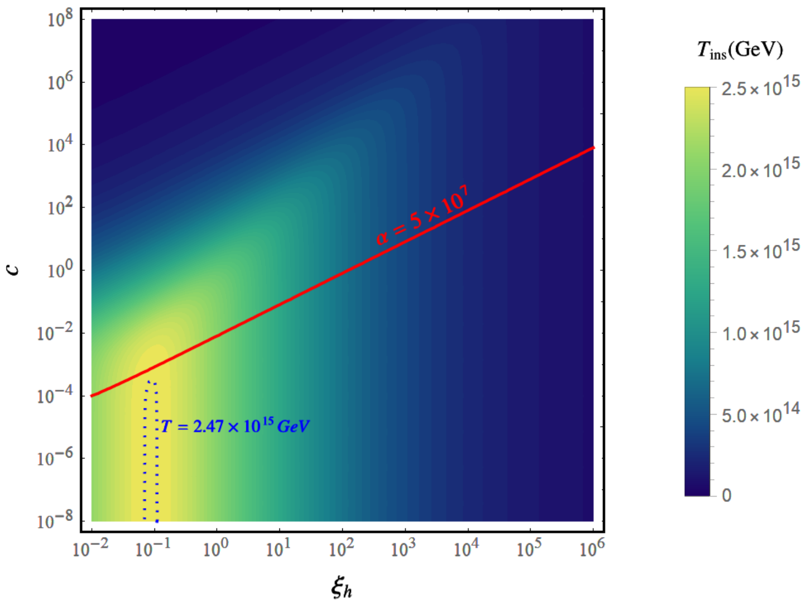

Figure 7.7: In the c, ξ_h plane we show the instantaneous reheating temperature, given by Eq. (7.84), for $N_\star = 55$. Light colors correspond to larger temperatures. The largest temperature, $T \simeq 2.47 \times 10^{15}$ GeV, is in the yellow region at $\xi_h \simeq 0.1$, whose limit is the blue dashed line. The red line is the locus of the points with $\alpha = 5 \times 10^7$.

where $R(\xi_h, c) = F(\xi_h, c)/c$. This gives it a very simple form in certain regions, and interestingly, this includes the region where $T_{\rm ins}$ gets its largest value.

The first region of interest is when $c/\xi_h^2 < 1$. As we noted earlier, Eq. (7.75) is easy to solve when c vanishes, since in this case it reduces to a quadratic equation for $h_{\rm end}^2$. For non-vanishing c, within the regime $c/\xi_h^2 < 1$, we can treat this ratio as a small parameter, to find the desired solution as a deviation from the zeroth-order solution, corresponding to $c = 0$. This is easy to implement and leads to a function $R(\xi_h, c)$ that is independent of c to the lowest order in c/ξ_h^2. In particular, it is found that,

$$R(\xi_h, c) \;=\; \left(\frac{1 + 16\xi_h - \sqrt{1 + 32\,\xi_h}}{16\,\xi_h^2} \right)^2 \;\equiv\; P(\xi_h)\,. \tag{7.85}$$

The function $P(\xi_h)$ is regular at $\xi_h = 0$, with limit $P(0) = 64$. Using this, we find from (7.84)

$$T_{\rm ins} \;=\; (0.968 \times 10^{-3})\;(\xi_h\,P(\xi_h))^{1/4}\quad . \tag{7.86}$$

In this we have set $55/N_\star \simeq 1$, and also assume that $\xi_h > 0.01$, which is actually the region we are interested in. Note that (7.86) is valid in the regime $c/\xi_h^2 < 1$ and it is a very convenient relation. Within the regime $c < \xi_h^2$ the maximum temperature is reached when $\xi_h P(\xi_h)$ reaches its maximum. This occurs at $\xi_h = 3/32$, *i.e.* very close to $\simeq 0.094$, and for this value $T_{\rm ins} \simeq 2.47 \times 10^{15}$ GeV, in natural units. This is independent of c as long as c is much smaller than ξ_h^2. Away from this maximum, $T_{\rm ins}$ decreases with increasing ξ_h increases and behaves like $T_{\rm ins} \simeq (0.968 \times 10^{-3})\,\xi_h^{-1/4}$. Another interesting region is when c is large and $c >> \xi_h^2$. In this region the function $F(\xi_h, c)$ that controls $\rho_{\rm end}$ in (7.83) is very close to unity. Note that the size of c alone is not sufficient to have $F(\xi_h, c) \simeq 1$, despite the fact that $h_{\rm end}^2$ is small. We must additionally require that $c >> \xi_h^2$. Then it turns out that $\rho_{\rm end}$ is inversely proportional to α, and thus the instantaneous reheating temperature is proportional to $\alpha^{-1/4}$, or equally proportional to $(\lambda_h/c)^{1/4}$. The latter is proportional to $(\xi_h/c)^{1/4}$ if (7.79)

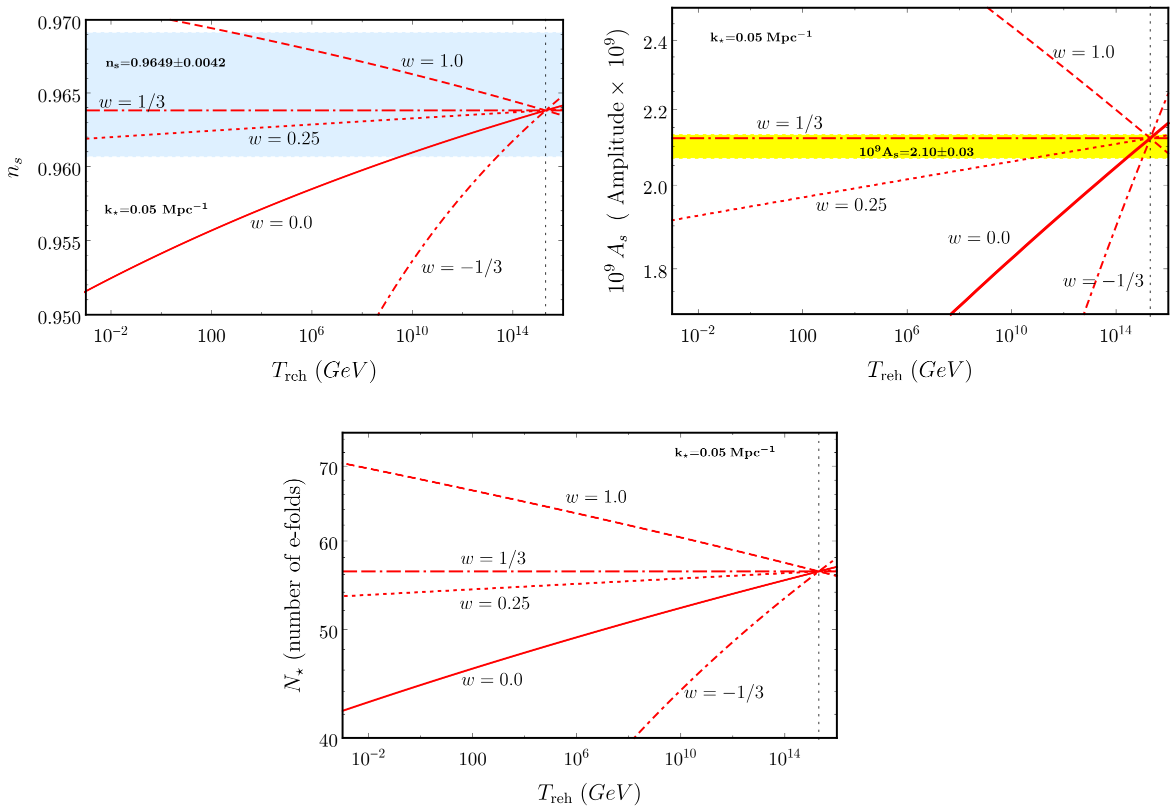

Figure 7.8: Top: The primordial tilt n_s, left, and the amplitude of the power spectrum A_s, right, vs. the reheating temperature $T_{\rm reh}$, for the Higgs model, for inputs $\xi_h = 0.06$, $\lambda_h = 4.875 \times 10^{-12}$ and $\alpha = 5 \times 10^5$. Bottom: For the Higgs models and same inputs, the number of e-folds is plotted against the reheating temperature.

is used. Then the analytic result for $T_{\rm ins}$ in this case is trivially found from (7.84),

$$T_{\rm ins} \simeq (0.968 \times 10^{-3}) \left(\frac{\xi_h}{c}\right)^{1/4} . \tag{7.87}$$

This applies to large c values, satisfying the condition $c \gg \xi_h^2$, and so cannot be arbitrarily large. The largest value within this regime is about $\simeq 10^{15}$ GeV, which is slightly smaller than the corresponding temperature of the $c << \xi_h^2$ region. This is obtained for $c \simeq 10^2$, which is relatively large, and values of ξ_h^2 about an order of magnitude smaller than c. Any other pair of values, for these parameters, within this particular regime, leads to lower values of $T_{\rm ins}$.

Unfortunately, there are no simple mathematical expressions to deal with outside of the above, and we will rely on a numerical treatment of (7.84). In fact, scanning the two-dimensional parameter space c, ξ_h^2, we found that the approximate formulas given earlier agree with the values obtained from (7.84) with very good accuracy in the corresponding regions. In Fig. 7.7 we show the instantaneous reheating temperature, as given by Eq. (7.84), for $N_\star = 55$. Light colors correspond to higher temperatures. From this figure, it is clear that the larger temperatures are obtained for values of the parameters within the small yellow region, located at the bottom and left. The region with the largest temperature $T_{\rm ins}$ is centered around $\xi_h \simeq 0.1$, and values $c \lesssim 10^{-4}$, having as boundary the blue dashed line corresponding to $T_{\rm ins} = 2.47 \times 10^{15}$ GeV. The maximum temperature reached is very close to it, confirming our previous arguments. Within this region $\xi_h \simeq 0.1$, and since Eq. (7.79) is used, $\lambda_h \simeq 10^{-12}$. Therefore $\alpha = c/2\lambda_h \lesssim 5 \times 10^7$ is needed for having the largest possible

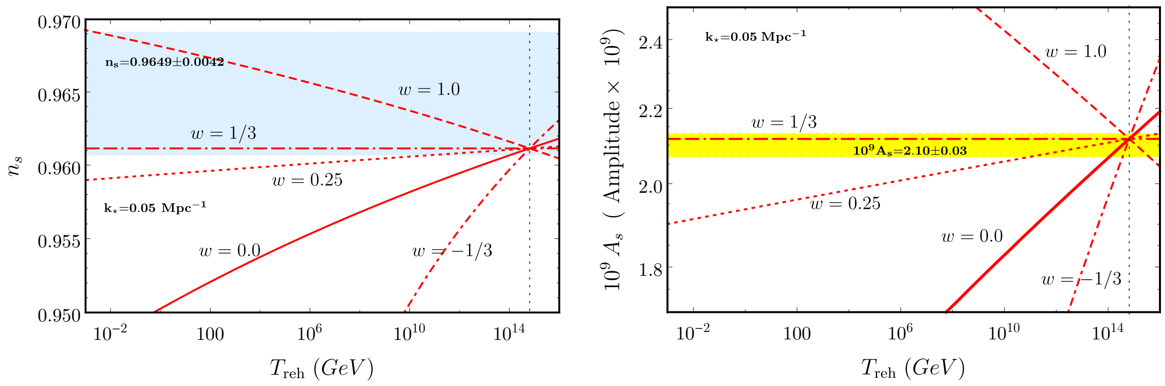

Figure 7.9: The primordial tilt n_s, left, and the power spectrum amplitude A_s, right, vs. the reheating temperature $T_{\rm reh}$, for the Higgs model, for inputs $\xi_h = 0.06$, $\lambda_h = 5.6 \times 10^{-12}$ and $\alpha = 5 \times 10^{11}$ (case - A).

$T_{\rm ins}$. This can also be seen by plotting the location of the points for which the parameter α has a constant value, $\alpha = 5 \times 10^7$. This is just above the range given above. Lower values, $\alpha < 5 \times 10^7$, will move this line downwards, crossing the largest $T_{\rm ins}$ region, and thus the maximum $T_{\rm ins}$ is obtainable.

Note that the analytic expressions for $T_{\rm ins}$, given so far, serve as an estimate of the magnitude of the instantaneous temperature. As we have already pointed out, the actual values are extracted by solving the pertinent equations of motion numerically. However, the numerical analysis reveals that these estimates are accurate enough. In fact, the results derived are lower by less than about 10 %. Only in a small region, for $c \leq 10^{-8}$ and for ξ_h values in the vicinity $\xi_h \simeq 0.1$, this difference augments to about 15 %, or so. This is in accord with the discussion following Eq. (7.47). As a result the maximum instantaneous reheating temperature mentioned before, $T_{\rm ins} = 2.47 \times 10^{15}$ GeV, drops to $T_{\rm ins} = 2.07 \times 10^{15}$ GeV.

Our numerical study can be summarized by the selection of the following representative inputs:

For the value $\xi_h = 0.06$, which according to the previous discussion sets the threshold for a sufficient number of e-folds, we choose the quartic coupling $\lambda_h = 4.875 \times 10^{-12}$. From (7.79) we can see that for $N_\star = 50 - 60$ the quartic coupling ranges between 4.29×10^{-12} (for $N_\star = 60$) and 6.22×10^{-12} (for $N_\star = 50$), so the chosen value is indeed in a reasonable range. However, this fine-tuned value was chosen such that the predicted amplitude A_s is within the observational limits, and such that instantaneous reheating is feasible. It should be noted that the approximate formula used for A_s may differ from the one provided by the numerical method. The latter gives more accurate results, since the exact numerical solution for the field h is used, and also because it incorporates corrections, which, although small in some cases, are of the same order of magnitude as the observational errors. For this reason, fine-tuning is necessary to make the instantaneous reheating mechanism a realistic possibility.

For these inputs $\xi_h^2/2\lambda_h \simeq 3.7 \times 10^8$, and thus for values $\alpha \ll 5 \times 10^7$ we are in the regime $a \ll \xi_h^2/2\lambda_h$ and, as we have discussed, the predictions are insensitive to the choice of α. Therefore, any value of α leads to the same results provided $\alpha \ll 5 \times 10^7$. We have verified this with our numerical code. For definiteness we take $\alpha = 5 \times 10^5$ which is three orders of magnitude smaller than $\xi_h^2/2\lambda_h$, as given above.

In Fig. 7.8, at the top, we show the primordial tilt and the power spectrum amplitude.We see that agreement with the n_s data is achieved for each temperature when the parameter w is $\simeq 0.25$ or larger but smaller than 1.0. However, for canonical reheating, $w = 0.0$, however a lower bound is imposed $T_{\rm reh} \gtrsim 10^{10}$ GeV, while for $w = 1.0$ the lower bound is

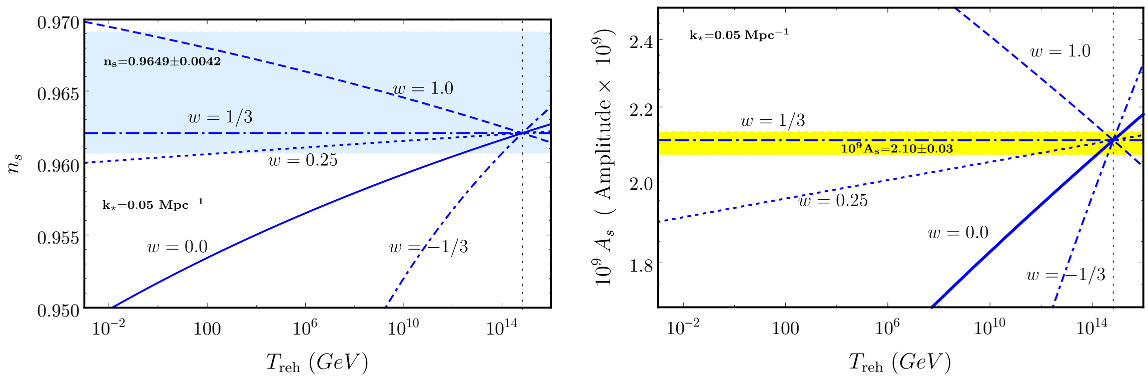

Figure 7.10: The same as in Figure 7.9, for inputs $\xi_h = 10.0$, $\lambda_h = 8.85 \times 10^{-10}$ and $\alpha = 5 \times 10^{11}$ (case B).

Table 7.2: Predictions of Higgs Model, for the input values shown above, for the cosmological observables $n_s, r, A_s, N_\star$ and for various values of the equation-of-state parameter w. The values shown for the reheating temperature $T_{\rm reh}$, in GeV, correspond to the minimum (upper rows) and maximum (lower rows) allowed when the observational limits for A_s and n_s are imposed.

Higgs Model (pivot scale $k_\star = 0.05\,Mpc^{-1}$)			
Input values	$\xi_h = 0.06$	$\lambda_h = 4.875 \times 10^{-12}$	$\alpha = 5 \times 10^5$
w - value	$w = 0.0$	$w = 0.25$	$w = 1.0$
$10^9\ A_s$	2.07	2.07	2.13
n_s	0.9634	0.9633	0.9639
r	0.0102	0.0102	0.0100
$N_\star$	55.67	55.67	56.45
$T_{\rm reh}$	2.562×10^{14}	6.695×10^{10}	1.569×10^{15}
$10^9\ A_s$	2.12	2.12	2.12
n_s	0.9638	0.9638	0.9638
r	0.0100	0.0100	0.0100
$N_\star$	56.36	56.36	56.36
$T_{\rm reh}$	2.027×10^{15}	2.027×10^{15}	2.027×10^{15}

about $T_{\rm reh} \gtrsim 100\,\mathrm{GeV}$. Looking at the A_s plot we observe, as advertised, that instantaneous reheating can occur, for the given ξ_h, λ_h inputs. We also observe that the constraints are more stringent than those imposed by n_s. Indeed, values of $w > 1/3$, allow temperatures very close to $T_{\rm ins}$. At the same time, a lower reheating temperature is imposed for the case $w = 0.25$, $T_{\rm reh} \gtrsim 10^{11}\,\mathrm{GeV}$, while for the canonical scenario the lower bound imposed by A_s is pushed to a much higher value, close to $T_{\rm ins}$. At the bottom of the same figure, the number of e-folds is shown. Although values of e-folds $N_\star$ as large as $\simeq 70$ for low $T_{\rm reh}$ are allowed, by n_s data, when $1 > w \geq 0.25$, the A_s measurements restrict the allowed temperature range in such a way that $N_\star$ is forced to fall within the range $\simeq 55.70 - 56.30$, as shown in Table 7.2. In this table the predictions for $A_s, n_s, r, N_\star$, corresponding to the minimum (upper rows) and maximum (lower rows) reheating temperature, are also shown. The maximum reheating temperature is the instantaneous temperature, $T_{\rm ins} = 2.027 \times 10^{15}\,\mathrm{GeV}$, and for this reason the predictions for the various w, in this case agree.

As a second example, we consider values of ξ_h in the range $\xi_h = 0.06 - 10.0$ when the parameter α is increased to $\alpha = 5 \times 10^{11}$. These cases fall in the regime $a > \xi_h^2/2\lambda_h$ if λ_h is

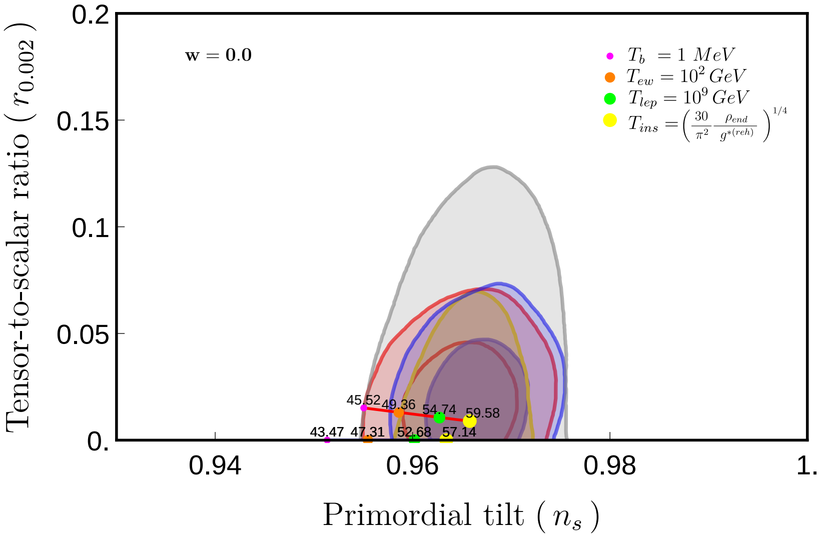

Figure 7.11: The tensor-to-scalar ratio $r_{0.002}$ vs. the primordial tilt n_s for the Higgs model. As in Fig 7.4 the numbers shown correspond to the e-folds and the circles denote different reheating temperatures. For the top line (in red) the parameters are $\alpha = 5 \times 10^5$, $\xi_h = 0.06$ and $\lambda_h = 4.875 \times 10^{-12}$, while for the bottom line (in blue) $\alpha = 5 \times 10^{11}$, $\xi_h = 0.06$ and $\lambda_h = 5.60 \times 10^{-12}$. Shown are only the cases for the canonical scenario, $w = 0$.

within the range suggested by (7.79). Following the same reasoning, we can consider values for the quartic coupling such that agreement with the A_s data is achieved while allowing the maximum reheating temperature to reach the instantaneous temperature $T_{\rm ins}$. For the smallest value of ξ_h in this range, $\xi_h = 0.06$, the quartic coupling can be assumed to be $\lambda_h = 5.60 \times 10^{-12}$, while for the largest, $\xi_h = 10$, the value $\lambda_h = 8.85 \times 10^{-10}$ meets our needs. For illustrative purposes, we call these cases A and B, respectively.

Note that by changing α, from $\alpha = 5 \times 10^5$ to $\alpha = 5 \times 10^{11}$, the predicted values for the cosmological parameters also change, and thus readjustments of λ_h are necessary to obtain a match with the data of A_s while having $T_{\rm ins}$ as the maximum temperature. This is the reason why the values of λ_h for the case $\xi_h = 0.06$ are slightly different for $\alpha = 5 \times 10^5$ and $\alpha = 5 \times 10^{11}$.

In Figs. 7.9 and 7.10 we show the predictions for the primordial tilt and the power spectrum amplitude for the cases A and B, respectively, discussed before. Comparing Fig. 7.9 with Fig. 7.8 (on top), we first see that $T_{\rm ins}$ is lowered, in comparison to the A - case. Indeed, from $T_{\rm ins} = 2.027 \times 10^{15}$ GeV it slides down to 6.522×10^{14} GeV. Also the lowest reheating temperatures change a little. For instance for $w = 0.25$ this is 1.065×10^{11} GeV, *i.e.* it has been slightly increased from the corresponding $\alpha = 5 \times 10^5$ case, which was 6.695×10^{10} GeV (see Table 7.2). Figure 7.10 shows the corresponding predictions for the B - case. In this case, $T_{\rm ins} = 6.647 \times 10^{14}$ GeV. That is, it is slightly larger than the A - case. Holding α fixed, the tendency for $T_{\rm ins}$ is to decrease, with increasing the parameter ξ_h, as long as $a > \xi_h^2/2\lambda_h$, where the quartic coupling is set to match the data of A_s.

In Fig. 7.11, we show the tensor-to-scalar ratio $r_{0.002}$ versus the primordial tilt n_s for the Higgs model. The numbers of the e-folds are shown, and the circles denote different reheating temperatures, exactly as in Fig. 7.4. The upper line (in red) corresponds to the parameters $\alpha = 5 \times 10^5$, $\xi_h = 0.06$ and $\lambda_h = 4.875 \times 10^{-12}$ while for the lower one (in blue) the parameters are $\alpha = 5 \times 10^{11}$, $\xi_h = 0.06$ and $\lambda_h = 5.60 \times 10^{-12}$. Shown are only the cases for canonical reheating, *i.e.* $w = 0$. Note that in drawing this figure, the constraints arising from A_s have not been taken into account. If they are, we are left with a small segment with temperature $T_{\rm ins}$. In any case, we see from these figures that as the parameter $\alpha$is increased, the tensor-to-scalar ratio becomes smaller and the predictions move downward and the mechanism of the instantaneous reheating temperature is in full agreement with the Planck 2018 cosmological constraints.

Chapter 8

Scale-invariance, dynamically induced Planck scale and inflation

In this section we construct a model of scale-invariant quadratic gravity in which the Planck scale is dynamically generated by the VEVs of a scalar field ϕ and the Higgs h, which are nonminimally coupled to gravity by terms of the form $\xi_i \Phi_i^2 R$, where $\Phi_i = \phi,\, h$. The additional scalar field ϕ comes from a general $U(1)_X$ extension of the SM gauge structure, which includes an additional gauge boson X_μ and three right-handed neutrinos N_R^i that can generate masses for the SM neutrinos via a type-I seesaw mechanism. The model can naturally accommodate DM and we outline three different possibilities. Moreover, the mass of the Higgs and the electroweak scale is generated by a portal coupling between ϕ and h of the form $\lambda_{h\phi} h^2 \phi^2$. Thus, the addition of the extra scalar field ϕ is necessary to preserve the scale invariance of our model, since the well-known Higgs mass term contained in the SM Lagrangian is not scale invariant.

8.1 Scale-invariant inflation in Palatini gravity

We begin the discussion of our model by describing the scale-invariant $U(1)_X$ extension of SM, which we use [389–407], containing a complex scalar field Φ, a gauge boson X_μ and three right-handed neutrinos N_R^i. We also outline three different ways in which the model can accommodate dark matter candidates. We then focus on the gravitational part of the theory and study it in the Palatini formalism.

8.1.1 $U(1)_X$ extension of the Standard Model

We consider the $U(1)_X$ extension of SM based on the gauge group $SU(3)_c \times SU(2)_L \times U(1)_Y \times U(1)_X$. In Table 8.1 we present the matter fields of this model, which in addition to the SM matter fields also contains three generations of right-handed neutrinos N_R^i $(i = 1, 2, 3)$ and a complex $U(1)_X$ scalar field Φ, whose VEV generates the mass of the vector boson X_μ as well as the masses of the right-handed neutrinos. This $U(1)_X$ extension can be recognized as a linear combination of the $U(1)_Y$ and the $U(1)_{B-L}$ gauge group, with the latter being free of gauge and gravitational anomalies. The existence of the three right-handed neutrinos plays a crucial role in this anomaly cancellation. Following [408], we introduce the real parameters x_H and x_Φ used in the determination of the $U(1)_X$ charge of the field Φ, which is given by

$$Q_X = Y x_H + Q_{BL}\, x_\Phi \,, \tag{8.1}$$

where Y and Q_{BL} are its hypercharge and $B-L$ charge, respectively. Two interesting choices for the parameters x_H and x_Φ are the choice $(x_H, x_\Phi) = (0, 1)$, which is consistent with the $U(1)_{B-L}$ model, and the choice $(x_H, x_\Phi) = (-2, 1)$, which is consistent with the SM with an additional $U(1)_R$ symmetry.

Table 8.1: The matter fields of the $U(1)_X$ extension of the SM with the associated charges. In addition to the SM particle content ($i = 1, 2, 3$), three right-handed neutrinos N_R^i ($i = 1, 2, 3$) and a $U(1)_X$ complex scalar field Φ are introduced. The $U(1)_X$ charge is determined by the two real parameters, x_H and x_Φ, as $Q_X = Y x_H + Q_{BL} x_\Phi$ with its hypercharge Y and $B-L$ charge Q_{BL}.

	$SU(3)_c$	$SU(2)_L$	$U(1)_Y$	$U(1)_X$
q_L^i	**3**	**2**	$1/6$	$(1/6)x_H + (1/3)x_\Phi$
u_R^i	**3**	**1**	$2/3$	$(2/3)x_H + (1/3)x_\Phi$
d_R^i	**3**	**1**	$-1/3$	$(-1/3)x_H + (1/3)x_\Phi$
ℓ_L^i	**1**	**2**	$-1/2$	$(-1/2)x_H + (-1)x_\Phi$
e_R^i	**1**	**1**	-1	$(-1)x_H + (-1)x_\Phi$
H	**1**	**2**	$1/2$	$(1/2)x_H$
N_R^i	**1**	**1**	0	$(-1)x_\Phi$
Φ	**1**	**1**	0	$(+2)x_\Phi$

The covariant derivative associated with the $U(1)_Y \times U(1)_X$ gauge interaction is defined as

$$D_\mu = \partial_\mu - i\left(g_1 Y + \tilde{g} Q_X\right) B_\mu - i g_X Q_X X_\mu \,, \tag{8.2}$$

where g_1 and g_X are the $U(1)_Y$ and $U(1)_X$ gauge couplings, respectively. In (8.2), the possible kinetic mixing between the two $U(1)$ gauge bosons can be neglected for simplicity if one assumes that the mixing coupling $\tilde{g}$ vanishes on the $U(1)_X$ symmetry breaking scale.

To the well-known SM Yukawa sector we need to add the BSM Yukawa sector resulting from the $U(1)_X$ extension, which reads.

$$\mathcal{L}_{\text{Yukawa}}^{\text{BSM}} = -y_D^{ij} \overline{\ell}_L^i H N_R^j - \frac{1}{2} y_M^i \Phi \overline{N}_R^{iC} N_R^i + h.c. \,, \tag{8.3}$$

where y_D and y_M are the Dirac and Majorana Yukawa couplings respectively. Without loss of generality, we also assume that the Majorana Yukawa couplings already diagonal in our basis. Furthermore, it is interesting to note that in this setting, lepton asymmetry can be produced by decays of the heavy right-handed neutrinos into SM leptons at high temperatures. Then the lepton asymmetry can be converted into a baryon asymmetry via electroweak sphalerons [409, 410] (see also [396, 411, 412]).

Assuming that the complex $U(1)_X$ scalar field Φ develops a nonzero VEV v_ϕ and working in the unitary gauge, we have that

$$\Phi = \frac{1}{\sqrt{2}}(\phi + v_\phi) \,. \tag{8.4}$$

Thus, the BSM scalar Lagrangian and the gravity Lagrangian are given by

$$\begin{aligned} \mathcal{L}_{\text{scalar}}^{\text{BSM}} &= \frac{1}{2} g^{\mu\nu} \partial_\mu \phi \partial_\nu \phi + \frac{1}{4} \lambda_\phi \phi^4 + \frac{1}{4} \lambda_{h\phi} h^2 \phi^2 \,, \\ \mathcal{L}_{\text{gravity}} &= \frac{1}{2}\left(\xi_\phi \phi^2 + \xi_h h^2\right) g^{\mu\nu} R_{\mu\nu} + \frac{\alpha}{2} R^2 + \frac{\beta}{2} R_{(\mu\nu)} R^{(\mu\nu)} \,, \end{aligned} \tag{8.5}$$

where h is the Higgs field also written in the unitary gauge, and ξ_ϕ, ξ_h are the nonminimal couplings between gravity and matter. Note that the Ricci tensor depends only on the connection Γ since we are working in the Palatini formalism. Moreover, there are no mass terms for either ϕ or h, since the theory must respect classical scale invariance. The reduced

Planck mass $M_{\rm P}$ is dynamically generated when ϕ and h develop their VEVs,

$$M_{\rm P}^2 = \xi_\phi v_\phi^2 + \xi_h v_h^2 \,. \tag{8.6}$$

In connexion with $U(1)_X$ and electroweak symmetry breaking, the $U(1)_X$ gauge boson X_μ and the right-handed Majorana neutrinos N_R^i obtain their masses as

$$M_X = \sqrt{(2x_\Phi g_X v_\phi)^2 + (x_H g_X v_h)^2} \simeq 2x_\Phi g_X v_\phi \,, \qquad M_{N_R^i} = \frac{y_M^i}{\sqrt{2}} v_\phi \,. \tag{8.7}$$

The part of the JF action that contains the scalar ϕ and the Higgs h is

$$\begin{aligned} S_{\rm JF} \;&=\; \int {\rm d}^4x\sqrt{-g}\left\{\frac{1}{2}\left[\left(\xi_\phi\phi^2+\xi_h h^2\right)g^{\mu\nu}R_{\mu\nu}+\alpha R^2+\beta R_{(\mu\nu)}R^{(\mu\nu)}\right]\right. \\ &\left. \qquad +\frac{1}{2}g^{\mu\nu}\partial_\mu\phi\partial_\nu\phi+\frac{1}{2}g^{\mu\nu}\partial_\mu h\partial_\nu h - V^{(0)}(\phi,h)\right\} , \end{aligned} \tag{8.8}$$

with the tree-level potential given by

$$V^{(0)}(\phi,h) = \frac{1}{4}\left(\lambda_\phi\phi^4 - \lambda_{h\phi}h^2\phi^2 + \lambda_h h^4\right) . \tag{8.9}$$

Note that the coupling constants λ_ϕ, λ_h and $\lambda_{h\phi}$ are dimensionless, assumed to be positive, and the minus sign is introduced in front of the portal coupling term to account for spontaneous symmetry breaking due to the running of the coupling constants.

With the goal of eventually reshaping the action (8.8) in the EF where the gravitational sector consists only of the Einstein-Hilbert -term, we begin by performing a Weyl rescaling of the metric of the form

$$g^{\mu\nu} \longrightarrow \Omega^2 g^{\mu\nu} \,, \quad \Omega^2 = \xi_\phi\phi^2 + \xi_h h^2 \,. \tag{8.10}$$

The quadratic in curvature terms are invariant under the rescaling (8.10) unlike the Einstein-Hilbert term which rescales as $R \longrightarrow \Omega^2 R$ and thus the action takes the form[1]

$$\begin{aligned} S_{\rm IF} \;&=\; \int {\rm d}^4x\sqrt{-g}\left\{\frac{1}{2}\left[g^{\mu\nu}R_{\mu\nu}+\alpha R^2+\beta R_{\mu\nu}R^{\mu\nu}\right] - \frac{1}{2\Omega^2}g^{\mu\nu}\partial_\mu\phi\partial_\nu\phi\right. \\ &\left. \qquad -\frac{1}{2\Omega^2}g^{\mu\nu}\partial_\mu h\partial_\nu h - \frac{V^{(0)}(\phi,h)}{\Omega^4}\right\} . \end{aligned} \tag{8.11}$$

Following the notation of [5] we will call this frame the "intermediate frame" (IF) to account for the fact that, even though we have eliminated the nonminimal coupling that appears in the JF, we have not dealt with the quadratic terms yet.

8.1.2 Potential dark matter candidates

An interesting property of the $U(1)_X$ model under consideration is that it can provide us with viable dark matter candidates in a minimal and natural way.

- A first possibility is that the extra gauge boson X_μ constitutes dark matter [413–415]. The $U(1)_X$ gauge group contains an intrinsic discrete Z_2 symmetry, that makes X_μ automatically stable. Note, however, that this statement holds only if the $U(1)_X$ is sequestered and has no tree-level mixing with the hypercharge. In this case, no one-loop level mixing can be generated either.

[1]From now on we consider only the symmetric Ricci tensor $R_{(\mu\nu)}$ and in order to speed up notation we discard the parentheses.

- A second possibility arises by introducing a Z_2 parity and imposing one of the three right-handed neutrinos to be odd, while the others are even [416, 417]. This makes the odd right-handed neutrino stable and a possible DM candidate. he remaining right-handed neutrinos are sufficient to produce the observed neutrino oscillations.

- A third possibility arises by adding an additional Dirac fermion ζ, which is singlet under the SM gauge group and having a generic $U(1)_X$ charge Q_X [418]. It is worth noting that the addition of the Dirac fermion does not disturb the anomaly cancellation of the $U(1)_X$ extended SM. The ζ field interacts with the SM particles due to $U(1)_X$ gauge interactions and its relic freeze-out abundance is determined by the processes $\zeta\bar{\zeta} \overset{X_\mu}{\longleftrightarrow} f\bar{f}$, where f is a SM fermion. On the other hand in [419], a freeze-in DM scenario is studied, where either X_μ or the right-handed neutrinos easily be on the order of 100 MeV to 1 GeV.

8.2 Gildener-Weinberg approach

Classically scale-invariant models containing multiple scalar fields are usually studied using the Gildener-Weinberg formalism [420][2]. In this approach, perturbative minimization at a certain energy scale is realized by the running of the coupling constants in the full quantum theory. First, one identifies the flat directions (FD) of the tree-level potential in the field space. These are directions along which the first derivatives of the potential with respect to each of the fields vanish. The flatness of the tree potential has the consequence that the dynamics of the system is governed by the one-loop corrections that dominate along the FD. In this way, the flatness is perturbatively removed and the physical vacuum of the theory is lifted out of the valley of degenerate minima along the FD. In this section we use the Gildener-Weinberg formalism and finally end with an inflationary single-field action.

8.2.1 Tree level minimization

The tree-level potential after the Weyl rescaling of the JF action is given by

$$U^{(0)}(\phi, h) \equiv \frac{V^{(0)}(\phi, h)}{\Omega^4} = \frac{(\lambda_\phi \phi^4 - \lambda_{h\phi} h^2 \phi^2 + \lambda_h h^4)}{4\left(\xi_\phi \phi^2 + \xi_h h^2\right)^2} \,. \tag{8.12}$$

The first derivatives of $U^{(0)}(\phi, h)$ with respect to the two fields vanish along the trajectories in field space that satisfy the following conditions

$$\partial_\phi U^{(0)}(\phi, h) = 0 \quad \Rightarrow \quad h^2 = \left(\frac{\lambda_{h\phi}\, \xi_\phi + 2\lambda_\phi\, \xi_h}{\lambda_{h\phi}\, \xi_h + 2\lambda_h\, \xi_\phi}\right) \phi^2 \,, \tag{8.13}$$

$$\partial_h U^{(0)}(\phi, h) = 0 \quad \Rightarrow \quad \phi^2 = \left(\frac{\lambda_{h\phi}\, \xi_h + 2\lambda_h\, \xi_\phi}{\lambda_{h\phi}\, \xi_\phi + 2\lambda_\phi\, \xi_h}\right) h^2 \,. \tag{8.14}$$

A trajectory is equivalent to an FD if it simultaneously satisfies the Eqs. (8.13) and (8.14). Note that in our model the two extremization conditions give the same constraint and consequently correspond directly to FDs of $U^{(0)}(\phi, h)$. The two different signs correspond to the two independent FDs of the tree-level potential. We consider ϕ and h to be positive definite

[2] See also [116, 390, 397, 399, 400, 421–460] for various applications of the formalism.

and therefore the relevant FD for our analysis is the one given by the condition

$$v_h = \sqrt{\frac{\lambda_{h\phi}\,\xi_\phi + 2\lambda_\phi\,\xi_h}{\lambda_{h\phi}\,\xi_h + 2\lambda_h\,\xi_\phi}}\,v_\phi\,, \tag{8.15}$$

where the fields are at their VEV along the FD since this corresponds to the minimum of the potential. Note that for $\xi_h \ll 1$, when $v_\phi \sim M_{\rm P}$ and $\lambda_h \sim 0.1$, the portal coupling must be extremely small, $\lambda_{h\phi} \sim 10^{-30}$. After applying Eq. (8.15), we can calculate the value of $U^{(0)}(\phi, h)$ along the FD in terms of the coupling constants of the model

$$U^{(0)}_{\rm min} \equiv U^{(0)}(v_\phi, v_h) = \frac{\left(4\lambda_h\lambda_\phi - \lambda_{h\phi}^2\right) M_{\rm P}^4}{16\left[\lambda_\phi\xi_h^2 + \xi_\phi\left(\lambda_{h\phi}\xi_h + \lambda_h\xi_\phi\right)\right]}\,. \tag{8.16}$$

Note that the minimum of the tree level potential (8.16) can be negative, zero or positive depending on the value of the combination $4\lambda_h\lambda_\phi - \lambda_{h\phi}^2$. If we had instead applied the Gildener-Weinberg approach to the JF tree-level potential (8.9), the identification of the resulting extremization conditions would impose the constraint $\lambda_{h\phi}^2 = 4\lambda_h\lambda_\phi$ and consequently, the minimum of (8.9) would be fixed to zero. This freedom in setting the minimum of the potential will play an important role in the next section, where the one-loop corrections will be considered.

Having identified the FD of the tree-level potential we can proceed to the computation of the mass matrix. Its elements are given by

$$M^2_{ij} \equiv \left.\frac{\partial^2 U^{(0)}}{\partial\Phi^i\,\partial\Phi^j}\right|_{\Phi^i = v_{\Phi^i},\,\Phi^j = v_{\Phi^j}}\,, \tag{8.17}$$

where we denote $(\Phi^1, \Phi^2) = (\phi, h)$ and v_{Φ^i} are their respective VEVs. Using the ratio of the two VEVs, we can define the mixing angle ω, which corresponds to the angle between the $h = 0$ axis in the field space and the FD (see Fig. (8.1)) as follows:

$$\omega \equiv \arctan\left(\frac{v_h}{v_\phi}\right) = \arctan\left(\sqrt{\frac{\lambda_{\phi h}\,\xi_\phi + 2\lambda_\phi\,\xi_h}{\lambda_{\phi h}\,\xi_h + 2\lambda_h\,\xi_\phi}}\right)\,, \tag{8.18}$$

where we have inserted the condition (8.15) in the last equation. We can now perform an orthogonal rotation given by the transformation

$$\begin{pmatrix} \phi \\ h \end{pmatrix} = \begin{pmatrix} \cos\omega & -\sin\omega \\ \sin\omega & \cos\omega \end{pmatrix} \begin{pmatrix} s \\ \sigma \end{pmatrix}\,, \tag{8.19}$$

in order to move from the initial field frame (ϕ, h) to the "FD frame" (s, σ), where the direction of the so-called "scalon" field s is identified with the FD and σ is the perpendicular direction.

Then we can write the potential in terms of the FD frame fields to compute the mass matrix directly in this frame with $(\Phi^1, \Phi^2) = (s, \sigma)$. The advantage of performing the rotation in the FD frame before calculating the mass matrix is that the resulting matrix is diagonal. Therefore, the mass eigenvalues for the fields (s, σ) lie on the main diagonal and are given by the following expressions:

$$m_s^2 = 0\,, \tag{8.20}$$

$$m_\sigma^2 = \frac{M_{\rm P}^4\left(\lambda_{h\phi}\xi_h + 2\lambda_h\xi_\phi\right)\left(2\lambda_\phi\xi_h + \lambda_{h\phi}\xi_\phi\right)^2\left[\left(\lambda_{h\phi} + 2\lambda_\phi\right)\xi_h + \left(2\lambda_h + \lambda_{h\phi}\right)\xi_\phi\right]}{8\,v_h^2\left[\lambda_\phi\xi_h^2 + \xi_\phi\left(\lambda_{h\phi}\xi_h + \lambda_h\xi_\phi\right)\right]^3}\,, \tag{8.21}$$

where we have once again employed Eq. (8.15). As expected, the mass of s is exactly zero at tree level since it corresponds to the pseudo-Goldstone boson of the broken classical scale symmetry. However, as we will see below, it acquires a non-zero mass when quantum corrections are taken into account. Moreover, we identify the mass m_σ with the measured value of the Higgs boson mass.

Along the FD ($\sigma = 0$), the only relevant DOF is the scalon s, which is related to ϕ and h via

$$s^2 = \phi^2 + h^2 \,, \qquad s = \frac{\phi}{\cos\omega} = \frac{h}{\sin\omega} \,. \tag{8.22}$$

The above relations can be easily verified by a simple inspection of the field space in Fig. (8.1). Using Eqs. (8.22) we can rewrite the noncanonical kinetic terms for h and ϕ in terms of s as

$$\frac{1}{\Omega^2}\left[\frac{1}{2}g^{\mu\nu}\partial_\mu\phi\partial_\nu\phi + \frac{1}{2}g^{\mu\nu}\partial_\mu h\partial_\nu h\right] = \frac{1}{\Omega^2}\left[\frac{1}{2}g^{\mu\nu}\partial_\mu s\partial_\nu s\right] ,$$

where, the nonminimal coupling functional expressed in terms of s has the following form:

$$\frac{1}{\Omega^2} = \frac{1}{\xi_\phi\phi^2 + \xi_h h^2} = \frac{1}{\xi_s s^2} \,. \tag{8.23}$$

In the last equation, we have defined an "effective" nonminimal coupling constant for the scalon as

$$\xi_s \equiv \xi_\phi \cos^2\omega + \xi_h \sin^2\omega \,. \tag{8.24}$$

Finally, we perform the following field redefinition in order to render the kinetic term of s canonical:

$$s_c - v_c = \int_{v_s}^{s} \frac{1}{\sqrt{\xi_s}}\frac{\mathrm{d}s'}{s'} = \frac{1}{\sqrt{\xi_s}} \ln\frac{s}{v_s} \,. \tag{8.25}$$

The field s_c is the one that drives inflation in our model and thus we shall refer to it as the inflaton field.

8.2.2 One loop effective potential

The one-loop corrections along the flat direction for the canonical field s_c at the scale Λ can be written as

$$U^{(1)}(s_c) = \mathbb{A}\, s_c^4 + \mathbb{B}\, s_c^4 \ln\frac{s_c^2}{\Lambda^2} \,, \tag{8.26}$$

where in our model

$$\begin{aligned}
\mathbb{A} &= \frac{1}{64\pi^2 v_s^4}\Bigg\{ M_h^4\left(\ln\frac{M_h^2}{v_s^2} - \frac{3}{2}\right) + 6M_W^4\left(\ln\frac{M_W^2}{v_s^2} - \frac{5}{6}\right) + 3M_Z^4\left(\ln\frac{M_Z^2}{v_s^2} - \frac{5}{6}\right) \\
&\quad + 3M_X^4\left(\ln\frac{M_X^2}{v_s^2} - \frac{5}{6}\right) - 6M_{N_R}^4\left(\ln\frac{M_{N_R}^2}{v_s^2} - 1\right) - 12M_t^4\left(\ln\frac{M_t^2}{v_s^2} - 1\right)\Bigg\} \,, \quad (8.27) \\
\mathbb{B} &= \frac{\mathcal{M}^4}{64\pi^2 v_s^4} \,, \qquad \mathcal{M}^4 \equiv M_h^4 + 3M_X^4 + 6M_W^4 + 3M_Z^4 - 6M_{N_R}^4 - 12M_t^4 \,. \quad (8.28)
\end{aligned}$$

Minimizing (8.26), we can determine the scale Λ as

$$\Lambda = v_s \exp\left[\frac{\mathbb{A}}{2\mathbb{B}} + \frac{1}{4}\right] . \tag{8.29}$$

Then, we can express the one-loop correction as

$$U^{(1)}(s_c) = \frac{\mathcal{M}^4}{64\pi^2 v_s^4} s_c^4 \left[\ln \frac{s_c^2}{v_s^2} - \frac{1}{2}\right] . \tag{8.30}$$

One sees that the addition of the $U(1)_X$ gauge symmetry, and in particular the mass of the extra gauge boson X_μ can make $\mathcal{M}^4$ positive if $3M_X^4 - 6M_{N_R}^4 \gtrsim (317\text{ GeV})^4$, which in turn implies that the one-loop potential is bounded from below at large field values. From the one-loop corrections we can obtain the radiatively-generated mass for the s scalar

$$m_s^2 = \frac{\mathcal{M}^4}{8\pi^2 v_s^2} . \tag{8.31}$$

Note that the one-loop correction (8.30) is negative in the minimum. This observation justifies the choice to consider the one-loop corrections in the "intermediate frame" (8.11) rather than in the JF action (8.8). If we had chosen the latter, the extremization conditions for the tree-level JF potential would set its value to zero along the flat direction, as we mentioned earlier, and thus the full one-loop effective potential (tree level + one loop) would correspond to an anti-de Sitter vacuum. This problem can of course be easily circumvented by including a positive cosmological constant in the effective potential to achieve a Minkowski vacuum, although in this case the model is no longer scale invariant and is instead characterized as quasi-scale invariant.

We now require that the full one-loop effective potential is zero at v_s which can be realized once we assume that $4\lambda_h\lambda_\phi - \lambda_{h\phi}^2 > 0$, so that $U_{\text{min}}^{(0)} > 0$. Then we may write

$$U_{\text{eff}}(v_s) = U_{\text{min}}^{(0)} + U^{(1)}(v_s) = 0 , \tag{8.32}$$

which finally yields

$$U_{\text{eff}}(s_c) = \frac{\mathcal{M}^4}{128\pi^2} \left[\frac{s_c^4}{v_s^4}\left(2\ln\frac{s_c^2}{v_s^2} - 1\right) + 1\right] . \tag{8.33}$$

Note that the condition (8.32) effectively means that the cosmological constant can potentially be generated from two or higher-order loop corrections.

The VEV of the inflaton s_c is associated with the reduced Planck mass via the value of the effective nonminimal coupling constant (8.24) as

$$v_s^2 = \frac{M_{\text{P}}^2}{\xi_s} , \tag{8.34}$$

and thus, it is evident that in principle v_s can be super-Planckian for $\xi_s < 1$. Indeed, as we will see in Sec. 8.4, this is exactly the case in our model since observationally viable inflation requires $\xi_s \lesssim \mathcal{O}(10^{-3})$.

Finally, the effective action along the FD, written explicitly in terms of the inflaton field, is as follows

$$S = \int \mathrm{d}^4x\sqrt{-g}\left\{\frac{1}{2}\left[g^{\mu\nu}R_{\mu\nu} + \alpha R^2 + \beta R_{\mu\nu}R^{\mu\nu}\right] - \frac{1}{2}g^{\mu\nu}\partial_\mu s_c \partial_\nu s_c - U_{\text{eff}}(s_c)\right\} . \tag{8.35}$$

In the next section, our goal is to identify and apply the appropriate transformations to remove the higher order curvature terms and finally reformulate the effective action (8.35) in the EF where the gravity sector consisting solely of the Einstein-Hilbert term.

8.3 Einstein frame representation

In this section, in order to obtain the predictions of the model for the cosmological observables, we will move from the "intermediate frame" of Eq. (8.11) or (8.35) to the EF using the procedure which was outlined in [219] (see also [461]).

8.3.1 The Legendre transformation

The action (8.35) can be cast in the form

$$S = \int \mathrm{d}^4x\sqrt{-g}\left[\frac{1}{2}C(g_{\mu\nu}, R_{\mu\nu}) + \mathcal{L}_m(g_{\mu\nu},\, s_c,\, \partial_\mu s_c)\right]\,, \tag{8.36}$$

where we have defined the "curvature" function

$$C(g_{\mu\nu}, R_{\mu\nu}) = g^{\mu\nu}R_{\mu\nu} + \alpha R^2 + \beta R_{\mu\nu}R^{\mu\nu}\,, \tag{8.37}$$

and the matter Lagrangian density

$$\mathcal{L}_m(g_{\mu\nu},\, s_c,\, \partial_\mu s_c) = \frac{1}{2}g^{\mu\nu}\partial_\mu s_c\partial_\nu s_c - U_{\text{eff}}(s_c)\,. \tag{8.38}$$

From this point on, the dependence of $\partial_\mu s_c$ in the argument of $\mathcal{L}_m$ is ignored for brevity. After introducing the auxiliary field $\Sigma_{\mu\nu}$, the action becomes

$$S = \int \mathrm{d}^4x\sqrt{-g}\left[\frac{1}{2}C(g_{\mu\nu}, \Sigma_{\mu\nu}, s_c) + \frac{1}{2}\frac{\partial C}{\partial\Sigma_{\mu\nu}}\left(R_{\mu\nu} - \Sigma_{\mu\nu}\right) + \mathcal{L}_m(g_{\mu\nu}, s_c)\right]\,. \tag{8.39}$$

It is trivial to see that the variation $\delta S/\delta\Sigma_{\mu\nu} = 0$ gives that $\Sigma_{\mu\nu} = R_{\mu\nu}$. The advantage of action (8.39) is that it is linear in the Ricci tensor, so it is one step closer to the final EF action. We introduce the new variable $q^{\mu\nu}$, which is defined as

$$\sqrt{-q}q^{\mu\nu} = \sqrt{-g}\frac{\partial C}{\partial\Sigma_{\mu\nu}}\,, \tag{8.40}$$

where $q = \det(q_{\mu\nu})$ and $q^{\mu\nu}q_{\mu\lambda} = \delta^{\nu}{}_{\lambda}$. Using (8.40) we can solve the $\Sigma_{\mu\nu}$ in terms of the $g_{\mu\nu}$, s_c and $q_{\mu\nu}$, so that the action can be written as

$$S = \int \mathrm{d}^4x\left\{\frac{\sqrt{-q}}{2}q^{\mu\nu}R_{\mu\nu} - \frac{\sqrt{-g}}{2}\left[\frac{\partial C}{\partial\Sigma_{\mu\nu}}\Sigma_{\mu\nu}(q_{\mu\nu}, g_{\mu\nu}, s_c) - C(q_{\mu\nu}, g_{\mu\nu}, s_c) - 2\mathcal{L}_m(g_{\mu\nu}, s_c)\right]\right\}\,. \tag{8.41}$$

The gravitational sector of (8.41) is the typical Einstein-Hilbert term for the metric $q_{\mu\nu}$. Varying the action (8.41) with respect to $g_{\mu\nu}$ (see Appendix D) will give us $g_{\mu\nu}$ as a function of $q_{\mu\nu}$, s_c and $\partial_\mu s_c$. In this way we obtain that

$$\begin{aligned}\frac{1}{\sqrt{-g}}\frac{\delta S}{\delta g^{\mu\nu}} \;=\; & -\frac{1}{4(\beta+4\alpha)}\frac{\sqrt{-q}}{\sqrt{-g}}q^{\sigma\lambda}g_{\sigma\mu}g_{\lambda\nu} \\ & +\frac{1}{4\beta}\frac{q}{g}\left(q^{\sigma\lambda}q^{\rho\delta}g_{\lambda\delta}g_{\rho\nu}g_{\sigma\mu} - \frac{\alpha}{\beta+4\alpha}q^{\delta\rho}g_{\delta\rho}q^{\sigma\lambda}g_{\sigma\mu}g_{\lambda\nu}\right) \\ & +\frac{1}{2}g_{\mu\nu}\left[\frac{1}{\beta+4\alpha}\left(\frac{1}{2}+\frac{\alpha}{8\beta}\frac{q}{g}q^{\lambda\sigma}g_{\lambda\sigma}q^{\rho\delta}g_{\rho\delta}\right) - \frac{q}{g}\frac{1}{8\beta}q^{\lambda\sigma}q^{\delta\rho}g_{\lambda\delta}g_{\sigma\rho}\right] \\ & +\frac{1}{2}g_{\mu\nu}\left(\frac{1}{2}g^{\lambda\sigma}\partial_\lambda s_c\partial_\sigma s_c + U_{\text{eff}}(s_c)\right) - \frac{1}{2}\partial_\mu s_c\partial_\nu s_c = 0\,.\end{aligned} \tag{8.42}$$

which will help us to solve the metric $g_{\mu\nu}$ in terms of the metric $q_{\mu\nu}$ and the inflaton field[3].

8.3.2 The disformal transformation

Another useful type of metric transformation is the disformal transformation [462–466], a generalisation of the well-known conformal transformation. It can be used to bring complicated actions, *e.g.* (8.35), into the EF. This is of the form

$$g_{\mu\nu} = A\, q_{\mu\nu} + B\, \partial_\mu s_c \partial_\nu s_c \,, \tag{8.43}$$

where the coefficients A and B are functions of s_c and X_q with

$$X_q \equiv \frac{1}{2} q^{\mu\nu} \partial_\mu s_c \partial_\nu s_c \,. \tag{8.44}$$

The relation correlating the determinants of the metrics $g_{\mu\nu}$ and $q_{\mu\nu}$ can be easily obtained by substituting the general form of the disformal transformation (8.43) into $\det\left(q^{\mu\sigma} g_{\mu\nu}\right) = q^{-1} g$. That is,

$$g = qA^3 \left(A - 2BX_q\right) \,. \tag{8.45}$$

For our computation we also need the inverse metric $g^{\mu\nu}$. Following [467] we obtain that

$$g^{\mu\nu} = \bar{A}\, q^{\mu\nu} + \bar{B} q^{\mu\lambda} q^{\nu\sigma} \partial_\lambda s_c \partial_\sigma s_c \,, \tag{8.46}$$

where

$$\bar{A} = \frac{1}{A} \,, \quad \bar{B} = -\frac{B}{A^2 - 2ABX_q} \,. \tag{8.47}$$

Finally, using (8.44) and (8.46) it is quite trivial to prove that the kinetic terms for the metric $g_{\mu\nu}$ can be expressed in terms of the kinetic terms for the metric $q_{\mu\nu}$ as

$$X_g = \bar{A} X_q - 2\bar{B} {X_q}^2 \,. \tag{8.48}$$

Now, we can substitute (8.43) and (8.48) in (8.42). This substitution gives us two algebraic equations. Each equation follows from the requirement that the coefficients of $q_{\mu\nu}$, and $\partial_\mu s_c \partial_\nu s_c$ must vanish identically. These equations are given below:

$$\begin{aligned} \frac{1}{16\beta(4\alpha+\beta)R_5} & \left(4(4\alpha+\beta)A^2 - 4\beta A\sqrt{R_5} - 4\alpha A R_2 - (4\alpha+\beta)R_3 + 4\beta R_5 + \alpha R_2^2\right) \\ & + \frac{U_{\text{eff}}(s_c)}{2} - \frac{X_g}{2} = 0 \,, \end{aligned} \tag{8.49}$$

$$\begin{aligned} \frac{1}{16\beta(4\alpha+\beta)R_5} & \Big(4(4\alpha+\beta)R_4 - 4\beta R_1\sqrt{R_5} - 4\alpha R_2 R_1 - (4\alpha+\beta)BR_3 + 4\beta BR_5 \\ & + \alpha BR_2^2\Big) + \frac{BU_{\text{eff}}(s_c)}{2} - \frac{BX_g}{2} - \frac{1}{2} = 0 \,, \end{aligned} \tag{8.50}$$

where the functions R_i are given in the Appendix D. Equations (8.49) and (8.50) accorded well with Eqs. (6.44) and (6.45) of [219]. Our goal is to solve the system (8.49)-(8.50), but this is a very difficult task. However, we can approximate the solutions by assuming that in the slow roll approximation the higher-order kinetic terms are negligible at least during

[3] Equation (8.42) has been also derived in [219], with a missing 1/2 factor in the parenthesis in the third line. We think that this is only a misprint as our final results are in absolutely agreement with these of [219].

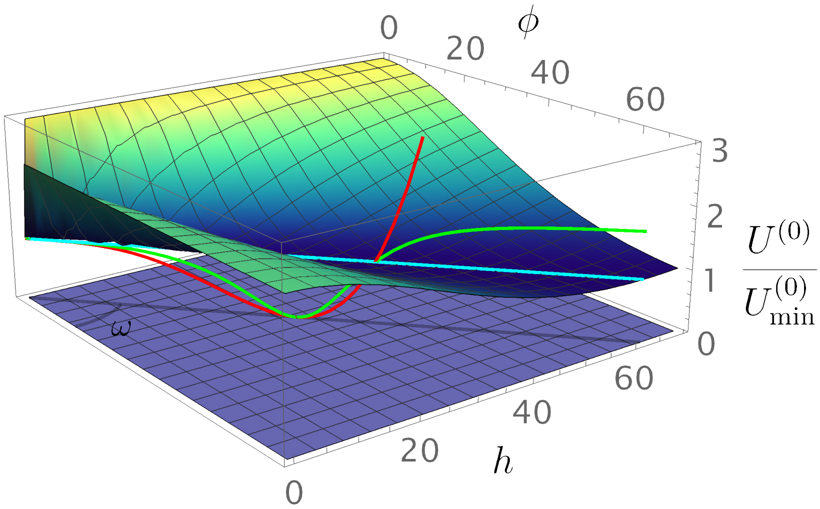

Figure 8.1: The normalized tree-level potential $U^{(0)}(\phi,h)/U^{(0)}_{\rm min}$ (8.12) and its flat direction (cyan line). We also plot the normalized one-loop corrected potential along the flat direction $U_{\rm eff}(s_c)/U_{\rm eff}(0)$ (8.33) (red curve) and the normalized inflaton potential $\bar{U}(s_c)/\bar{U}(0)$ (8.53) (green curve). The values of the parameters are $\tilde{\alpha}=10^9$, $\xi_s=10^{-3}$, and $\mathcal{M}\simeq 0.0357$. For illustrative purposes we have chosen the values of the couplings λ_ϕ, λ_h, $\lambda_{h\phi}$ such that the mixing angle (8.18) has the unrealistic value of $\omega\simeq 0.732$.

inflation [210], but also during reheating [217]. Thus, the approximate solution has the form

$$\begin{aligned} A &= a_0 + a_1 X_q + \mathcal{O}(X_q^2)\,, \\ B &= b_0 + b_1 X_q + \mathcal{O}(X_q^2)\,. \end{aligned} \tag{8.51}$$

By substituting (8.51) into the system (8.49)-(8.50) and expanding in terms of the kinetic term (8.44), we can solve for the coefficients a_i, and b_i after forcing that the coefficient of each order vanishes identically. These coefficients are listed in Appendix D.

Having done all the preliminary work, we can put the solution (8.51) with the coefficients (D.7) to the matter sector (D.3) and expand it again in the kinetic term. This gives us the final EF action

$$S_{\rm EF} = \int d^4x\sqrt{-q}\left[\frac{1}{2}q^{\mu\nu}R_{\mu\nu} + K(s_c)X_q - \bar{U}(s_c) + \mathcal{O}(X_q^2)\right]\,, \tag{8.52}$$

with

$$K(s_c) = \frac{1}{1+\tilde{\alpha}\,U_{\rm eff}(s_c)} \quad \text{and} \quad \bar{U}(s_c) = \frac{U_{\rm eff}(s_c)}{1+\tilde{\alpha}\,U_{\rm eff}(s_c)}\,, \tag{8.53}$$

where we have defined the "effective" higher-curvature coupling $\tilde{\alpha}\equiv 2\beta+8\alpha$. To avoid ghosts we assume that $K>0$ and hence $\tilde{\alpha}>0$. his is the case when both α and β are positive, but also when $\beta>-4\alpha$. As for the size of the parameter $\tilde{\alpha}$, according to [217] unitarity considerations suggest that $\tilde{\alpha} is \lesssim 10^{21}$.

We have mentioned various potentials so far, and to demonstrate their qualitative differences we plot them together in Fig. 8.1.The area with the color gradient corresponds to the normalized two-field tree-level JF potential $U^{(0)}(\phi,h)/U^{(0)}_{\rm min}$ as given in Eq. (8.12). Its FD, which we identified using the GW approach, is shown with the cyan line. After accounting for quantum corrections, we obtain the one-loop corrected potential (8.33) with a unique minimum singled-out from the valley of degenerate vacua along the FD, and we plot it with the red curve in its normalized form $U_{\rm eff}(s_c)/U_{\rm eff}(0)$. Finally, the normalized inflationary potential $\bar{U}(s_c)/\bar{U}(0)$ for our model (8.53) is shown with the green curve. Notice that $\bar{U}(s_c)$

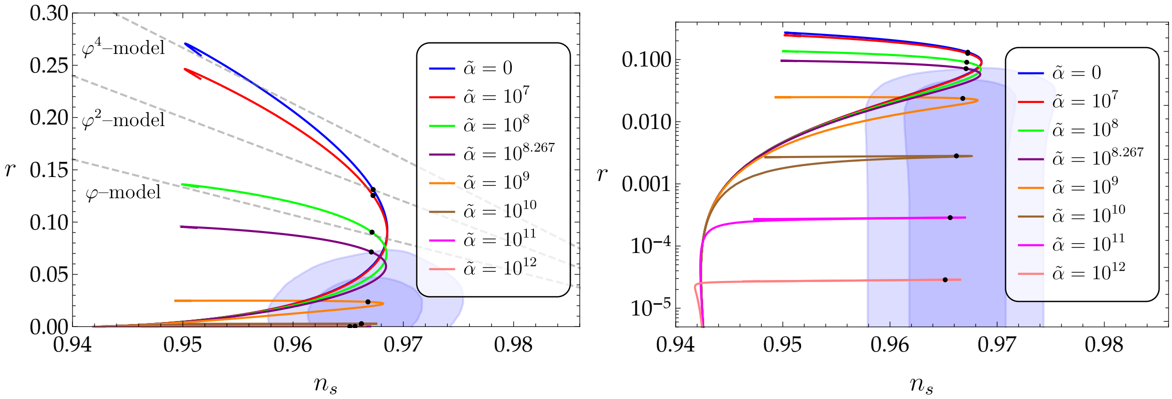

Figure 8.2: The predictions for the tensor-to-scalar ratio (r) and the tilt of the scalar spectrum (n_s) as ξ_s range from $\xi_s \ll 1$ to $\xi_s \gg 1$ for various values of $\tilde{\alpha}$. For each of the curves, the black dot corresponds to the $\xi_s \to 0$ limit (see Table 8.2) and ξ_s increases monotonically as we move away from it along each one of the two directions on the curve. The upper (lower) part of a curve with respect to its $\xi_s \to 0$ limit, corresponds to the predictions of large (small) field inflation. On the left (right) panel, the predictions are shown in linear (logarithmic) scale.

has plateaus on both sides of the minimum and thus it is suitable for both small field inflation and large field inflation *i.e.* excursions of the inflaton field in the regions $s_c < v_s$ and $s_c > v_s$ respectively.

In the end, after starting with a general scale invariant action involving adimensional matter-gravity and matter-matter couplings, we have obtained an action with a noncanonical scalar field minimally coupled to the usual Einstein-Hilbert action at the cost of negligible higher-order kinetic terms and a modified potential, which, as we will see next, is suitable for successful inflation in agreement with the observations.

8.4 Slow roll approximation and contact with observations

To constrain the parametric space of our model, in this section we compare its predictions for the cosmological obervables with the corresponding latest observational bounds established by the Planck collaboration.

The number of e-folds elapsed during the inflationary phase can be obtained in terms of the potential $\bar{U}(s_c)$ and the kinetic term coupling function $K(s_c)$ using the equations (6.6) and (7.23)

$$N_\star \equiv N(s_{c\star}) = \int_{s_{c,\mathrm{end}}}^{s_{c\star}} K(s_c)\frac{\bar{U}(s_c)}{\bar{U}'(s_c)}\mathrm{d}s_c\,. \tag{8.54}$$

To be more precise, we should calculate ρ_{end} by considering that the HFF parameter $\epsilon_1 \equiv -\dot{H}/H^2$ is exactly $\epsilon_1 = 1$ at the end of inflation. This condition gives that $\rho_{\mathrm{end}} = 3\bar{U}(s_{c,\mathrm{end}})/2$. Using this, and a pivot scale $k_\star = 0.002\,\mathrm{Mpc}^{-1}$, we can make explicit the dependence of the number of e-folds on the parameter $\tilde{\alpha}$, *i.e.*

$$N_\star = 64.3 + \frac{1}{4}\ln\left(\frac{2{U^\star_{\mathrm{eff}}}^2(1+\tilde{\alpha}U^{\mathrm{end}}_{\mathrm{eff}})}{3U^{\mathrm{end}}_{\mathrm{eff}}(1+\tilde{\alpha}U^\star_{\mathrm{eff}})^2}\right)\,. \tag{8.55}$$

In [3, 5], the higher-order kinetic terms appearing in the action (8.52) have been taken into account in the computation of ρ_{end}, but as shown there there is only an insignificant correction in the numerical factor of the number of e-folds. Moreover, in [3, 218] the reheating mechanism in R^2 Palatini inflationary models has been studied, but beyond the case of

Table 8.2: The predicted values for the tensor-to-scalar ratio (r), tilt of the scalar spectrum (n_s) and number of efolds ($N_\star$), in the limit $\xi_s \to 0$ for various values of $\tilde{\alpha}$.

$\tilde{\alpha}$	0	10^7	10^8	1.85×10^8	10^9	10^{10}	10^{11}	10^{12}
r	0.13090	0.12526	0.09022	0.07134	0.02368	0.00282	0.00029	0.00003
n_s	0.96727	0.96726	0.96717	0.96711	0.96681	0.96621	0.96563	0.96517
$N_\star$	60.6	60.6	60.4	60.3	59.8	58.8	58.0	57.3

instantaneous reheating, allowing a wider range for the number of e-folds for different values of the equation-of-state parameter.

Before performing the full parametric space study for the inflationary predictions of the model, we mention some asymptotic limits in terms of the value of the effective nonminimal coupling ξ_s. For $\xi_s \ll 1$ and $\tilde{\alpha} = 0$ we find that the predictions for both small filed inflation (SFI) and large field inflation (LFI) are equivalent to those of quadratic inflation,

$$n_s \simeq 1 - \frac{2}{N_\star}\,, \qquad r_0 \simeq \frac{8}{N_\star}\,, \tag{8.56}$$

where r_0 denotes the tensor-to-scalar ratio for $\tilde{\alpha} = 0$. On the other hand, for $\xi_s \gg 1$ we find

$$n_s \simeq 1 - \frac{3}{N_\star}\,, \tag{8.57}$$

for both SFI and LFI, while

$$r_0 \simeq \frac{16}{N_\star} \quad (\text{for LFI})\,, \qquad r_0 \simeq 0 \quad (\text{for SFI})\,, \tag{8.58}$$

Note that the first limit corresponds to the prediction of quartic inflation. When $\tilde{\alpha} \neq 0$, the predictions for n_s remain the same but r is changed as [5, 202]

$$r = \frac{r_0}{1 + \tilde{\alpha} U^\star_{\text{eff}}} = \frac{r_0}{1 + \frac{3}{2}\pi^2 \tilde{\alpha} A_s r_0}\,, \tag{8.59}$$

therefore, the presence of the parameter $\tilde{\alpha}$ results in a suppression of the value of tensor-to-scalar ratio.

Table 8.3: For $\tilde{\alpha} \lesssim 10^{8.267} \simeq 1.85 \times 10^8$, only small field inflation yields viable values for r and n_s (see Fig. 8.2). Here, we give the minimum and maximum values of ξ_s for which we obtain viable predictions for various $\tilde{\alpha}$. We also give the values of $\mathcal{M}$, r, n_s and $N_\star$ for these marginal values of ξ_s.

Small field inflation					
$\tilde{\alpha}$	$\xi_s^{(\text{min})}$	$\mathcal{M}$	r	n_s	$N_\star$
0	0.0006267	0.0502432	0.0729636	0.968159	60.3
10^7	0.0005830	0.0510926	0.0730490	0.968233	60.3
10^8	0.0002017	0.0651665	0.0732724	0.968439	60.3
$\tilde{\alpha}$	$\xi_s^{(\text{max})}$	$\mathcal{M}$	r	n_s	$N_\star$
0	0.0041417	0.0297085	0.0161109	0.957741	59.6
10^7	0.0041389	0.0297168	0.0160355	0.957747	59.6
10^8	0.0041367	0.0297308	0.0152745	0.957739	59.6

Let us now turn to the full analysis of the parametric space of our model in terms of its predictions for the cosmological observables. For each given set of values for the parameters

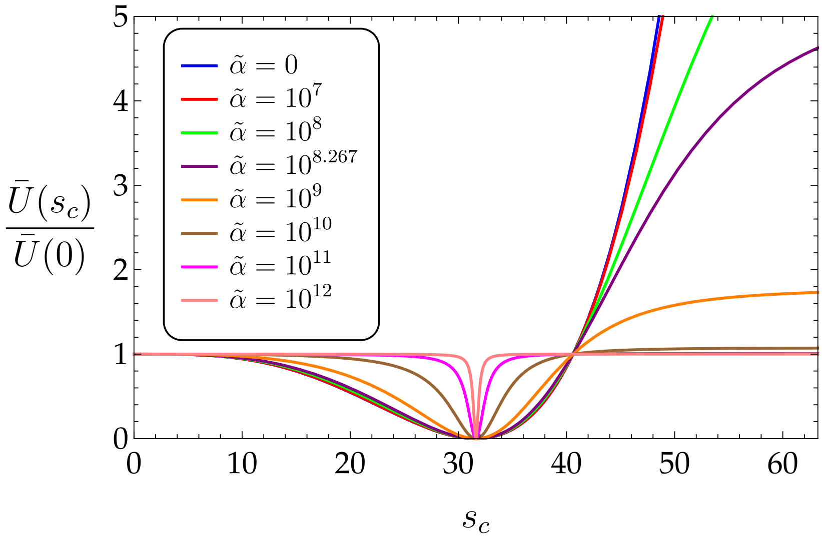

Figure 8.3: The normalized potential $\bar{U}(s_c)$ for $\xi_s = 0.001$ and various values of $\tilde{\alpha}$. In the limit $\tilde{\alpha} \gg 1$, the potential becomes symmetric about its VEV and consequently the predictions for small and large field inflation are identical.

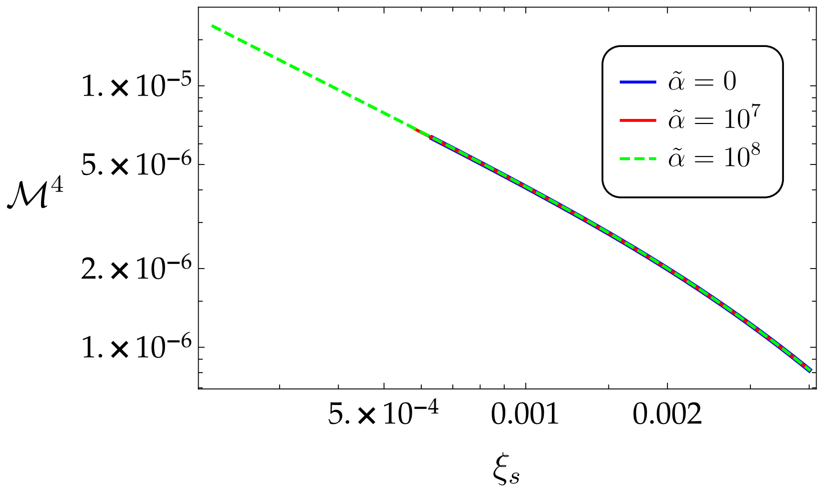

Figure 8.4: The parameter $\mathcal{M}^4$ as a function of ξ_s, for the viable range of values for ξ_s as given in Table 8.3 for small field inflation. For $\tilde{\alpha} \gtrsim 10^{8.267} \simeq 1.85 \times 10^8$, the $\xi_s \to 0$ limit is located in the observationally viable 95% CL region of the r-n_s plot and thus there is no lower cutoff for the value of ξ_s. Consequently in this case there is no upper cutoff for $\mathcal{M}^4$.

$\tilde{\alpha}$ and ξ_s, we used equation (8.55) to obtain the number of e-folds consistent with the constraints from reheating, while the value of $\mathcal{M}$ was fixed in each case so that we always have $A_s = 2.1 \times 10^{-9}$ at $k_\star = 0.05\,\mathrm{Mpc}^{-1}$ in agreement with the bounds set by the Planck collaboration. For both SFI and LFI, we have considered various values of $\tilde{\alpha}$ and a wide range of values for ξ_s ranging from $\xi_s \ll 1$ to $\xi_s \gg 1$ and in Fig. 8.2 we plot the corresponding predictions for the tensor-to-scalar ratio and the scalar tilt against the 68% (dark blue) and 95% (light blue) CL regions for n_s and r at $k_* = 0.002\,\mathrm{Mpc}^{-1}$ as obtained with the combined data of Planck+BK15+BAO [87].

The various curves correspond to fixed values of $\tilde{\alpha}$, while ξ_s moves along the curves, with the black dot on each curve being the $\xi_s \to 0$ limit. These dots also denote the transition point between the predictions of SFI and LFI with the lower (upper) part of each curve corresponding to small (large) field inflation. Obviously, in the limit of small ξ_s the predictions of SFI and LFI are identical. As we move away from the $\xi_s \to 0$ limit along a given curve

Table 8.4: For various $\tilde{\alpha} \gtrsim 10^{8.267} \simeq 1.85 \times 10^8$, and for both SFI and LFI, we give the corresponding maximum values of ξ_s that yield predictions that comply with the observational bounds. We also give the values of $\mathcal{M}$, r, n_s and $N_\star$ for these marginal values of ξ_s.

Small field inflation					
$\tilde{\alpha}$	$\xi_s^{(\max)}$	$\mathcal{M}$	r	n_s	$N_\star$
10^9	0.0040967	0.0299033	0.0103843	0.957734	59.4
10^{10}	0.0039033	0.0306853	0.0024263	0.957835	58.8
10^{11}	0.0036767	0.0316817	0.0002763	0.957919	58.0
10^{12}	0.0035200	0.0324432	0.0000280	0.957921	57.3
Large field inflation					
$\tilde{\alpha}$	$\xi_s^{(\max)}$	$\mathcal{M}$	r	n_s	$N_\star$
10^9	0.0028733	0.0245332	0.0248280	0.958142	60.0
10^{10}	0.0025667	0.0259176	0.0027631	0.957819	59.0
10^{11}	0.0020250	0.0286194	0.0002796	0.957922	58.1
10^{12}	0.0017108	0.0306805	0.0000280	0.957918	57.4

in both directions ξ_s increases monotonically with the top end of the curves having ξ_s values of $\mathcal{O}(10^8)$ and the bottom end (more evident in the right panel of Fig. 8.2) to values of $\mathcal{O}(10^{-1})$.

The effect of $\tilde{\alpha}$ on inflationary predictions is to suppress the value of r (cf. Eq. (8.59)). This effect becomes important for values $\tilde{\alpha} \gtrsim 10^6 - 10^7$. As the right panel of Fig. 8.2 shows, for sufficiently large values of $\tilde{\alpha}$ the predictions of SFI and LFI are identical along an extended range of values of ξ_s. This can be understood via the shape of the inflationary potential, which becomes symmetric about the location of the VEV for $\tilde{\alpha} \gg 1$, see Fig. 8.3.

Further inspection of Fig. 8.2 shows that for values of $\tilde{\alpha} \lesssim 10^{8.267} \simeq 1.85 \times 10^8$, LFI is not viable since its predictions are outside the 95% CL region for the measured values for r and n_s. On the other hand, SFI agrees with observations for a finite range of values of ξ_s, where the smallest (largest) viable value of ξ_s gives the largest (smallest) predicted value for r for a given $\tilde{\alpha}$, see also Table 8.3. This range is $2 \times 10^{-4} \lesssim \xi_s \lesssim 4 \times 10^{-3}$ and consequently, via (8.34) the VEV of the inflaton is restricted to $15\, M_\mathrm{P} \lesssim v_s \lesssim 70\, M_\mathrm{P}$. Moreover, the finite range of admissible values for ξ_s implies a corresponding finite range of viable values for the parameter $\mathcal{M}$ as can be seen in Fig. 8.4.

For values of $\tilde{\alpha} \gtrsim 10^{8.267} \simeq 1.85 \times 10^8$ the $\xi_s \to 0$ limit is located within the observationally viable 95% CL region of the r-n_s plot (see Fig. 8.2) and thus SFI and LFI have only an upper cutoff, $\xi_s \lesssim 4 \times 10^{-3}$, for the viable values of ξ_s as it is shown in Table 8.4. This in turn implies a lower cutoff, $15\, M_\mathrm{P} \lesssim v_s$, for the VEV of the inflaton.

In summary, v_s must be super-Planckian in all cases, implying that $v_s \simeq v_\phi$ as $v_h \sim \mathcal{O}(10^{-16})\, M_\mathrm{P}$. It is then obvious that the mixing angle as defined in Eq. (8.18) will satisfy $\omega \simeq 0$ and thus the flat direction, for values of the parameters lying in the viable regions of the parametric space is almost identified with the direction of the field ϕ in the field space, see Fig. 8.1.

8.5 Coleman-Weinberg inflation in Palatini gravity

In this section we study the predictions of nonminimal Coleman-Weinberg (CW) inflation [468] in presence of an $\frac{\alpha}{2}R^2$ term in the Palatini formulation of gravity, as in Chapter 7. As in

Sec. 8.1 a dynamical generation of the Planck scale takes place due to the inflaton nonminimal coupling.

We consider the following scalar potential

$$V(\phi) = \frac{1}{4}\lambda(\phi)\phi^4 + \Lambda^4, \tag{8.60}$$

containing a running[4] quartic coupling $\lambda(\phi)$ and a cosmological constant Λ which is adjusted so that at the minimum the potential value is zero, *i.e.*

$$V(v_\phi) = \frac{1}{4}\lambda(v_\phi)v_\phi^4 + \Lambda^4 = 0\,, \tag{8.61}$$

where v_ϕ is the VEV of the inflaton. We assume the following nonminimal coupling to gravity (see (7.8)):

$$g(\phi) = \xi_\phi \phi^2\,. \tag{8.62}$$

Therefore, the Planck scale is dynamically generated by a non vanishing inflaton VEV that satisfies

$$v_\phi = \frac{M_\mathrm{P}^2}{\sqrt{\xi_\phi}}. \tag{8.63}$$

Note that such a relation automatically implies that ξ_ϕ can only take positive values. We discuss now the possible scenarios that arise from the minimization of the scalar potential. A complete discussion was already presented in [168], however for the sake of clarity we review the relevant details. Given the scalar potential in Eq. (8.60), the general minimum equation is

$$\frac{1}{4}\beta(v_\phi) + \lambda(v_\phi) = 0\,, \tag{8.64}$$

where $\beta(\mu) = \mu\frac{\partial}{\partial\mu}\lambda(\mu)$ is the beta-function of the quartic coupling $\lambda(\mu)$. Therefore, several possibilities are open according to how we solve the equation:

$$\text{a)} \quad \beta(v_\phi) = \lambda(v_\phi) = 0, \tag{8.65}$$

$$\text{b)} \quad \beta(v_\phi) > 0,\ \lambda(v_\phi) < 0, \tag{8.66}$$

$$\text{c)} \quad \beta(v_\phi) < 0,\ \lambda(v_\phi) > 0. \tag{8.67}$$

It is easy to show that c) is actually a local maximum of the potential, so the only admissible solutions are a) or b). Using Eq. (8.61), the first option also implies that $\Lambda = 0$, thus realizing a fully classical scale invariant setup, while the second option requires $\Lambda \neq 0$ (it can be proven that the scale invariance is only softly broken *i.e.* $\Lambda \ll 1$ [168]). The quartic coupling prefactor in Eq. (8.60) can be model-independently written as a Taylor expansion around the VEV

$$\lambda(\phi) = \lambda(v_\phi) + \beta(v_\phi)\ln\frac{\phi}{v} + \frac{1}{2!}\beta'(v_\phi)\ln^2\frac{\phi}{v} + \frac{1}{3!}\beta''(v_\phi)\ln^3\frac{\phi}{v} + \cdots\,, \tag{8.68}$$

where $\beta'(\mu)$ and $\beta''(\mu)$ are respectively the first and second derivative of $\beta(\mu)$ with respect to $t = \ln\mu$ and we assumed without loss of generality that $\phi > 0$. Therefore for case a) described in Eq. (8.65) we have that the leading order expression is

$$\lambda^a(\phi) \simeq \frac{\beta'(v_\phi)}{2}\ln^2\frac{\phi}{v_\phi}\,, \tag{8.69}$$

[4]The careful reader might notice that also ξ_ϕ and α are subject to quantum corrections. However, it can be proven that their running is suppressed and can be safely ignored because of the constraint on the amplitude of scalar perturbations [87, 469] and perturbativity of the theory (*e.g.* [122, 140, 152, 470] and refs. therein.)

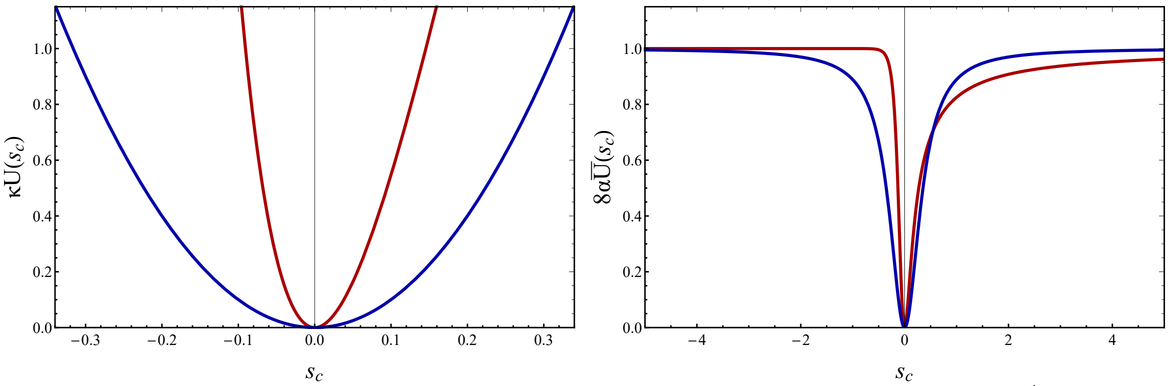

Figure 8.5: The scalar IF potential $U(s_c)$ for the 1st order CW model (red line) with $\kappa = \Lambda^{-4}$ and for the 2nd order CW model (blue line) with $\kappa = \xi_\phi^2/\beta'$ (left). The scalar EF potential $\bar{U}(s_c)$ of Eq. (8.53) for the 1st order CW model (red line) and for the 2nd order CW model (blue line) (right).

while for case b) we get

$$\lambda^b(\phi) \simeq \lambda(v_\phi) + \beta(v_\phi) \ln \frac{\phi}{v_\phi} \,. \tag{8.70}$$

In the following subsections we discuss separately each case, starting from case b). In order to avoid a cumbersome notation, from now on we omit the argument "(v_ϕ)" and restore it only when needed.

8.5.1 1st order Coleman - Weinberg potential

By using eqs. (8.61), (8.63) and (8.70) the potential can be rewritten as [113, 168]

$$V_1(\phi) \quad = \quad \Lambda^4 \left\{ 1 + \left[4 \ln \left(\frac{\phi}{v_\phi} \right) - 1 \right] \frac{\phi^4}{v_\phi^4} \right\}. \tag{8.71}$$

In presence of the nonminimal coupling to gravity (8.62) but before the effect of the R^2 term, the inflaton potential in the IF becomes [113, 168]

$$U_1(s_c) = \Lambda^4 \left(4\sqrt{\xi_\phi} \frac{s_c}{M_{\rm Pl}} + e^{-4\sqrt{\xi_\phi}\frac{s_c}{M_{\rm Pl}}} - 1 \right) \,, \tag{8.72}$$

where s_c is the canonically normalized field in the IF. We can immediately appreciate two relevant limit cases [113, 168]. For $\xi_\phi \gg 1$ and $s_c > 0$, the potential becomes

$$U_1(s_c) \approx a_s s_c \,, \tag{8.73}$$

with $a_s = 4\frac{\Lambda^4}{v_\phi}$. On the other hand for $\xi_\phi \ll 1$, the potential reduces to

$$U_1(s_c) \approx \frac{m^2}{2} {s_c}^2 \,, \tag{8.74}$$

with $m = m_1 = 4\frac{\Lambda^2}{v_\phi}$. Therefore in the IF, the model includes linear and quadratic inflation as limit solutions respectively for big ξ_ϕ and small ξ_ϕ.

In order to have an understanding of the overall shape of the potential, in Fig. 8.5, red line, we plot the 1st order CW potential as a function of s_c for the reference values $\xi_\phi = 10$, $\Lambda = 0.0015$. In the left panel we show U_1, *i.e.* the potential in the IF, while on the right panel we show $\bar{U}_1$ (see (8.53)), *i.e.* the potential in the EF after the effect of the $\frac{\alpha}{2}R^2$ term, with

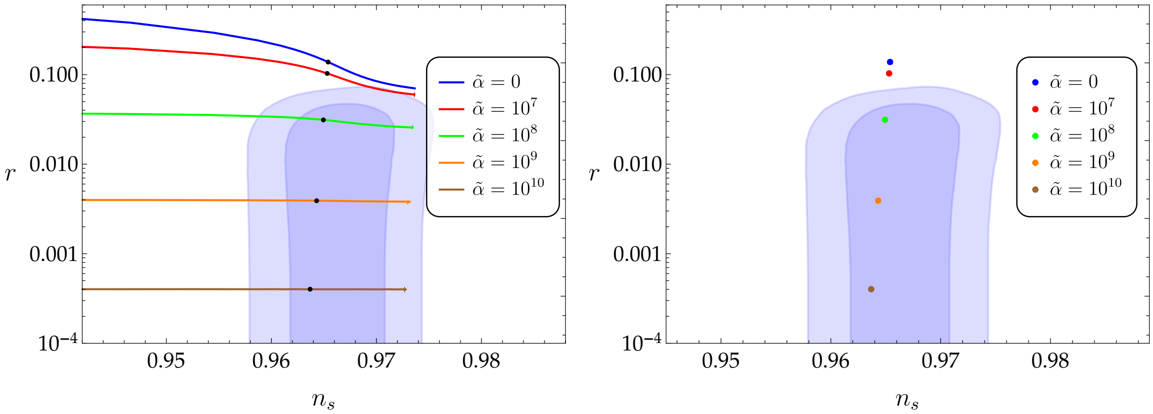

Figure 8.6: The predictions for the tensor-to-scalar ratio (r) and the spectral index (n_s) for the 1st order CW potential (left) and for the 2nd order CW potential (right).

$\alpha = 10^{10}$. We can notice that since U_1 is asymmetrical under the transformation $s_c \to -s_c$, the same holds for $\bar{U}_1$.

8.5.2 2nd order Coleman - Weinberg potential

By using eqs. (8.61), (8.63) and (8.69) the potential can be rewritten as [112]

$$V_2(\phi) = \frac{1}{8}\beta' \phi^4 \ln^2\left(\frac{\phi}{v_\phi}\right) \tag{8.75}$$

and the nonminimal coupling satisfies again Eq. (8.63). In the IF the model reproduces the quadratic inflationary potential (8.74),

$$U_2(s_c) = \frac{\beta' M_{\rm Pl}^2}{8\xi_\phi} s_c^2 \,. \tag{8.76}$$

where now [112]

$$m^2 = m_2^2 = \frac{\beta' M_{\rm P}^2}{4\xi_\phi} \,. \tag{8.77}$$

In Fig. 8.5, blue line, we plot the 2nd order CW potential as a function of s_c for the reference values $\xi_\phi = 10$ and $\beta' = 10^{-9}$. In the left panel we show U_2, *i.e.* the IF potential, while on the right panel we show $\bar{U}_2$, *i.e.* the potential in the EF, with $\alpha = 10^{10}$. We can notice that since U_2 is now symmetrical under the transformation $s_c \to -s_c$, the same holds for $\bar{U}_2$. We can also appreciate that the asymptotic limit of $\bar{U} \to 1/8\alpha$ holds for both models regardless of the starting potential (provided that their asymptotic limit is $U \to \infty$), in agreement with [202].

8.5.3 Inflationary predictions

Finally, in Fig. 8.6 we present the inflationary predictions for the 1st (left) and 2nd (right) order potentials, for various values of the parameter α. For each curve, in the 1st order potential, the black dot corresponds to the $\xi_\phi \to 0$ limit. The parts of the curves in the left of the black dots correspond to small field SFI, while the right ones to LFI. For the 2nd order CW potential, the predictions are v_ϕ independent as they depend only on the mass parameter given in (8.77), which is constrained from the amplitude of the scalar power spectrum. The number of e-folds in both models are predefined by Eq. (6.6) for $k_\star = 0.05\,\mathrm{Mpc}^{-1}$.

Chapter 9

Conclusions

In the first part of this thesis, Chapters 3-5, we calculated the thermal gravitino abundance using the full one-loop thermally corrected gravitino self-energy. After correcting the main analytical formulas for the gravitino production rate, we calculated it numerically without approximation. We provide a simple and useful parameterization of our final result. In the context of minimal supergravity models that assume unification of the gaugino masses, we have updated the bounds on the reheating temperature for certain gravitino masses. In particular, the saturation of the current LHC gaugino mass limit $m_{\tilde{g}} \gtrsim 2100\text{GeV}$, we find that a maximum reheating temperature $T_{\text{reh}} \simeq 10^9\,\text{GeV}$ is compatible to a gravitino mass $m_{3/2} \simeq 500 - 600\,\text{GeV}$.

It should be noted that attempting to constrain the reheating temperature by applying the cosmological data to gravitino DM scenarios illuminates for us whether or not thermal leptogenesis is a possible mechanism for producing the baryon asymmetry. Successful thermal leptogenesis requires a high temperature, $T_{\text{reh}} \gtrsim 2\times10^9\,\text{GeV}$ [471–473], which is slightly larger than the maximum reheating temperature obtained in our model using the lowest $m_{1/2}$ mass demonstrated in the recent LHC data [313, 314]. In any case, there are many alternative models for baryogenesis. Moreover, as mentioned earlier, thermal gravitino abundance is generally a part of the total DM density and the inclusion of other components will affect the phenomenological analysis.

In the second part of this thesis we have examined various models of inflation in the context of the Palatini formulation of gravity. In Chapter 7, we have carried out this investigation without invoking any particular reheating temperature mechanism,and show that the measurements of the amplitude of the primordial power spectrum impose very stringent constraints.These, in combination with the constraints imposed by the measurements of other cosmological observables, in particular the primordial tilt n_s and the tensor-to-scalar ratio r, significantly constrain these models.

For the quadratic model $V = \frac{m^2}{2}\phi^2$ we have seen that amplitude of the scalar power spectrum A_s puts constraints on the parameter m, and agreement with the data is obtained for values of this parameter that lie in a narrow range. The maximum reheating, or instantaneous, temperature T_{ins}, is of order $\sim 10^{15}\,\text{GeV}$, and this is achieved for fine-tuned values of m, within this range. For these fine-tuned values, the range of the allowed temperatures is quite narrow and depends on the effective equation-of-state parameter w, with a lowest temperature not far from the instantaneous temperature. For the canonical scenario, this is smaller but of the same order as T_{ins}. If we allow small deviations from these fine-tuned values, agreement with the data is still possible. However, these deviations, while not significantly perturbing the observable n_s, should be in a narrow range outside of which agreement with A_s data is difficult to achieve. In these cases, the allowed temperatures are well below T_{ins} and rapid thermalization is not possible. Moreover, depending on the value of m, not every value of w in the range $-1/3 < w < 1$ is allowed. The conclusion for this model is that agreement with all cosmological data is possible for values of the potential coupling m that are in a narrow range. Instantaneous reheating is possible at the cost of a very fine-tuned value of m.

The model with the quartic potential $V \sim \phi^4$ is at odds with the spectral index data n_s. Only marginal agreement with the primordial tilt can be obtained, with $n_s \simeq 0.960$, but this occurs for very low reheating temperatures close to Nucleosynthesis $T_{\rm reh} \sim MeV$, and for values of w close to $w = 1.0$. On the other hand, the amplitude A_s favors smaller values of the equation-of-state parameter $w \lesssim 0.25$. The conclusion is that, this model is difficult to reconcile with n_s, the measurements of the scalar power spectrum and reheating temperatures that are reasonably larger than $T_{\rm reh} \sim$ MeV so that we do not run into problems with Big Bang Nucleosynthesis. As our qualitative arguments have shown, the situation is even worse for the descending models, $V \sim \phi^n$ with $n > 4$, the situation is even worse.

The situation with the quartic potential is rescued in the Higgs model when the scalar field couples to gravity in a nonminimal manner, specified by a parameter ξ_h. This helps in that, as we have explicitly shown, the value of n_s depends on ξ_h allowing for larger values of n_s. Consistency with n_s observations requires that ξ_h be no smaller than, say, ~ 0.06. For a given ξ_h, the measurement of the primordial spectrum in the Higgs model strongly constrains the quartic coupling λ_h. The larger the value of ξ_h, the larger the values of the allowed λ_h. The quartic coupling is small, smaller than $\sim 10^{-6}$, for values ξ_h not exceeding $\sim 10^4$. Higher λ_h values are allowed in principle, but these require very large values of ξ_h, leading to instantaneous reheating temperatures smaller than $\sim 10^{15} GeV$.

In Chapter 8 we have studied scale-invariant models, again in the context of the Palatini formulation of gravity. The Planck scale is dynamically generated via the Coleman-Weinberg formalism by the VEVs of the scalar field ϕ and the Higgs field h. These scalar fields have been nonminimally coupled to gravity via terms of the form $\xi_i \Phi_i^2 R$, where $\Phi_i = \phi, h$. The additional scalar field ϕ comes from a $U(1)_X$ extension of the SM, which contains an additional gauge boson X_μ and three right-handed neutrinos N_R^i. The Higgs mass was produced by the portal coupling $\lambda_{h\phi} h^2 \phi^2$. This is exactly the meaning of the addition of the extra scalar field ϕ. Without it, the necessity of the existence of a Higgs mass term with a dimensionful coupling would have broken the scale invariance of our model. A possible additional Z_2 symmetry facilitates the stability of the potential dark matter candidates in the framework of our model. As discussed, these can be either the new fermions of the model *e.g.* the right-handed neutrinos or the additional Dirac fermion ζ, or the additional $U(1)_X$ gauge boson.

We have used the Gildener-Weinberg approach, the generalisation of the Coleman-Weinberg mechanism to the case of multiple fields, to identify the flat direction of the tree-level potential. Along the flat direction, the theory effectively becomes single field and by calculating the quantum corrections we obtain the one-loop effective potential, stabilised by the additional $U(1)_X$ gauge boson. In the effective single-field description, two parameters are important for our analysis namely the effective nonminimal coupling ξ_s, which is composed of the nonminimal couplings of ϕ and h and their mixing angle ω, and the effective higher-curvature coupling $\tilde{\alpha}$ which corresponds to a combination of the coupling constants of the quadratic curvature corrections in the action. These quadratic in curvature terms are the usual scale invariant terms R^2 and $R_{(\mu\nu)} R^{(\mu\nu)}$. The fact that their effect on the inflationary observables can be jointly described by the common coupling $\tilde{\alpha}$ shows that their contribution to the final EF potential is the same. On the other hand, the higher order kinetic terms generated in EF are not of the same form, since the R^2 term gives us only a second order kinetic term, while the $R_{(\mu\nu)} R^{(\mu\nu)}$ term gives higher than the second order terms. The study of such kinetic terms was beyond the scope of this thesis, since they are negligible at least during slow roll.

Transforming the action into the EF and comparing the predictions of the model with the observations, requires the use of both conformal and disformal transformations. The one-loop corrections are taken in the IF, *i.e.* after the conformal transformation is performed, which decouples the scalar fields from the Einstein-Hilbert term, but before the disformal transformation, which removes the quadratic in curvature terms from the gravitational sector.

In this IF, we can have an one-loop effective potential with a minimum at zero without using a cosmological constant term that would make our model "quasi scale invariant". After transforming the action to EF, we obtain a modified effective potential $\bar{U}(s_c)$ in terms of a canonical scalar field s_c playing the role of the inflaton. The shape of the potential $\bar{U}(s_c)$ has plateaus on both sides of the minimum and thus both SFI and LFI can be accommodated in our model. The additional higher-order kinetic terms that appear in the EF are negligible in the slow roll approximation, and so we have retained only liner order terms in our analysis. By applying the cosmological data on inflation we were able to constrain the size of the VEV of these scalar fields, and consequently the masses of the extra gauge boson and right-handed neutrinos.

To constrain the parameter space, we have considered the most recent bounds on cosmological observables established by the Planck collaboration and we have found that our model agrees with observations for a wide range of parameters. More specifically, for values of the parameter $\tilde{\alpha}$ in the range $\tilde{\alpha} \gtrsim 1.85 \times 10^8$, both SFI and LFI support viable inflation when $\xi_s \lesssim \mathcal{O}(10^{-3})$. In the large $\tilde{\alpha}$ limit, the inflationary potential becomes symmetric about its minimum and consequently the predictions for the SFI and LFI observables are identical.

When $\tilde{\alpha} \lesssim 1.85 \times 10^8$, and regardless of the value of ξ_s, LFI is not feasible because the predicted values for the tensor-to-scalar ratio and the tilt of the scalar power spectrum are outside the 95% CL region. On the other hand, SFI exhibits regions in the parametric space that are viable for any $\tilde{\alpha}$ with ξ_s interpolating between a maximum and a minimum value. Finally, the largest viable value for ξ_s in our model arises in the context of SFI and is approximately $\xi_s \simeq 4 \times 10^{-3}$, corresponding to a minimum value for the VEV of s_c near $15\, M_{\mathrm{P}}$.

Finally, at the end of Chapter 8 we studied the Coleman-Weinberg model of inflation in the presence of a R^2 term. We show that this model can also be compatible with latest observational data, for a wide range of the parameters used.

Appendix A

Conventions and notation

In flat spacetime the metric is given by

$$g_{\mu\nu} \equiv \mathrm{diag}(+1, -1, -1, -1)\,, \tag{A.1}$$

where $\mu, \nu = 0, 1, 2, 3$.

We define the Pauli σ matrices with lower Lorentz indices $\sigma_\mu \equiv (\mathbb{I}, \sigma_i) = (\sigma_0, \sigma_i)$ where

$$\begin{aligned} \sigma_0 &\equiv \begin{pmatrix} 1 & 0 \\ 0 & 1 \end{pmatrix}, \qquad & \sigma_1 &\equiv \begin{pmatrix} 0 & 1 \\ 1 & 0 \end{pmatrix}, \\ \sigma_2 &\equiv \begin{pmatrix} 0 & -i \\ i & 0 \end{pmatrix}, \qquad & \sigma_3 &\equiv \begin{pmatrix} 1 & 0 \\ 0 & -1 \end{pmatrix}. \end{aligned} \tag{A.2}$$

The raising and lowering of spinor indices is made using the $\varepsilon-$tensors

$$\varepsilon_{\alpha\beta} \equiv \begin{pmatrix} 0 & -1 \\ 1 & 0 \end{pmatrix}, \qquad \varepsilon^{\alpha\beta} \equiv \begin{pmatrix} 0 & 1 \\ -1 & 0 \end{pmatrix}. \tag{A.3}$$

The spinor index structure of the matrices σ_μ is such that $\sigma_\mu \equiv (\sigma_\mu)_{\alpha\dot{\alpha}}$ and the indices may be raised as

$$\begin{aligned} (\overline{\sigma}_\mu)^{\dot{\alpha}\alpha} &\equiv \varepsilon^{\alpha\beta}\varepsilon^{\dot{\alpha}\dot{\beta}}\,(\sigma_\mu)_{\beta\dot{\beta}}\,, \\ (\sigma_\mu)_{\alpha\dot{\alpha}} &\equiv \varepsilon_{\alpha\beta}\varepsilon_{\dot{\alpha}\dot{\beta}}\,(\overline{\sigma}_\mu)^{\dot{\beta}\beta}\,. \end{aligned} \tag{A.4}$$

Also, we define

$$\begin{aligned} (\sigma^{\mu\nu})_\alpha^{\ \beta} &\equiv \frac{i}{4}\left(\sigma^\mu_{\ \alpha\dot{\alpha}}\,\overline{\sigma}^{\nu\,\dot{\alpha}\beta} - \sigma^\nu_{\ \alpha\dot{\alpha}}\,\overline{\sigma}^{\mu\,\dot{\alpha}\beta}\right), \\ (\overline{\sigma}^{\mu\nu})^{\dot{\alpha}}_{\ \dot{\beta}} &\equiv \frac{i}{4}\left(\overline{\sigma}^{\mu\,\dot{\alpha}\alpha}\,\sigma^\nu_{\ \alpha\dot{\beta}} - \overline{\sigma}^{\nu\,\dot{\alpha}\alpha}\,\sigma^\mu_{\ \alpha\dot{\beta}}\right). \end{aligned} \tag{A.5}$$

It is easy to see that $\overline{\sigma}_0 = \sigma_0$ and $\overline{\sigma}_i = -\sigma_i$ with $i = 1, 2, 3$. Using the Pauli σ matrices we can define the Dirac γ matrices which in the Weyl basis read

$$\gamma_\mu = \begin{pmatrix} 0 & \sigma_\mu \\ \overline{\sigma}_\mu & 0 \end{pmatrix}, \qquad \gamma_5 = \begin{pmatrix} \mathbb{I} & 0 \\ 0 & -\mathbb{I} \end{pmatrix}. \tag{A.6}$$

A.1 Weyl, Dirac and Majorana spinors

A two-component left-handed Weyl spinor ξ_α transforms in the $\left(\mathbf{\frac{1}{2}}, \mathbf{0}\right)$ representation of the $SO(3,1)$ Lorentz group, while the right-handed one $\overline{\xi}_{\dot{\alpha}}$ is in the conjugate representation

$\left(\mathbf{0}, \mathbf{\frac{1}{2}}\right)$. These spinors are hermitian conjugate, *i.e.* $(\xi_\alpha)^\dagger = \bar{\xi}_{\dot{\alpha}}$ and $\left(\bar{\xi}_{\dot{\alpha}}\right)^\dagger = \xi_\alpha$ and their spinor indices are pulled using (A.3), namely,

$$\xi_\alpha = \varepsilon_{\alpha\beta}\xi^\beta, \qquad \xi^\alpha = \varepsilon^{\alpha\beta}\xi_\beta\,, \tag{A.7}$$

$$\bar{\xi}_{\dot{\alpha}} = \varepsilon_{\dot{\alpha}\dot{\beta}}\bar{\xi}^{\dot{\beta}}, \qquad \bar{\xi}^{\dot{\alpha}} = \varepsilon^{\dot{\alpha}\dot{\beta}}\bar{\xi}_{\dot{\beta}}\,. \tag{A.8}$$

A Dirac spinor can be written in terms of a left and a right-handed Weyl spinor as

$$\psi_{\mathrm{D}} = \begin{pmatrix} \xi_\alpha \\ \bar{\eta}^{\dot{\alpha}} \end{pmatrix}, \tag{A.9}$$

and its adjoint as

$$\overline{\psi}_{\mathrm{D}} \equiv {\psi_{\mathrm{D}}}^\dagger\gamma^0 = \begin{pmatrix} \eta^\alpha & \bar{\xi}_{\dot{\alpha}} \end{pmatrix}\,. \tag{A.10}$$

Using the projectors $P_L = \frac{1}{2}(\mathbb{I} + \gamma_5)$ and $P_R = \frac{1}{2}(\mathbb{I} - \gamma_5)$ left and right-handed Dirac spinors are given by

$$\begin{aligned} \psi_L \equiv P_L\psi_{\mathrm{D}} &= \begin{pmatrix} \mathbb{I} & 0 \\ 0 & 0 \end{pmatrix}\begin{pmatrix} \xi_\alpha \\ \bar{\eta}^{\dot{\alpha}} \end{pmatrix} = \begin{pmatrix} \xi_\alpha \\ 0 \end{pmatrix}\,, \\ \psi_R \equiv P_R\psi_{\mathrm{D}} &= \begin{pmatrix} 0 & 0 \\ 0 & \mathbb{I} \end{pmatrix}\begin{pmatrix} \xi_\alpha \\ \bar{\eta}^{\dot{\alpha}} \end{pmatrix} = \begin{pmatrix} 0 \\ \bar{\eta}^{\dot{\alpha}} \end{pmatrix}\,. \end{aligned} \tag{A.11}$$

For the adjoint spinor (A.10) one obtains $\overline{\psi}_L = \overline{\psi}_{\mathrm{D}}P_R$ and $\overline{\psi}_R = \overline{\psi}_{\mathrm{D}}P_L$.

The charge conjugate Dirac spinor reads

$$\psi^c_{\mathrm{D}} = \mathcal{C}\overline{\psi}^T_{\mathrm{D}} = \begin{pmatrix} \eta_\alpha \\ \bar{\xi}_{\dot{\alpha}} \end{pmatrix}\,, \tag{A.12}$$

where the charge conjugation matrix is written as $\mathcal{C} = i\gamma^2\gamma^0$. Majorana spinors ψ_{M} are equal to their own charge conjugate, so

$$\psi_{\mathrm{M}} = \begin{pmatrix} \xi_\alpha \\ \bar{\xi}_{\dot{\alpha}} \end{pmatrix}\,. \tag{A.13}$$

A.2 Structure constants

The structure constants $f^{(\alpha)\,abc}$ for the three gauge groups are given by

$$\begin{aligned} f^{(1)\,abc} &= 0\,, \\ f^{(2)\,abc} &= \epsilon^{abc}\,, \\ f^{(3)\,abc} &= f^{abc}\,, \end{aligned} \tag{A.14}$$

where ϵ^{abc} is the totally antisymmetric Levi-Civita symbol with $\epsilon^{123} = 1$. The corresponding $SU(3)_c$ totally antisymmetric structure constants are given by

$$\begin{aligned} f^{123} &= 1\,, \\ f^{147} &= -f^{156} = f^{246} = f^{257} = f^{345} = -f^{367} = \frac{1}{2}\,, \\ f^{458} &= f^{678} = \frac{\sqrt{3}}{2}\,, \end{aligned} \tag{A.15}$$

and all the other f^{abc} not related to these by permuting indices are zero.

Appendix B

Basic integrals for spectral densities

In the previous sections of the main text we have used the basic integrals:

$$
\begin{aligned}
L_1^{F,B}(P) &= \int \frac{\mathrm{d}^4K}{(2\pi)^3}\frac{\delta(K^2)}{(K-P)^2}n_{F,B}(K) = -\frac{1}{4p}\int_0^\infty \frac{\mathrm{d}k}{(2\pi)^2}L_-(k)n_{F,B}(k)\,, && \text{(B.1)}\\
L_2^{F,B}(P) &= \int \frac{\mathrm{d}^4K}{(2\pi)^3}k_0\frac{\delta(K^2)}{(K-P)^2}n_{F,B}(K)\\
&= \frac{1}{4p}\int_0^\infty \frac{\mathrm{d}k}{(2\pi)^2}k\left[-2\ln\frac{\omega_+}{\omega_-}+L_+(k)\right]n_{F,B}(k)\,, && \text{(B.2)}\\
L_3^{F,B}(P) &= \int \frac{\mathrm{d}^4K}{(2\pi)^3}k_0^2\frac{\delta(K^2)}{(K-P)^2}n_{F,B}(K) = -\frac{1}{4p}\int_0^\infty \frac{\mathrm{d}k}{(2\pi)^2}k^2L_-(k)n_{F,B}(k)\,, && \text{(B.3)}\\
L_4^{F,B}(P) &= \int \frac{\mathrm{d}^4K}{(2\pi)^3}\mathbf{p}\cdot\mathbf{k}\frac{\delta(K^2)}{(K-P)^2}n_{F,B}(K)\\
&= \frac{1}{4}\int_0^\infty \frac{\mathrm{d}k}{(2\pi)^2}\left[4k+\frac{P^2}{2p}L_-(k)-\frac{p_0k}{p}\left(2\ln\frac{\omega_+}{\omega_-}-L_+(k)\right)\right]n_{F,B}(k)\,, && \text{(B.4)}\\
L_5^{F,B}(P) &= \int \frac{\mathrm{d}^4K}{(2\pi)^3}P\cdot K\frac{\delta(K^2)}{(K-P)^2}\,n_{F,B}(K)\\
&= -\frac{1}{4}\int_0^\infty \frac{\mathrm{d}k}{(2\pi)^2}\left[4k+\frac{P^2}{2p}L_-(k)\right]n_{F,B}(k)\,, && \text{(B.5)}
\end{aligned}
$$

where

$$
\begin{aligned}
L_\pm(k) &= \ln\frac{k+\omega_+}{k+\omega_-}\pm\ln\frac{k-\omega_+}{k-\omega_-}\,, && \text{(B.6)}\\
\omega_\pm &= \frac{1}{2}(p_0\pm p)\,. && \text{(B.7)}
\end{aligned}
$$

In addition we define

$$
\begin{aligned}
L &= 1-\frac{p_0}{p}\ln\frac{\omega_+}{\omega_-}\,, && \text{(B.8)}\\
M(k) &= (k+\omega_+)(k+\omega_-)\ln\frac{k+\omega_+}{k+\omega_-}-(k-\omega_+)(k-\omega_-)\ln\frac{k-\omega_+}{k-\omega_-}\,. && \text{(B.9)}
\end{aligned}
$$

Moreover, one gets

$$
M(k) = \left(\frac{P^2}{4}+k^2\right)L_-(k)+kp_0L_+(k)\,. \qquad \text{(B.10)}
$$

Actually $L_5^{F,B}(P)$ can be evaluated using the relation $P\cdot K = k_0\,p_0-\mathbf{p}\cdot\mathbf{k}$, as $L_5^{F,B}(P) = p_0\,L_2^{F,B}(P)-L_4^{F,B}(P)$.

For illustration we will calculate $L_1^{F,B}(P)$ in (B.1). To perform the integration we use that

$$\begin{aligned} \mathrm{d}^4K &= 2\pi k^2 \mathrm{d}k_0 \mathrm{d}k \mathrm{d}\eta_k\,, \\ \delta(K^2) &= \frac{1}{2|k_0|}\left[\delta(k+k_0)+\delta(k-k_0)\right], \end{aligned} \tag{B.11}$$

where $\eta_k \equiv \hat{\mathbf{p}}\cdot\hat{\mathbf{k}}$ and $K\cdot P = k_0 p_0 - \eta_k p k$. We remind that p, k denote the measures of the corresponding momentum 3-vectors, eg. $p = |\mathbf{p}|$ and the same for k. In addition we get

$$(K-P)^2 = P^2 - 2K\cdot P = 2\eta_k k p - 2k_0 p_0 + P^2\,, \tag{B.12}$$

assuming that particles in the loop are massless $K^2 = 0$. Thus we proceed as

$$\begin{aligned} L_1^{F,B}(P) &= \int \frac{\mathrm{d}^4K}{(2\pi)^3}\frac{\delta(K^2)}{(K-P)^2} n_{F,B}(K) \\ &= \int \frac{2\pi k^2 \mathrm{d}k_0 \mathrm{d}k \mathrm{d}\eta_k}{(2\pi^3)}\frac{1}{2|k_0|}\frac{\delta(k+k_0)+\delta(k-k_0)}{2\eta_k k p - 2k_0 p_0 + P^2} n_{F,B}(K) \\ &= \int \frac{\mathrm{d}k}{(2\pi)^2}\frac{k}{2}\int_{-1}^{+1}\mathrm{d}\eta_k\left[\frac{1}{2\eta_k k p + P^2 - 2kp_0} + \frac{1}{2\eta_k k p + P^2 + 2kp_0}\right] n_{F,B}(k)\,. \end{aligned} \tag{B.13}$$

We will apply

$$\int_{-1}^{+1}\frac{\mathrm{d}\eta_k}{a\eta_k + b} = \frac{1}{a}\ln\frac{b+a}{b-a}\,, \tag{B.14}$$

with $a = 2pk$ and $b_{1,2} = P^2 \mp 2kp_0$ at the first (second) term respectively. Therefore we obtain

$$\begin{aligned} L_1^{F,B}(P) &= \int_0^\infty \frac{\mathrm{d}k}{(2\pi)^2}\frac{k}{2a}\left[\ln\frac{b_1+a}{b_1-a} + \ln\frac{b_2+a}{b_2-a}\right] n_{F,B}(k) \\ &= \frac{1}{4p}\int_0^\infty \frac{\mathrm{d}k}{(2\pi)^2}\left[\ln\frac{(p_0-p)(p_0+p-2k)}{(p_0+p)(p_0-p-2k)} + \ln\frac{(p_0+p)(p_0-p+2k)}{(p_0-p)(p_0+p+2k)}\right] n_{F,B}(k) \\ &= \frac{1}{4p}\int_0^\infty \frac{\mathrm{d}k}{(2\pi)^2}\left[\ln\frac{k-\omega_+}{k-\omega_-} + \ln\frac{k+\omega_-}{k+\omega_+}\right] n_{F,B}(k) \\ &= -\frac{1}{4p}\int_0^\infty \frac{\mathrm{d}k}{(2\pi)^2} L_-(k) n_{F,B}(k)\,, \end{aligned} \tag{B.15}$$

which is the final result. Similarly one can obtain the Eqs. (B.2)–(B.5).

We have also used the integrals[1]

$$\int_0^\infty \frac{\mathrm{d}k}{2\pi^2} k n_F(k) = \frac{T^2}{24} \quad \text{and} \quad \int_0^\infty \frac{\mathrm{d}k}{2\pi^2} k n_B(k) = \frac{T^2}{12}\,. \tag{B.16}$$

$$I_1^{B,F}(p_0,p) = \int_0^\infty \mathrm{d}k L_-(k,p_0,p)\, n_{B,F}(k), \tag{B.17}$$

$$I_2^{B,F}(p_0,p) = \int_0^\infty \mathrm{d}k k^2 L_-(k,p_0,p)\, n_{B,F}(k), \tag{B.18}$$

and

$$I_3^{B,F}(p_0,p) = \int_0^\infty \mathrm{d}k k L_+(k,p_0,p)\, n_{B,F}(k). \tag{B.19}$$

[1] The real and imaginary parts of logarithms are given by $\ln(x) = \ln|x| - i\pi\Theta(-x)$.

Appendix C

Calculation of the collision term

For the process $a + b \to c + \widetilde{G}$ the collision term is given by

$$\mathcal{C} = \frac{1}{(2\pi)^8} \int \frac{\mathrm{d}^3\mathbf{p_1}}{2E_1} \frac{\mathrm{d}^3\mathbf{p_2}}{2E_2} \frac{\mathrm{d}^3\mathbf{p_3}}{2E_3} \frac{\mathrm{d}^3\mathbf{p}}{2E} \delta^4(P_1 + P_2 - P_3 - P)|\mathcal{M}|^2 f_a f_b (1 \pm f_c) \,. \tag{C.1}$$

Firstly, our aim is to calculate the quantity $\frac{d\mathcal{C}}{\mathrm{d}^3p}$, where $\mathrm{d}^3\mathbf{p} = p^2\,\mathrm{d}p\,\mathrm{d}\Omega_p = \mathrm{d}^3p\,\mathrm{d}\Omega_p$. Thus,

$$\frac{d\mathcal{C}}{\mathrm{d}^3p} = \frac{1}{2^9\pi^8 E} \int \frac{\mathrm{d}^3\mathbf{p_1}}{2E_1} \frac{\mathrm{d}^3\mathbf{p_2}}{2E_2} \frac{\mathrm{d}^3\mathbf{p_3}}{2E_3} \int \mathrm{d}\Omega_p\, \delta^4(P_1 + P_2 - P_3 - P)|\mathcal{M}|^2 f_a f_b (1 \pm f_c) \,. \tag{C.2}$$

This calculation will be done in the so-called t-frame, in which the reference momentum is the t-channel momentum $\mathbf{k} = \mathbf{p_1} - \mathbf{p_3}$. Of course the results are frame independent. Thus we will express the other momenta defining first $\hat{\mathbf{k}} = \hat{\mathbf{z}}$,

$$\begin{aligned} \mathbf{k} &= k(0,0,1)\,, \\ \mathbf{p} &= E(0, \sin\tilde{\theta}, \cos\tilde{\theta})\,, \\ \mathbf{p}_3 &= E_3(\cos\phi\sin\theta, \sin\phi\sin\theta, \cos\theta)\,. \end{aligned} \tag{C.3}$$

In this frame the Mandelstam variables are

$$\begin{aligned} s &= (P_1 + P_2)^2 = (P_3 + P)^2 = 2E\,E_3(1 - \cos\theta\cos\tilde{\theta} - \sin\theta\sin\tilde{\theta}\sin\phi)\,, \\ t &= (P_1 - P_3)^2 = (P - P_2)^2 = (E_1 - E_3)^2 - k^2\,. \end{aligned} \tag{C.4}$$

Before we continue with the computation of (C.2), we will prove some useful identities. We will use the identity

$$\frac{\mathrm{d}^3\mathbf{p_1}}{2E_1} = \mathrm{d}^4P_1\,\delta^4(P_1^2)\,\Theta(E_1) = \mathrm{d}E_1\,\mathrm{d}^3\mathbf{p_1}\,\delta^4(P_1^2)\,\Theta(E_1)\,, \tag{C.5}$$

and we will insert $\int \mathrm{d}^3\mathbf{k}\,\delta^3(\mathbf{k} - \mathbf{p_1} + \mathbf{p_3}) = 1$, then

$$\begin{aligned} \frac{\mathrm{d}^3\mathbf{p_1}}{2E_1} &= \int \mathrm{d}^3\mathbf{k}\,\delta^3(\mathbf{k} - \mathbf{p_1} + \mathbf{p_3})\mathrm{d}E_1\mathrm{d}^3\mathbf{p_1}\delta^4(P_1^2)\Theta(E_1) \\ &= \int \mathrm{d}^3\mathbf{q}\,\delta^3(\mathbf{k} - \mathbf{p_1} + \mathbf{p_3})\mathrm{d}E_1\mathrm{d}^3\mathbf{p_1}\delta^4(E_1^2 - |\mathbf{p_1}^2|)\Theta(E_1)\,, \end{aligned} \tag{C.6}$$

and after integrating over $\mathrm{d}^3\mathbf{p_1}$ using the $\delta-$function we get

$$\frac{\mathrm{d}^3\mathbf{p_1}}{2E_1} = \delta(E_1^2 - |\mathbf{k} + \mathbf{p_3}|^2)\Theta(E_1)\mathrm{d}E_1\mathrm{d}^3\mathbf{k}\,. \tag{C.7}$$

Another usefull identity is

$$\begin{aligned}\frac{\mathrm{d}^3\mathbf{p_1}}{2E_1} &= \mathrm{d}E_1\mathrm{d}^3\mathbf{p_1}\delta^4(P_1^2)\Theta(E_1) \\ &= \mathrm{d}E_1\mathrm{d}^3\mathbf{p_1}\delta^4(E_1^2-|\mathbf{p_1}|^2)\Theta(E_1) \\ &= \frac{\delta(E_1-|\mathbf{p_1}|)}{2|\mathbf{p_1}|}\Theta(E_1)\mathrm{d}E_1\mathrm{d}^3\mathbf{p_1}\,,\end{aligned} \tag{C.8}$$

which after multiplying by $\delta^4(P_1+P_2-P_3-P)$ becomes

$$\frac{\mathrm{d}^3\mathbf{p_1}}{2E_1}\,\delta^4(P_1+P_2-P_3-P) = \delta((E_3+E-E_2)^2-|\mathbf{k}+\mathbf{p_3}|^2)\Theta(E_3+E-E_2)\,. \tag{C.9}$$

In this calculation, we will use (C.7) as it is and (C.9) expressed in terms of $\mathbf{p_2}$ and E_2

$$\frac{\mathrm{d}^3\mathbf{p_2}}{2E_2}\,\delta^4(P_1+P_2-P_3-P) = \delta((E_3+E-E_1)^2-|\mathbf{p}-\mathbf{k}|^2)\Theta(E_3+E-E_1)\,. \tag{C.10}$$

Now, the next step is to rewrite the $\delta-$functions in terms of $\cos\theta$ and $\cos\tilde{\theta}$. We have

$$\begin{aligned}\delta\left(E_1^2-|\mathbf{k}+\mathbf{p_3}|^2\right) &= \delta\left(E_1^2-E_3^2-k^2-2E_3k\cos\theta\right) \\ &= \frac{1}{2E_3k}\delta\left(\cos\theta-\frac{E_1^2-E_3^2-k^2}{2E_3k}\right)\,,\end{aligned} \tag{C.11}$$

and

$$\begin{aligned}\delta\left((E+E_3-E_1)^2-|\mathbf{p}-\mathbf{k}|^2\right) &= \delta\left((E+E_3-E_1)^2-E^2-k^2+2Ek\cos\tilde{\theta}\right) \\ &= \frac{1}{2Ek}\delta\left(\cos\tilde{\theta}-\frac{E^2+k^2-(E+E_3-E_1)^2}{2Ek}\right)\,.\end{aligned} \tag{C.12}$$

Substituting (C.7), (C.10), (C.11) and (C.12) in (C.2) we get

$$\begin{aligned}\frac{d\mathcal{C}}{\mathrm{d}^3p} &= \frac{1}{2^{12}\pi^8E^2}\int \mathrm{d}\cos\tilde{\theta}\,\mathrm{d}\tilde{\phi}\,\mathrm{d}\cos\theta\,\mathrm{d}\phi\,\mathrm{d}E_1\,\mathrm{d}E_3\,\mathrm{d}k\,\mathrm{d}\Omega_k \\ &\times\delta\left(\cos\theta-\frac{E_1^2-E_3^2-k^2}{2E_3k}\right)\,\delta\left(\cos\tilde{\theta}-\frac{E^2+k^2-(E+E_3-E_1)^2}{2Ek}\right) \\ &\times|\mathcal{M}|^2f_af_b(1\pm f_c)\Theta(E_1)\Theta(E_3)\Theta(E+E_3-E_1)\,.\end{aligned} \tag{C.13}$$

Nothing depends on $\mathrm{d}\tilde{\phi}$ and $\mathrm{d}\Omega_k$, so after these integrations we get an additional $8\pi^2$ factor. After the θ and $\tilde{\theta}$ integrations we have to substitute

$$\cos\theta = \frac{E_1^2-E_3^2-k^2}{2E_3k} \qquad \text{and} \qquad \cos\tilde{\theta} = \frac{E^2+k^2-(E+E_3-E_1)^2}{2Ek}\,. \tag{C.14}$$

From the integrations over the $\delta-$functions, we find that

$$-1\leq\cos\theta\leq 1 \Rightarrow \begin{cases}E_3-E_1\leq k\leq E_1+E_3 \\ E_1-E_3\leq k\,,\end{cases} \tag{C.15}$$

$$-1\leq\cos\tilde{\theta}\leq 1 \Rightarrow \begin{cases}E_1-E_3\leq k\leq 2E+E_3-E_1 \\ E_3-E_1\leq k\,,\end{cases} \tag{C.16}$$

which yield the $\Theta-$functions $\Theta(k-|E_1-E_3|)$, $\Theta(E_1+E_3-k)$ and $\Theta(2E+E_3-E_1-k)$. After performing the remaining angular integrations we find that

$$\frac{d\mathcal{C}}{\mathrm{d}^3p} = \frac{1}{2^9\pi^6E^2}\int \mathrm{d}E_1\,\mathrm{d}E_3\,\mathrm{d}q\,\mathrm{d}\phi\,|\mathcal{M}|^2 f_a f_b(1\pm f_c)(Theta)\,, \tag{C.17}$$

where

$$\begin{aligned} Theta = {} & \Theta(k-|E_1-E_3|)\Theta(E_1+E_3-k) \\ & \Theta(2E+E_3-E_1-k)\Theta(E+E_3-E_1)\Theta(E_1)\Theta(E_3) \end{aligned} \tag{C.18}$$

and in $|\mathcal{M}|^2$ we have substituted θ and $\tilde{\theta}$ from (C.14). Now, we use the identities

$$\Theta(E_1+E_3-k) = 1-\Theta(k-E_1-E_3)\,, \tag{C.19}$$

and

$$\Theta(k-E_1-E_3)\Theta(k-|E_1-E_3|) = \Theta(k-E_1-E_3)\,, \tag{C.20}$$

in order to split (C.18), that is,

$$\begin{aligned} Theta = {} & \Theta(k-|E_1-E_3|)\Theta(2E+E_3-E_1-k)\Theta(E+E_3-E_1)\Theta(E_1)\Theta(E_3) \\ & -\Theta(k-E_1-E_3)\Theta(2E+E_3-E_1-k)\Theta(E+E_3-E_1)\Theta(E_1)\Theta(E_3)\,. \end{aligned} \tag{C.21}$$

Now, we insert

$$1 = \Theta(E_1-E_3)+\Theta(E_3-E_1)\,,$$

so

$$\begin{aligned} Theta = {} & \Theta(k-E_1+E_3)\Theta(2E+E_3-E_1-k)\Theta(E+E_3-E_1)\Theta(E_1-E_3)\Theta(E_1)\Theta(E_3) \\ & +\Theta(k+E_1-E_3)\Theta(2E+E_3-E_1-k)\Theta(E+E_3-E_1)\Theta(E_3-E_1)\Theta(E_1)\Theta(E_3) \\ & -\Theta(k-E_1-E_3)\Theta(2E+E_3-E_1-k)\Theta(E+E_3-E_1)\Theta(E_1)\Theta(E_3)\,. \end{aligned} \tag{C.22}$$

Note that

$$\Theta(k-E_1-E_3)\Theta(2E+E_3-E_1-k) \Rightarrow E_1<E\,, \tag{C.23}$$

so we have to include the corresponding $\Theta-$function. It is obvious that we will need to calculate 3 different integrals because of the 3 different combinations of $\Theta-$functions in (C.22). We have

$$Theta = Theta_1+Theta_2+Theta_3\,, \tag{C.24}$$

where

$$\begin{aligned} Theta_1 &= \Theta(k-E_1+E_3)\Theta(2E+E_3-E_1-k)\Theta(E+E_3-E_1)\Theta(E_1-E_3)\Theta(E_1)\Theta(E_3)\,, \\ Theta_2 &= \Theta(k+E_1-E_3)\Theta(2E+E_3-E_1-k)\Theta(E+E_3-E_1)\Theta(E_3-E_1)\Theta(E_1)\Theta(E_3)\,, \\ Theta_3 &= -\Theta(k-E_1-E_3)\Theta(2E+E_3-E_1-k)\Theta(E+E_3-E_1)\Theta(E-E_1)\Theta(E_1)\Theta(E_3)\,. \end{aligned} \tag{C.25}$$

After splitting the $Theta$ into three terms as in (C.24) we can write

$$\frac{d\mathcal{C}^{|\mathcal{M}|^2}}{\mathrm{d}^3p} = \sum_A g_A^{|\mathcal{M}|^2}\,, \tag{C.26}$$

where $|\mathcal{M}|^2 = \{s,t,s^2,t^2,st\}$ and $A=\{1,2,3\}$. We have defined

$$g_A^{|\mathcal{M}|^2} = \frac{1}{2^9\pi^6E^2}\int_0^\infty \mathrm{d}E_3\int_0^{E+E_3}\mathrm{d}E_1\int \mathrm{d}k\int_0^{2\pi}\mathrm{d}\phi\,|\mathcal{M}|^2\,f_{abc}\,Theta_A\,, \tag{C.27}$$

Table C.1: The integration limits for k for the various cases.

A	k-limits
1	$E_1 - E_3 \leq k \leq 2E + E_3 - E_1$
2	$E_3 - E_1 \leq k \leq 2E + E_3 - E_1$
3	$E_1 + E_3 \leq k \leq 2E + E_3 - E_1$

and the statistical factor is

$$f_{abc} = f_a(E_1) f_b(E_2)(1 \pm f_c(E_3))\,. \tag{C.28}$$

The integration limits for the dk integration are dictated by the theta functions in (C.25). As we have mentioned we will calculate five different amplitudes $|\mathcal{M}|^2$ for completeness. These are $|\mathcal{M}|^2 = s, t, s^2, t^2$ and st. Moreover, since we will integrate analytically over k and ϕ, it will be useful to define the function

$$\tilde{g}_A^{|\mathcal{M}|^2}(E, E_1, E_3) = \frac{1}{2\pi} \int \mathrm{d}k \int_0^{2\pi} \mathrm{d}\phi \, |\mathcal{M}|^2\,. \tag{C.29}$$

Thus from (C.27) and (C.29), we obtain that

$$g_A^{|\mathcal{M}|^2} = \frac{1}{2^8 \pi^5 E^2} \int_0^{\infty} \mathrm{d}E_3 \int_0^{E+E_3} \mathrm{d}E_1 \, \tilde{g}_A^{|\mathcal{M}|^2}(E, E_1, E_3)\, f_{abc}\, Theta_A\,. \tag{C.30}$$

Using now the limits from the Table C.1 based on (C.25), we are ready to calculate $\tilde{g}_A^{|\mathcal{M}|^2}(E, E_1, E_3)$. In details we have

- For $|\mathcal{M}|^2 = s$

$$\begin{aligned}
\tilde{g}_1^s &= \frac{4}{3} (E - E_1 + E_3)^2 (E + 2E_1 + E_3)\ , \\
\tilde{g}_2^s &= \frac{4}{3} E^2 (E + 3E_3)\ , \\
\tilde{g}_3^s &= \frac{4}{3} (E - E_1) \left(E^2 + 3E_3(E + E_1) + EE_1 - 2E_1^2 \right)\ .
\end{aligned}$$

- For $|\mathcal{M}|^2 = t$

$$\begin{aligned}
\tilde{g}_1^t &= -\frac{4}{3} (E - E_1 + E_3)^2 (2E + E_1 - E_3)\ , \\
\tilde{g}_2^t &= -\frac{4}{3} E^2 (2E - 3E_1 + 3E_3)\ , \\
\tilde{g}_3^t &= -\frac{4}{3} (E - E_1) (3E_3(E + E_1) + (E - E_1)(2E + E_1))\ .
\end{aligned}$$

- For $|\mathcal{M}|^2 = s^2$

$$\begin{aligned}
\tilde{g}_1^{s^2} &= \frac{16}{15} (E - E_1 + E_3)^3 \left(E^2 + 3EE_1 + 2EE_3 + 6E_1^2 + 3E_1E_3 + E_3^2 \right)\ , \\
\tilde{g}_2^{s^2} &= \frac{16}{15} E^3 \left(E^2 + 5EE_3 + 10E_3^2 \right)\ , \\
\tilde{g}_3^{s^2} &= \frac{16}{15} \left(5E_3(E^4 - 4EE_1^3 + 3E_1^4) + 10E_3^2(E^3 - E_1^3) + (E^2 + 3EE_1 + 6E_1^2)(E - E_1)^3 \right)\ .
\end{aligned}$$

Table C.2: The values of the collision term normalised by $1/T^6$, for the possible statistical factors and the five basic squared amplitudes.

$\lvert\mathcal{M}\rvert^2$	BBF	BFB	FFF
s	$0.25957 \cdot 10^{-3}$	$0.27138 \cdot 10^{-3}$	$0.15116 \cdot 10^{-3}$
t	$-0.12978 \cdot 10^{-3}$	$-0.13286 \cdot 10^{-3}$	$-0.75581 \cdot 10^{-4}$
s^2	$0.53955 \cdot 10^{-2}$	$0.54574 \cdot 10^{-2}$	$0.41807 \cdot 10^{-2}$
t^2	$0.17981 \cdot 10^{-2}$	$0.18055 \cdot 10^{-2}$	$0.13937 \cdot 10^{-2}$
st	$-0.26977 \cdot 10^{-2}$	$-0.27144 \cdot 10^{-2}$	$-0.20903 \cdot 10^{-2}$

- For $|\mathcal{M}|^2 = t^2$

$$\begin{aligned}
\tilde{g}_1^{t^2} &= \frac{16}{15}\left(6E^2 + 3E(E_1 - E_3) + (E_1 - E_3)^2\right)(E - E_1 + E_3)^3 \,, \\
\tilde{g}_2^{t^2} &= \frac{16}{15}E^3\left(6E^2 + 15E(E_3 - E_1) + 10(E_1 - E_3)^2\right) \,, \\
\tilde{g}_3^{t^2} &= \frac{16}{15}\left(6E^5 + 15E^4(E_3 - E_1) + 10E^3(E_1 - E_3)^2 - E_1^3(E_1^2 - 5E_1E_3 + 10E_3^2)\right) \,.
\end{aligned}$$

- Finally, for $|\mathcal{M}|^2 = s\,t$

$$\begin{aligned}
\tilde{g}_1^{s\,t} &= -\frac{16}{15}(E - E_1 + E_3)^3\left(3E^2 + E(4E_1 + E_3) + (E_1 - E_3)(3E_1 + 2E_3)\right) \,, \\
\tilde{g}_2^{s\,t} &= -\frac{16}{15}E^3\left(3E^2 - 5E(E_1 - 2E_3) + 10E_3(E_3 - E_1)\right) \,, \\
\tilde{g}_3^{s\,t} &= -\frac{16}{15}\left(10E_3^2\left(E^3 - E_1^3\right) + 10E_3\left(E^2 + EE_1 + E_1^2\right)(E - E_1)^2 + \left(3E^2 + 4EE_1 + 3E_1^2\right)(E - E_1)^3\right) \,.
\end{aligned}$$

Based on the previous analytical results for the $\tilde{g}_A^{|\mathcal{M}|^2}(E, E_1, E_3)$ we will use the relation

$$\mathcal{C}_{abc}^{|\mathcal{M}|^2} = \frac{1}{2^8\pi^5}\int_0^\infty \mathrm{d}E \int_0^\infty \mathrm{d}E_3 \int_0^{E+E_3} \mathrm{d}E_1 \sum_A \{\tilde{g}_A^{|\mathcal{M}|^2}(E, E_1, E_3)\, Theta_A\}\, f_{abc} \,, \tag{C.31}$$

in order to perform numerically the integrations over E_1, E_3 and E. The $Theta_A$ is taken from (C.24) and the statistical factor f_{abc} can be f_{BBF}, f_{BFB} or f_{FFF}. For all these cases the numerical values for the collision terms, normalised by $1/T^6$ are summarized in the Table C.2. For our calculation of the subtracted rate we need only the numerical factors $\mathcal{C}^s_{\text{BBF}} = 0.25957 \times 10^{-3}$ and $\mathcal{C}^t_{\text{BFB}} = -0.13286 \times 10^{-3}$.

Table C.3: The $\mathcal{C}'$ collision term normalised by $1/T^6$, where the statistical factor f_c has been neglected. The percentages in the parentheses are the deviations from the value of $\mathcal{C}$, namely $(\mathcal{C}' - \mathcal{C})/\mathcal{C}\,\%$.

$\lvert\mathcal{M}\rvert^2$	BBF	BFB	FFF
s	$0.29511 \cdot 10^{-3}$ (+13.69%)	$0.22133 \cdot 10^{-3}$ (−18.44%)	$0.16600 \cdot 10^{-3}$ (+9.82%)
t	$-0.14755 \cdot 10^{-3}$ (+13.69%)	$-0.11067 \cdot 10^{-3}$ (−16.70%)	$-0.82999 \cdot 10^{-4}$ (+9.81%)
s^2	$0.57419 \cdot 10^{-2}$ (+6.42%)	$0.50242 \cdot 10^{-2}$ (−7.94%)	$0.43961 \cdot 10^{-2}$ (+5.15%)
t^2	$0.19140 \cdot 10^{-2}$ (+6.45%)	$0.16747 \cdot 10^{-2}$ (−7.24%)	$0.14654 \cdot 10^{-2}$ (+5.14%)
st	$-0.28710 \cdot 10^{-2}$ (+6.42%)	$-0.25121 \cdot 10^{-2}$ (−7.45%)	$-0.21981 \cdot 10^{-2}$ (+5.16%)

Moreover ignoring the statistical factor for the accompanying particle of gravitino, that is $1 \pm f_c(E_3) = 1$, we can calculate the collision factor $\mathcal{C}'$ defined as

$$\mathcal{C}' = \frac{1}{(2\pi)^8} \int \frac{\mathrm{d}^3\mathbf{p_1}}{2E_1} \frac{\mathrm{d}^3\mathbf{p_2}}{2E_2} \frac{\mathrm{d}^3\mathbf{p_3}}{2E_3} \frac{\mathrm{d}^3\mathbf{p}}{2E} \delta^4(P_1 + P_2 - P_3 - P) |\mathcal{M}|^2 f_a f_b \,, \tag{C.32}$$

analytically. The numerical values for $\mathcal{C}'$ along with the deviations from the value of $\mathcal{C}$ are given in Table C.3.

Appendix D

Details on the variations

Substituting (8.37) in (8.40) gives us that the auxiliary field $\Sigma_{\mu\nu}$ in terms of $q_{\mu\nu}$ and $g_{\mu\nu}$ reads

$$\Sigma_{\mu\nu} = \frac{1}{2\beta}\frac{\sqrt{-q}}{\sqrt{-g}}q^{\kappa\lambda}g_{\kappa\mu}g_{\lambda\nu} - \frac{1}{2\beta+8\alpha}\left(1+\frac{\alpha}{\beta}\frac{\sqrt{-q}}{\sqrt{-g}}q^{\kappa\lambda}g_{\kappa\lambda}\right)g_{\mu\nu}\,, \tag{D.1}$$

and its trace is

$$\Sigma = g^{\mu\nu}\Sigma_{\mu\nu} = \frac{-4}{2\beta+8\alpha} + \frac{1}{2\beta+8\alpha}\frac{\sqrt{-q}}{\sqrt{-g}}q^{\kappa\lambda}g_{\kappa\lambda}\,. \tag{D.2}$$

The part of the Lagrangian density that has to be varied with respect to $g_{\mu\nu}$ is

$$\begin{aligned}\sqrt{-g}\mathcal{L}_g &= -\sqrt{-g}\left(\frac{1}{2}\frac{\partial C}{\partial\Sigma_{\mu\nu}}\Sigma_{\mu\nu} - \frac{1}{2}C - \mathcal{L}_m\right)\\ &= -\sqrt{-g}\left(\frac{\alpha}{2}\Sigma^2 + \frac{\beta}{2}\Sigma_{\mu\nu}\Sigma^{\mu\nu} + \frac{1}{2}g^{\mu\nu}\partial_\mu s_c\partial_\nu s_c + U_{\text{eff}}(s_c)\right)\,.\end{aligned} \tag{D.3}$$

Varying (D.3) we obtain that

$$\begin{aligned}\delta\left(\sqrt{-g}\mathcal{L}_g\right) &= -\sqrt{-g}\Big[\alpha\Sigma\delta\Sigma + \beta g^{\mu\gamma}\Sigma_{\mu\nu}\delta\left(g^{\rho\nu}\Sigma_{\gamma\rho}\right) + \frac{1}{2}\partial_\mu s_c\partial_\nu s_c\delta g^{\mu\nu}\Big]\\ &\quad -\frac{1}{2}\sqrt{-g}g_{\mu\nu}\delta g^{\mu\nu}\Big[-\frac{\alpha}{2}\Sigma^2 - \frac{\beta}{2}\Sigma_{\mu\nu}\Sigma^{\mu\nu} - U_{\text{eff}}(s_c) - \frac{1}{2}g^{\kappa\lambda}\partial_\kappa s_c\partial_\lambda s_c\Big].\end{aligned} \tag{D.4}$$

Substituting (D.1) and (D.2) in (D.4) and after manipulations we have that

$$\begin{aligned}\frac{1}{\sqrt{-g}}\frac{\delta S}{\delta g^{\mu\nu}} &= -\frac{1}{4(\beta+4\alpha)}\frac{\sqrt{-q}}{\sqrt{-g}}q^{\sigma\lambda}g_{\sigma\mu}g_{\lambda\nu}\\ &\quad+\frac{1}{4\beta}\frac{q}{g}\left(q^{\sigma\lambda}q^{\rho\delta}g_{\lambda\delta}g_{\rho\nu}g_{\sigma\mu} - \frac{\alpha}{\beta+4\alpha}q^{\delta\rho}g_{\delta\rho}q^{\sigma\lambda}g_{\sigma\mu}g_{\lambda\nu}\right)\\ &\quad+\frac{1}{2}g_{\mu\nu}\left[\frac{1}{\beta+4\alpha}\left(\frac{1}{2}+\frac{\alpha}{8\beta}\frac{q}{g}q^{\lambda\sigma}g_{\lambda\sigma}q^{\rho\delta}g_{\rho\delta}\right) - \frac{q}{g}\frac{1}{8\beta}q^{\lambda\sigma}q^{\delta\rho}g_{\lambda\delta}g_{\sigma\rho}\right]\\ &\quad+\frac{1}{2}g_{\mu\nu}\left(\frac{1}{2}g^{\lambda\sigma}\partial_\lambda s_c\partial_\sigma s_c + U_{\text{eff}}(s_c)\right) - \frac{1}{2}\partial_\mu s_c\partial_\nu s_c = 0\,.\end{aligned} \tag{D.5}$$

The functions R_i which has been displayed in Eqs. (8.49)-(8.50) are listed below

$$\begin{aligned}R_1 &= B\left(2A - 2BX_q\right)\,,\\ R_2 &= 4A - 2BX_q\,,\\ R_3 &= 4A^2 - 4ABX_q + 4B^2X_q^2\,,\\ R_4 &= A(R_1 + AB) - 2BR_1X_q\,,\\ R_5 &= A^3\left(A - 2BX_q\right)\,.\end{aligned} \tag{D.6}$$

The coefficients a_i, and b_i which has been displayed in Eq. (8.51) are[1]

$$
\begin{aligned}
a_0 &= \frac{1}{1+\tilde{\alpha}U_{\rm eff}}\,,\\
b_0 &= \frac{(\tilde{\beta}-\tilde{\alpha})}{(1+\tilde{\alpha}U_{\rm eff})(1+\tilde{\beta}U_{\rm eff})}\,,\\
a_1 &= \frac{\tilde{\beta}}{2(1+\tilde{\beta}U_{\rm eff})}\,,\\
b_1 &= \frac{(\tilde{\beta}-\tilde{\alpha})\left(3\tilde{\beta}-2\tilde{\alpha}+(2\tilde{\beta}-\tilde{\alpha})(\tilde{\alpha}+\tilde{\beta})U_{\rm eff}+\tilde{\alpha}\tilde{\beta}^2U_{\rm eff}^2\right)}{(1+\tilde{\alpha}U_{\rm eff})(1+\tilde{\beta}U_{\rm eff})^3}\,,
\end{aligned}
\tag{D.7}
$$

where we have defined $\tilde{\alpha}=2\beta+8\alpha$, $\tilde{\beta}=4\beta+8\alpha$ and $U_{\rm eff}=U_{\rm eff}(s_c)$. As it seems, for $\tilde{\alpha}=\tilde{\beta}$, the coefficients b_0 and b_1, like the rest higher order b coefficients of the same series (8.51), are equal to zero. This is expected, as the equality of the tilted factors is translated to an elimination of the $R_{\mu\nu}R^{\mu\nu}$ term and so the disformal transformation is reduced again to the usual conformal.

[1] These coefficients have been also found in [219].

Bibliography

[1] H. Eberl, I. D. Gialamas, and V. C. Spanos, "Gravitino thermal production revisited," *Phys. Rev. D* **103** no. 7, (2021) 075025, arXiv:2010.14621 [hep-ph].

[2] H. Eberl, I. D. Gialamas, and V. C. Spanos, "In preparation ," (2021) .

[3] I. D. Gialamas and A. Lahanas, "Reheating in R^2 Palatini inflationary models," *Phys. Rev. D* **101** no. 8, (2020) 084007, arXiv:1911.11513 [gr-qc].

[4] I. D. Gialamas, A. Karam, T. D. Pappas, and V. C. Spanos, "Scale-invariant quadratic gravity and inflation in the Palatini formalism," *Phys. Rev. D* **104** no. 2, (2021) 023521, arXiv:2104.04550 [astro-ph.CO].

[5] I. D. Gialamas, A. Karam, and A. Racioppi, "Dynamically induced Planck scale and inflation in the Palatini formulation," *JCAP* **11** (2020) 014, arXiv:2006.09124 [gr-qc].

[6] D. Canko, I. Gialamas, G. Jelic-Cizmek, A. Riotto, and N. Tetradis, "On the Catalysis of the Electroweak Vacuum Decay by Black Holes at High Temperature," *Eur. Phys. J. C* **78** no. 4, (2018) 328, arXiv:1706.01364 [hep-th].

[7] D. D. Canko, I. D. Gialamas, and G. P. Kodaxis, "A simple $F(\mathcal{R}, \phi)$ deformation of Starobinsky inflationary model," *Eur. Phys. J. C* **80** no. 5, (2020) 458, arXiv:1901.06296 [hep-th].

[8] I. D. Gialamas, A. Karam, A. Lykkas, and T. D. Pappas, "Palatini-Higgs inflation with nonminimal derivative coupling," *Phys. Rev. D* **102** no. 6, (2020) 063522, arXiv:2008.06371 [gr-qc].

[9] I. D. Gialamas, A. Karam, T. D. Pappas, A. Racioppi, and V. C. Spanos, "Scale-invariance, dynamically induced Planck scale and inflation in the Palatini formulation," in *Conference on recent developments in high energy physics and cosmology*. 7, 2021. arXiv:2107.04408 [gr-qc].

[10] H. Eberl, I. D. Gialamas, and V. C. Spanos, "Gravitino thermal production," 7, 2021. arXiv:2107.09319 [hep-ph].

[11] R. Kallosh, L. Kofman, A. D. Linde, and A. Van Proeyen, "Gravitino production after inflation," *Phys. Rev. D* **61** (2000) 103503, arXiv:hep-th/9907124.

[12] G. Giudice, A. Riotto, and I. Tkachev, "Thermal and nonthermal production of gravitinos in the early universe," *JHEP* **11** (1999) 036, arXiv:hep-ph/9911302.

[13] H. P. Nilles, M. Peloso, and L. Sorbo, "Nonthermal production of gravitinos and inflatinos," *Phys. Rev. Lett.* **87** (2001) 051302, arXiv:hep-ph/0102264.

[14] M. Kawasaki, F. Takahashi, and T. T. Yanagida, "Gravitino overproduction in inflaton decay," *Phys. Lett. B* **638** (2006) 8–12, arXiv:hep-ph/0603265.

[15] M. Endo, M. Kawasaki, F. Takahashi, and T. T. Yanagida, "Inflaton decay through supergravity effects," *Phys. Lett. B* **642** (2006) 518–524, arXiv:hep-ph/0607170.

[16] J. Ellis, M. A. G. Garcia, D. V. Nanopoulos, K. A. Olive, and M. Peloso, "Post-Inflationary Gravitino Production Revisited," *JCAP* **03** (2016) 008, arXiv:1512.05701 [astro-ph.CO].

[17] E. Dudas, Y. Mambrini, and K. Olive, "Case for an EeV Gravitino," *Phys. Rev. Lett.* **119** no. 5, (2017) 051801, arXiv:1704.03008 [hep-ph].

[18] K. Kaneta, Y. Mambrini, and K. A. Olive, "Radiative production of nonthermal dark matter," *Phys. Rev. D* **99** no. 6, (2019) 063508, arXiv:1901.04449 [hep-ph].

[19] M. Kawasaki, K. Kohri, T. Moroi, and A. Yotsuyanagi, "Big-Bang Nucleosynthesis and Gravitino," *Phys. Rev. D* **78** (2008) 065011, arXiv:0804.3745 [hep-ph].

[20] M. Kawasaki, K. Kohri, T. Moroi, and Y. Takaesu, "Revisiting big-bang nucleosynthesis constraints on long-lived decaying particles," *Phys. Rev. D* **97** no. 2, (2018) 023502, arXiv:1709.01211 [hep-ph].

[21] R. H. Cyburt, J. R. Ellis, B. D. Fields, K. A. Olive, and V. C. Spanos, "Bound-State Effects on Light-Element Abundances in Gravitino Dark Matter Scenarios," *JCAP* **11** (2006) 014, arXiv:astro-ph/0608562.

[22] R. H. Cyburt, J. Ellis, B. D. Fields, F. Luo, K. A. Olive, and V. C. Spanos, "Metastable charged sparticles and the cosmological ^{7}Li problem," *JCAP* **12** (2012) 037, arXiv:1209.1347 [astro-ph.CO].

[23] S. Weinberg, "Cosmological Constraints on the Scale of Supersymmetry Breaking," *Phys. Rev. Lett.* **48** (1982) 1303.

[24] J. R. Ellis, J. E. Kim, and D. V. Nanopoulos, "Cosmological Gravitino Regeneration and Decay," *Phys. Lett. B* **145** (1984) 181–186.

[25] M. Khlopov and A. D. Linde, "Is it easy to save the gravitino?," *Phys. Lett. B* **138** (1984) 265–268.

[26] T. Moroi, H. Murayama, and M. Yamaguchi, "Cosmological constraints on the light stable gravitino," *Phys. Lett. B* **303** (1993) 289–294.

[27] M. Kawasaki and T. Moroi, "Gravitino production in the inflationary universe and the effects on big bang nucleosynthesis," *Prog. Theor. Phys.* **93** (1995) 879–900, arXiv:hep-ph/9403364.

[28] T. Moroi, *Effects of the gravitino on the inflationary universe*. Phd thesis, 1995. arXiv:hep-ph/9503210.

[29] J. Ellis, D. V. Nanopoulos, K. A. Olive, and S.-J. Rey, "On the thermal regeneration rate for light gravitinos in the early universe," *Astropart. Phys.* **4** (1996) 371–386, arXiv:hep-ph/9505438.

[30] M. Bolz, W. Buchmuller, and M. Plumacher, "Baryon asymmetry and dark matter," *Phys. Lett. B* **443** (1998) 209–213, arXiv:hep-ph/9809381.

[31] M. Bolz, A. Brandenburg, and W. Buchmuller, "Thermal production of gravitinos," *Nucl. Phys. B* **606** (2001) 518–544, arXiv:hep-ph/0012052. [Erratum: Nucl.Phys.B 790, 336–337 (2008)].

[32] M. Bolz, *Thermal Production of Gravitinos*. PhD thesis, Hamburg U., 2000.

[33] F. D. Steffen, "Gravitino dark matter and cosmological constraints," *JCAP* **0609** (2006) 001, arXiv:hep-ph/0605306 [hep-ph].

[34] J. Pradler and F. D. Steffen, "Thermal gravitino production and collider tests of leptogenesis," *Phys. Rev. D* **75** (2007) 023509, arXiv:hep-ph/0608344.

[35] J. Pradler and F. D. Steffen, "Constraints on the Reheating Temperature in Gravitino Dark Matter Scenarios," *Phys. Lett. B* **648** (2007) 224–235, arXiv:hep-ph/0612291.

[36] V. S. Rychkov and A. Strumia, "Thermal production of gravitinos," *Phys. Rev. D* **75** (2007) 075011, arXiv:hep-ph/0701104.

[37] J. Pradler, "Electroweak Contributions to Thermal Gravitino Production," Master's thesis, Vienna U., 2006.

[38] G. F. Giudice and R. Rattazzi, "Theories with gauge mediated supersymmetry breaking," *Phys. Rept.* **322** (1999) 419–499, arXiv:hep-ph/9801271.

[39] K. Choi, K. Hwang, H. B. Kim, and T. Lee, "Cosmological gravitino production in gauge mediated supersymmetry breaking models," *Phys. Lett. B* **467** (1999) 211–217, arXiv:hep-ph/9902291.

[40] T. Asaka, K. Hamaguchi, and K. Suzuki, "Cosmological gravitino problem in gauge mediated supersymmetry breaking models," *Phys. Lett. B* **490** (2000) 136–146, arXiv:hep-ph/0005136.

[41] K. Jedamzik, M. Lemoine, and G. Moultaka, "Gravitino dark matter in gauge mediated supersymmetry breaking," *Phys. Rev. D* **73** (2006) 043514, arXiv:hep-ph/0506129.

[42] H. Fujisaki, K. Kumekawa, M. Yamaguchi, and M. Yoshimura, "Particle production and gravitino abundance after inflation," *Phys. Rev. D* **54** (1996) 2494–2503, arXiv:hep-ph/9511381.

[43] M. Hashimoto, K. I. Izawa, M. Yamaguchi, and T. Yanagida, "Gravitino overproduction through moduli decay," *Prog. Theor. Phys.* **100** (1998) 395–398, arXiv:hep-ph/9804411.

[44] M. Lemoine, "Gravitational production of gravitinos," *Phys. Rev. D* **60** (1999) 103522, arXiv:hep-ph/9908333.

[45] A. L. Maroto and J. R. Pelaez, "The Equivalence theorem and the production of gravitinos after inflation," *Phys. Rev. D* **62** (2000) 023518, arXiv:hep-ph/9912212.

[46] D. H. Lyth, "Late time creation of gravitinos from the vacuum," *Phys. Lett. B* **476** (2000) 356–362, arXiv:hep-ph/9912313.

[47] F. Takayama and M. Yamaguchi, "Gravitino dark matter without R-parity," *Phys. Lett. B* **485** (2000) 388–392, arXiv:hep-ph/0005214.

[48] J. R. Ellis, K. A. Olive, Y. Santoso, and V. C. Spanos, "Gravitino dark matter in the CMSSM," *Phys. Lett. B* **588** (2004) 7–16, arXiv:hep-ph/0312262.

[49] K. Kohri, M. Yamaguchi, and J. Yokoyama, "Production and dilution of gravitinos by modulus decay," *Phys. Rev. D* **70** (2004) 043522, arXiv:hep-ph/0403043.

[50] R. Allahverdi, A. Jokinen, and A. Mazumdar, "Gravitino production from reheating in split supersymmetry," *Phys. Rev. D* **71** (2005) 043505, arXiv:hep-ph/0410169.

[51] E. J. Copeland and O. Seto, "Reheating and gravitino production in braneworld inflation," *Phys. Rev. D* **72** (2005) 023506, arXiv:hep-ph/0505149.

[52] R. Rangarajan and N. Sahu, "Gravitino production in an inflationary universe and implications for leptogenesis," *Mod. Phys. Lett. A* **23** (2008) 427–436, arXiv:hep-ph/0606228.

[53] S. Antusch and K. Dutta, "Non-thermal Gravitino Production in Tribrid Inflation," *Phys. Rev. D* **92** (2015) 083503, arXiv:1505.04022 [hep-ph].

[54] Y. Ema, K. Mukaida, K. Nakayama, and T. Terada, "Nonthermal Gravitino Production after Large Field Inflation," *JHEP* **11** (2016) 184, arXiv:1609.04716 [hep-ph].

[55] R. Arya, N. Mahajan, and R. Rangarajan, "Gravitino production in a thermal Universe revisited," *Phys. Lett. B* **772** (2017) 258–264, arXiv:1608.03386 [astro-ph.CO].

[56] I. Dalianis, "R-Symmetry and Gravitino Abundance," *Phys. Rev. D* **85** (2012) 061301, arXiv:1110.2072 [hep-ph].

[57] I. Dalianis, "Gravitino dark matter production at finite temperature," *JHEP* **11** (2013) 162, arXiv:1304.7673 [hep-ph].

[58] H. Fukushima and R. Kitano, "Gravitino thermal production revisited and a new cosmological scenario of gauge mediation," *JHEP* **01** (2014) 081, arXiv:1311.6228 [hep-ph].

[59] M. Badziak, I. Dalianis, and Z. Lalak, "Suppressing gravitino thermal production with a temperature-dependent messenger coupling," *JHEP* **02** (2016) 173, arXiv:1512.06795 [hep-ph].

[60] F. Hasegawa, K. Mukaida, K. Nakayama, T. Terada, and Y. Yamada, "Gravitino Problem in Minimal Supergravity Inflation," *Phys. Lett. B* **767** (2017) 392–397, arXiv:1701.03106 [hep-ph].

[61] E. W. Kolb, A. J. Long, and E. Mcdonough, "Catastrophic Production of Slow Gravitinos," arXiv:2102.10113 [hep-th].

[62] E. W. Kolb, A. J. Long, and E. Mcdonough, "The Gravitino Swampland Conjecture," arXiv:2103.10437 [hep-th].

[63] E. Dudas, M. A. G. Garcia, Y. Mambrini, K. A. Olive, M. Peloso, and S. Verner, "Slow and Safe Gravitinos," *Phys. Rev. D* **103** (2021) 123519, arXiv:2104.03749 [hep-th].

[64] T. Terada, "Minimal supergravity inflation without slow gravitino," *Phys. Rev. D* **103** no. 12, (2021) 125022, arXiv:2104.05731 [hep-th].

[65] N. Cribiori, D. Lust, and M. Scalisi, "The gravitino and the swampland," *JHEP* **06** (2021) 071, arXiv:2104.08288 [hep-th].

[66] A. Castellano, A. Font, A. Herraez, and L. E. Ibáñez, "A Gravitino Distance Conjecture," `arXiv:2104.10181 [hep-th]`.

[67] I. Antoniadis, K. Benakli, and W. Ke, "Salvage of Too Slow Gravitinos," `arXiv:2105.03784 [hep-th]`.

[68] D. Lindley, "Cosmological Constraints on the Lifetime of Massive Particles," *Astrophys. J.* **294** (1985) 1–8.

[69] D. Lindley, "Hadronic Decays of Cosmological Gravitinos," *Phys. Lett. B* **171** (1986) 235–238.

[70] J. R. Ellis, D. V. Nanopoulos, and S. Sarkar, "The Cosmology of Decaying Gravitinos," *Nucl. Phys. B* **259** (1985) 175–188.

[71] A. B. Lahanas, D. V. Nanopoulos, and V. C. Spanos, "Neutralino relic density in a universe with nonvanishing cosmological constant," *Phys. Rev. D* **62** (2000) 023515, `arXiv:hep-ph/9909497`.

[72] A. B. Lahanas, D. V. Nanopoulos, and V. C. Spanos, "Neutralino dark matter elastic scattering in a flat and accelerating universe," *Mod. Phys. Lett. A* **16** (2001) 1229–1242, `arXiv:hep-ph/0009065`.

[73] R. H. Cyburt, J. R. Ellis, B. D. Fields, and K. A. Olive, "Updated nucleosynthesis constraints on unstable relic particles," *Phys. Rev. D* **67** (2003) 103521, `arXiv:astro-ph/0211258`.

[74] K. Jedamzik, "Did something decay, evaporate, or annihilate during Big Bang nucleosynthesis?," *Phys. Rev. D* **70** (2004) 063524, `arXiv:astro-ph/0402344`.

[75] R. H. Cyburt, J. Ellis, B. D. Fields, F. Luo, K. A. Olive, and V. C. Spanos, "Gravitino Decays and the Cosmological Lithium Problem in Light of the LHC Higgs and Supersymmetry Searches," *JCAP* **05** (2013) 014, `arXiv:1303.0574 [astro-ph.CO]`.

[76] R. H. Cyburt, J. Ellis, B. D. Fields, F. Luo, K. A. Olive, and V. C. Spanos, "Nucleosynthesis Constraints on a Massive Gravitino in Neutralino Dark Matter Scenarios," *JCAP* **10** (2009) 021, `arXiv:0907.5003 [astro-ph.CO]`.

[77] N. E. Mavromatos and V. C. Spanos, "Gravitino properties in a conformal supergravity model," *Phys. Rev. D* **87** no. 3, (2013) 035025, `arXiv:1212.6386 [hep-ph]`.

[78] H. Eberl and V. C. Spanos, "GravitinoPack and decays of supersymmetric metastable particles," *Comput. Phys. Commun.* **202** (2016) 310–325, `arXiv:1509.09159 [hep-ph]`.

[79] H. Eberl and V. C. Spanos, "Three-body gravitino decays in the MSSM," *JHEP* **08** (2013) 055, `arXiv:1305.6934 [hep-ph]`.

[80] E. Braaten and R. D. Pisarski, "Soft Amplitudes in Hot Gauge Theories: A General Analysis," *Nucl. Phys. B* **337** (1990) 569–634.

[81] E. Braaten and T. C. Yuan, "Calculation of screening in a hot plasma," *Phys. Rev. Lett.* **66** (1991) 2183–2186.

[82] **Planck** Collaboration, N. Aghanim *et al.*, "Planck 2018 results. VI. Cosmological parameters," `arXiv:1807.06209 [astro-ph.CO]`.

[83] A. H. Guth, "The Inflationary Universe: A Possible Solution to the Horizon and Flatness Problems," *Phys. Rev.* **D23** (1981) 347–356.

[84] A. A. Starobinsky, "Dynamics of Phase Transition in the New Inflationary Universe Scenario and Generation of Perturbations," *Phys. Lett.* **117B** (1982) 175–178.

[85] A. D. Linde, "A New Inflationary Universe Scenario: A Possible Solution of the Horizon, Flatness, Homogeneity, Isotropy and Primordial Monopole Problems," *Phys. Lett.* **108B** (1982) 389–393.

[86] A. Albrecht and P. J. Steinhardt, "Cosmology for Grand Unified Theories with Radiatively Induced Symmetry Breaking," *Phys. Rev. Lett.* **48** (1982) 1220–1223.

[87] **Planck** Collaboration, Y. Akrami *et al.*, "Planck 2018 results. X. Constraints on inflation," `arXiv:1807.06211 [astro-ph.CO]`.

[88] A. A. Starobinsky, "A New Type of Isotropic Cosmological Models Without Singularity," *Phys. Lett.* **91B** (1980) 99–102.

[89] V. Faraoni, E. Gunzig, and P. Nardone, "Conformal transformations in classical gravitational theories and in cosmology," *Fund. Cosmic Phys.* **20** (1999) 121, `arXiv:gr-qc/9811047`.

[90] V. Faraoni, *Cosmology in scalar tensor gravity*. 2004.

[91] E. E. Flanagan, "The Conformal frame freedom in theories of gravitation," *Class. Quant. Grav.* **21** (2004) 3817, `arXiv:gr-qc/0403063`.

[92] L. Jarv, P. Kuusk, and M. Saal, "Scalar-tensor cosmology at the general relativity limit: Jordan versus Einstein frame," *Phys. Rev. D* **76** (2007) 103506, `arXiv:0705.4644 [gr-qc]`.

[93] T. Chiba and M. Yamaguchi, "Conformal-Frame (In)dependence of Cosmological Observations in Scalar-Tensor Theory," *JCAP* **10** (2013) 040, `arXiv:1308.1142 [gr-qc]`.

[94] M. Postma and M. Volponi, "Equivalence of the Einstein and Jordan frames," *Phys. Rev. D* **90** no. 10, (2014) 103516, `arXiv:1407.6874 [astro-ph.CO]`.

[95] L. Järv, P. Kuusk, M. Saal, and O. Vilson, "Invariant quantities in the scalar-tensor theories of gravitation," *Phys. Rev. D* **91** no. 2, (2015) 024041, `arXiv:1411.1947 [gr-qc]`.

[96] L. Järv, P. Kuusk, M. Saal, and O. Vilson, "Transformation properties and general relativity regime in scalar–tensor theories," *Class. Quant. Grav.* **32** (2015) 235013, `arXiv:1504.02686 [gr-qc]`.

[97] P. Kuusk, M. Rünkla, M. Saal, and O. Vilson, "Invariant slow-roll parameters in scalar–tensor theories," *Class. Quant. Grav.* **33** no. 19, (2016) 195008, `arXiv:1605.07033 [gr-qc]`.

[98] L. Järv, K. Kannike, L. Marzola, A. Racioppi, M. Raidal, M. Rünkla, M. Saal, and H. Veermäe, "Frame-Independent Classification of Single-Field Inflationary Models," *Phys. Rev. Lett.* **118** no. 15, (2017) 151302, `arXiv:1612.06863 [hep-ph]`.

[99] A. Karam, T. Pappas, and K. Tamvakis, "Frame-dependence of higher-order inflationary observables in scalar-tensor theories," *Phys. Rev. D* **96** no. 6, (2017) 064036, arXiv:1707.00984 [gr-qc].

[100] D. Burns, S. Karamitsos, and A. Pilaftsis, "Frame-Covariant Formulation of Inflation in Scalar-Curvature Theories," *Nucl. Phys.* **B907** (2016) 785–819, arXiv:1603.03730 [hep-ph].

[101] S. Karamitsos and A. Pilaftsis, "On the Cosmological Frame Problem," *PoS* **CORFU2017** (2018) 036, arXiv:1801.07151 [hep-th].

[102] L. Järv, A. Karam, A. Kozak, A. Lykkas, A. Racioppi, and M. Saal, "Equivalence of inflationary models between the metric and Palatini formulation of scalar-tensor theories," *Phys. Rev. D* **102** no. 4, (2020) 044029, arXiv:2005.14571 [gr-qc].

[103] A. Karam, S. Karamitsos, and M. Saal, "β-function reconstruction of Palatini inflationary attractors," arXiv:2103.01182 [gr-qc].

[104] M. Shaposhnikov and D. Zenhausern, "Scale invariance, unimodular gravity and dark energy," *Phys. Lett.* **B671** (2009) 187–192, arXiv:0809.3395 [hep-th].

[105] J. Garcia-Bellido, J. Rubio, M. Shaposhnikov, and D. Zenhausern, "Higgs-Dilaton Cosmology: From the Early to the Late Universe," *Phys. Rev. D* **84** (2011) 123504, arXiv:1107.2163 [hep-ph].

[106] F. Bezrukov, G. K. Karananas, J. Rubio, and M. Shaposhnikov, "Higgs-Dilaton Cosmology: an effective field theory approach," *Phys. Rev. D* **87** no. 9, (2013) 096001, arXiv:1212.4148 [hep-ph].

[107] V. V. Khoze, "Inflation and Dark Matter in the Higgs Portal of Classically Scale Invariant Standard Model," *JHEP* **1311** (2013) 215, arXiv:1308.6338 [hep-ph].

[108] T. G. Steele, Z.-W. Wang, D. Contreras, and R. B. Mann, "Viable dark matter via radiative symmetry breaking in a scalar singlet Higgs portal extension of the standard model," *Phys. Rev. Lett.* **112** no. 17, (2014) 171602, arXiv:1310.1960 [hep-ph].

[109] J. Ren, Z.-Z. Xianyu, and H.-J. He, "Higgs Gravitational Interaction, Weak Boson Scattering, and Higgs Inflation in Jordan and Einstein Frames," *JCAP* **06** (2014) 032, arXiv:1404.4627 [gr-qc].

[110] K. Kannike, A. Racioppi, and M. Raidal, "Embedding inflation into the Standard Model - more evidence for classical scale invariance," *JHEP* **1406** (2014) 154, arXiv:1405.3987 [hep-ph].

[111] C. Csaki, N. Kaloper, J. Serra, and J. Terning, "Inflation from Broken Scale Invariance," *Phys. Rev. Lett.* **113** (2014) 161302, arXiv:1406.5192 [hep-th].

[112] K. Kannike, G. Hütsi, L. Pizza, A. Racioppi, M. Raidal, *et al.*, "Dynamically Induced Planck Scale and Inflation," *JHEP* **1505** (2015) 065, arXiv:1502.01334 [astro-ph.CO].

[113] K. Kannike, A. Racioppi, and M. Raidal, "Linear inflation from quartic potential," *JHEP* **01** (2016) 035, arXiv:1509.05423 [hep-ph].

[114] Z.-W. Wang, T. G. Steele, T. Hanif, and R. B. Mann, "Conformal Complex Singlet Extension of the Standard Model: Scenario for Dark Matter and a Second Higgs Boson," *JHEP* **08** (2016) 065, arXiv:1510.04321 [hep-ph].

[115] A. Barvinsky, A. Y. Kamenshchik, and D. Nesterov, "Origin of inflation in CFT driven cosmology: R^2-gravity and non-minimally coupled inflaton models," *Eur. Phys. J. C* **75** no. 12, (2015) 584, arXiv:1510.06858 [hep-th].

[116] A. Farzinnia and S. Kouwn, "Classically scale invariant inflation, supermassive WIMPs, and adimensional gravity," *Phys. Rev. D* **93** no. 6, (2016) 063528, arXiv:1512.05890 [hep-ph].

[117] M. Rinaldi and L. Vanzo, "Inflation and reheating in theories with spontaneous scale invariance symmetry breaking," *Phys. Rev.* **D94** no. 2, (2016) 024009, arXiv:1512.07186 [gr-qc].

[118] L. Marzola, A. Racioppi, M. Raidal, F. R. Urban, and H. Veermäe, "Non-minimal CW inflation, electroweak symmetry breaking and the 750 GeV anomaly," *JHEP* **03** (2016) 190, arXiv:1512.09136 [hep-ph].

[119] N. D. Barrie, A. Kobakhidze, and S. Liang, "Natural Inflation with Hidden Scale Invariance," *Phys. Lett.* **B756** (2016) 390–393, arXiv:1602.04901 [gr-qc].

[120] P. G. Ferreira, C. T. Hill, and G. G. Ross, "Scale-Independent Inflation and Hierarchy Generation," *Submitted to: Phys. Rev. Lett.* (2016) , arXiv:1603.05983 [hep-th].

[121] K. Kannike, A. Racioppi, and M. Raidal, "Super-heavy dark matter – Towards predictive scenarios from inflation," *Nucl. Phys.* **B918** (2017) 162–177, arXiv:1605.09378 [hep-ph].

[122] L. Marzola and A. Racioppi, "Minimal but non-minimal inflation and electroweak symmetry breaking," *JCAP* **1610** no. 10, (2016) 010, arXiv:1606.06887 [hep-ph].

[123] G. K. Karananas and J. Rubio, "On the geometrical interpretation of scale-invariant models of inflation," *Phys. Lett.* **B761** (2016) 223–228, arXiv:1606.08848 [hep-ph].

[124] G. Tambalo and M. Rinaldi, "Inflation and reheating in scale-invariant scalar-tensor gravity," *Gen. Rel. Grav.* **49** no. 4, (2017) 52, arXiv:1610.06478 [gr-qc].

[125] K. Kannike, M. Raidal, C. Spethmann, and H. Veermäe, "The evolving Planck mass in classically scale-invariant theories," *JHEP* **04** (2017) 026, arXiv:1610.06571 [hep-ph].

[126] M. Artymowski and A. Racioppi, "Scalar-tensor linear inflation," *JCAP* **1704** no. 04, (2017) 007, arXiv:1610.09120 [astro-ph.CO].

[127] P. G. Ferreira, C. T. Hill, and G. G. Ross, "Weyl Current, Scale-Invariant Inflation and Planck Scale Generation," *Phys. Rev. D* **95** no. 4, (2017) 043507, arXiv:1610.09243 [hep-th].

[128] A. Salvio, "Inflationary Perturbations in No-Scale Theories," *Eur. Phys. J.* **C77** no. 4, (2017) 267, arXiv:1703.08012 [astro-ph.CO].

[129] A. Karam, T. Pappas, and K. Tamvakis, "Frame-dependence of higher-order inflationary observables in scalar-tensor theories," *Phys. Rev.* **D96** no. 6, (2017) 064036, arXiv:1707.00984 [gr-qc].

[130] K. Kaneta, O. Seto, and R. Takahashi, "Very low scale Coleman-Weinberg inflation with non-minimal coupling," *Phys. Rev.* **D97** no. 6, (2017) 063004, arXiv:1708.06455 [hep-ph].

[131] A. Karam, L. Marzola, T. Pappas, A. Racioppi, and K. Tamvakis, "Constant-Roll (Quasi-)Linear Inflation," *JCAP* **05** (2018) 011, arXiv:1711.09861 [astro-ph.CO].

[132] A. Racioppi, "New universal attractor in nonminimally coupled gravity: Linear inflation," *Phys. Rev. D* **97** no. 12, (2018) 123514, arXiv:1801.08810 [astro-ph.CO].

[133] P. G. Ferreira, C. T. Hill, J. Noller, and G. G. Ross, "Inflation in a scale invariant universe," *Phys. Rev. D* **97** no. 12, (2018) 123516, arXiv:1802.06069 [astro-ph.CO].

[134] D. Benisty and E. I. Guendelman, "Two scalar fields inflation from scale-invariant gravity with modified measure," *Class. Quant. Grav.* **36** no. 9, (2019) 095001, arXiv:1809.09866 [gr-qc].

[135] A. Barnaveli, S. Lucat, and T. Prokopec, "Inflation as a spontaneous symmetry breaking of Weyl symmetry," *JCAP* **01** (2019) 022, arXiv:1809.10586 [gr-qc].

[136] J. Kubo, M. Lindner, K. Schmitz, and M. Yamada, "Planck mass and inflation as consequences of dynamically broken scale invariance," *Phys. Rev. D* **100** no. 1, (2019) 015037, arXiv:1811.05950 [hep-ph].

[137] S. Mooij, M. Shaposhnikov, and T. Voumard, "Hidden and explicit quantum scale invariance," *Phys. Rev. D* **99** no. 8, (2019) 085013, arXiv:1812.07946 [hep-th].

[138] M. Shaposhnikov and K. Shimada, "Asymptotic Scale Invariance and its Consequences," *Phys. Rev. D* **99** no. 10, (2019) 103528, arXiv:1812.08706 [hep-ph].

[139] C. Wetterich, "Quantum scale symmetry," arXiv:1901.04741 [hep-th].

[140] S. Vicentini, L. Vanzo, and M. Rinaldi, "Scale-invariant inflation with one-loop quantum corrections," *Phys. Rev. D* **99** no. 10, (2019) 103516, arXiv:1902.04434 [gr-qc].

[141] A. Shkerin, "Dilaton-assisted generation of the Fermi scale from the Planck scale," *Phys. Rev. D* **99** no. 11, (2019) 115018, arXiv:1903.11317 [hep-th].

[142] P. G. Ferreira, C. T. Hill, J. Noller, and G. G. Ross, "Scale-independent R^2 inflation," *Phys. Rev. D* **100** no. 12, (2019) 123516, arXiv:1906.03415 [gr-qc].

[143] D. Ghilencea, "Weyl R^2 inflation with an emergent Planck scale," *JHEP* **10** (2019) 209, arXiv:1906.11572 [gr-qc].

[144] I. Oda, "Planck Scale from Broken Local Conformal Invariance in Weyl Geometry," *Adv. Stud. Theor. Phys.* **14** no. 1-4, (2020) 9–28, arXiv:1909.09889 [hep-th].

[145] A. Racioppi, "Non-Minimal (Self-)Running Inflation: Metric vs. Palatini Formulation," *JHEP* **21** (2020) 011, arXiv:1912.10038 [hep-ph].

[146] D. Benisty, E. Guendelman, E. Nissimov, and S. Pacheva, "Dynamically Generated Inflationary Lambda-CDM," *Symmetry* **12** no. 3, (2020) 481, arXiv:2002.04110 [gr-qc].

[147] D. Benisty, E. Guendelman, E. Nissimov, and S. Pacheva, "Quintessential Inflation with Dynamical Higgs Generation as an Affine Gravity," *Symmetry* **12** (2020) 734, arXiv:2003.04723 [gr-qc].

[148] Y. Tang and Y.-L. Wu, "Weyl scaling invariant R^2 gravity for inflation and dark matter," *Phys. Lett. B* **809** (2020) 135716, arXiv:2006.02811 [hep-ph].

[149] D. M. Ghilencea, "Gauging scale symmetry and inflation: Weyl versus Palatini gravity," *Eur. Phys. J. C* **81** no. 6, (2021) 510, arXiv:2007.14733 [hep-th].

[150] K. Stelle, "Renormalization of Higher Derivative Quantum Gravity," *Phys. Rev. D* **16** (1977) 953–969.

[151] T. Biswas, A. Mazumdar, and W. Siegel, "Bouncing universes in string-inspired gravity," *JCAP* **03** (2006) 009, arXiv:hep-th/0508194.

[152] A. Salvio and A. Strumia, "Agravity," *JHEP* **06** (2014) 080, arXiv:1403.4226 [hep-ph].

[153] A. Edery and Y. Nakayama, "Restricted Weyl invariance in four-dimensional curved spacetime," *Phys. Rev. D* **90** (2014) 043007, arXiv:1406.0060 [hep-th].

[154] L. Alvarez-Gaume, A. Kehagias, C. Kounnas, D. Lüst, and A. Riotto, "Aspects of Quadratic Gravity," *Fortsch. Phys.* **64** no. 2-3, (2016) 176–189, arXiv:1505.07657 [hep-th].

[155] A. Salvio, "Quadratic Gravity," *Front. in Phys.* **6** (2018) 77, arXiv:1804.09944 [hep-th].

[156] A. Edery and Y. Nakayama, "Critical gravity from four dimensional scale invariant gravity," *JHEP* **11** (2019) 169, arXiv:1908.08778 [hep-th].

[157] A. Salvio and H. Veermäe, "Horizonless ultracompact objects and dark matter in quadratic gravity," *JCAP* **02** (2020) 018, arXiv:1912.13333 [gr-qc].

[158] D. M. Ghilencea, "Palatini quadratic gravity: spontaneous breaking of gauged scale symmetry and inflation," *Eur. Phys. J. C* **80** no. 12, (4, 2020) 1147, arXiv:2003.08516 [hep-th].

[159] A. Salvio, "Dimensional Transmutation in Gravity and Cosmology," arXiv:2012.11608 [hep-th].

[160] A. Palatini, "Deduzione invariantiva delle equazioni gravitazionali dal principio di hamilton," *Rendiconti del Circolo Matematico di Palermo (1884-1940)* **43** no. 1, (Dec, 1919) 203–212.

[161] M. Ferraris, M. Francaviglia, and C. Reina, "Variational formulation of general relativity from 1915 to 1925 "palatini's method" discovered by einstein in 1925," *General Relativity and Gravitation* **14** no. 3, (Mar, 1982) 243–254.

[162] F. Bauer and D. A. Demir, "Inflation with Non-Minimal Coupling: Metric versus Palatini Formulations," *Phys. Lett. B* **665** (2008) 222–226, arXiv:0803.2664 [hep-ph].

[163] F. Bauer, "Filtering out the cosmological constant in the Palatini formalism of modified gravity," *Gen. Rel. Grav.* **43** (2011) 1733–1757, arXiv:1007.2546 [gr-qc].

[164] N. Tamanini and C. R. Contaldi, "Inflationary Perturbations in Palatini Generalised Gravity," *Phys. Rev. D* **83** (2011) 044018, arXiv:1010.0689 [gr-qc].

[165] F. Bauer and D. A. Demir, "Higgs-Palatini Inflation and Unitarity," *Phys. Lett. B* **698** (2011) 425–429, arXiv:1012.2900 [hep-ph].

[166] S. Rasanen and P. Wahlman, "Higgs inflation with loop corrections in the Palatini formulation," *JCAP* **11** (2017) 047, arXiv:1709.07853 [astro-ph.CO].

[167] T. Tenkanen, "Resurrecting Quadratic Inflation with a non-minimal coupling to gravity," *JCAP* **12** (2017) 001, arXiv:1710.02758 [astro-ph.CO].

[168] A. Racioppi, "Coleman-Weinberg linear inflation: metric vs. Palatini formulation," *JCAP* **12** (2017) 041, arXiv:1710.04853 [astro-ph.CO].

[169] T. Markkanen, T. Tenkanen, V. Vaskonen, and H. Veermäe, "Quantum corrections to quartic inflation with a non-minimal coupling: metric vs. Palatini," *JCAP* **03** (2018) 029, arXiv:1712.04874 [gr-qc].

[170] L. Järv, A. Racioppi, and T. Tenkanen, "Palatini side of inflationary attractors," *Phys. Rev. D* **97** no. 8, (2018) 083513, arXiv:1712.08471 [gr-qc].

[171] C. Fu, P. Wu, and H. Yu, "Inflationary dynamics and preheating of the nonminimally coupled inflaton field in the metric and Palatini formalisms," *Phys. Rev. D* **96** no. 10, (2017) 103542, arXiv:1801.04089 [gr-qc].

[172] A. Racioppi, "New universal attractor in nonminimally coupled gravity: Linear inflation," *Phys. Rev. D* **97** no. 12, (2018) 123514, arXiv:1801.08810 [astro-ph.CO].

[173] P. Carrilho, D. Mulryne, J. Ronayne, and T. Tenkanen, "Attractor Behaviour in Multifield Inflation," *JCAP* **06** (2018) 032, arXiv:1804.10489 [astro-ph.CO].

[174] A. Kozak and A. Borowiec, "Palatini frames in scalar–tensor theories of gravity," *Eur. Phys. J. C* **79** no. 4, (2019) 335, arXiv:1808.05598 [hep-th].

[175] S. Rasanen and E. Tomberg, "Planck scale black hole dark matter from Higgs inflation," *JCAP* **01** (2019) 038, arXiv:1810.12608 [astro-ph.CO].

[176] S. Rasanen, "Higgs inflation in the Palatini formulation with kinetic terms for the metric," *Open J. Astrophys.* **2** no. 1, (2019) , arXiv:1811.09514 [gr-qc].

[177] J. P. B. Almeida, N. Bernal, J. Rubio, and T. Tenkanen, "Hidden Inflaton Dark Matter," *JCAP* **03** (2019) 012, arXiv:1811.09640 [hep-ph].

[178] K. Shimada, K. Aoki, and K.-i. Maeda, "Metric-affine Gravity and Inflation," *Phys. Rev. D* **99** no. 10, (2019) 104020, arXiv:1812.03420 [gr-qc].

[179] T. Takahashi and T. Tenkanen, "Towards distinguishing variants of non-minimal inflation," *JCAP* **04** (2019) 035, arXiv:1812.08492 [astro-ph.CO].

[180] R. Jinno, K. Kaneta, K.-y. Oda, and S. C. Park, "Hillclimbing inflation in metric and Palatini formulations," *Phys. Lett. B* **791** (2019) 396–402, arXiv:1812.11077 [gr-qc].

[181] J. Rubio and E. S. Tomberg, "Preheating in Palatini Higgs inflation," *JCAP* **04** (2019) 021, arXiv:1902.10148 [hep-ph].

[182] N. Bostan, "Non-minimally coupled quartic inflation with Coleman-Weinberg one-loop corrections in the Palatini formulation," *Phys. Lett. B* **811** (2020) 135954, arXiv:1907.13235 [gr-qc].

[183] N. Bostan, "Quadratic, Higgs and hilltop potentials in the Palatini gravity," *Commun. Theor. Phys.* **72** (2020) 085401, arXiv:1908.09674 [astro-ph.CO].

[184] T. Tenkanen and L. Visinelli, "Axion dark matter from Higgs inflation with an intermediate H_*," *JCAP* **08** (2019) 033, arXiv:1906.11837 [astro-ph.CO].

[185] T. Tenkanen, "Tracing the high energy theory of gravity: an introduction to Palatini inflation," *Gen. Rel. Grav.* **52** no. 4, (2020) 33, arXiv:2001.10135 [astro-ph.CO].

[186] M. Shaposhnikov, A. Shkerin, and S. Zell, "Quantum Effects in Palatini Higgs Inflation," *JCAP* **07** (2020) 064, arXiv:2002.07105 [hep-ph].

[187] A. Borowiec and A. Kozak, "New class of hybrid metric-Palatini scalar-tensor theories of gravity," *JCAP* **07** (2020) 003, arXiv:2003.02741 [gr-qc].

[188] A. Karam, M. Raidal, and E. Tomberg, "Gravitational dark matter production in Palatini preheating," *JCAP* **03** (2021) 064, arXiv:2007.03484 [astro-ph.CO].

[189] J. McDonald, "Does Palatini Higgs Inflation Conserve Unitarity?," *JCAP* **04** (2021) 069, arXiv:2007.04111 [hep-ph].

[190] M. Långvik, J.-M. Ojanperä, S. Raatikainen, and S. Räsänen, "Higgs inflation with the Holst and the Nieh–Yan term," *Phys. Rev. D* **103** no. 8, (2021) 083514, arXiv:2007.12595 [astro-ph.CO].

[191] M. Shaposhnikov, A. Shkerin, I. Timiryasov, and S. Zell, "Higgs inflation in Einstein-Cartan gravity," *JCAP* **02** (2021) 008, arXiv:2007.14978 [hep-ph].

[192] M. Shaposhnikov, A. Shkerin, I. Timiryasov, and S. Zell, "Einstein-Cartan gravity, matter, and scale-invariant generalization," *JHEP* **10** (2020) 177, arXiv:2007.16158 [hep-th].

[193] Y. Mikura, Y. Tada, and S. Yokoyama, "Conformal inflation in the metric-affine geometry," *EPL* **132** no. 3, (2020) 39001, arXiv:2008.00628 [hep-th].

[194] S. Verner, "Quintessential Inflation in Palatini Gravity," arXiv:2010.11201 [gr-qc].

[195] V.-M. Enckell, S. Nurmi, S. Räsänen, and E. Tomberg, "Critical point Higgs inflation in the Palatini formulation," *JHEP* **04** (2021) 059, arXiv:2012.03660 [astro-ph.CO].

[196] Y. Reyimuaji and X. Zhang, "Natural inflation with a nonminimal coupling to gravity," *JCAP* **03** (2021) 059, arXiv:2012.14248 [astro-ph.CO].

[197] Y. Mikura, Y. Tada, and S. Yokoyama, "Minimal k-inflation in light of the conformal metric-affine geometry," *Phys. Rev. D* **103** no. 10, (2021) L101303, arXiv:2103.13045 [hep-th].

[198] M. Kubota, K.-Y. Oda, K. Shimada, and M. Yamaguchi, "Cosmological Perturbations in Palatini Formalism," *JCAP* **03** (2021) 006, arXiv:2010.07867 [hep-th].

[199] D. Sáez-Chillón Gómez, "3+1 decomposition in modified gravities within the Palatini formalism and some applications," arXiv:2103.16319 [gr-qc].

[200] G. J. Olmo, "Palatini Approach to Modified Gravity: f(R) Theories and Beyond," *Int. J. Mod. Phys. D* **20** (2011) 413–462, arXiv:1101.3864 [gr-qc].

[201] F. Bombacigno and G. Montani, "Big bounce cosmology for Palatini R^2 gravity with a Nieh–Yan term," *Eur. Phys. J. C* **79** no. 5, (2019) 405, arXiv:1809.07563 [gr-qc].

[202] V.-M. Enckell, K. Enqvist, S. Rasanen, and L.-P. Wahlman, "Inflation with R^2 term in the Palatini formalism," *JCAP* **02** (2019) 022, arXiv:1810.05536 [gr-qc].

[203] I. Antoniadis, A. Karam, A. Lykkas, and K. Tamvakis, "Palatini inflation in models with an R^2 term," *JCAP* **11** (2018) 028, arXiv:1810.10418 [gr-qc].

[204] I. Antoniadis, A. Karam, A. Lykkas, T. Pappas, and K. Tamvakis, "Rescuing Quartic and Natural Inflation in the Palatini Formalism," *JCAP* **03** (2019) 005, arXiv:1812.00847 [gr-qc].

[205] T. Tenkanen, "Minimal Higgs inflation with an R^2 term in Palatini gravity," *Phys. Rev. D* **99** no. 6, (2019) 063528, arXiv:1901.01794 [astro-ph.CO].

[206] A. Edery and Y. Nakayama, "Palatini formulation of pure R^2 gravity yields Einstein gravity with no massless scalar," *Phys. Rev. D* **99** no. 12, (2019) 124018, arXiv:1902.07876 [hep-th].

[207] M. Giovannini, "Post-inflationary phases stiffer than radiation and Palatini formulation," *Class. Quant. Grav.* **36** no. 23, (2019) 235017, arXiv:1905.06182 [gr-qc].

[208] T. Tenkanen, "Trans-Planckian censorship, inflation, and dark matter," *Phys. Rev. D* **101** no. 6, (2020) 063517, arXiv:1910.00521 [astro-ph.CO].

[209] I. Antoniadis, A. Karam, A. Lykkas, T. Pappas, and K. Tamvakis, "Single-field inflation in models with an R^2 term," *PoS* **CORFU2019** (2020) 073, arXiv:1912.12757 [gr-qc].

[210] T. Tenkanen and E. Tomberg, "Initial conditions for plateau inflation: a case study," *JCAP* **04** (2020) 050, arXiv:2002.02420 [astro-ph.CO].

[211] A. Lloyd-Stubbs and J. McDonald, "Sub-Planckian ϕ^2 inflation in the Palatini formulation of gravity with an R^2 term," *Phys. Rev. D* **101** no. 12, (2020) 123515, arXiv:2002.08324 [hep-ph].

[212] I. Antoniadis, A. Lykkas, and K. Tamvakis, "Constant-roll in the Palatini-R^2 models," *JCAP* **04** no. 04, (2020) 033, arXiv:2002.12681 [gr-qc].

[213] N. Das and S. Panda, "Inflation and Reheating in f(R,h) theory formulated in the Palatini formalism," *JCAP* **05** (2021) 019, arXiv:2005.14054 [gr-qc].

[214] S. Bekov, K. Myrzakulov, R. Myrzakulov, and D. S.-C. Gómez, "General slow-roll inflation in $f(R)$ gravity under the Palatini approach," *Symmetry* **12** no. 12, (2020) 1958, arXiv:2010.12360 [gr-qc].

[215] K. Dimopoulos and S. Sánchez López, "Quintessential inflation in Palatini $f(R)$ gravity," *Phys. Rev. D* **103** no. 4, (2021) 043533, arXiv:2012.06831 [gr-qc].

[216] D. S.-C. Gómez, "Variational principle and boundary terms in gravity à la Palatini," *Phys. Lett. B* **814** (2021) 136103, arXiv:2011.11568 [gr-qc].

[217] A. Karam, E. Tomberg, and H. Veermäe, "Tachyonic preheating in Palatini R 2 inflation," *JCAP* **06** (2021) 023, arXiv:2102.02712 [astro-ph.CO].

[218] A. Lykkas and K. Tamvakis, "Extended interactions in the Palatini-R^2 inflation," arXiv:2103.10136 [gr-qc].

[219] J. Annala, "Higgs inflation and higher-order gravity in Palatini formulation, Masters's thesis, Helsinki U. ," arXiv:2106.09438 [gr-qc].

[220] J. Annala and S. Rasanen, "Inflation with $R_{(\alpha\beta)}$ terms in the Palatini formulation," arXiv:2106.12422 [astro-ph.CO].

[221] S. P. Martin, "A Supersymmetry primer," *Adv. Ser. Direct. High Energy Phys.* **18** (1998) 1–98, arXiv:hep-ph/9709356.

[222] H. P. Nilles, "Supersymmetry, Supergravity and Particle Physics," *Phys. Rept.* **110** (1984) 1–162.

[223] E. Cremmer, S. Ferrara, C. Kounnas, and D. V. Nanopoulos, "Naturally Vanishing Cosmological Constant in N=1 Supergravity," *Phys. Lett. B* **133** (1983) 61.

[224] J. R. Ellis, C. Kounnas, and D. V. Nanopoulos, "Phenomenological SU(1,1) Supergravity," *Nucl. Phys. B* **241** (1984) 406–428.

[225] J. R. Ellis, A. B. Lahanas, D. V. Nanopoulos, and K. Tamvakis, "No-Scale Supersymmetric Standard Model," *Phys. Lett. B* **134** (1984) 429.

[226] J. R. Ellis, C. Kounnas, and D. V. Nanopoulos, "No Scale Supersymmetric Guts," *Nucl. Phys. B* **247** (1984) 373–395.

[227] A. B. Lahanas and D. V. Nanopoulos, "The Road to No Scale Supergravity," *Phys. Rept.* **145** (1987) 1.

[228] J. Ellis, D. V. Nanopoulos, and K. A. Olive, "A no-scale supergravity framework for sub-Planckian physics," *Phys. Rev. D* **89** no. 4, (2014) 043502, arXiv:1310.4770 [hep-ph].

[229] J. Ellis, M. A. G. Garcia, D. V. Nanopoulos, and K. A. Olive, "Phenomenological Aspects of No-Scale Inflation Models," *JCAP* **10** (2015) 003, arXiv:1503.08867 [hep-ph].

[230] J. Ellis, M. A. G. Garcia, N. Nagata, D. V. Nanopoulos, and K. A. Olive, "Starobinsky-Like Inflation and Neutrino Masses in a No-Scale SO(10) Model," *JCAP* **11** (2016) 018, arXiv:1609.05849 [hep-ph].

[231] J. Ellis, M. A. G. Garcia, N. Nagata, D. V. Nanopoulos, and K. A. Olive, "Starobinsky-like Inflation, Supercosmology and Neutrino Masses in No-Scale Flipped SU(5)," *JCAP* **07** (2017) 006, arXiv:1704.07331 [hep-ph].

[232] E. Dudas, T. Gherghetta, Y. Mambrini, and K. A. Olive, "Inflation and High-Scale Supersymmetry with an EeV Gravitino," *Phys. Rev. D* **96** no. 11, (2017) 115032, arXiv:1710.07341 [hep-ph].

[233] J. Ellis, M. A. G. Garcia, N. Nagata, D. V. Nanopoulos, and K. A. Olive, "Symmetry Breaking and Reheating after Inflation in No-Scale Flipped SU(5)," *JCAP* **04** (2019) 009, arXiv:1812.08184 [hep-ph].

[234] S. F. King and E. Perdomo, "Starobinsky-like inflation and soft-SUSY breaking," *JHEP* **05** (2019) 211, arXiv:1903.08448 [hep-ph].

[235] J. Ellis, M. A. G. Garcia, N. Nagata, D. V. Nanopoulos, and K. A. Olive, "Cosmology with a master coupling in flipped SU(5) $\times$ U(1): the λ_6 universe," *Phys. Lett. B* **797** (2019) 134864, arXiv:1906.08483 [hep-ph].

[236] J. Ellis, M. A. G. Garcia, N. Nagata, D. V. Nanopoulos, and K. A. Olive, "Superstring-Inspired Particle Cosmology: Inflation, Neutrino Masses, Leptogenesis, Dark Matter & the SUSY Scale," *JCAP* **01** (2020) 035, arXiv:1910.11755 [hep-ph].

[237] J. Ellis, D. V. Nanopoulos, K. A. Olive, and S. Verner, "Phenomenology and Cosmology of No-Scale Attractor Models of Inflation," *JCAP* **08** (2020) 037, arXiv:2004.00643 [hep-ph].

[238] J. Ellis, D. V. Nanopoulos, K. A. Olive, and S. Verner, "Non-Oscillatory No-Scale Inflation," *JCAP* **03** (2021) 052, arXiv:2008.09099 [hep-ph].

[239] J. Ellis, M. A. G. Garcia, N. Nagata, N. D. V., K. A. Olive, and S. Verner, "Building models of inflation in no-scale supergravity," *Int. J. Mod. Phys. D* **29** no. 16, (2020) 2030011, arXiv:2009.01709 [hep-ph].

[240] J. Ellis, D. V. Nanopoulos, and K. A. Olive, "No-Scale Supergravity Realization of the Starobinsky Model of Inflation," *Phys. Rev. Lett.* **111** (2013) 111301, arXiv:1305.1247 [hep-th]. [Erratum: Phys.Rev.Lett. 111, 129902 (2013)].

[241] J. Ellis, D. V. Nanopoulos, and K. A. Olive, "Starobinsky-like Inflationary Models as Avatars of No-Scale Supergravity," *JCAP* **10** (2013) 009, arXiv:1307.3537 [hep-th].

[242] R. Kallosh and A. Linde, "Superconformal generalizations of the Starobinsky model," *JCAP* **06** (2013) 028, arXiv:1306.3214 [hep-th].

[243] F. Farakos, A. Kehagias, and A. Riotto, "On the Starobinsky Model of Inflation from Supergravity," *Nucl. Phys. B* **876** (2013) 187–200, arXiv:1307.1137 [hep-th].

[244] S. Ferrara, A. Kehagias, and A. Riotto, "The Imaginary Starobinsky Model," *Fortsch. Phys.* **62** (2014) 573–583, arXiv:1403.5531 [hep-th].

[245] S. Ferrara, A. Kehagias, and A. Riotto, "The Imaginary Starobinsky Model and Higher Curvature Corrections," *Fortsch. Phys.* **63** (2015) 2–11, arXiv:1405.2353 [hep-th].

[246] R. Kallosh, A. Linde, B. Vercnocke, and W. Chemissany, "Is Imaginary Starobinsky Model Real?," *JCAP* **07** (2014) 053, arXiv:1403.7189 [hep-th].

[247] K. Hamaguchi, T. Moroi, and T. Terada, "Complexified Starobinsky Inflation in Supergravity in the Light of Recent BICEP2 Result," *Phys. Lett. B* **733** (2014) 305–308, arXiv:1403.7521 [hep-ph].

[248] J. Ellis, M. A. G. García, D. V. Nanopoulos, and K. A. Olive, "Resurrecting Quadratic Inflation in No-Scale Supergravity in Light of BICEP2," *JCAP* **05** (2014) 037, arXiv:1403.7518 [hep-ph].

[249] J. Ellis, M. A. G. Garcia, D. V. Nanopoulos, and K. A. Olive, "A No-Scale Inflationary Model to Fit Them All," *JCAP* **08** (2014) 044, arXiv:1405.0271 [hep-ph].

[250] A. B. Lahanas and K. Tamvakis, "Inflation in no-scale supergravity," *Phys. Rev. D* **91** no. 8, (2015) 085001, arXiv:1501.06547 [hep-th].

[251] M. C. Romao and S. F. King, "Starobinsky-like inflation in no-scale supergravity Wess-Zumino model with Polonyi term," *JHEP* **07** (2017) 033, arXiv:1703.08333 [hep-ph].

[252] J. Ellis, D. V. Nanopoulos, and K. A. Olive, "From R^2 gravity to no-scale supergravity," *Phys. Rev. D* **97** no. 4, (2018) 043530, arXiv:1711.11051 [hep-th].

[253] S. Ferrara, R. Kallosh, A. Linde, and M. Porrati, "Minimal Supergravity Models of Inflation," *Phys. Rev. D* **88** no. 8, (2013) 085038, arXiv:1307.7696 [hep-th].

[254] C. Pallis, "Induced-Gravity Inflation in no-Scale Supergravity and Beyond," *JCAP* **08** (2014) 057, arXiv:1403.5486 [hep-ph].

[255] J. Ellis, M. A. G. García, D. V. Nanopoulos, and K. A. Olive, "Two-Field Analysis of No-Scale Supergravity Inflation," *JCAP* **01** (2015) 010, arXiv:1409.8197 [hep-ph].

[256] G. A. Diamandis, B. C. Georgalas, K. Kaskavelis, P. Kouroumalou, A. B. Lahanas, and G. Pavlopoulos, "Inflation in R^2 supergravity with non-minimal superpotentials," *Phys. Lett. B* **744** (2015) 74–81, arXiv:1411.5785 [hep-th].

[257] T. Terada, Y. Watanabe, Y. Yamada, and J. Yokoyama, "Reheating processes after Starobinsky inflation in old-minimal supergravity," *JHEP* **02** (2015) 105, arXiv:1411.6746 [hep-ph].

[258] W. Buchmuller, E. Dudas, L. Heurtier, A. Westphal, C. Wieck, and M. W. Winkler, "Challenges for Large-Field Inflation and Moduli Stabilization," *JHEP* **04** (2015) 058, arXiv:1501.05812 [hep-th].

[259] I. Dalianis and F. Farakos, "On the initial conditions for inflation with plateau potentials: the $R + R^2$ (super)gravity case," *JCAP* **07** (2015) 044, arXiv:1502.01246 [gr-qc].

[260] I. Garg and S. Mohanty, "No scale SUGRA SO(10) derived Starobinsky Model of Inflation," *Phys. Lett. B* **751** (2015) 7–11, arXiv:1504.07725 [hep-ph].

[261] J. Ellis, M. A. G. Garcia, D. V. Nanopoulos, and K. A. Olive, "Calculations of Inflaton Decays and Reheating: with Applications to No-Scale Inflation Models," *JCAP* **07** (2015) 050, arXiv:1505.06986 [hep-ph].

[262] E. Dudas and C. Wieck, "Moduli backreaction and supersymmetry breaking in string-inspired inflation models," *JHEP* **10** (2015) 062, arXiv:1506.01253 [hep-th].

[263] S. Ferrara, A. Kehagias, and M. Porrati, "$\mathcal{R}^2$ Supergravity," *JHEP* **08** (2015) 001, arXiv:1506.01566 [hep-th].

[264] J. Ellis, M. A. G. Garcia, D. V. Nanopoulos, and K. A. Olive, "No-Scale Inflation," *Class. Quant. Grav.* **33** no. 9, (2016) 094001, arXiv:1507.02308 [hep-ph].

[265] A. Addazi and M. Y. Khlopov, "Dark matter and inflation in $R + \zeta R^2$ supergravity," *Phys. Lett. B* **766** (2017) 17–22, arXiv:1612.06417 [gr-qc].

[266] C. Pallis and N. Toumbas, "Starobinsky Inflation: From Non-SUSY To SUGRA Realizations," *Adv. High Energy Phys.* **2017** (2017) 6759267, arXiv:1612.09202 [hep-ph].

[267] G. D. Diamandis, A. B. Lahanas, and K. Tamvakis, "Towards a formulation of $f(R)$ supergravity," *Phys. Rev. D* **92** no. 10, (2015) 105023, arXiv:1509.01065 [hep-th].

[268] G. A. Diamandis, B. C. Georgalas, K. Kaskavelis, A. B. Lahanas, and G. Pavlopoulos, "Deforming the Starobinsky model in ghost-free higher derivative supergravities," *Phys. Rev. D* **96** no. 4, (2017) 044033, arXiv:1704.07617 [hep-th].

[269] I. Garg and S. Mohanty, "No-scale SUGRA Inflation and Type-I seesaw," *Int. J. Mod. Phys. A* **33** no. 21, (2018) 1850127, arXiv:1711.01979 [hep-ph].

[270] W. Ahmed and A. Karozas, "Inflation from a no-scale supersymmetric $SU(4)_c \times SU(2)_L \times SU(2)_R$ model," *Phys. Rev. D* **98** no. 2, (2018) 023538, arXiv:1804.04822 [hep-ph].

[271] S. Khalil, A. Moursy, A. K. Saha, and A. Sil, "$U(1)_R$ inspired inflation model in no-scale supergravity," *Phys. Rev. D* **99** no. 9, (2019) 095022, arXiv:1810.06408 [hep-ph].

[272] J. Ellis, D. V. Nanopoulos, K. A. Olive, and S. Verner, "A general classification of Starobinsky-like inflationary avatars of SU(2,1)/SU(2) × U(1) no-scale supergravity," *JHEP* **03** (2019) 099, arXiv:1812.02192 [hep-th].

[273] J. Ellis, D. V. Nanopoulos, K. A. Olive, and S. Verner, "Unified no-scale model of modulus fixing, inflation, supersymmetry breaking, and dark energy," *Phys. Rev. D* **100** no. 2, (2019) 025009, arXiv:1903.05267 [hep-ph].

[274] G. A. Diamandis, B. C. Georgalas, K. Kaskavelis, and G. Pavlopoulos, "Multi-field inflation from a higher derivative N = 1 Supergravity model," arXiv:2010.14917 [hep-th].

[275] D. V. Nanopoulos, V. C. Spanos, and I. D. Stamou, "Primordial Black Holes from No-Scale Supergravity," *Phys. Rev. D* **102** no. 8, (2020) 083536, arXiv:2008.01457 [astro-ph.CO].

[276] S. Weinberg, "Implications of dynamical symmetry breaking," *Phys. Rev. D* **13** (1976) 974–996. [Addendum: Phys.Rev.D 19, 1277–1280 (1979)].

[277] E. Gildener, "Radiatively Induced Spontaneous Symmetry Breaking for Asymptotically Free Gauge Theories," *Phys.Rev.* **D13** (1976) 1025.

[278] L. Susskind, "Dynamics of Spontaneous Symmetry Breaking in the Weinberg-Salam Theory," *Phys. Rev.* **D20** (1979) 2619–2625.

[279] **ATLAS** Collaboration, G. Aad *et al.*, "Observation of a new particle in the search for the Standard Model Higgs boson with the ATLAS detector at the LHC," *Phys.Lett.* **B716** (2012) 1–29, arXiv:1207.7214 [hep-ex].

[280] **CMS** Collaboration, S. Chatrchyan *et al.*, "Observation of a new boson at a mass of 125 GeV with the CMS experiment at the LHC," *Phys.Lett.* **B716** (2012) 30–61, arXiv:1207.7235 [hep-ex].

[281] S. Dimopoulos and S. Raby, "Supercolor," *Nucl. Phys. B* **192** (1981) 353–368.

[282] E. Witten, "Dynamical breaking of supersymmetry," *Nucl. Phys. B* **188** (1981) 513.

[283] M. Dine, W. Fischler, and M. Srednicki, "Supersymmetric technicolor," *Nucl. Phys. B* **189** (1981) 575–593.

[284] S. Dimopoulos and H. Georgi, "Softly broken supersymmetry and su(5)," *Nucl. Phys. B* **193** (1981) 150–162.

[285] N. Sakai, "Naturalness in supersymmetric guts," *Z. Phys. C* **11** (1981) 153.

[286] H. Georgi, H. R. Quinn, and S. Weinberg, "Hierarchy of interactions in unified gauge theories," *Phys. Rev. Lett.* **33** (1974) 451–454.

[287] J. R. Ellis, S. Kelley, and D. V. Nanopoulos, "Probing the desert using gauge coupling unification," *Phys. Lett. B* **260** (1991) 131–137.

[288] U. Amaldi, W. de Boer, and H. Furstenau, "Comparison of grand unified theories with electroweak and strong coupling constants measured at lep," *Phys. Lett. B* **260** (1991) 447–455.

[289] P. Langacker and M.-x. Luo, "Implications of precision electroweak experiments for m_t, ρ_0, $\sin^2\theta_w$ and grand unification," *Phys. Rev. D* **44** (1991) 817–822.

[290] C. Giunti, C. W. Kim, and U. W. Lee, "Running coupling constants and grand unification models," *Mod. Phys. Lett. A* **6** (1991) 1745–1755.

[291] G. G. Ross and R. G. Roberts, "Minimal supersymmetric unification predictions," *Nucl. Phys. B* **377** (1992) 571–592.

[292] J. Wess and J. Bagger, *Supersymmetry and supergravity.* Princeton University Press, Princeton, NJ, USA, 1992.

[293] S. Deser and B. Zumino, "Broken Supersymmetry and Supergravity," *Phys. Rev. Lett.* **38** (1977) 1433–1436.

[294] E. Cremmer, B. Julia, J. Scherk, P. van Nieuwenhuizen, S. Ferrara, and L. Girardello, "Super-higgs effect in supergravity with general scalar interactions," *Phys. Lett. B* **79** (1978) 231–234.

[295] W. Rarita and J. Schwinger, "On a theory of particles with half integral spin," *Phys. Rev.* **60** (1941) 61.

[296] A. Denner, H. Eck, O. Hahn, and J. Kublbeck, "Feynman rules for fermion number violating interactions," *Nucl. Phys. B* **387** (1992) 467–481.

[297] H. Eberl, *Strahlungskorrekturen im minimalen supersymmetrischen Standardmodell.* PhD thesis, TU Vienna, 1998.

[298] R. Casalbuoni, S. De Curtis, D. Dominici, F. Feruglio, and R. Gatto, "A GRAVITINO - GOLDSTINO HIGH-ENERGY EQUIVALENCE THEOREM," *Phys. Lett. B* **215** (1988) 313–316.

[299] T. Lee and G.-H. Wu, "Interactions of a single goldstino," *Phys. Lett. B* **447** (1999) 83–88, arXiv:hep-ph/9805512.

[300] M. L. Bellac, *Thermal Field Theory*. Cambridge Monographs on Mathematical Physics. Cambridge University Press, 2011.

[301] H. Weldon, "Effective Fermion Masses of Order gT in High Temperature Gauge Theories with Exact Chiral Invariance," *Phys. Rev. D* **26** (1982) 2789.

[302] A. Das, A. Bandyopadhyay, P. K. Roy, and M. G. Mustafa, "General structure of fermion two-point function and its spectral representation in a hot magnetized medium," *Phys. Rev. D* **97** no. 3, (2018) 034024, arXiv:1709.08365 [hep-ph].

[303] A. Peshier, K. Schertler, and M. H. Thoma, "One loop selfenergies at finite temperature," *Annals Phys.* **266** (1998) 162–177, arXiv:hep-ph/9708434.

[304] J. Kapusta and C. Gale, *Finite-temperature field theory: Principles and applications*. Cambridge Monographs on Mathematical Physics. Cambridge University Press, 2011.

[305] M. H. Thoma, "Applications of high temperature field theory to heavy ion collisions," arXiv:hep-ph/9503400.

[306] T. Hahn, "CUBA: A Library for multidimensional numerical integration," *Comput. Phys. Commun.* **168** (2005) 78–95, arXiv:hep-ph/0404043.

[307] H. Weldon, "Covariant Calculations at Finite Temperature: The Relativistic Plasma," *Phys. Rev. D* **26** (1982) 1394.

[308] H. Weldon, "Dynamical Holes in the Quark - Gluon Plasma," *Phys. Rev. D* **40** (1989) 2410.

[309] H. Weldon, "Structure of the gluon propagator at finite temperature," *Annals Phys.* **271** (1999) 141–156, arXiv:hep-ph/9701279.

[310] H. Weldon, "Structure of the quark propagator at high temperature," *Phys. Rev. D* **61** (2000) 036003, arXiv:hep-ph/9908204.

[311] E. W. Kolb and M. S. Turner, *The Early Universe*, vol. 69. 1990.

[312] M. A. G. Garcia, Y. Mambrini, K. A. Olive, and M. Peloso, "Enhancement of the Dark Matter Abundance Before Reheating: Applications to Gravitino Dark Matter," *Phys. Rev. D* **96** no. 10, (2017) 103510, arXiv:1709.01549 [hep-ph].

[313] **ATLAS** Collaboration, M. Aaboud *et al.*, "Search for supersymmetry in final states with missing transverse momentum and multiple b-jets in proton-proton collisions at $\sqrt{s}$ = 13 tev with the atlas detector," *JHEP* **06** (2018) 107, arXiv:1711.01901 [hep-ex].

[314] **CMS** Collaboration, A. M. Sirunyan *et al.*, "Search for supersymmetry in proton-proton collisions at 13 TeV in final states with jets and missing transverse momentum," *JHEP* **10** (2019) 244, arXiv:1908.04722 [hep-ex].

[315] A. R. Liddle and S. M. Leach, "How long before the end of inflation were observable perturbations produced?," *Phys. Rev. D* **68** (2003) 103503, arXiv:astro-ph/0305263.

[316] R. Allahverdi, R. Brandenberger, F.-Y. Cyr-Racine, and A. Mazumdar, "Reheating in Inflationary Cosmology: Theory and Applications," *Ann. Rev. Nucl. Part. Sci.* **60** (2010) 27–51, `arXiv:1001.2600 [hep-th]`.

[317] D. I. Podolsky, G. N. Felder, L. Kofman, and M. Peloso, "Equation of state and beginning of thermalization after preheating," `hep-ph/0507096v1`.

[318] J. Martin and C. Ringeval, "First CMB Constraints on the Inflationary Reheating Temperature," *Phys. Rev. D* **82** (2010) 023511, `arXiv:1004.5525 [astro-ph.CO]`.

[319] P. Adshead, R. Easther, J. Pritchard, and A. Loeb, "Inflation and the Scale Dependent Spectral Index: Prospects and Strategies," *JCAP* **02** (2011) 021, `arXiv:1007.3748 [astro-ph.CO]`.

[320] J. Mielczarek, "Reheating temperature from the CMB," *Phys. Rev. D* **83** (2011) 023502, `arXiv:1009.2359 [astro-ph.CO]`.

[321] R. Easther and H. V. Peiris, "Bayesian Analysis of Inflation II: Model Selection and Constraints on Reheating," *Phys. Rev. D* **85** (2012) 103533, `arXiv:1112.0326 [astro-ph.CO]`.

[322] L. Dai, M. Kamionkowski, and J. Wang, "Reheating constraints to inflationary models," *Phys. Rev. Lett.* **113** (2014) 041302, `arXiv:1404.6704 [astro-ph.CO]`.

[323] J. B. Munoz and M. Kamionkowski, "Equation-of-State Parameter for Reheating," *Phys. Rev.* **D91** no. 4, (2015) 043521, `arXiv:1412.0656 [astro-ph.CO]`.

[324] J. L. Cook, E. Dimastrogiovanni, D. A. Easson, and L. M. Krauss, "Reheating predictions in single field inflation," *JCAP* **04** (2015) 047, `arXiv:1502.04673 [astro-ph.CO]`.

[325] J.-O. Gong, S. Pi, and G. Leung, "Probing reheating with primordial spectrum," *JCAP* **05** (2015) 027, `arXiv:1501.03604 [hep-ph]`.

[326] T. Rehagen and G. B. Gelmini, "Low reheating temperatures in monomial and binomial inflationary potentials," *JCAP* **06** (2015) 039, `arXiv:1504.03768 [hep-ph]`.

[327] K. D. Lozanov and M. A. Amin, "Self-resonance after inflation: oscillons, transients and radiation domination," *Phys. Rev. D* **97** no. 2, (2018) 023533, `arXiv:1710.06851 [astro-ph.CO]`.

[328] K. D. Lozanov and M. A. Amin, "Equation of State and Duration to Radiation Domination after Inflation," *Phys. Rev. Lett.* **119** no. 6, (2017) 061301, `arXiv:1608.01213 [astro-ph.CO]`.

[329] M. Kawasaki, K. Kohri, and N. Sugiyama, "Cosmological constraints on late time entropy production," *Phys. Rev. Lett.* **82** (1999) 4168, `arXiv:astro-ph/9811437`.

[330] T. Hasegawa, N. Hiroshima, K. Kohri, R. S. Hansen, T. Tram, and S. Hannestad, "MeV-scale reheating temperature and thermalization of oscillating neutrinos by radiative and hadronic decays of massive particles," *JCAP* **12** no. 12, (2019) 012, `arXiv:1908.10189 [hep-ph]`.

[331] F. Lucchin and S. Matarrese, "Power Law Inflation," *Phys. Rev. D* **32** (1985) 1316.

[332] E. D. Stewart and D. H. Lyth, "A More accurate analytic calculation of the spectrum of cosmological perturbations produced during inflation," *Phys. Lett. B* **302** (1993) 171–175, arXiv:gr-qc/9302019.

[333] J.-O. Gong and E. D. Stewart, "The Density perturbation power spectrum to second order corrections in the slow roll expansion," *Phys. Lett. B* **510** (2001) 1–9, arXiv:astro-ph/0101225.

[334] D. J. Schwarz, C. A. Terrero-Escalante, and A. A. Garcia, "Higher order corrections to primordial spectra from cosmological inflation," *Phys. Lett. B* **517** (2001) 243–249, arXiv:astro-ph/0106020.

[335] J. Martin and D. J. Schwarz, "WKB approximation for inflationary cosmological perturbations," *Phys. Rev. D* **67** (2003) 083512, arXiv:astro-ph/0210090.

[336] S. Habib, K. Heitmann, G. Jungman, and C. Molina-Paris, "The Inflationary perturbation spectrum," *Phys. Rev. Lett.* **89** (2002) 281301, arXiv:astro-ph/0208443.

[337] S. M. Leach, A. R. Liddle, J. Martin, and D. J. Schwarz, "Cosmological parameter estimation and the inflationary cosmology," *Phys. Rev. D* **66** (2002) 023515, arXiv:astro-ph/0202094.

[338] S. Habib, A. Heinen, K. Heitmann, G. Jungman, and C. Molina-Paris, "Characterizing inflationary perturbations: The Uniform approximation," *Phys. Rev. D* **70** (2004) 083507, arXiv:astro-ph/0406134.

[339] R. Casadio, F. Finelli, M. Luzzi, and G. Venturi, "Improved WKB analysis of cosmological perturbations," *Phys. Rev. D* **71** (2005) 043517, arXiv:gr-qc/0410092.

[340] H. Wei, R.-G. Cai, and A. Wang, "Second-order corrections to the power spectrum in the slow-roll expansion with a time-dependent sound speed," *Phys. Lett. B* **603** (2004) 95–106, arXiv:hep-th/0409130.

[341] R. Casadio, F. Finelli, M. Luzzi, and G. Venturi, "Higher order slow-roll predictions for inflation," *Phys. Lett. B* **625** (2005) 1–6, arXiv:gr-qc/0506043.

[342] W. H. Kinney and K. Tzirakis, "Quantum modes in DBI inflation: exact solutions and constraints from vacuum selection," *Phys. Rev. D* **77** (2008) 103517, arXiv:0712.2043 [astro-ph].

[343] L. Lorenz, J. Martin, and C. Ringeval, "Constraints on Kinetically Modified Inflation from WMAP5," *Phys. Rev. D* **78** (2008) 063543, arXiv:0807.2414 [astro-ph].

[344] L. Lorenz, J. Martin, and C. Ringeval, "K-inflationary Power Spectra in the Uniform Approximation," *Phys. Rev. D* **78** (2008) 083513, arXiv:0807.3037 [astro-ph].

[345] N. Agarwal and R. Bean, "Cosmological constraints on general, single field inflation," *Phys. Rev. D* **79** (2009) 023503, arXiv:0809.2798 [astro-ph].

[346] J. Martin, C. Ringeval, and V. Vennin, "K-inflationary Power Spectra at Second Order," *JCAP* **06** (2013) 021, arXiv:1303.2120 [astro-ph.CO].

[347] J. Beltran Jimenez, M. Musso, and C. Ringeval, "Exact Mapping between Tensor and Most General Scalar Power Spectra," *Phys. Rev.* **D88** (2013) 043524, arXiv:1303.2788 [astro-ph.CO].

[348] A. L. Alinea, T. Kubota, and W. Naylor, "Logarithmic divergences in the k-inflationary power spectra computed through the uniform approximation," *JCAP* **02** (2016) 028, arXiv:1506.08344 [gr-qc].

[349] A. A. Starobinsky, "A New Type of Isotropic Cosmological Models Without Singularity," *Adv. Ser. Astrophys. Cosmol.* **3** (1987) 130–133.

[350] V. F. Mukhanov and G. V. Chibisov, "Quantum Fluctuations and a Nonsingular Universe," *JETP Lett.* **33** (1981) 532–535.

[351] A. A. Starobinsky, "The Perturbation Spectrum Evolving from a Nonsingular Initially De-Sitter Cosmology and the Microwave Background Anisotropy," *Sov. Astron. Lett.* **9** (1983) 302.

[352] T. P. Sotiriou and V. Faraoni, "f(R) Theories Of Gravity," *Rev. Mod. Phys.* **82** (2010) 451–497, arXiv:0805.1726 [gr-qc].

[353] T. Koivisto and H. Kurki-Suonio, "Cosmological perturbations in the palatini formulation of modified gravity," *Class. Quant. Grav.* **23** (2006) 2355–2369, arXiv:astro-ph/0509422.

[354] K. Enqvist, T. Koivisto, and G. Rigopoulos, "Non-metric chaotic inflation," *JCAP* **05** (2012) 023, arXiv:1107.3739 [astro-ph.CO].

[355] A. Borowiec, M. Kamionka, A. Kurek, and M. Szydlowski, "Cosmic acceleration from modified gravity with Palatini formalism," *JCAP* **02** (2012) 027, arXiv:1109.3420 [gr-qc].

[356] A. Stachowski, M. Szydł owski, and A. Borowiec, "Starobinsky cosmological model in Palatini formalism," *Eur. Phys. J. C* **77** no. 6, (2017) 406, arXiv:1608.03196 [gr-qc].

[357] V.-M. Enckell, K. Enqvist, S. Rasanen, and E. Tomberg, "Higgs inflation at the hilltop," *JCAP* **06** (2018) 005, arXiv:1802.09299 [astro-ph.CO].

[358] K. Kannike, A. Kubarski, L. Marzola, and A. Racioppi, "A minimal model of inflation and dark radiation," *Phys. Lett. B* **792** (2019) 74–80, arXiv:1810.12689 [hep-ph].

[359] J. Wu, G. Li, T. Harko, and S.-D. Liang, "Palatini formulation of $f(R,T)$ gravity theory, and its cosmological implications," *Eur. Phys. J. C* **78** no. 5, (2018) 430, arXiv:1805.07419 [gr-qc].

[360] R. Jinno, M. Kubota, K.-y. Oda, and S. C. Park, "Higgs inflation in metric and Palatini formalisms: Required suppression of higher dimensional operators," *JCAP* **03** (2020) 063, arXiv:1904.05699 [hep-ph].

[361] C. Armendariz-Picon, T. Damour, and V. F. Mukhanov, "k - inflation," *Phys. Lett. B* **458** (1999) 209–218, arXiv:hep-th/9904075.

[362] J. Garriga and V. F. Mukhanov, "Perturbations in k-inflation," *Phys. Lett. B* **458** (1999) 219–225, arXiv:hep-th/9904176.

[363] S. Li and A. R. Liddle, "Observational constraints on K-inflation models," *JCAP* **10** (2012) 011, arXiv:1204.6214 [astro-ph.CO].

[364] J. J. M. Carrasco, R. Kallosh, and A. Linde, "Cosmological Attractors and Initial Conditions for Inflation," *Phys. Rev. D* **92** no. 6, (2015) 063519, arXiv:1506.00936 [hep-th].

[365] F. L. Bezrukov and M. Shaposhnikov, "The Standard Model Higgs boson as the inflaton," *Phys. Lett.* **B659** (2008) 703–706, arXiv:0710.3755 [hep-th].

[366] F. L. Bezrukov, A. Magnin, and M. Shaposhnikov, "Standard Model Higgs boson mass from inflation," *Phys. Lett.* **B675** (2009) 88–92, arXiv:0812.4950 [hep-ph].

[367] J. L. F. Barbon and J. R. Espinosa, "On the Naturalness of Higgs Inflation," *Phys. Rev.* **D79** (2009) 081302, arXiv:0903.0355 [hep-ph].

[368] A. O. Barvinsky, A. Yu. Kamenshchik, C. Kiefer, A. A. Starobinsky, and C. Steinwachs, "Asymptotic freedom in inflationary cosmology with a non-minimally coupled Higgs field," *JCAP* **0912** (2009) 003, arXiv:0904.1698 [hep-ph].

[369] A. O. Barvinsky, A. Y. Kamenshchik, C. Kiefer, A. A. Starobinsky, and C. F. Steinwachs, "Higgs boson, renormalization group, and naturalness in cosmology," *Eur. Phys. J. C* **72** (2012) 2219, arXiv:0910.1041 [hep-ph].

[370] C. Germani and A. Kehagias, "New Model of Inflation with Non-minimal Derivative Coupling of Standard Model Higgs Boson to Gravity," *Phys. Rev. Lett.* **105** (2010) 011302, arXiv:1003.2635 [hep-ph].

[371] C. Germani and A. Kehagias, "Cosmological Perturbations in the New Higgs Inflation," *JCAP* **05** (2010) 019, arXiv:1003.4285 [astro-ph.CO]. [Erratum: JCAP 06, E01 (2010)].

[372] R. N. Lerner and J. McDonald, "A Unitarity-Conserving Higgs Inflation Model," *Phys. Rev.* **D82** (2010) 103525, arXiv:1005.2978 [hep-ph].

[373] F. Bezrukov, A. Magnin, M. Shaposhnikov, and S. Sibiryakov, "Higgs inflation: consistency and generalisations," *JHEP* **01** (2011) 016, arXiv:1008.5157 [hep-ph].

[374] K. Kamada, T. Kobayashi, M. Yamaguchi, and J. Yokoyama, "Higgs G-inflation," *Phys. Rev. D* **83** (2011) 083515, arXiv:1012.4238 [astro-ph.CO].

[375] K. Kamada, T. Kobayashi, T. Takahashi, M. Yamaguchi, and J. Yokoyama, "Generalized Higgs inflation," *Phys. Rev.* **D86** (2012) 023504, arXiv:1203.4059 [hep-ph].

[376] F. Bezrukov, "The Higgs field as an inflaton," *Class. Quant. Grav.* **30** (2013) 214001, arXiv:1307.0708 [hep-ph].

[377] K. Allison, "Higgs xi-inflation for the 125-126 GeV Higgs: a two-loop analysis," *JHEP* **02** (2014) 040, arXiv:1306.6931 [hep-ph].

[378] F. Bezrukov and M. Shaposhnikov, "Higgs inflation at the critical point," *Phys. Lett.* **B734** (2014) 249–254, arXiv:1403.6078 [hep-ph].

[379] Y. Hamada, H. Kawai, K.-y. Oda, and S. C. Park, "Higgs inflation from Standard Model criticality," *Phys. Rev.* **D91** (2015) 053008, arXiv:1408.4864 [hep-ph].

[380] A. Salvio and A. Mazumdar, "Classical and Quantum Initial Conditions for Higgs Inflation," *Phys. Lett.* **B750** (2015) 194–200, arXiv:1506.07520 [hep-ph].

[381] X. Calmet and I. Kuntz, "Higgs Starobinsky Inflation," *Eur. Phys. J.* **C76** no. 5, (2016) 289, arXiv:1605.02236 [hep-th].

[382] R. Jinno, K. Kaneta, and K.-y. Oda, "Hill-climbing Higgs inflation," *Phys. Rev. D* **97** no. 2, (2018) 023523, arXiv:1705.03696 [hep-ph].

[383] F. Bezrukov, M. Pauly, and J. Rubio, "On the robustness of the primordial power spectrum in renormalized Higgs inflation," *JCAP* **02** (2018) 040, arXiv:1706.05007 [hep-ph].

[384] M. He, A. A. Starobinsky, and J. Yokoyama, "Inflation in the mixed Higgs-R^2 model," *JCAP* **05** (2018) 064, arXiv:1804.00409 [astro-ph.CO].

[385] A. Gundhi and C. F. Steinwachs, "Scalaron-Higgs inflation," *Nucl. Phys. B* **954** (2020) 114989, arXiv:1810.10546 [hep-th].

[386] J. Rubio, "Higgs inflation," *Front. Astron. Space Sci.* **5** (2019) 50, arXiv:1807.02376 [hep-ph].

[387] M. He, R. Jinno, K. Kamada, S. C. Park, A. A. Starobinsky, and J. Yokoyama, "On the violent preheating in the mixed Higgs-R^2 inflationary model," *Phys. Lett. B* **791** (2019) 36–42, arXiv:1812.10099 [hep-ph].

[388] C. F. Steinwachs, "Higgs field in cosmology," *Fundam. Theor. Phys.* **199** (2020) 253–287, arXiv:1909.10528 [hep-ph].

[389] R. Hempfling, "The Next-to-minimal Coleman-Weinberg model," *Phys.Lett.* **B379** (1996) 153–158, arXiv:hep-ph/9604278 [hep-ph].

[390] W.-F. Chang, J. N. Ng, and J. M. S. Wu, "Shadow Higgs from a scale-invariant hidden U(1)(s) model," *Phys. Rev. D* **75** (2007) 115016, arXiv:hep-ph/0701254.

[391] S. Iso, N. Okada, and Y. Orikasa, "Classically conformal $B-L$ extended Standard Model," *Phys.Lett.* **B676** (2009) 81–87, arXiv:0902.4050 [hep-ph].

[392] S. Iso, N. Okada, and Y. Orikasa, "The minimal $B-L$ model naturally realized at TeV scale," *Phys.Rev.* **D80** (2009) 115007, arXiv:0909.0128 [hep-ph].

[393] S. Iso and Y. Orikasa, "TeV Scale B-L model with a flat Higgs potential at the Planck scale - in view of the hierarchy problem -," *PTEP* **2013** (2013) 023B08, arXiv:1210.2848 [hep-ph].

[394] C. Englert, J. Jaeckel, V. Khoze, and M. Spannowsky, "Emergence of the Electroweak Scale through the Higgs Portal," *JHEP* **1304** (2013) 060, arXiv:1301.4224 [hep-ph].

[395] E. J. Chun, S. Jung, and H. M. Lee, "Radiative generation of the Higgs potential," *Phys. Lett. B* **725** (2013) 158–163, arXiv:1304.5815 [hep-ph]. [Erratum: Phys.Lett.B 730, 357–359 (2014)].

[396] V. V. Khoze and G. Ro, "Leptogenesis and Neutrino Oscillations in the Classically Conformal Standard Model with the Higgs Portal," *JHEP* **1310** (2013) 075, arXiv:1307.3764.

[397] S. Benic and B. Radovcic, "Electroweak breaking and Dark Matter from the common scale," *Phys. Lett. B* **732** (2014) 91–94, arXiv:1401.8183 [hep-ph].

[398] V. V. Khoze, C. McCabe, and G. Ro, "Higgs vacuum stability from the dark matter portal," *JHEP* **1408** (2014) 026, arXiv:1403.4953 [hep-ph].

[399] S. Benic and B. Radovcic, "Majorana dark matter in a classically scale invariant model," *JHEP* **01** (2015) 143, arXiv:1409.5776 [hep-ph].

[400] J. Guo, Z. Kang, P. Ko, and Y. Orikasa, "Accidental dark matter: Case in the scale invariant local B-L model," *Phys. Rev. D* **91** no. 11, (2015) 115017, arXiv:1502.00508 [hep-ph].

[401] Z.-W. Wang, F. S. Sage, T. G. Steele, and R. B. Mann, "Asymptotic Safety in the Conformal Hidden Sector?," *J. Phys. G* **45** no. 9, (2018) 095002, arXiv:1511.02531 [hep-ph].

[402] W. Altmannshofer, W. A. Bardeen, M. Bauer, M. Carena, and J. D. Lykken, "Light Dark Matter, Naturalness, and the Radiative Origin of the Electroweak Scale," *JHEP* **1501** (2015) 032, arXiv:1408.3429 [hep-ph].

[403] A. Das, N. Okada, and N. Papapietro, "Electroweak vacuum stability in classically conformal B-L extension of the Standard Model," *Eur. Phys. J. C* **77** no. 2, (2017) 122, arXiv:1509.01466 [hep-ph].

[404] R. Jinno and M. Takimoto, "Probing a classically conformal B-L model with gravitational waves," *Phys. Rev. D* **95** no. 1, (2017) 015020, arXiv:1604.05035 [hep-ph].

[405] A. Das, S. Oda, N. Okada, and D.-s. Takahashi, "Classically conformal U(1)' extended standard model, electroweak vacuum stability, and LHC Run-2 bounds," *Phys. Rev.* **D93** no. 11, (2016) 115038, arXiv:1605.01157 [hep-ph].

[406] S. Oda, N. Okada, and D.-s. Takahashi, "Right-handed neutrino dark matter in the classically conformal U(1)' extended standard model," *Phys. Rev. D* **96** no. 9, (2017) 095032, arXiv:1704.05023 [hep-ph].

[407] C. Marzo, L. Marzola, and V. Vaskonen, "Phase transition and vacuum stability in the classically conformal B–L model," *Eur. Phys. J. C* **79** no. 7, (2019) 601, arXiv:1811.11169 [hep-ph].

[408] S. Oda, N. Okada, D. Raut, and D.-s. Takahashi, "Nonminimal quartic inflation in classically conformal U$(1)_X$ extended standard model," *Phys. Rev. D* **97** no. 5, (2018) 055001, arXiv:1711.09850 [hep-ph].

[409] S. Davidson and A. Ibarra, "A Lower bound on the right-handed neutrino mass from leptogenesis," *Phys. Lett. B* **535** (2002) 25–32, arXiv:hep-ph/0202239.

[410] S. Davidson, E. Nardi, and Y. Nir, "Leptogenesis," *Phys. Rept.* **466** (2008) 105–177, arXiv:0802.2962 [hep-ph].

[411] V. V. Khoze and A. D. Plascencia, "Dark Matter and Leptogenesis Linked by Classical Scale Invariance," *JHEP* **11** (2016) 025, arXiv:1605.06834 [hep-ph].

[412] A. Biswas, S. Choubey, and S. Khan, "Neutrino mass, leptogenesis and FIMP dark matter in a U$(1)_{B-L}$ model," *Eur. Phys. J. C* **77** no. 12, (2017) 875, arXiv:1704.00819 [hep-ph].

[413] O. Lebedev, H. M. Lee, and Y. Mambrini, "Vector Higgs-portal dark matter and the invisible Higgs," *Phys.Lett.* **B707** (2012) 570–576, arXiv:1111.4482 [hep-ph].

[414] S. Baek, P. Ko, W.-I. Park, and E. Senaha, "Higgs Portal Vector Dark Matter : Revisited," *JHEP* **1305** (2013) 036, arXiv:1212.2131 [hep-ph].

[415] C. Gross, O. Lebedev, and Y. Mambrini, "Non-Abelian gauge fields as dark matter," *JHEP* **08** (2015) 158, arXiv:1505.07480 [hep-ph].

[416] N. Okada and O. Seto, "Higgs portal dark matter in the minimal gauged $U(1)_{B-L}$ model," *Phys. Rev. D* **82** (2010) 023507, arXiv:1002.2525 [hep-ph].

[417] S. Benic and B. Radovcic, "Majorana dark matter in a classically scale invariant model," *JHEP* **1501** (2015) 143, arXiv:1409.5776 [hep-ph].

[418] S. Kawai, N. Okada, and S. Okada, "Low-energy implications of cosmological data in $\mathrm{U}(1)_X$ Higgs inflation," *Phys. Rev. D* **103** no. 3, (2021) 035026, arXiv:2012.06637 [hep-ph].

[419] N. Okada, S. Okada, and Q. Shafi, "Light Z' and dark matter from $\mathrm{U}(1)_X$ gauge symmetry," *Phys. Lett. B* **810** (2020) 135845, arXiv:2003.02667 [hep-ph].

[420] E. Gildener and S. Weinberg, "Symmetry Breaking and Scalar Bosons," *Phys. Rev. D* **13** (1976) 3333.

[421] R. Foot, A. Kobakhidze, and R. R. Volkas, "Electroweak Higgs as a pseudo-Goldstone boson of broken scale invariance," *Phys. Lett. B* **655** (2007) 156–161, arXiv:0704.1165 [hep-ph].

[422] R. Foot, A. Kobakhidze, K. L. McDonald, and R. R. Volkas, "Neutrino mass in radiatively-broken scale-invariant models," *Phys. Rev. D* **76** (2007) 075014, arXiv:0706.1829 [hep-ph].

[423] R. Foot, A. Kobakhidze, K. L. McDonald, and R. R. Volkas, "A Solution to the hierarchy problem from an almost decoupled hidden sector within a classically scale invariant theory," *Phys. Rev. D* **77** (2008) 035006, arXiv:0709.2750 [hep-ph].

[424] M. Holthausen, M. Lindner, and M. A. Schmidt, "Radiative Symmetry Breaking of the Minimal Left-Right Symmetric Model," *Phys. Rev. D* **82** (2010) 055002, arXiv:0911.0710 [hep-ph].

[425] R. Foot, A. Kobakhidze, and R. R. Volkas, "Stable mass hierarchies and dark matter from hidden sectors in the scale-invariant standard model," *Phys. Rev. D* **82** (2010) 035005, arXiv:1006.0131 [hep-ph].

[426] L. Alexander-Nunneley and A. Pilaftsis, "The Minimal Scale Invariant Extension of the Standard Model," *JHEP* **09** (2010) 021, arXiv:1006.5916 [hep-ph].

[427] R. Foot, A. Kobakhidze, and R. R. Volkas, "Cosmological constant in scale-invariant theories," *Phys. Rev. D* **84** (2011) 075010, arXiv:1012.4848 [hep-ph].

[428] R. Foot and A. Kobakhidze, "Electroweak Scale Invariant Models with Small Cosmological Constant," *Int. J. Mod. Phys. A* **30** no. 21, (2015) 1550126, arXiv:1112.0607 [hep-ph].

[429] J. S. Lee and A. Pilaftsis, "Radiative Corrections to Scalar Masses and Mixing in a Scale Invariant Two Higgs Doublet Model," *Phys. Rev. D* **86** (2012) 035004, arXiv:1201.4891 [hep-ph].

[430] A. Farzinnia, H.-J. He, and J. Ren, "Natural Electroweak Symmetry Breaking from Scale Invariant Higgs Mechanism," *Phys. Lett. B* **727** (2013) 141–150, arXiv:1308.0295 [hep-ph].

[431] O. Antipin, M. Mojaza, and F. Sannino, "Conformal Extensions of the Standard Model with Veltman Conditions," *Phys. Rev. D* **89** no. 8, (2014) 085015, arXiv:1310.0957 [hep-ph].

[432] J. Guo and Z. Kang, "Higgs Naturalness and Dark Matter Stability by Scale Invariance," *Nucl. Phys. B* **898** (2015) 415–430, arXiv:1401.5609 [hep-ph].

[433] A. Farzinnia and J. Ren, "Higgs Partner Searches and Dark Matter Phenomenology in a Classically Scale Invariant Higgs Boson Sector," *Phys. Rev. D* **90** no. 1, (2014) 015019, arXiv:1405.0498 [hep-ph].

[434] M. Lindner, S. Schmidt, and J. Smirnov, "Neutrino Masses and Conformal Electro-Weak Symmetry Breaking," *JHEP* **10** (2014) 177, arXiv:1405.6204 [hep-ph].

[435] Z. Kang, "Upgrading sterile neutrino dark matter to FImP using scale invariance," *Eur. Phys. J. C* **75** no. 10, (2015) 471, arXiv:1411.2773 [hep-ph].

[436] A. Karam and K. Tamvakis, "Dark matter and neutrino masses from a scale-invariant multi-Higgs portal," *Phys. Rev. D* **92** no. 7, (2015) 075010, arXiv:1508.03031 [hep-ph].

[437] K. Ghorbani and H. Ghorbani, "Scalar Dark Matter in Scale Invariant Standard Model," *JHEP* **04** (2016) 024, arXiv:1511.08432 [hep-ph].

[438] A. J. Helmboldt, P. Humbert, M. Lindner, and J. Smirnov, "Minimal conformal extensions of the Higgs sector," *JHEP* **07** (2017) 113, arXiv:1603.03603 [hep-ph].

[439] K. Hashino, M. Kakizaki, S. Kanemura, and T. Matsui, "Synergy between measurements of gravitational waves and the triple-Higgs coupling in probing the first-order electroweak phase transition," *Phys. Rev. D* **94** no. 1, (2016) 015005, arXiv:1604.02069 [hep-ph].

[440] A. Ahriche, K. L. McDonald, and S. Nasri, "The Scale-Invariant Scotogenic Model," *JHEP* **06** (2016) 182, arXiv:1604.05569 [hep-ph].

[441] V. V. Khoze and A. D. Plascencia, "Dark Matter and Leptogenesis Linked by Classical Scale Invariance," *JHEP* **11** (2016) 025, arXiv:1605.06834 [hep-ph].

[442] F. Wu, "Aspects of a nonminimal conformal extension of the standard model," *Phys. Rev. D* **94** no. 5, (2016) 055011, arXiv:1606.08112 [hep-ph].

[443] A. Karam and K. Tamvakis, "Dark Matter from a Classically Scale-Invariant $SU(3)_X$," *Phys. Rev. D* **94** no. 5, (2016) 055004, arXiv:1607.01001 [hep-ph].

[444] L. Chataignier, T. Prokopec, M. G. Schmidt, and B. Świeżewska, "Systematic analysis of radiative symmetry breaking in models with extended scalar sector," *JHEP* **08** (2018) 083, arXiv:1805.09292 [hep-ph].

[445] F. Loebbert, J. Miczajka, and J. Plefka, "Consistent Conformal Extensions of the Standard Model," *Phys. Rev. D* **99** no. 1, (2019) 015026, arXiv:1805.09727 [hep-ph].

[446] V. Brdar, Y. Emonds, A. J. Helmboldt, and M. Lindner, "Conformal Realization of the Neutrino Option," *Phys. Rev. D* **99** no. 5, (2019) 055014, arXiv:1807.11490 [hep-ph].

[447] S. Yaser Ayazi and A. Mohamadnejad, "Scale-Invariant Two Component Dark Matter," *Eur. Phys. J. C* **79** no. 2, (2019) 140, arXiv:1808.08706 [hep-ph].

[448] T. Prokopec, J. Rezacek, and B. Świeżewska, "Gravitational waves from conformal symmetry breaking," *JCAP* **02** (2019) 009, arXiv:1809.11129 [hep-ph].

[449] A. Karam, T. Pappas, and K. Tamvakis, "Nonminimal Coleman–Weinberg Inflation with an R^2 term," *JCAP* **02** (2019) 006, arXiv:1810.12884 [gr-qc].

[450] S. Yaser Ayazi and A. Mohamadnejad, "Conformal vector dark matter and strongly first-order electroweak phase transition," *JHEP* **03** (2019) 181, arXiv:1901.04168 [hep-ph].

[451] A. Mohamadnejad, "Accidental scale-invariant Majorana dark matter in leptoquark-Higgs portals," *Nucl. Phys. B* **949** (2019) 114793, arXiv:1904.03857 [hep-ph].

[452] K. Kannike, A. Kubarski, and L. Marzola, "Geometry of Flat Directions in Scale-Invariant Potentials," *Phys. Rev. D* **99** no. 11, (2019) 115034, arXiv:1904.07867 [hep-ph].

[453] D.-W. Jung, J. Lee, and S.-H. Nam, "Scalar dark matter in the conformally invariant extension of the standard model," *Phys. Lett. B* **797** (2019) 134823, arXiv:1904.10209 [hep-ph].

[454] A. Mohamadnejad, "Gravitational waves from scale-invariant vector dark matter model: Probing below the neutrino-floor," *Eur. Phys. J. C* **80** no. 3, (2020) 197, arXiv:1907.08899 [hep-ph].

[455] K. Lane and E. Pilon, "Phenomenology of the new light Higgs bosons in Gildener-Weinberg models," *Phys. Rev. D* **101** no. 5, (2020) 055032, arXiv:1909.02111 [hep-ph].

[456] Z. Kang and J. Zhu, "Scale-genesis by Dark Matter and Its Gravitational Wave Signal," *Phys. Rev. D* **102** no. 5, (2020) 053011, arXiv:2003.02465 [hep-ph].

[457] A. G. Dias, J. Leite, B. L. Sánchez-Vega, and W. C. Vieira, "Dynamical symmetry breaking and fermion mass hierarchy in the scale-invariant 3-3-1 model," *Phys. Rev. D* **102** no. 1, (2020) 015021, arXiv:2005.00556 [hep-ph].

[458] J. Braathen, S. Kanemura, and M. Shimoda, "Two-loop analysis of classically scale-invariant models with extended Higgs sectors," *JHEP* **03** (2021) 297, arXiv:2011.07580 [hep-ph].

[459] K. Kannike, K. Loos, and L. Marzola, "Minima of Classically Scale-Invariant Potentials," arXiv:2011.12304 [hep-ph].

[460] K. Kannike, L. Marzola, M. Raidal, and A. Strumia, "Light Higgs boson from multi-phase criticality in dynamical symmetry breaking," *Phys. Lett. B* **816** (2021) 136241, arXiv:2102.01084 [hep-ph].

[461] V. I. Afonso, C. Bejarano, J. Beltran Jimenez, G. J. Olmo, and E. Orazi, "The trivial role of torsion in projective invariant theories of gravity with non-minimally coupled matter fields," *Class. Quant. Grav.* **34** no. 23, (2017) 235003, arXiv:1705.03806 [gr-qc].

[462] J. D. Bekenstein, "The Relation between physical and gravitational geometry," *Phys. Rev. D* **48** (1993) 3641–3647, arXiv:gr-qc/9211017.

[463] M. Zumalacárregui and J. Garcia-Bellido, "Transforming gravity: from derivative couplings to matter to second-order scalar-tensor theories beyond the Horndeski Lagrangian," *Phys. Rev. D* **89** (2014) 064046, arXiv:1308.4685 [gr-qc].

[464] M. Minamitsuji, "Disformal transformation of cosmological perturbations," *Phys. Lett. B* **737** (2014) 139–150, arXiv:1409.1566 [astro-ph.CO].

[465] S. Tsujikawa, "Disformal invariance of cosmological perturbations in a generalized class of Horndeski theories," *JCAP* **04** (2015) 043, arXiv:1412.6210 [hep-th].

[466] G. Domènech, A. Naruko, and M. Sasaki, "Cosmological disformal invariance," *JCAP* **10** (2015) 067, arXiv:1505.00174 [gr-qc].

[467] H. Firouzjahi, M. A. Gorji, S. A. Hosseini Mansoori, A. Karami, and T. Rostami, "Two-field disformal transformation and mimetic cosmology," *JCAP* **11** (2018) 046, arXiv:1806.11472 [gr-qc].

[468] S. R. Coleman and E. J. Weinberg, "Radiative Corrections as the Origin of Spontaneous Symmetry Breaking," *Phys.Rev.* **D7** (1973) 1888–1910.

[469] **BICEP2, Keck Array** Collaboration, P. Ade *et al.*, "BICEP2 / Keck Array x: Constraints on Primordial Gravitational Waves using Planck, WMAP, and New BICEP2/Keck Observations through the 2015 Season," *Phys. Rev. Lett.* **121** (2018) 221301, arXiv:1810.05216 [astro-ph.CO].

[470] T. Markkanen, S. Nurmi, A. Rajantie, and S. Stopyra, "The 1-loop effective potential for the Standard Model in curved spacetime," *JHEP* **06** (2018) 040, arXiv:1804.02020 [hep-ph].

[471] G. Giudice, A. Notari, M. Raidal, A. Riotto, and A. Strumia, "Towards a complete theory of thermal leptogenesis in the SM and MSSM," *Nucl. Phys. B* **685** (2004) 89–149, arXiv:hep-ph/0310123.

[472] S. Antusch and A. Teixeira, "Towards constraints on the SUSY seesaw from flavour-dependent leptogenesis," *JCAP* **02** (2007) 024, arXiv:hep-ph/0611232.

[473] W. Buchmuller, R. D. Peccei, and T. Yanagida, "Leptogenesis as the origin of matter," *Ann. Rev. Nucl. Part. Sci.* **55** (2005) 311–355, arXiv:hep-ph/0502169.